UNIVERSITY
OF TASMANIA

The Development and Evaluation of Supracolloidal Monolithic Structures for Applications in Separation Science

By

Christopher Desire

A thesis submitted in fulfillment of the requirements for

the degree of

Doctor of Philosophy

School of Physical Sciences
University of Tasmania

Submitted August 2017

Declarations

This thesis contains no material which has been accepted for a degree or diploma by the University or any other institution, except by way of background information and duly acknowledged in the thesis, and to the best of my knowledge and belief no material previously published or written by another person except where due acknowledgement is made in the text of the thesis, nor does the thesis contain any material that infringes copyright.

The publishers of the papers comprising Chapters 1 and 3 to 7 hold the copyright for that content, and access to the material should be sought from the respective journals. The remaining non published content of the thesis may be made available for loan and limited copying and communication in accordance with the Copyright Act 1968.

This thesis also consists of my own work, with the following exceptions:

- Chapter 3 - Mechanical testing was performed at the Department of Materials Engineering, Monash University (Clayton, Victoria, Australia) by Tara L. Schiller with the assistance of Mr Silvio Mattievich.

- Chapter 5 – Elemental analysis was performed by Thomas Rodemann from the Central Science Laboratory (CSL) at the University of Tasmania (Hobart, Tasmania, Australia).

- Chapter 6 - Crystal structures were obtained by Guy Clarkson (Department of Chemistry, University of Warwick, United Kingdom).

Christopher Desire

August 2017

Acknowledgements

Firstly, I would like to acknowledge my supervisors Prof. Emily Hilder and Dr Dario Arrua. I am extremely grateful for their support and the opportunities they enabled me to pursue during my PhD candidature. I would also like to acknowledge Prof. Stefan Bon who provided me with the opportunity to spend part of my PhD under his supervision and be an active member of his research team. His kindness and support is much appreciated. In addition I would like to thank Dr Tara Schiller for her support during my early candidature and when I spent time overseas.

I would also like to take the opportunity to thank Dr Peter Smith for his ongoing support and interest in my endeavours during both my undergraduate degree and PhD candidature. His passion for chemistry and supporting the next generation of students is one of the reasons this thesis exists.

To all the wonderful people I have had the privilege to work with over the past four years, including Andrea Loiterzo, Brooke Longbottom, Ross Jaggers, Samuel Wilson-Whitford, Matt Donald, Adam Sutton, Farhan Cecil, Umme Kalsoom, Amin Khodabandeh, Fotouh Rasheed, Daniel Gstöttenmayr, Sara Thomas, Neeraj Verma, James Hsian-Meng Chan, Mohammad Talebi, Laura Tedone, Anton Peristyy, Eli Fornells Vernet, Joan Marc Cabot, Niall Macdonald, Sinéad Currivan, Disha Choudhury and Esme Candish, you made the lab and office fun to be in. In particular I would like to thank all the members of ACROSS and the Discipline of Chemistry for their support during this time.

I would also like to thank the staff (past and present) from the Discipline of Chemistry for their support over my candidature, including Brendon Schollum, Graham Meridith, Andrew Grosse, and Murray Frith. In addition I would like to acknowledge the support and guidance I received from the Central Science Laboratory (CSL) including the following members, Dr Karsten Gömann, Dr Sandrin Feig and Dr Thomas Rodemann.

It has been an eventful past four years and I would like to thank my friends who have supported me during this time, including Lewis Russell and James Howard. In particular I would like to thank the friends I spent many evenings with on the PS4, including Brendon Schollum, Tristan Davies, Reyne Pullen, Daniel Chaffelson, Daniel Bukofzer, and Andrew Herron. Hopefully there will be many more evenings like this to come and I thank you for my sanity, I think.

In addition, I would like to thank Bungie who created and maintained an immersive online world that I have spent much of the past three years in with those mentioned above. My immersion in the world of Destiny helped me to maintain my creativity and focus in order to overcome the challenges of PhD. I would also like to thank the members of the Destiny Community Podcast who provided a much-needed distraction during the last six months of candidature.

Finally, to my family, I am deeply grateful for your continued support over this time and thank you for sharing this journey with me.

Statement of Co-Authorship

The following people and institutions contributed to the publication of the work undertaken as part of this thesis:

Christopher Desire, School of Physical Sciences, UTAS = **Candidate**

Aminreza Khodabandeh, School of Physical Sciences, UTAS = **Author 1**

Tara L. Schiller, WMG, The University of Warwick = **Author 2**

Russell Wilson, School of Physical Sciences, UTAS = **Author 3**

R. Dario Arrua, Future Industries Institute, University of South Australia = **Author 4**

Stefan A. F. Bon, Department of Chemistry, The University of Warwick = **Author 5**

Emily F. Hilder, Future Industries Institute, University of South Australia = **Author 6**

Fotouh R. Mansour, Department of Pharmaceutical Analytical Chemistry, Tanta University = **Author 7**

Andrea Lotierzo, Department of Chemistry, The University of Warwick = **Author 8**

Author details and their roles:

Paper 1, <Monolithic High-performance Liquid Chromatography Columns>

Located in chapter 1

Candidate was the primary author (50%) with author 4 (40 %). Author 6 (10%) assisted with refinement and presentation.

Paper 2, <Preparation of highly interconnected hydrophilic polymers from emulsion templates with improved mechanical properties>

Located in chapter 3 & 2

Candidate was the primary author (65%) with author 3 and 4 (5% respectively). Author 5 and 6 (10% respectively) contributed to the idea, and its formalisation and development. Author 2 assisted with materials characterisation (5%). Author 1 and 3 assisted with refinement and presentation.

Paper 3, <Effect of shearing stress on the radial heterogeneity and chromatographic performance of styrene-based polymerised high internal phase emulsions prepared in capillary format>

Located in chapter 4, 1 & 2

Candidate was the primary author (60%) with author 4 (10%). Author 5, 6 and 7 (10% respectively) contributed to the idea, and its formalisation and development. Author 1 and 3 assisted with refinement and presentation.

Paper 4, <The preparation of styrene-based polymerised high internal phase emulsions functionalised with monomers from the internal phase for liquid chromatography>

Located in chapter 5, 1 & 2

Candidate was the primary author (60%) with author 4 (10%). Author 5, 6 and 7 (10% respectively) contributed to the idea, and its formalisation and development. Author 1 and 3 assisted with refinement and presentation.

Paper 5, <The preparation of polymer monoliths using latexes prepared from the soap-free emulsion polymerisation of styrene>

Located in chapter 6 & 1

Candidate was the primary author (60%) with author 5 (10%). Author 4, 6 and 8 (10% respectively) contributed to the idea, and its formalisation and development.

We the undersigned agree with the above stated "proportion of work undertaken" for each of the above published (or submitted) peer-reviewed manuscripts contributing to this thesis:

Signed:

	Emily Hilder	*John Dickey*
	School of Physical Sciences	*School of Physical Sciences*
	University of Tasmania	*University of Tasmania*
Date:	08/08/17	8/8/17

List of Publications and Presentations

Papers in peer-reviewed journals:

1. Desire, C.T., Arrua, R.D. & Hilder, E.F. Monolithic High-performance Liquid Chromatography Columns. *Encyclopedia of Analytical Chemistry*. DOI: 10.1002/9780470027318.a9386. (Chapter 1).

2. Desire, C.T., Khodabandeh, A., Schiller, T.L., Wilson, R., Arrua, R.D., Bon, S.A.F. & Hilder, E.F. Preparation of highly interconnected hydrophilic polymers from emulsion templates with improved mechanical properties. *European Polymer Journal*. *Accepted*. (Chapter 3).

3. Desire, C.T., Arrua, R.D., Mansour, F.R., Bon, S.A.F. & Hilder, E.F. Effect of shearing stress on the radial heterogeneity and chromatographic performance of styrene-based polymerised high internal phase emulsions prepared in capillary format. *RSC. Advances*. *In Preparation*. (Chapter 4).

4. Desire, C.T., Arrua, R.D., Mansour, F.R., Bon, S.A.F. & Hilder, E.F. The preparation of styrene-based polymerised high internal phase emulsions functionalised with monomers from the internal phase for liquid chromatography. *RSC. Advances*. *In Preparation*. (Chapter 5).

5. Desire, C.T., Lotierzo, A., Arrua, R.D., Hilder, E.F. & Bon, S.A.F. The preparation of polymer monoliths using latexes prepared from the soap-free emulsion polymerisation of styrene. *Green Chem*. *In Preparation*. (Chapter 6).

Conferences:

1. Desire, C.T., Lotierzo, A., Hilder, E.F. & Bon, S.A.F. Preparation of Polymer Monoliths using Crosslinked Colloidal Gels (oral presentation). *RACI Centenary Congress*, 23 - 28 July 2017. Melbourne. Australia.

2. Desire, C.T., Lotierzo, A., Bon, S.A.F. & Hilder, E.F. Crosslinked colloidal gels as potential analytical devices (poster presentation). *ASSAS 2 – ACROSS International Symposium on Separation Science*, Nov 30 - Dec 2 2016. Hobart. Australia.

3. Desire, C.T., Khodabandeh, A., Arrua, R.D., Bon, S.A.F. & Hilder, E.F. Development of Porous Polymers from Emulsion Templates for Separation Science (poster presentation). *Warwick Polymer Conference 2016*, 11 - 14 July 2016. University of Warwick, Coventry, CV4 7AL, United Kingdom.

4. Desire, C.T., Khodabandeh, A., Arrua, R.D. & Hilder, E.F. The Development of Porous Polymers from Emulsion Templates for Separation Science (poster presentation). *23rd Annual Research and Development Conference in Analytical and Environmental Chemistry*, 6 - 9 Dec 2015. University of Melbourne, Parkville, Victoria, Australia.

5. Desire, C.T., Khodabandeh, A., Arrua, R.D. & Hilder, E.F. Preparation of Porous Polymers from Emulsion Templates for Applications in Separation Science (poster presentation). *22nd Annual Research and Development Conference in Analytical and Environmental Chemistry*, 13 - 15 Dec 2014. Flinders University, Adelaide, Australia.

6. Desire, C.T., Khodabandeh, A., Arrua, R.D., Bon, S.A.F. & Hilder, E.F. Preparation of Hydrophilic Porous Polymers from Reduced Internal Phase Emulsions (oral presentation). *RACI National Congress*, 7 - 12 Dec 2014. Adelaide, Australia.

7. Hilder, E.F., Arrua, R.D., Desire, C.T., Khodabandeh, A. & Wilson, R. Preparation and characterisation of ordered porous polymer monoliths (oral presentation). *248th ACS National Meeting & Exposition*, 10 - 14 Aug 2014. San Francisco, CA, USA.

8. Hilder, E.F., Arrua, R.D., Khodabandeh, A., Desire, C.T. & Bon, S.A.F. Preparation and Characterization of Ordered Porous Polymer Monoliths for Chromatography (oral presentation). *41st International Symposium on High Performance Liquid Phase Separations and Related Techniques*, 11 - 15 May 2014. New Orleans, Louisiana, USA.

Abstract

This thesis focuses on the development of polymer monoliths from emulsions for applications in liquid chromatography, in particular the use of high internal phase emulsions to produce monoliths with controlled morphology.

An initial study focused on the preparation of hydrophilic polymer monoliths using oil-in-water emulsions. Here, the internal phase volume of the emulsion was varied to produce monoliths with improved mechanical properties under compression. A systematic study was then employed focusing on the influence of the internal phase volume, surfactant concentration and the emulsification energy on the interconnectivity of the resulting monolith. It was found that monoliths with significantly improved mechanical properties that maintained a high level of interconnectivity could be obtained by selecting an appropriate combination of these parameters. The monoliths obtained were found to be responsive to different solvent environments, with significant changes in their volume. This suggested their applicability for use as absorbents or for controlled release but made them unsuitable for liquid chromatography involving a solvent gradient. In addition, when prepared in capillary format, these monoliths were observed to detach from the capillary wall during purification as a result of shrinkage.

As such, the preparation of hydrophobic polymer monoliths from water-in-oil emulsions, in capillary format, for chromatographic applications was explored, as these exhibited minimal change in volume when exposed to different solvent environments. Particular attention was paid to the effect that the preparation in capillary format had on the morphology of the resulting monoliths. It was found that when these materials were prepared in capillaries of internal diameter less than 540 µm using low shear emulsification, significant alterations in their porous morphology were observed. In addition, all columns prepared possessed significant radial heterogeneity. When high shear emulsification was employed the morphology of the resulting monoliths mirrored that of those prepared within glass vials and no

significant radial heterogeneity was observed. As a result these monoliths exhibited significantly improved chromatographic performance for the separation of a standard mixture of proteins using reversed-phase liquid chromatography with a solvent gradient.

Given these monoliths exhibited a rigid backbone, which did not appear to be compromised by a solvent gradient, they were surface modified by simply incorporating monomers into the internal phase of the emulsion. Initial work focused on the incorporation of the hydrophilic monomer acrylamide in order to increase the hydrophilicity of the monolithic surface. The influence of the inclusion of monomer in the internal phase and choice of initiator on the resulting morphology of these monoliths was investigated. It was found that increases in the monomer content coupled with the use of either a water-soluble or oil-soluble initiator resulted in monoliths with varied morphology and surface chemistry. The increase in hydrophilicity of this scaffold was observed through the separation of some components of a peptide mixture using hydrophilic interaction liquid chromatography, which was not possible using the unmodified scaffold. Finally, a weakly hydrophilic monomer poly(ethylene glycol) diacrylate (M_w 258) was incorporated into the internal phase where it was observed to act as an efficient co-stabiliser resulting in an increase in the homogeneity of the column, and this material was found to be capable of separating a more complex protein mixture by reversed phase liquid chromatography.

The final section of this thesis focused on the preparation of polymer monoliths using latex particles prepared from the soap-free emulsion polymerisation of styrene as a new approach for their preparation. Here, two oppositely charged latexes were combined which resulted in the formation of a colloidal gel that was porous in nature. Chemical cross-linking was then employed, by including a cross-linking monomer in the formulation, to form a rigid polymer monolith. These materials could also be prepared from a single latex by promoting the formation of the gel through the inclusion of a salt, in this case the initiator used for the cross-linking process. It was found that the pore size of these materials was predictable as it

directly correlated to the particle diameter. The mouldability and freestanding nature of these gels also easily allowed for their preparation in a variety of formats, even without a mould. These materials were also capable of rapidly absorbing solvents of varying polarity though capillary action suggesting their applicability for thin-layer chromatography or for extraction.

Table of Contents

List of Abbreviations

AA	Acrylic acid
AAm	Acrylamide
ACN	Acetonitrile
AIBN	2,2'-azobis(2-methylpropionitrile)
AMPS	2-acrylamido-2-methyl-1-propanesulfonic acid
APS	Ammonium persulfate
BET	Brunauer-Emmett-Teller
BuMA	Butyl methacrylate
CEC	Capillary Electrochromatography
CHDF	Capillary Hydrodynamic Fractionation
COC	Cycloolefin copolymer
CIM	Convective Interactive Media
DEA	Diethylamine
DEAE	Diethylaminoethyl
DEGDA	Di(ethylene glycol) diacrylate
DLS	Dynamic Light Scattering
DMSO	Dimethyl sulfoxide
DVB	Divinylbenzene
EDMA	Ethylene dimethacrylate
EHA	2-ethylhexyl acrylate
EHMA	2-ethylhexyl methacrylate
EtOH	Ethanol
GMA	Glycidyl methacrylate
HEMA	2-hydroxyethyl methacrylate
HIC	Hydrophobic Interaction Chromatography
HILIC	Hydrophilic Interaction Liquid Chromatography
HIPE	High Internal Phase Emulsion
HLB	Hydrophilic-Lipophilic Balance
i.d.	internal diameter

IC	Ion Chromatography
IEX	Ion-Exchange Chromatography
IP	Internal Phase
IUPAC	International Union of Pure and Applied Chemistry
KPS	Potassium persulfate
LC	Liquid Chromatography
LIPE	Low Internal Phase Emulsion
MBAm	*N,N*'-methylenebisacrylamide
MIP	Mercury Intrusion Porosimetry
MIPE	Medium Internal Phase Emulsion
MMA	Methacrylic acid
MS	Mass Spectrometry
NIPAM	N-isopropyl acrylamide
NMR	Nuclear magnetic resonance
o.d.	outer diameter
PEEK	Polyether ether ketone
PEG	Poly(ethylene glycol)
PEGDA	Poly(ethylene glycol) diacrylate
PLGA	Poly(D,L-lactic-*co*-glycolic acid)
RAFT	Reversible Addition-Fragmentation Chain Transfer
RPLC	Reversed-Phase Liquid Chromatography
SEM	Scanning Electron Microscopy
Sty	Styrene
TEMED	N,N,N',N'-tetramethylethylenediamine
TEVBAC	Triethyl(4-vinylbenzyl)ammonium chloride
TLC	Thin-layer chromatography
TMVBAC	Trimethyl(vinylbenzyl)ammonium chloride
V-50	2,2-azobis(2-methylpropanimidamide) dihydrochloride

Chapter 1 has been removed for copyright or proprietary reasons.

It has been published as: Desire, C. T., Arrua, R. D., Hilder, E. F. Monolithic High-performance Liquid Chromatography Columns, in, Encyclopedia of Analytical Chemistry. DOI: 10.1002/9780470027318.a9386.

Chapter 2

Experimental

This section briefly summarises the materials, instrumentation and general procedures used throughout this research, unless specified otherwise in specific chapters.

2.1 Materials

Unless otherwise specified the chemicals listed in **Tables 2.1 - 2.6** were used as received. The H_2O used in all experiments was first purified using a Milli-Q system (18 MΩ cm, Millipore, USA).

Table 2.1 Chemicals used for the preparation and/or characterisation of the emulsion templated porous polymers

Chemical	Purity/Conc	Supplier
Acetone	AR grade	Chem-Supply
Acrylamide (AAm)	≥98.0%	Fluka
2,2′-azobis(2-methylpropionitrile) (AIBN) [a]		MP Biomedicals
Basic alumina (Brockman activity I, 60-325 mesh)		Sigma-Aldrich
Ammonium persulfate (APS)	≥98.0%	Ajax Chemicals
Calcium chloride dihydrate	≥98.0%	Ajax Chemicals
Dichloromethane	>99%	Unilab
Divinylbenzene (DVB) [b]	80%	Sigma-Aldrich
Methanol (MeOH)	AR grade	Chem-Supply
N,*N*′-methylenebisacrylamide (MBAm)	≥99.5%	Sigma-Aldrich
Paraffin-oil	Puriss	Sigma-Aldrich
PEG diacrylate (PEGDA, Mn 258) [c]		Sigma-Aldrich
Potassium persulfate (KPS) [d]	≥99.0%	Sigma-Aldrich
Sodium carbonate (anhydrous)	≥99.9%	Merck
Sodium sulfate (anhydrous)	≥99.0%	Sigma-Aldrich
Span® 80	≥60%	Fluka
Styrene (Sty) [b]	99%	Sigma-Aldrich
Tween® 85	≥50% aqueous solution	Sigma-Aldrich

[a] Was re-crystalised from MeOH. [b] Were passed through a column of basic alumina to remove inhibitors. [c] Was purified according to the procedure in **Section 2.4.2**. [d] Was re-crystalised from H_2O.

Table 2.2 Chemicals used for the surface modification of fused-silica capillaries

Chemical	Purity/Conc	Supplier
Acetone	AR grade	Chem-Supply
Acetic acid	≥99.7%	Sigma-Aldrich
Ethanol (EtOH)	>99%	Chem-Supply
Hydrochloric acid (HCl)	37% aqueous solution	Merck
Sodium hydroxide (NaOH)	≥98.0%	Sigma-Aldrich
3-(trimethoxysilyl)propyl methacrylate	≥98%	Sigma-Aldrich

Table 2.3 Chemicals used for the preparation of mobile phases for LC

Chemical	Purity	Supplier
Acetonitrile (ACN)	≥99.8%	VWR
Formic acid	≥98.0%	Fluka
Methanol (MeOH)	99.9%	Fisher Scientific

Table 2.4 Analytes used for LC

Chemical	Purity	Supplier
Albumin from chicken egg white (ovalbumin)	(≥98%)	Sigma-Aldrich
α-chymotrypsinogen A from bovine pancreas		Sigma-Aldrich
Cytidine	≥99%	Fluka
Cytochrome *c* from equine heart	≥95%	Sigma-Aldrich
Guanosine	≥99%	Fluka
HPLC peptide standard mixture (consisting of angiotensin II, Gly-Tyr, Leu encephalin, Met encephalin and Val-Tyr-Val)		Sigma-Aldrich
Lysozyme from chicken egg white	≥90%	Sigma-Aldrich
Myoglobin from horse heart	≥90%	Sigma-Aldrich
Ribonuclease A, type I-A, from bovine pancreas	≥60%	Sigma-Aldrich
Thiourea	≥99.0%	Ajax Chemicals

Table 2.5 Chemicals used for the preparation and/or characterisation of cross-linked colloidal gels

Chemical	Purity	Supplier
Acetone	≥99%	Sigma-Aldrich
Ammonium persulfate (APS)	98%	Sigma-Aldrich
2,2-azobis(2-methylpropanimidamide) dihydrochloride (V-50)	98%	Acros Organics
2,2′-azobis(2-methylpropionitrile) (AIBN) [a]		BDH
Di(ethylene glycol) diacrylate (DEGDA)	75%	Sigma-Aldrich
Dimethyl sulfoxide-d_6 (DMSO)		Sigma-Aldrich
Divinylbenzene (DVB)	80%	Sigma-Aldrich
Methanol (MeOH)	AR grade	VWR
Styrene (Sty)	≥99%	Sigma-Aldrich
4-styrenesulfonic acid sodium salt		Sigma-Aldrich
Triethylamine	≥99%	Sigma-Aldrich
N,N,N′,N′-tetramethylethylenediamine (TEMED)	≥99%	Sigma-Aldrich
4-vinylbenzyl chloride	90%	Sigma-Aldrich

[a] Was re-crystalised from MeOH.

Table 2.6 Chemicals used for the characterisation of cross-linked colloidal gels

Chemical	Purity	Supplier
Acetonitrile (ACN)	≥99.8%	VWR
Ethanol (EtOH)	>99%	Chem-Supply
Hexadecane	≥98.5%	Acros Organics
Methanol (MeOH)	AR grade	VWR
Sunflower oil		Woolworths Essentials

Polyimide-coated capillaries of 150 µm i.d. (360 µm o.d.), 250 µm i.d. (360 µm o.d.) and 540 µm i.d. (670 µm o.d.) were obtained from Polymicro Technologies.

2.2 Characterisation

2.2.1 Optical Microscopy

Optical microscopy images of emulsions were obtained using a Nikon Eclipse E200 microscope equipped with a 10× objective (Nikon Corporation, Chiyoda, Tokyo, Tokyo, Japan) and a 30.5 mm 0.5× C-mount adapter connected to a 5.0 MP Tucsen IS500 Camera (Fuzhou Xintu Photonics Co., Ltd, Fujian, China). A few drops of emulsion were placed on a glass slide, which had a piece of Teflon (500 µm thick) covering the perimeter. The Teflon had been adhered using a two-part epoxy adhesive (Araldite 5 Minute Everyday, Shelley Pty. Ltd. NSW, Australia). Another glass slide was placed over the top to limit any evaporation that may occur. The Teflon limited any compression of the emulsion droplets, and this setup allowed more stable images to be obtained. The droplet size distributions were obtained by directly measuring the droplet diameters from the images using the image analysis software ImageJ (NIH image). This was performed for at least 300 droplets. Optical microscopy images were obtained immediately after preparation, and 24 h later for selected samples.

2.2.2 Dynamic Light Scattering

Dynamic light scattering (DLS) was attempted for the emulsions prepared in **Chapter 3** on a Malvern Nano-ZS (ATA Scientific Pty. Ltd, NSW, Australia) with diluted emulsion in order to estimate the droplet size. The particle size and particle size distributions for the latexes prepared in **Chapter 6** were also measured by DLS using a Malvern Instruments Zetasizer (Nano-ZS) instrument using dilute latex samples. Zeta potentials were also measured using this instrument with dilute latex samples.

2.2.3 Scanning Electron Microscopy

The polymer morphologies for the samples prepared in **Chapters 3, 4** & **5** were investigated using a Hitachi SU-70 field emission scanning electron microscope (Hitachi, Pleasanton, CA, USA) operated in high vacuum mode with an acceleration voltage of 1.5 kV. Secondary electrons were detected using a Hitachi scintillator-type detector. The samples were platinum coated (2-3 nm thick coating) using a Bal-Tec SCD 050 Sputter Coater (Bal-Tec AG, Balzers, Liechtenstein). The average void and window sizes were obtained (where applicable) using ImageJ, where the diameter of at least 300 voids and windows were measured.

The values obtained are actually an underestimation of the true values and it is therefore necessary to introduce a statistical correction [1-2], the derivation of which is described by Barbetta and Cameron [2], where essentially the values obtained are multiplied by a factor of $2/(3^{1/2})$. The average number of windows per void was also estimated for some samples by counting the number of observed windows for 300 voids, however this is a rough estimate as all the windows present for a void are not visible from the SEM images and this is not easily corrected for. The average degree of interconnectivity was also calculated for the samples in **Chapter 3** by dividing the average window diameter by the average void diameter [1, 3]. For **Chapters 4** & **5** the radial distribution of voids for the capillary cross-sections was determined by calculating the average diameter of the voids present within the

annulus formed from concentric circles, which differed in diameter by 25 μm for **Chapter 4** and 15 μm for **Chapter 5**, originating from the capillary wall.

SEM micrographs were obtained for the materials prepared in **Chapter 6** using a Zeiss Supra™ 55VP field emission scanning electron microscope (Carl Zeiss AG, Oberkochen, Germany), with secondary electron detection, operating in high vacuum mode with an acceleration voltage of 15 kV. Samples were first dispersed in H_2O and evaporated onto silicon wafers attached to aluminium stubs, before being sputter-coated with carbon using an Emitech K950X sputter-coater (Quorum Technologies, Kent, United Kingdom) or gold coated using a Polaron Range sputter coater (Quorum Technologies, Kent, United Kingdom). The average pore size for some of these materials was estimated by measuring the diameter of 500 pores. Histograms were obtained from these data sets using 22 bins, where the bin width was calculated by dividing the range of values by the number of bins. Theoretical normal distributions were also obtained based on the mean and standard deviation over a range of ± 3 standard deviations using 200 points.

2.2.4 Surface Area Analysis

The specific surface area of the materials prepared in **Chapters 3-6** was determined by nitrogen adsorption with the Brunauer-Emmett-Teller (BET) method [4] using a Micromeritics Tristar II 2020 automated gas sorption–desorption instrument (Micromeritics, Norcross, GA, USA). Prior to analysis, all samples were dried in a Micromeritics SmartPrep at 80 °C for 48 h. This was performed in triplicate with 100-200 mg of sample.

2.2.5 Mercury Intrusion Porosimetry

Mercury intrusion porosimetry (MIP) was performed on selected samples in **Chapter 3** using a Micromeritics AutoPore IV 9505 porosimeter (Micromeritics, Norcross, GA, USA). Penetrometers with a stem volume of 0.4120 mL and a bulb volume of 3 mL were used. Intrusion pressure was started at 1.5 psi and was increased to a final

value of 33, 000 psi. This was also performed in triplicate. Between 100 and 200 mg of sample was used each time depending on the stem volumes obtained (more sample was required for the less porous materials). The pore size distributions obtained were redrawn using Origin® 8.5 (OriginLab Corporation, Northampton, MA, USA).

2.2.6 Mechanical Properties

An Instron 5500R Advanced Materials Testing System (Instron, Norwood, MA, USA) was used to measure the mechanical properties under compression for selected polymer disks prepared in **Chapter 3**. The samples were compressed at a rate of 5 mm/min. At least five cylindrical disks of ~11.5 mm in diameter and ~16 mm in height were analysed for each sample. The average Young's modulus was determined from the slope of the initial elastic region (strain values of 0 to 0.02) of the compressive stress-strain curves obtained. The crush strength was also calculated, which was defined as the maximum stress at the end of the initial elastic region [5]. The stress-strain curves were plotted using Origin® 8.5 and were shifted so each curve started at the origin. Depending on the maximum load, either a 1 kN or 5 kN load cell was used. All sample ends were sanded to ensure they were tangential and allow maximum contact with the testing plates to ensure repeatability of the results when possible. All tests were conducted at room temperature.

2.2.7 Porosity and Swelling Studies

Dry polymer disks prepared in **Chapters 3-5** were immersed in three different solvents; Milli-Q H_2O, acetone and MeOH. At least four disks for each sample were used for each solvent. Their mass and dimensions (diameter and height) were recorded prior to immersion in these solvents. When Milli-Q H_2O was utilised as the solvent the disks in **Chapter 3** were immersed for 24 h before their mass was again determined by flicking the sample before weighing. The dimensions of the swollen disks were also measured.

For acetone and MeOH (and H_2O for the disks in **Chapters 4** & **5**) a method adapted from Greig and Sherrington [6] was employed where these disks were placed in centrifuge tubes with the respective solvent for 1 h before being centrifuged at ~2600 rpm for 15 min. Their mass was re-measured and the disks were re-immersed in the solvent for 5 min before being centrifuged for a further 15 min at ~2600 rpm, after which their mass was again determined. This process was repeated until a constant mass was achieved and the dimensions of the polymer disks were re-measured. Centrifugation was employed to force the solvent into the pores of the porous polymer.

The polymer disks prepared in **Chapter 6** were immersed in a variety of solvents including; Milli-Q H_2O, MeOH, EtOH, ACN, hexadecane and sunflower oil. At least three disks for each sample were immersed in each solvent for 24 h and their mass and dimensions were recorded both prior and after immersion. At least one of the disks for each sample was immersed in the solvents for only 30 min.

The dry state porosity (ϕ_d) is defined as the total pore volume (V_{pd}) of the dry disk divided by the total volume of the dry polymer disk (V_d) (Equation 1).

$$\phi_d = \frac{V_{pd}}{V_d} \qquad \text{(Equation 1)}$$

When immersed in a solvent that enters the pores, the pore volume (V_{pw}) of the wet disk is equivalent to the change in the mass of the polymer disk (Δm) divided by the density of the solvent (ρ) (Equation 2).

$$V_{pw} = \frac{\Delta m}{\rho} \qquad \text{(Equation 2)}$$

As well as entering the pores, the solvent may also swell the polymer changing the total volume of the polymer disk and this new volume is denoted as V_w. The wet state porosity (ϕ_w) is therefore given by Equation 3.

$$\phi_w = \frac{\Delta m/\rho}{V_w} \qquad \text{(Equation 3)}$$

For the disks prepared in **Chapter 3** the swelling in acetone was negligible so $V_w \cong V_d$, which implies that $V_{pw} \cong V_{pd}$. The porosity measurements for this solvent were therefore a good approximation for the porosity of these dry polymer disks (ϕ_d). For the disks prepared in **Chapters 4** & **5** the swelling in MeOH and acetone was negligible, while for the disks prepared in **Chapter 6** the swelling or shrinkage in all solvents, except ACN, was negligible.

As well as the porosity, the change in volume (ΔV) as a result of any swelling in the different solvents was calculated as a percentage relative to the original disk volume (V_d). The mass of solvent taken up by the pores (m_s) was also calculated and represented as a percentage relative to the original mass of the disk. The densities used for acetone, ACN, EtOH, hexadecane, MeOH, Milli-Q H_2O and sunflower oil at 25 °C were 0.791, 0.786, 0.789, 0.773, 0.792, 1.00 and 0.914 g/mL, respectively.

2.2.8 Additional Characterisation Techniques

The nitrogen and sulfur content for selected poly(HIPE)s was determined with a Thermo Finnigan EA 1112 Series Flash Elemental Analyser, while FTIR spectra were recorded using a Bruker Vertex 70 infrared spectrometer equipped with an ATR probe. Nuclear magnetic resonance (NMR) spectra were recorded in DMSO-d_6 on a Bruker Advance III HD operating at 300 MHz at room temperature. NMR and FTIR spectra were exported and redrawn using Origin® 8.5.

Crystal structures were determined by mounting suitable crystals on a glass fiber with Fomblin oil®, which were then placed on an Xcalibur Gemini diffractometer with a CCD area detector. Crystals were kept at 150 K during the data collection [7] and the structure was solved using Olex2 [8] with the ShelXS [7] structure solution program using Direct Methods and refined with the ShelXL [9] refinement package using least squares minimisation.

2.3 Chromatography

2.3.1 Capillary LC

Chromatographic separations were performed using a Dionex UltiMate™ 3000 RSLCnano system equipped with a NCS-3500RS capillary LC gradient pump including a membrane degasser unit and integrated column compartment, a VWD-3400RS UV detector equipped with a 45 nL flow cell and a WPS-3000TPLC RS autosampler fitted with a 1 µL sample loop. Chromeleon® software (Ver. 6.80) was used for system control and data processing (data collection rate was 2.5 Hz). Chromatograms were converted to ASCII files and redrawn using Origin® 8.5. The LC experiments were conducted under gradient conditions and 1 µL injections were performed with the aid of an autosampler. UV detection was employed at both 214 and 280 nm. For all chromatograms the baseline drift caused by the gradient was subtracted. Comparisons were made to the original chromatograms to ensure that structures observed were not artefacts of the subtraction process.

For the RPLC separations eluent A consisted of 0.1 vol% formic acid in H_2O and eluent B consisted of 0.1 vol% formic acid in ACN and these were degassed prior to use. Samples were dissolved in and diluted with H_2O to the appropriate concentrations. For the HILIC separations eluent A was ACN and eluent B was Milli-Q H_2O and these were also degassed prior to use. Here, samples were dissolved in and diluted with ACN to the appropriate concentrations.

2.3.2 Permeability Measurements

Permeability measurements were performed for columns of various lengths by recording the column back pressure at various flow rates ranging between 0.5 and 9 µL/min in both MeOH and H_2O at 25°C. Before being recorded the pressure was allowed to stabilise for 5 to 10 min. The permeability was then calculated using Darcy's law [10-11] as follows:

Starting with Darcy's law which states,

$$k_{p,f} = \frac{L}{\Delta P}\eta\mu_{SF} \qquad \text{(Equation 4)}$$

where Δ*P* is the pressure drop, L is the length of the column, $k_{p,f}$ is the permeability of the monolithic column, η is the mobile phase viscosity and μ_{sf} is the superficial velocity. The superficial velocity is assumed in this derivation to have the same value as for a generic "empty" tube. This can therefore be rearranged to,

$$\Delta P = \frac{L}{k_{p,f}}\eta\mu_{SF} \qquad \text{(Equation 4a)}$$

The superficial velocity is related to the volumetric flow rate (F_v) by the inverse of the cross-sectional area (A) of the capillary, so the equation becomes,

$$\Delta P = \frac{L\eta}{k_{p,f}A}F_v \qquad \text{(Equation 4b)}$$

In terms of units, if ΔP is expressed in MPa, the column length in m, the viscosity in MPa·s, the volumetric flow rate in m^3/s and the cross-section area in m^2 then the permeability will be in m^2. In order for the volumetric flow rate to be used in units of µL/min the following conversion can be utilised,

$$\mathrm{F}_v\left(\frac{\mu L}{min}\right) = (1.67 \times 10^{-11})\, F_v(\frac{m^3}{s})$$

Equation 4b can therefore be re-written as,

$$\Delta P = \frac{1.67 \times 10^{-11} L\eta}{k_{p,f}A}F_v \quad \text{(Equation 4c)}$$

with the units as above, except the volumetric flow rate is expressed in µL/min. A plot of pressure drop against volumetric flow rate will therefore yield a gradient (m),

$$\mathrm{m} = \frac{1.67 \times 10^{-11} L\eta}{k_{p,f} A}$$

Thus allowing the permeability to be calculated as follows,

$$k_{p,f} = \frac{1.67 \times 10^{-11} L\eta}{mA} \quad \text{(Equation 5)}$$

The pressure values measured actually contain contributions from the back pressure of the system [12], so this was corrected for by subtracting the slope obtained from a plot of back pressure against flow rate, over the same range of flow rates, in the absence of the column from m. The resulting value was then used to calculate the permeability. Viscosities of 0.544 mPa·s and 0.890 mPa·s for MeOH and H_2O at 25°C, respectively, were used in the calculations [11], and this was performed for at least three columns prepared from the same batch.

2.4 General Procedures

2.4.1 Surface modification of fused-silica capillaries

The polyimide-coated capillaries were surface modified based on a procedure by Rohr et al. [13]. Briefly, capillaries were rinsed with acetone and H_2O, activated by pumping a solution of 0.2 M NaOH through the capillaries using a syringe pump at a rate of 30 µL/h for 30 min. The capillaries were then rinsed with H_2O, before 0.2 M HCl was pumped through them at the same rate for 30 min. After which these were rinsed with H_2O and then EtOH at pH 5 (adjusted using acetic acid). A 20 wt% solution of 3-(trimethoxysilyl)propyl methacrylate in EtOH at pH 5 was then pumped through the capillaries at 30 µL/h for 1 h. Finally the capillaries were rinsed with acetone and purged with nitrogen for 2 min before being left at room temperature for 24 h to allow for the completion of the condensation reaction.

2.4.2 Purification of PEGDA

PEGDA was purified according to the procedure by Liu et al. [14] to remove impurities and inhibitor. Briefly, 25 mL of monomer and 15 mL of aqueous saturated sodium carbonate solution were added to a 100 mL separating funnel and shaken vigorously. The funnel was then placed on a ring stand and phase separation was allowed to occur before the lower layer (the carbonate solution) was removed. This washing procedure was repeated twice more, followed by rinsing with 3 × 25 mL of Milli-Q H_2O to remove residual carbonate solution (the organic layer was the lower layer this time). The monomer was then extracted from the remaining aqueous layer (the upper layer) using 3 × 25 mL aliquots of dichloromethane. The extracts were then combined and dried with anhydrous sodium sulfate. This was filtered through Whatman cellulose-based filter paper (Maidstone, Kent, UK) before the dichloromethane was removed under reduced pressure.

2.5 References

[1] Carnachan, R. J.; Bokhari, M.; Przyborski, S. A.; Cameron, N. R. *Soft Matter.* **2006**, *2*, 608-616.
[2] Barbetta, A.; Cameron, N. R. *Macromolecules.* **2004**, *37*, 3188-3201.
[3] Kimmins, S. D.; Wyman, P.; Cameron, N. R. *Reactive and Functional Polymers.* **2012**, *72*, 947-954.
[4] Brunauer, S.; Emmett, P. H.; Teller, E. *J. Am. Chem. Soc.* **1938**, *60*, 309-319.
[5] Menner, A.; Haibach, K.; Powell, R.; Bismarck, A. *Polymer.* **2006**, *47*, 7628-7635.
[6] Greig, J. A.; Sherrington, D. C. *Polymer.* **1978**, *19*, 163-172.
[7] Sheldrick, G. M. *Acta Cryst.* **2008**, *A64*, 112-122.
[8] Dolomanov, O. V.; Bourhis, L. J.; Gildea, R. J.; Howard, J. A. K.; Puschmann, H. *J. Appl. Cryst.* **2009**, *42*, 339-341.
[9] Sheldrick, G. M. *Acta Cryst.* **2015**, *C71*, 3-8.
[10] Nischang, I.; Svec, F.; Fréchet, J. M. *J. Chromatogr. A.* **2009**, *1216*, 2355-2361.
[11] Li, Y.; Tolley, H. D.; Lee, M. L. *J. Chromatogr. A.* **2010**, *1217*, 4934-4945.
[12] Geiser, L.; Eeltink, S.; Svec, F.; Fréchet, J. M. *J. Chromatogr. A.* **2007**, *1140*, 140-146.
[13] Rohr, T.; Hilder, E. F.; Donovan, J. J.; Svec, F.; Fréchet, J. M. J. *Macromolecules.* **2003**, *36*, 1677-1684.
[14] Liu, J.; Sun, X.; Lee, M. L. *Anal. Chem.* **2007**, *79*, 1926-1931.

Chapter 3

Preparation of highly interconnected hydrophilic polymers from emulsion templates with improved mechanical properties

3.1 Introduction

The preparation of poly(HIPE)s for LC has so far been limited to those materials prepared from water-in-oil emulsions, which limits the hydrophilicity of the resulting materials. This therefore reduces the applicability of these poly(HIPE)s for different chromatographic modes, without further modification. Hydrophilic polymer monoliths have been found to be suitable for separations using HILIC [1], which is not possible with a hydrophobic surface. For example, acrylamide (AAm)-based monoliths have been applied as stationary phases for HILIC for the separation of pyrimidines and purines [2], and for peptides [3].

Hydrophilic poly(HIPE)s can be prepared from oil-in-water emulsions, however difficulties associated with stabilising these systems [4] and the removal of the oil phase [5], which can be problematic, has been attributed to the limited nature of these reports. However stable systems have been reported in the literature, for example Hua et al. [6] prepared (paraffin-oil)-in-water HIPEs stabilised by Tween® 85 with and without titanium dioxide nanoparticles, which resulted in open cellular poly(HIPE)s upon curing with AAm and *N,N*'-methylenebisacrylamide (MBAm) in the continuous phase. These hydrophilic porous polymers are not only potentially useful as chromatographic stationary phases but can also find applications as tissue engineering scaffolds [7], for cell culture [8], controlled release devices [9-10] and as absorbents [5, 11].

The high porosity of these poly(HIPE)s is not without its disadvantages, for example poly(HIPE)s generally have poor mechanical properties, for instance when exposed to external mechanical compression, which has limited their use [12-18]. Poor mechanical properties, as a result of high porosity, are known to result in difficulties for

chromatographic applications [19]. While poly(HIPE)s prepared from water-in-oil emulsions have so far exhibited rigid behavior when applied in LC under reasonable pressures [20-21], this could be an issue for their hydrophilic counterparts prepared from oil-in-water emulsions, or if higher operating pressures are required. As such it is desirable to investigate strategies that can improve the mechanical properties of these systems.

Strategies do exist to improve the mechanical properties of poly(HIPE)s, including reinforcement with inorganic particles [14, 22-23] and the utilisation of alternative monomers to influence the physical and mechanical properties of the continuous copolymer phase [12, 18, 24-25]. The simplest approach is to increase the polymer foam density [18, 26-28], which can be achieved by reducing the internal phase volume of the emulsion.

Lissant [29] defines medium internal phase emulsions (MIPEs) as emulsions with internal phases between 30 and 70 vol% and low internal phase emulsions (LIPEs) as having an internal phase less than 30 vol%, with those above 70 vol% being (HIPEs). The polymerisation of such emulsions has been shown to lead to an increase in the mechanical properties [16, 18, 22, 26-27, 30]. For example, Luo et al. [30] prepared poly(Sty-*co*-DVB) based poly(MIPE)s using a miniemulsion template where internal phases of 60, 50 and 40 vol% were employed. Under compression, the resulting materials had elastic moduli of 160 ± 10, 300 ± 10 and 410 ± 10 MPa respectively. Increases in elastic moduli were also previously observed by Williams and Wrobleski [31] for poly(Sty-*co*-DVB) foams when the polymer foam density was increased from 0.025 g/cm^3 to 0.200 g/cm^3, with values of 6 MPa and 186 MPa, respectively.

This clearly demonstrates the benefit reducing the internal phase volume has on the mechanical properties. The drawback is the detrimental effect this can have on the open cellular nature of these materials, with a decrease in the interconnectivity commonly observed [14, 26, 30]. In some cases this even results in predominately closed cellular structures [30]. However, Luo et al. [30] also demonstrated that the interconnectivity could be improved using increased emulsification energies, specifically sonication, in the preparation of the emulsion templates. Even though the total dispersed volume stays the

same the total area increases as well as the total number of emulsion droplets, when sonication was utilised, which increased the likelihood for window formation and hence promoted improved interconnectivity.

Published work to date involving a reduction in internal phase has so far been limited to hydrophobic-based systems prepared from water-in-oil emulsions. It is therefore desirable to explore the possibility to obtain highly interconnected hydrophilic polymers with improved mechanical properties from oil-in-water emulsions using this approach. In this chapter, the possibility of preparing hydrophilic porous polymers from (paraffin-oil)-in-water emulsions with improved mechanical properties was investigated by reducing the internal phase volume. The emulsification energy was varied to establish the influence this had over the materials open cellular network. The impact of the internal phase volume and surfactant level on the materials morphology was also investigated. Additionally, the behaviour of these materials in different solvent environments was explored, as well as their preparation in capillary format with the intention to apply these materials for capillary LC.

3.2 Experimental

3.2.1 Preparation of hydrophilic porous polymers

The preparation of hydrophilic porous polymers was based on a modified procedure from Hua et al. [6]. The monomer AAm (82 wt% w.r.t. total monomers), the cross-linker MBAm (18 wt% w.r.t. total monomers) and the surfactant Tween® 85 were dissolved with stirring in Milli-Q H_2O. Once dissolved the initiator Ammonium persulfate (APS) (2.31 wt% w.r.t. total monomers) was also added. The internal paraffin-oil phase was added dropwise at a rate of approximately one drop per second with gentle stirring on a magnetic stirrer. Emulsions were then obtained by emulsification either with the Ultra Turrax T 25 homogeniser (IKA, Janke u. Kunkel- Straße, Staufen im Breisgau, Germany) equipped with an S 25 N 10 G dispersing element (7.5-mm rotor) or with a Branson digital sonifier® model 450 equipped with a disruptor horn with a 0.5 inch tip diameter (Branson

Ultrasonics Corporation, Danbury, Connecticut, USA). When the digital sonifier® was used the beaker was immersed in an ice bath to avoid significant increases in temperature during the sonication process, which would increase the rate of polymerisation.

Once the emulsions were obtained the majority was transferred to a 25 mL glass vial, while some was transferred to a 4 mL glass vial. These vials were sealed and the 25 mL sample vial was placed in a water bath at 50 °C and polymerised for 24 h, while the 4 mL sample vial was left at room temperature to evaluate the emulsion's stability over time. This sample is referred to as the stability sample. The polymerised sample from the water bath was removed from the vial, cut into smaller pieces and washed with acetone using a Soxhlet apparatus for 48 h to remove the internal paraffin-oil phase as well as any additional impurities. The porous polymers were then left to dry at 25 °C in a vacuum oven for one week.

The total monomer concentration in the continuous water phase was fixed at 43 wt% (w.r.t. continuous phase), while the total volume of both the internal phase and continuous phase was fixed at 20 mL for all experiments. The differences in the samples lies in the internal phase volumes used, surfactant level and the emulsification energy (see **Tables 3.1** & **3.5** for a detailed composition of the emulsion templates utilised in this work).

Polymer disks for compression tests were obtained by first preparing the emulsion as described above, however 10 mL disposable syringes (~1.5 cm in diameter) were filled with this mixture. These syringes were sealed and placed in the water bath at 50 °C at an angle of ~45° from the horizontal (to ensure any air bubbles migrated to the top of the syringe) and polymerised for 24 h. Once cured, the polymer was removed from the syringe and cut into 2 cm thick pieces. These were first washed in vials of MeOH at room temperature with an orbital shaker for 24 h, then with MeOH using a Soxhlet apparatus for 24 h and finally with acetone with the Soxhlet apparatus for 24 h. This modified washing procedure was implemented to limit the cracking that occurred with the samples upon shrinkage when exposed to acetone. These samples were then dried in a vacuum oven at 25 °C.

Polymer disks for porosity determination and swelling studies were also prepared using 10 mL disposable syringes with the exception that the disks were cut into ~0.5 cm thick pieces.

For the preparation in capillary format, the emulsions were passed through 20 cm of 150 µm i.d. surface-modified fused silica capillaries. These were filled multiple times to limit the number of air bubbles or voids present and the ends were sealed with rubber, before being placed horizontally in the water bath. Vertical placement was avoided as this has been observed to result in column heterogeneity due to the influence of gravity for conventional polymer monoliths [32].

3.2.2 Characterisation of Emulsions

Optical microscopy images were obtained immediately after preparation and 24 h later using the stability samples. Unfortunately, the resolution of the optical microscope was insufficient to observe the droplet size distributions of the sonicated emulsions. Dynamic light scattering was attempted for these samples with diluted emulsion to estimate the droplet size, however significant creaming resulted in unreliable results. Digital photographs were also obtained of the stability samples immediately after preparation and 24 h later.

3.3 Results and Discussion

3.3.1 Porous polymer preparation and morphology tuning

A series of porous hydrophilic polymers were prepared using an internal phase of 60 vol%. In order to investigate the structural pore morphology obtained from the emulsion droplet templating strategy, different emulsification energies were employed in their preparation. These are samples 2-7 (**Table 3.1**) and all possessed porosities consistent with the internal phase volume used (**Table 3.2**). The emulsions were stable over a 24 h period (**Table 3.2**, **Figures A1** & **A2** in **Appendix A**).

Table 3.1 Composition of emulsion templates for samples 1-14

	Oil Phase / mL		Aqueous Phase / g					
No.	Paraffin-oil	IP [a]	AAm	MBAm	Tween® 85	H_2O	APS	Emulsification
1	16	80%	1.42	0.309	0.2 [5 wt%] [b]	4	0.04	[14 000 rpm, 2 min^{H}]
2	12	60%	2.84	0.618	0.4 [5 wt%] [b]	8	0.08	[10 000 rpm, 2 min^{H}]
3	12	60%	2.84	0.618	0.4 [5 wt%] [b]	8	0.08	[14 000 rpm, 2 min^{H}]
4	12	60%	2.84	0.618	0.4 [5 wt%] [b]	8	0.08	[18 000 rpm, 2 min^{H}]
5	12	60%	2.84	0.618	0.4 [5 wt%] [b]	8	0.08	[30% amp, 5 min^{U}]
6	12	60%	2.84	0.618	0.4 [5 wt%] [b]	8	0.08	[30% amp, 10 min^{U}]
7	12	60%	2.84	0.618	0.4 [5 wt%] [b]	8	0.08	[50% amp, 5 min^{U}]
8	12	60%	2.84	0.618	0.8 [10 wt%] [b]	8	0.08	[30% amp, 5 min^{U}]
9	12	60%	2.84	0.618	1.2 [15 wt%] [b]	8	0.08	[30% amp, 5 min^{U}]
10	12	60%	2.84	0.618	1.6 [20 wt%] [b]	8	0.08	[30% amp, 5 min^{U}]
11	10	50%	3.55	0.7725	0.5 [5 wt%] [b]	10	0.1	[30% amp, 5 min^{U}]
12	8	40%	4.26	0.927	0.6 [5 wt%] [b]	12	0.12	[30% amp, 5 min^{U}]
13	4	20%	5.68	1.236	0.8 [5 wt%] [b]	16	0.16	[30% amp, 5 min^{U}]
14	4	20%	5.68	1.236	3.2 [20 wt%] [b]	16	0.16	[30% amp, 5 min^{U}]

[a] The percentage of internal phase (IP) utilised with respect to the total volume of oil and water. [b] Percentage of Tween® 85 solution with respect to the continuous water phase. [H] Emulsification with the homogeniser, the homogenisation time is provided. [U] Emulsification with the digital sonifier®, the amplitude (amp) and sonication time is provided.

Table 3.2 Morphological features of the porous polymers for samples 1-7

Sample	V / μm [a]	D1 / μm [b]	D2 / μm [c]	W / μm [d]	BET / m^2g^{-1} [e]	φ_d / % [f]	Preparation
1	5 ± 2	6 ± 3	6 ± 2	1.0 ± 0.5	2.2 ± 0.3	69 ± 2	[80% IP, 14 000 rpm, 2 min^{H}, 5 wt%]
2	15 ± 5	13 ± 6	13 ± 7	2 ± 1	1.2 ± 0.1	58 ± 3	[60% IP, 10 000 rpm, 2 min^{H}, 5 wt%]
3	8 ± 3	7 ± 3	9 ± 4	1.0 ± 0.7	1.0 ± 0.2	53 ± 9	[60% IP, 14 000 rpm, 2 min^{H}, 5 wt%]
4	6 ± 2	6 ± 3	6 ± 3	0.8 ± 0.5	1.3 ± 0.2	53 ± 3	[60% IP, 18 000 rpm, 2 min^{H}, 5 wt%]
5	0.7 ± 0.4	-	-	0.2 ± 0.1	7.5 ± 0.4	63 ± 3	[60% IP, 30% amp, 5 min^{U}, 5 wt%]
6	0.5 ± 0.3	-	-	0.1 ± 0.1	8.5 ± 0.1	59 ± 4	[60% IP, 30% amp, 10 min^{U}, 5 wt%]
7	0.5 ± 0.2	-	-	0.11 ± 0.08	8.3 ± 0.4	55 ± 5	[60% IP, 50% amp, 5 min^{U}, 5 wt%]

[a] Average void diameter as determined from SEM. [b] Average droplet diameter immediately after preparation as determined from optical microscopy. [c] Average droplet diameter 24 h after preparation as determined from optical microscopy. [d] Average window diameter as determined from SEM. [e] Average specific surface area as determined from the Brunauer-Emmett-Teller (BET) method. [f] Average dry state porosity as determined by immersion in acetone. [H] Emulsification with the homogeniser, the homogenisation time is provided. [U] Emulsification with the digital sonifier®, the amplitude (amp) and sonication time is provided.

Fabrication of porous monoliths with lower dispersed volume fractions is typically associated with a reduction in the interconnectivity of the material, which has an impact on their open cellular nature. Open cellular poly(HIPE) and poly(MIPE) materials possess interconnectivity due to the presence of interconnecting pores or windows in their structure [33], the formation of which is suggested to occur due to volume contraction of the thin film between adjacent droplets at the gel point [34], or from the removal of a surfactant rich phase from these thin films during the washing and drying process [15]. Regardless of the mechanism, the distance between the internal phase droplets is extremely important for the formation of windows, with increases in droplet contact reported to promote greater window formation [30]. This occurs because the continuous

phase film becomes thinner at the point of contact as the distance between adjacent droplets decreases. This can be achieved by increasing the emulsification energy, which results in a larger number of smaller droplets, and hence increased droplet contact.

For samples 2-5 (**Figure 3.1** and **Table 3.2**) increases in the emulsification energy corresponded to a decrease in the average droplet and subsequent void size. For example, when the emulsion was prepared with the homogeniser at 10 000 rpm for 2 min (sample 2) the average void size obtained was 15 ± 5 µm, however this was reduced to 6 ± 2 µm when the emulsion was prepared with the homogeniser at 18 000 rpm for 2 min (sample 4). This was further reduced to 0.7 ± 0.4 µm when the digital sonifier® was utilised at 30% amplitude for 5 min (sample 5). Interestingly, the average window sizes were comparable, around 1 µm, for samples 2-4 and were only significantly reduced for sample 5, which had an average window size of 0.2 ± 0.1 µm. The surface areas obtained were consistent with the observed void and window sizes with samples 2-4 possessing similar surface areas of ~ 1 m^2/g, while sample 5, which possessed considerably smaller voids and windows, possessed a significantly larger surface area of 7.5 ± 0.4 m^2/g.

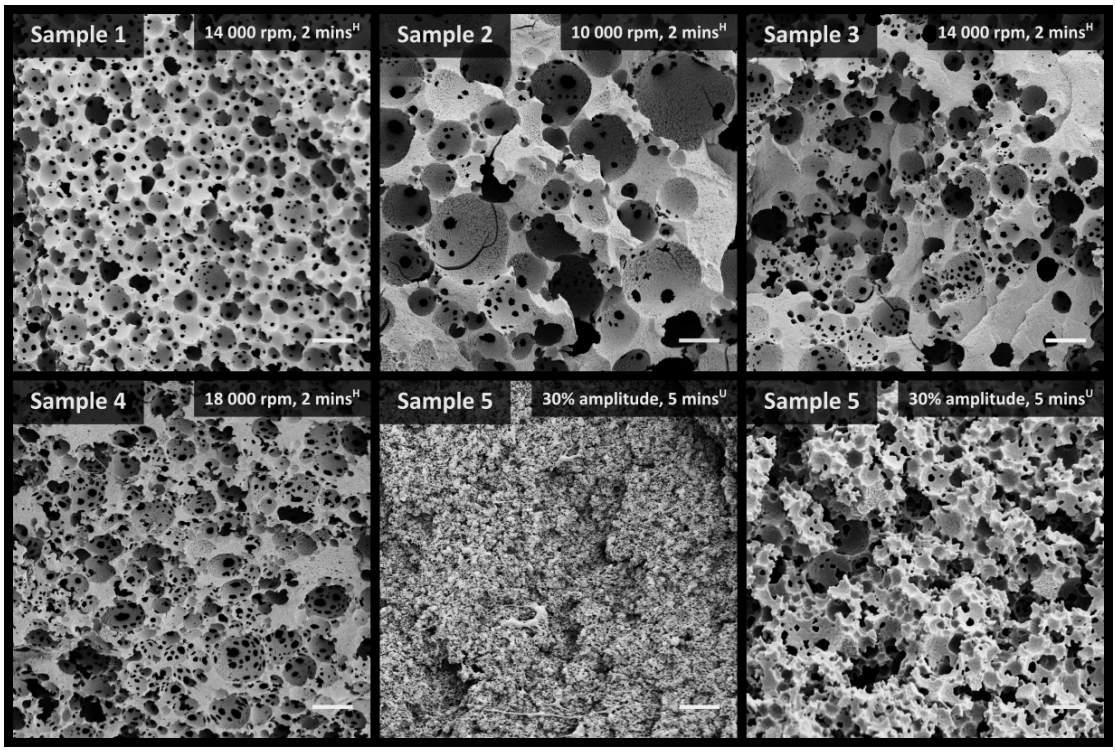

Figure 3.1. SEM images of samples 1-5, prepared with different emulsification energies. Sample 1 was prepared from an 80 vol% internal phase, while this was 60 vol% for samples 2-5. Scale bar is 10 µm for all but the second image for sample 5, which is 1 µm.

Table 3.3 Interconnectivity of the porous polymers for samples 1-7

Sample	N_w [a]	[W/V] [b]	$[W_A/V_{SA}]$ [c]	$N_w \times [W_A/V_{SA}]$ [d]	Preparation
1	4	0.19	0.0090	0.036	[80% IP, 14 000 rpm, 2 min^H, 5 wt%]
2	4	0.13	0.0042	0.017	[60% IP, 10 000 rpm, 2 min^H, 5 wt%]
3	4	0.13	0.0039	0.016	[60% IP, 14 000 rpm, 2 min^H, 5 wt%]
4	5	0.12	0.0035	0.018	[60% IP, 18 000 rpm, 2 min^H, 5 wt%]
5	2	0.25	0.016	0.032	[60% IP, 30% amp, 5 min^U, 5 wt%]
6	2	0.28	0.020	0.040	[60% IP, 30% amp, 10 min^U, 5 wt%]
7	2	0.25	0.015	0.030	[60% IP, 50% amp, 5 min^U, 5 wt%]

[a] Average number of windows per void as determined from SEM. [b] Average degree of interconnectivity calculated by dividing the average window diameter by the average void diameter. [c] Average degree of interconnectivity calculated by dividing the average area of the windows by the average surface area of the voids (both calculated using the average window and void diameters, respectively, as determined from SEM). [d] The product of the average number of windows per void by the average degree of interconnectivity (relative to the surface area of the voids). Otherwise known as the openness [4]. [H] Emulsification with the homogeniser, the homogenisation time is provided. [U] Emulsification with the digital sonifier®, the amplitude (amp) and sonication time is provided.

For the homogenised samples (samples 2-4) the observed decrease in void size appeared to result in an increase in the average number of windows present per void, from 4 for samples 2 & 3 to 5 for sample 4 (**Table 3.3**), consistent with the increase in interconnectivity previously reported when increased emulsification energy was employed [30]. It is important to note that the number of windows determined from the SEM images is an underestimation of the true value, as not all the windows which were present will be visible given the cross sectioning of the sample during preparation for analysis. However, given all the samples were prepared in this way, comparisons made between samples are expected to be more reliable, even though the values being compared are not a true reflection of the actual number of windows present in each case.

The average number of windows present per void, while providing an insight into the interconnectivity of the material, is not the only important factor in determining the open cellular nature of these materials, as the relative size of the windows compared to the voids is also important. The average degree of interconnectivity provides an insight into their relative size, allowing for comparisons between samples, and is defined as the average window diameter divided by the average void diameter [35-36]. However, this does not provide an estimate of the proportion of the voids surface that is open for two reasons. Firstly, a window can be approximated to be a small circle sitting on the surface of a much larger sphere, and simply taking the ratio of diameters ignores the higher dimensionality of the spherical voids. As such, taking the ratio of the average area of the

windows against the average surface area of the voids provides a more accurate estimate of the proportion of the voids surface that a single window occupies.

Secondly, this does not take into account the actual number of windows that are present. It is proposed that the product of the average number of windows per void with the average degree of interconnectivity (relative to the surface area of the voids) would provide a more representative interpretation of the relative open cellular nature of these materials (Table 3), and this has previously been termed the openness [4]. If the number of windows could be measured more accurately this would provide an estimate of the actual percentage of the voids surface that was open, however, as discussed above comparisons made between samples are still expected to be reliable.

The average degree of interconnectivity was similar for samples 2-4 (**Table 3.3**) and multiplying this by the average number of windows also resulted in similar values, however sample 4 possessed the highest value of 1.8×10^{-2} (compared to 1.7×10^{-2} and 1.6×10^{-2} for samples 2 and 3 respectively), which was consistent with the increase in the number of windows observed for this sample. However, the small difference between these values makes interpreting their significance difficult, but this does suggest that increasing the emulsification energy with the homogeniser is only having a small effect on the open cellular nature of these materials. For the sonicated sample (sample 5) the decrease in the void size did not correspond to an increase in the average number of windows per void as expected, as this actually decreased from 5 windows per void to 2. This could be as a result of the increased Laplace pressure associated with smaller droplets [37-38] making droplet deformation more difficult.

An increase in Laplace pressure would also be expected as a result of the increase in the total surface area of the droplets, which requires more surfactant to stabilise the interfacial area and thus the interfacial tension would be higher. It should be noted that in a HIPE the droplets are not perfectly spherical due to the high packing density [39] and this deviation allows the internal phase to exceed that of 74 vol%, resulting in greater contact between the droplets. The deformation of the droplets therefore aids in the formation of windows [40] and it is expected that the ability for these droplets to deform

will be another factor that influences window formation. In this case, the increase in Laplace pressure may have resulted in a reduction in the ability for these droplets to deform and thus reduced window formation.

Interestingly, the average degree of interconnectivity appeared larger suggesting that once a window formed it occupied a greater percentage of the voids surface, this has also been observed for other systems when the void size was decreased [41-42]. Decreases in the droplet size typically correspond to the presence of thinner films between adjacent droplets at their point of contact [28, 30], as such it is possible in this case that a larger proportion of the film between droplets has contracted (or been removed) resulting in larger windows relative to the size of the voids. This could also explain why a lower number of windows were observed, as these were actually larger in relative size. The product of the average number of windows by the average degree of interconnectivity for this sample resulted in a value of 3.2×10^{-2}, higher than that achieved when using the homogeniser, which suggests that, overall, this material possessed voids that were more open in nature.

It should be noted that the openness values calculated are low, and do not appear to correlate to how open the voids appear from examining the SEM images, (**Figure 3.1**) and there are two main reasons for this. Firstly, the surface of the void (since it is curved and not two-dimensional as it appears in the SEM image) is significantly larger than the area of the windows (which is approximated as two-dimensional). Therefore the area that a window occupies is expected to be significantly less than that of the voids surface. This higher dimensionality of the voids surface, while appearing two-dimensional, is the reason why direct interpretation of the SEM images, in regards to openness, can be misleading. Secondly, the exact number of windows is not known due to the sectioning of the samples, hence the values calculated are an underestimation of the true openness of the material. However, as discussed above, since each sample was prepared in the same way comparisons of these values are expected to be representative.

A conventional poly(HIPE) material was also prepared from an 80 vol% internal phase and was denoted as sample 1 (**Table 3.1**). This appeared to possess a slightly smaller average

void diameter (**Table 3.2**) to that of sample 3 (prepared at the same emulsification energy but with a 60 vol% internal phase) although their window sizes were the same on average. In accordance, sample 1 possessed a higher degree of interconnectivity (**Table 3.3**). The average number of windows per void was the same for both samples, and the product of this with the average degree of interconnectivity therefore resulted in a higher value of 3.6×10^{-2} for sample 1 compared to 1.6×10^{-2} for sample 3. This suggests that sample 1 possessed voids that were more open and is consistent with previous reports where a reduction in the internal phase volume has been detrimental to the open cellular nature of emulsion templated materials [14, 26, 30].

Interestingly, this value was not too different from the value obtained of 3.2×10^{-2} when sonication was utilised with the lower internal phase volume (sample 5). In addition, the average specific surface area was higher for sample 1 with a value of 2.2 ± 0.3 m^2/g compared to 1.0 ± 0.2 m^2/g for sample 3. This was presumably due to the presence of larger regions of bulk polymer observed for sample 3 (**Figure 3.1**), or inaccuracies in the surface area measurements. This has also previously been reported for other poly(MIPE)s prepared with this internal phase volume [16, 18, 22] and is a result of the reduced packing density. Even though it appears that the reduction in internal phase volume has compromised the open cellular nature of these materials to a degree, it is clear that by increasing the emulsification energy, in particular when sonication was employed, this

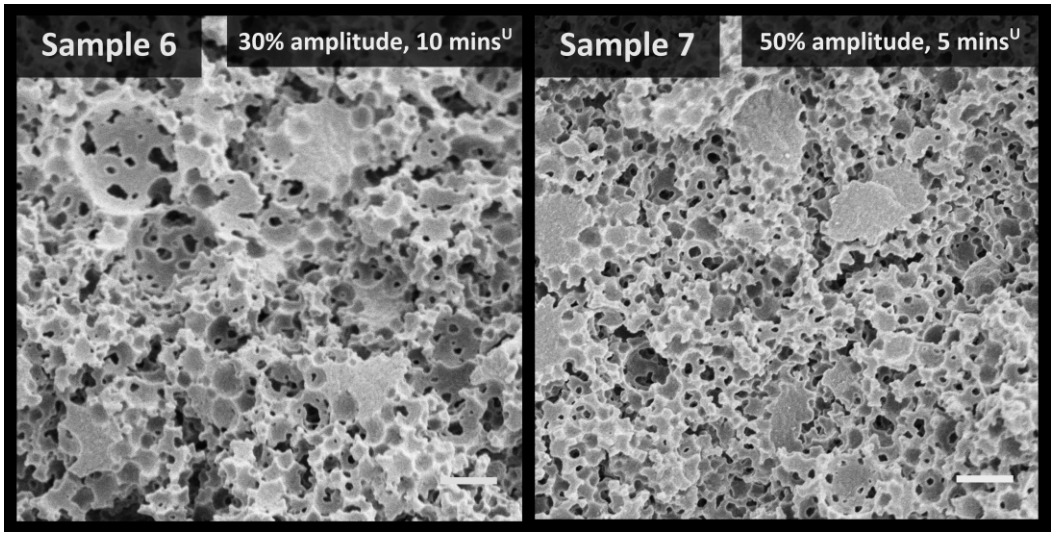

Figure 3.2. SEM images of samples 6 & 7, prepared from 60 vol% internal phase emulsions with different emulsification energies. Scale bar is 1 μm.

Table 3.4 Morphological features of the porous polymers for Samples 5 & 8-14

Sample	V / μm [a]	P / μm [b]	BET / m^2g^{-1} [c]	φ_d / % [d]	Preparation
5	0.7 ± 0.4	0.26 ± 0.01	7.5 ± 0.4	63 ± 3	[60% IP, 30% amp, 5 min[U], 5 wt%]
8	0.5 ± 0.3	0.45 ± 0.01	4.5 ± 0.3	62 ± 3	[60% IP, 30% amp, 5 min[U], 10 wt%]
9	-	0.61 ± 0.02	3.2 ± 0.7	59 ± 1	[60% IP, 30% amp, 5 min[U], 15 wt%]
10	-	0.72 ± 0.01	6.4 ± 0.1	62 ± 2	[60% IP, 30% amp, 5 min[U], 20 wt%]
11	0.4 ± 0.2	0.295 ± 0.001	6.1 ± 0.3	48 ± 5	[50% IP, 30% amp, 5 min[U], 5 wt%]
12	0.7 ± 0.3	0.437 ± 0.004	3.0 ± 0.1	36 ± 3	[40% IP, 30% amp, 5 min[U], 5 wt%]
13	1 ± 1	0.68 ± 0.01	0.20 ± 0.01	-	[20% IP, 30% amp, 5 min[U], 5 wt%]
14	-	0.62 ± 0.06	3.9 ± 0.4	39 ± 1	[20% IP, 30% amp, 5 min[U], 20 wt%]

[a] Average void diameter as determined from SEM. [b] Average median pore diameter (volume) as determined from Mercury Intrusion Porosimetry (MIP). [c] Average specific surface area as determined from the BET method. [d] Average dry state porosity as determined by immersion in acetone. [U] Emulsification with the digital sonifier®, the amplitude (amp) and sonication time is provided.

effect can be reduced resulting in the obtainment of highly interconnected hydrophilic structures from emulsion templates with internal phases below 74 vol%.

Sonication for the preparation of these materials was investigated further as, in addition to providing an open cellular nature similar to that observed with the higher internal phase volume (albeit with a lower number of windows), it also resulted in surface areas that appeared larger than that of the homogenised samples. Materials with larger surface areas are important for several applications including catalysis [43], chromatography [44], sample preparation and extraction [45]. Increasing the duration of sonication (sample 6) or the sonication amplitude (sample 7) did not appear to result in significant alterations in the morphology for these materials (**Tables 3.2** & **3.3** and **Figure 3.2**), however increases in the surfactant level with fixed emulsification energy (digital sonifier at 30% amplitude for 5 min) did appear to have a significant effect (**Figure 3.3**). The samples prepared with

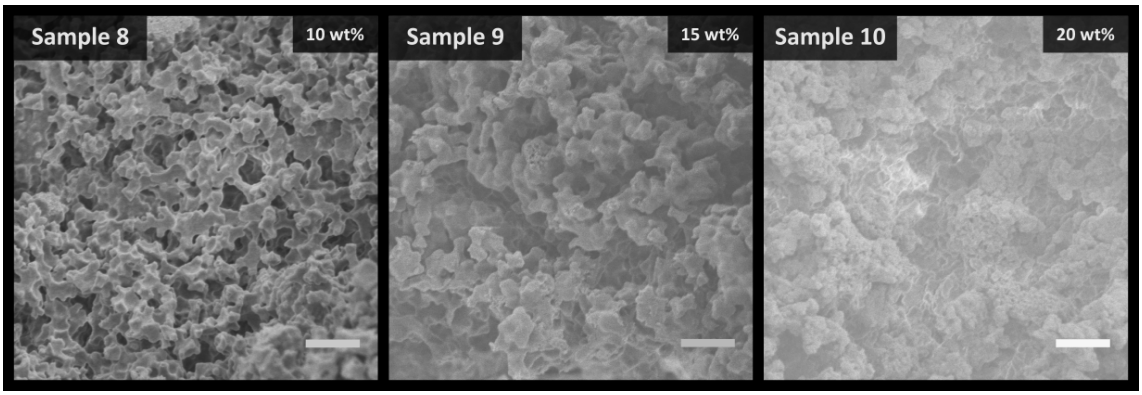

Figure 3.3. SEM images of samples 8-10, prepared from a 60 vol% internal phase but with different surfactant levels. Scale bar is 1 μm.

10, 15 and 20 wt% Tween® 85 were denoted as samples 8-10 (**Table 3.1**) respectively and their morphological features are shown in **Table 3.4**.

An increase from 5 to 10 wt% Tween® 85 appeared to result in the loss of the void/window structure, however open pores that appeared to be cellular in nature were still observed, consistent with a material prepared from a templated approach. Hence their size could be estimated by SEM and these voids possessed an average diameter of 0.5 ± 0.3 µm. This appeared lower than the average void diameter of 0.7 ± 0.4 µm observed when 5 wt% Tween® 85 was utilised, though not statistically different. Given the cross-section of these open pores did not appear to be perfectly circular MIP was also employed (the pore size distributions for these samples can be found in **Figure A4** in **Appendix A**) and provided a similar estimate of 0.45 ± 0.01 µm.

It is important to note that in the case of traditional poly(HIPE) morphologies possessing voids and windows the value obtained by MIP is an estimate of the window size only [46]. This is because the windows fill with mercury before the voids, and hence the intrusion volume of the voids is assigned to the windows. In accordance, the value determined from MIP for sample 5 (5 wt% Tween® 85) of 0.26 ± 0.01 µm was consistent with its window size of 0.2 ± 0.1 µm determined from SEM. In contrast, sample 8 (10 wt% Tween® 85) did not possess the void and window structure and hence the value obtained by MIP is an estimate of the open pores observed in its structure (**Figure 3.3**). This was also consistent with the estimate obtained by SEM. Increasing the surfactant concentration beyond 10 wt% to 15 and 20 wt% resulted in materials that better resembled the random globular structures typical for conventional AAm monoliths [47-48] prepared by phase separation from a solvent mixture, as the cellular nature appeared to have been lost. Despite the obvious alteration in structure, no macroscopic changes in the emulsions were evident for these samples (**Figure A1** in **Appendix A)**.

Typically, an increase in the surfactant level simply results in a reduction in the droplet size and an associated decrease in the void size for emulsion templated materials [15, 49]. Decreases in the droplet size have already been shown in this work to result in an increase in the degree of interconnectivity (relative window to void size) when the emulsification

energy was increased with sonication, presumably due to the presence of thinner continuous phase films as a result of increased droplet contact. Any further reduction in the droplet size would therefore be expected to result in windows of larger relative size and a situation could potentially arise when these voids appear to become predominately open in nature. This is consistent with the void size of sample 8 appearing to be lower than the void size of sample 5. However, the increase in the degree of interconnectivity observed was only significant over a very large variation in the droplet size (**Tables 3.2** & **3.3**) and the reduction in size (if any) when the surfactant level was increased from 5 wt% to 10 wt% was not statistically significant.

Williams and Wrobleski [31] have observed similar effects for poly(Sty-co-DVB) based foams when the surfactant level was increased. They suggested that the increase in surfactant level simply resulted in increased thinning of the continuous phase film between adjacent droplets, therefore enhancing droplet contact and resulting in larger relative window sizes. It was also observed in their work that this did eventually reach a point where the film disappears completely resulting in the loss of the void structure. Increases in the degree of interconnectivity with increased surfactant levels have also been observed for other systems [40], and this is the more likely explanation for sample 8 (10 wt% Tween 85) appearing to possess voids that have become predominately open in nature. Williams and Wrobleski [31] also reported that increasing the surfactant level beyond this point results in materials that no longer reflect that of the emulsions they are prepared from as they are unable to maintain their structure when dried. This appears to occur for these materials at surfactant concentrations of 15 and 20 wt%.

The pores present for these samples were difficult to estimate by SEM, however MIP indicated that the increase in surfactant beyond 10 wt% resulted in an increase in the average pore diameter (**Table 3.4**). For example, increasing the surfactant level from 10 to 15 wt% resulted in an increase in the average pore diameter from 0.45 ± 0.01 µm to 0.61 ± 0.02 µm, and then to 0.72 ± 0.01 µm when 20 wt% Tween 85 was utilised. Since these structures resembled that of conventional AAm monoliths, the values obtained by MIP are a measure of the pores located between the globular structures. If these pores were

originally the voids, this would suggest that they increased in size when the surfactant was increased above 10 wt%.

Williams and Wrobleski [31] also noted that when the surfactant level was increased above that required to saturate the droplet interface excess surfactant is relegated to the continuous phase where it can modify the physiochemistry of that phase. Here, the excess surfactant could be self-assembling into cylindrical type structures enhancing the viscosity of this phase, making the generation of smaller droplets more difficult upon shear. As such, larger droplets would be obtained at the same energy input, however, given the surfactant is present in significant excess full contraction (or removal) of the thin film would still be expected resulting in the obtainment of predominately open voids even though they are larger in size. Alternatively, the difference in pore size could simply have been an artefact associated with the shift in structure from a cellular material to a random globular structure upon drying [31].

The decrease in average specific surface area from 4.5 ± 0.3 to 3.2 ± 0.7 m^2/g (**Table 3.4**) when the surfactant level was increased from 10 to 15 wt% was also consistent with materials possessing a larger pore size. However, when the surfactant level was increased to 20 wt% this material actually possessed a larger surface area of 6.4 ± 0.1 m^2/g, even though it possessed the largest pore size (**Table 3.4**). This could be associated with some additional templating of the structure due to the presence of a non-conventional continuous phase, or again simply an artefact associated with the compromised structure. The porosities of these samples were also as expected. Regardless of the mechanism responsible for these different morphologies, it is clear that increasing the level of surfactant in addition to increases in the emulsification energy is also having a profound influence on the materials morphology.

In order to investigate the possibility of preparing open cellular structures from internal phases less than 60 vol%, both the surfactant level (5 wt% relative to the continuous phase) and the emulsification energy (digital sonifier at 30% amplitude for 5 min) were fixed and internal phases of 50, 40 and 20 vol% were investigated. These were denoted as samples 11-13 (**Table 3.1**) respectively and their resulting morphologies are shown in

Figure 3.4. It was apparent that open cellular materials could be obtained with internal phases as low as 40 vol%, however these materials were also without the void/window structure. The porosities for these samples were as expected (**Table 3.4**), which is consistent with these materials being open cellular in nature, given the porosity was determined by filling the pores with liquid. The shift in morphology can potentially be explained by considering that a reduction in the internal phase volume with fixed surfactant level relative to the continuous phase, results in an increase in the surfactant-to-oil ratio, which has already been demonstrated to result in the obtainment of this open cellular structure (**Figure 3.3**). Again no macroscopic change in the emulsions was observed for these samples (**Figure A1** in **Appendix A**).

A reduction in the internal phase volume might also be expected to result in the obtainment of smaller emulsion droplets from the increase in surfactant-to-oil ratio and/or a lower viscosity due to the reduced oil content [42], however estimates of the void size for the material prepared with 50 vol% internal phase of 0.4 ± 0.2 µm by SEM

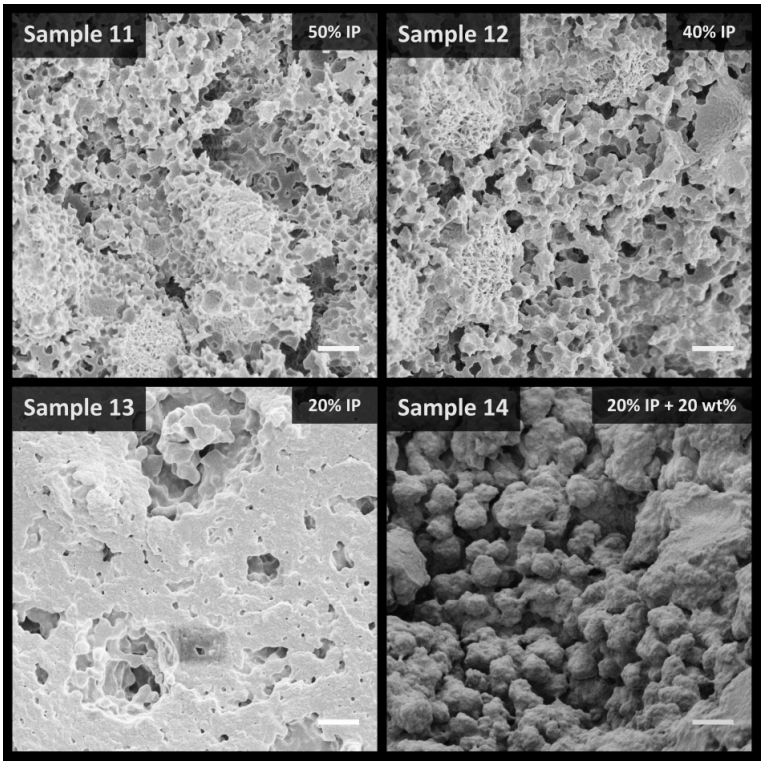

Figure 3.4. SEM images of samples 11-14, prepared with different internal phase volumes. Samples were prepared with 5 wt% Tween® 85, except sample 14, which was prepared with 20 wt% Tween® 85. Scale bar is 1 µm.

and 0.295 ± 0.001 µm by MIP (**Table 3.4**) revealed there was only a slight reduction in the droplet and void size when compared to the material prepared with 60 vol% internal phase. MIP was again providing an estimate of these open pores, given the loss of the void and window structure. This is in agreement with the expectation that excess surfactant is predominately contributing to the increased thinning of the continuous phase film, instead of a significant reduction in the droplet size. Interestingly, closer inspection of this material revealed the presence of what appeared to be the occasional void that possessed a small number of windows (**Figure 3.4**), suggesting it was actually an intermediate between the two contrasting morphologies. Reducing the internal phase further to 40 vol% resulted in an increase in the average pore diameter to 0.7 ± 0.3 µm by SEM and 0.437 ± 0.004 µm by MIP. As described previously, the presence of excess surfactant, as a result of a further increase in surfactant-to-oil ratio, can result in an increase in the continuous phase viscosity and thus larger voids that are open in nature can be formed. Alternatively, the presence of larger droplets could have been due to coalescence as a result of the lower droplet packing density. The decrease in average specific surface area from 6.1 ± 0.3 m^2/g for the 50 vol% internal phase to 3.0 ± 0.1 m^2/g for the 40 vol% internal phase was also consistent with the presence of larger pores.

An increase in the void size was also observed when the internal phase was reduced to 20 vol% with an average size of 0.68 ± 0.01 µm by MIP, however these voids were fewer in number with significant regions of bulk polymer resulting in the material appearing to be predominately non-porous. This is consistent with its significantly lower average specific surface area of 0.20 ± 0.01 m^2/g. Interestingly, increasing the surfactant level to 20 wt% while maintaining the 20 vol% internal phase (sample 14) resulted in a material that appeared to be more porous in nature with a similar average pore size of 0.62 ± 0.06 µm by MIP, however these pores were not cellular in nature. A significantly higher surface area of 3.9 ± 0.4 m^2/g was obtained for this sample, consistent with its increased porous nature. As described above, the increase in surfactant level could simply have compromised the integrity of this material upon drying, which resulted in the shift in morphology observed. The increase in its porous nature was also consistent with its increased porosity of 39 ± 1 %, much higher than the internal phase utilised of 20 vol%.

Another explanation for the presence of additional porosity is the presence of a non-conventional continuous phase, as a result of the low oil content and relatively high surfactant level, further templating the structure. This is also consistent with the suggestion that the removal of surfactant, during purification, can result in the obtainment of materials with higher porosity [42]. Finally, this could have been as a result of creaming, however this was not visually evident over a 24 h period (**Figure A1** in **Appendix A**).

These results demonstrate that the emulsification energy and the surfactant-to-oil ratio appear to have a significant influence over the morphology of the resulting materials. Given that both can significantly influence the thickness of the continuous phase film between adjacent droplets, these parameters are expected to act in conjunction to influence the resulting morphology. This was therefore investigated using an experimental design approach [50].

3.3.2 Screening the parameters which influence morphology through experimental design

For clarity in this section the following nomenclature is used: Sample number (Internal phase volume, emulsification conditions, duration of emulsification, surfactant level). Polymers prepared with the Ultra Turrax T 25 homogeniser have a superscript H, while polymers prepared using the digital sonifier® have a superscript U.

It is clear from this work that several parameters are influencing the morphology of these materials, including the emulsification energy and the surfactant-to-oil ratio. From the proposed mechanism it is expected that these parameters will act in conjunction, and not independently, to influence the resulting morphology of these materials, in particular when it comes to a shift in morphology from the traditional void and window structure to one with predominantly open voids. Increases in the emulsification energy have already been shown in this work to result in an increase in the degree of interconnectivity (**Figure 3.1** and **Table 3.3**), through the generation of smaller droplets and therefore thinner continuous phase films between them at the point of contact.

However, it is known that a reduction in the droplet size can also be achieved through the utilisation of increased surfactant concentrations [15, 49]. Increases in the surfactant-to-oil ratio were also shown to have a significant influence over the degree of interconnectivity at fixed emulsification energy when the variation in droplet size was minimal (**Figures 3.3** & **3.4** and **Table 3.4**), due to increased thinning of the continuous phase films. In addition, reductions in the internal phase volume have also been extensively reported in the literature to result in a reduction in the open cellular nature of these materials due to the reduced contact between droplets [14, 26, 30].

It is expected that in order for a shift in the morphology away from the traditional void and window structure to one where the voids are predominately open to occur, the droplets must be sufficiently small and in sufficient contact, while the continuous phase film between adjacent droplets must also be sufficiently thin, all of which can be influenced by the parameters mentioned above. An understanding of which of these parameters or combination thereof (and at what levels) that most strongly influence the morphology may allow for the preparation of materials with better tailored morphologies.

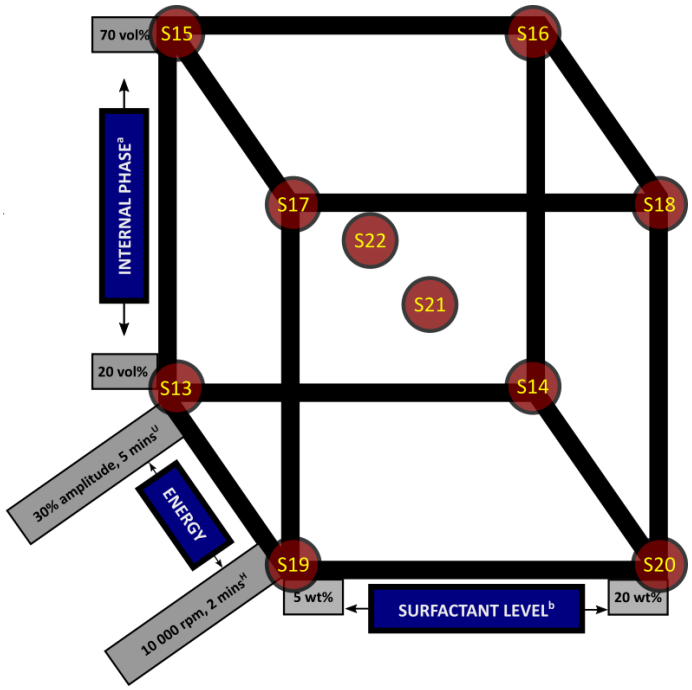

Figure 3.5. Experimental design scheme with the low and high values for the internal phase volume, surfactant level and emulsification energy, which are represented by the vertices of the cube. [a] With respect to the total volume of oil and water. [b] With respect to the continuous water phase. [H] Emulsification with the homogeniser, the homogenisation time is provided. [U] Emulsification with the digital sonifier®, the amplitude and sonication time is provided. S = sample.

Table 3.5 Composition of emulsion templates for samples 13-25

	Oil Phase / mL		Aqueous Phase / g					
No.	Paraffin-oil	IP [a]	AAm	MBAm	Tween® 85	H_2O	APS	Emulsification
13	4	20%	5.68	1.236	0.8 [5 wt%] [b]	16	0.16	[30% amp, 5 min^{U}]
14	4	20%	5.68	1.236	3.2 [20 wt%] [b]	16	0.16	[30% amp, 5 min^{U}]
15	14	70%	2.13	0.4635	0.3 [5 wt%] [b]	6	0.06	[30% amp, 5 min^{U}]
16	14	70%	2.13	0.4635	1.2 [20 wt%] [b]	6	0.06	[30% amp, 5 min^{U}]
17	14	70%	2.13	0.4635	0.3 [5 wt%] [b]	6	0.06	[10 000 rpm, 2 min^{H}]
18	14	70%	2.13	0.4635	1.2 [20 wt%] [b]	6	0.06	[10 000 rpm, 2 min^{H}]
19	4	20%	5.68	1.236	0.8 [5 wt%] [b]	16	0.16	[10 000 rpm, 2 min^{H}]
20	4	20%	5.68	1.236	3.2 [20 wt%] [b]	16	0.16	[10 000 rpm, 2 min^{H}]
21	9	45%	3.905	0.8498	1.375 [12.5 wt%] [b]	11	0.11	[14 000 rpm, 2 min^{H}]
22	9	45%	3.905	0.8498	1.375 [12.5 wt%] [b]	11	0.11	[30% amp, 5 min^{U}]
23	8	40 vol%	4.26	0.927	0.6 [5 wt%] [b]	12	0.12	[14 000 rpm, 2 min^{H}]
24	8	40 vol%	4.26	0.927	0.6 [5 wt%] [b]	12	0.12	[18 000 rpm, 2 min^{H}]
25	8	40 vol%	4.26	0.927	2.4 [20 wt%] [b]	12	0.12	[18 000 rpm, 2 min^{H}]

[a] With respect to the total volume of oil and water. [b] Percentage of Tween® 85 solution with respect to the continuous water phase. [H] Emulsification with the homogeniser, the homogenisation time is provided. [U] Emulsification with the digital sonifier®, the amplitude (amp) and sonication time is provided.

Table 3.6 Combined levels for samples 13-22

Sample	IP [a]	S [b]	E [c]
13	-	-	+
14	-	+	-
15	+	-	+
16	+	+	+
17	+	-	-
18	+	+	-
19	-	-	-
20	-	+	-
21	0	0	0
22	0	0	+

[a] Level of the internal phase volume. [b] Level for the surfactant concentration. [c] Level for the emulsification energy. + high level, - low level, 0 centre point.

A full factorial experimental design approach was employed to investigate the potential of interrelationship between these parameters, by preparing a series of samples from combinations of high and low values for each parameter, an approach commonly referred to as screening [50]. The surfactant level was varied based on its concentration relative to the continuous phase, as this would potentially highlight the influence of the surfactant-to-oil ratio on the materials morphology, without assuming it to be its own parameter. The composition of the samples utilised in this study (samples 13-22) are shown in **Table 3.5**, while **Table 3.6** demonstrates how each sample related to the combination of high and low values for each parameter. Each sample can be thought to lie on one of the vertices of a cube, which is represented in **Figure 3.5**, while samples 21 and 22 were included to investigate curvature (non-linear variation in morphology).

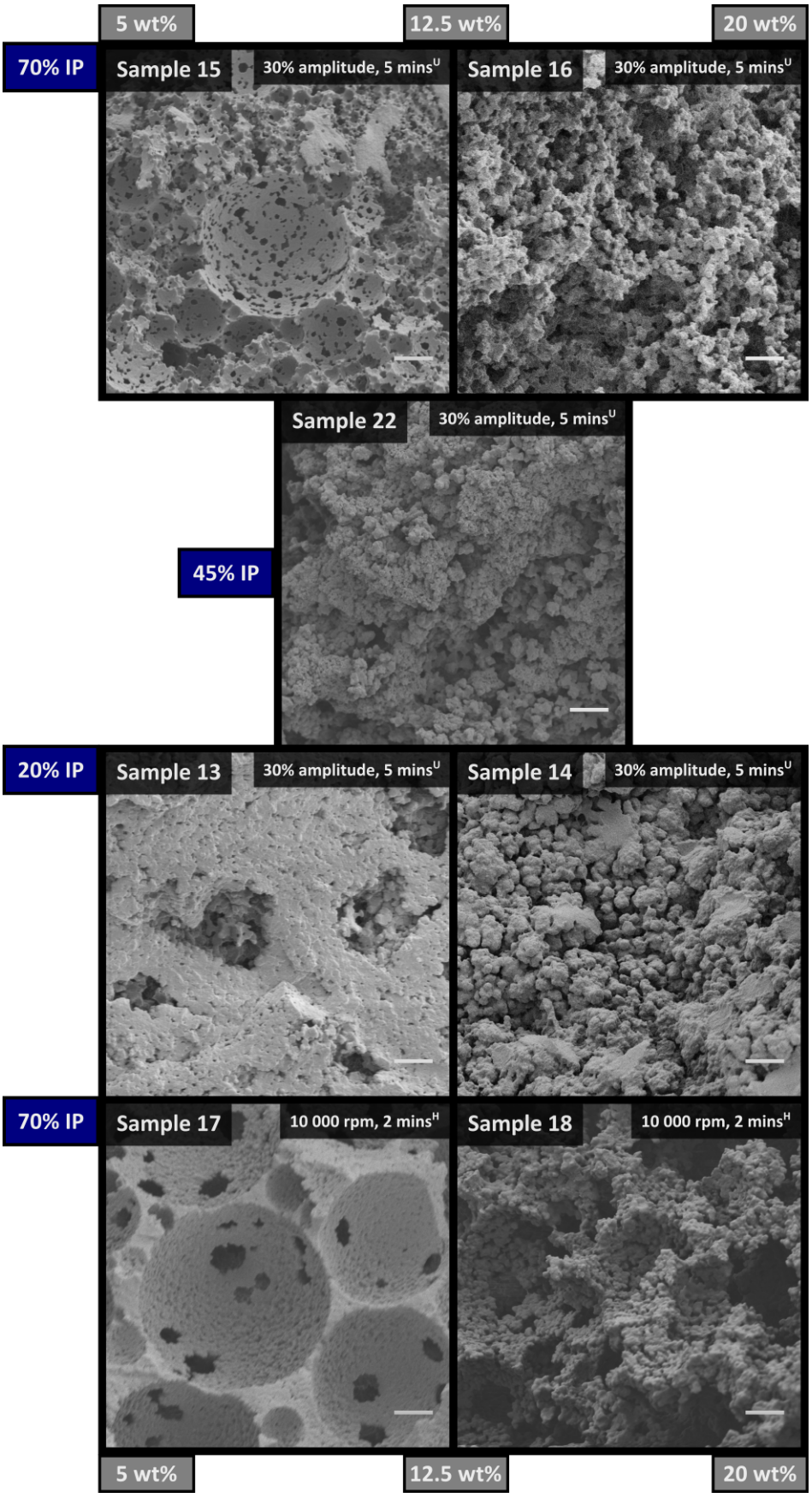

Figure 3.6. SEM images of samples 13-18 & 22, prepared with various emulsification energies, surfactant levels and internal phase volumes. Scale bar is 2 µm.

Table 3.7 Morphological features of the porous polymers for samples 13-18 & 22

Sample	V / μm [a]	D1 / μm [b]	D2 / μm [c]	W / μm [d]	P / μm [e]	BET / m^2g^{-1} [f]	φ_d / % [g]	Preparation
13	-	-	-	-	0.68 ± 0.01	0.20 ± 0.01	-	[20% IP, 30% amp, 5 min[U], 5 wt%]
14	-	-	-	-	0.62 ± 0.06	3.9 ± 0.4	39 ± 1	[20% IP, 30% amp, 5 min[U], 20 wt%]
15	3 ± 2	-	-	0.2 ± 0.1	0.389 ± 0.004	5.3 ± 0.2	67 ± 2	[70% IP, 30% amp, 5 min[U], 5 wt%]
16	-	-	-	-	0.769 ± 0.004	5.6 ± 0.6	60 ± 10	[70% IP, 30% amp, 5 min[U], 20 wt%]
17	6 ± 3	8 ± 4	8 ± 3	0.8 ± 0.4	1.7 ± 0.1	1.8 ± 0.2	55 ± 3	[70% IP, 10 000 rpm, 2 min[H], 5 wt%]
18	4 ± 2	6 ± 3	7 ± 3	0.8 ± 0.4	1.9 ± 0.1	3.9 ± 0.2	67 ± 3	[70% IP, 10 000 rpm, 2 min[H], 20 wt%]
22	-	-	-	-	0.69 ± 0.01	5.2 ± 0.3	48 ± 1	[45% IP, 30% amp, 5 min[U], 12.5 wt%]

[a] Average void diameter as determined from SEM. [b] Average droplet diameter immediately after preparation as determined from optical microscopy. [c] Average droplet diameter 24 h after preparation as determined from optical microscopy. [d] Average window diameter as determined from SEM. [e] Average median pore diameter (volume) as determined from MIP. [f] Average specific surface area as determined from the BET method. [g] Average dry state porosity as determined by immersion in acetone. [H] Emulsification with the homogeniser, the homogenisation time is provided. [U] Emulsification with the digital sonifier®, the amplitude (amp) and sonication time is provided.

The morphology of the materials obtained is shown in **Figure 3.6**, while their porous properties can be found in **Table 3.7**. Materials could not be obtained for samples 19, 20 and 21 as they exhibited significant creaming (**Figure A1** in **Appendix A**) suggesting the contact between droplets is having a profound effect on the emulsions stability towards creaming. Samples 17 and 18 exhibited a small degree of creaming, however this did not result in an increase in their porosity, although the porosity for sample 17 was lower than expected. This could have been due to the presence of some closed pores as a result of the lower emulsification energy utilised. All other samples appeared stable and possessed porosities consistent with the internal phase volume utilised, except for sample 14, which has been discussed previously.

Starting with sample 17 (70% IP, 10 000 rpm, 2 min, 5 wt%), which possessed a traditional void and window structure, and increasing the emulsification energy using the digital sonifier® at 30% amplitude for 5 min (sample 15) simply resulted in a material with smaller voids and windows (**Table 3.7**). If the surfactant level was increased, instead of the emulsification energy, to 20 wt% (sample 18) a similar material was also obtained possessing voids and windows. However this sample appeared to possess an additional porous structure in its void walls, consistent with its higher surface area of 3.9 ± 0.4 m^2/g compared to 1.8 ± 0.2 m^2/g for sample 17, as both samples possessed similar void and window sizes (**Table 3.7**). This could be related to the presence of a non-conventional continuous phase, due to the increased surfactant concentration, further templating the structure, however the porosity was as expected.

As mentioned, sample 17 possessed a lower than expected porosity of 55 ± 3 %, which was suggested to be due to the presence of some closed pores, however both samples 15 and 18 possessed porosities as expected. This is consistent with both the emulsification energy and the surfactant level influencing the open cellular nature of these materials. If both the emulsification energy and surfactant level were increased (sample 16) a material without the traditional void/window structure, that did not resemble that of the original emulsion, was obtained. This suggests, that in fact, both the emulsification energy and the surfactant level contribute to the shift in morphology and their combination is important for when this occurs. In other words, there is no fixed value for either parameter that results in a particular morphology.

Starting from sample 14 (20% IP, 30% amp, 5 min^{U}, 20 wt%), which did not possess voids and windows and did not resemble that of the emulsion it was prepared from, and increasing the internal phase to 70 vol% (sample 16) simply resulted in a similar morphology, as described above. However when the surfactant level was reduced to 5 wt% (sample 13), while maintaining the 20 vol% internal phase and emulsification energy, a cellular material was obtained, albeit with a very low number of voids. This material was also without the void and window structure. This would suggest that the surfactant level is more important than the internal phase volume utilised. However, when the internal phase was increased to 70 vol% (sample 15), using the surfactant concentration of 5 wt% and the same emulsification energy, the traditional void and window structure was obtained. This demonstrates that both the internal phase volume and the surfactant concentration (relative to the continuous phase) are both influencing the shift in morphology, that is the surfactant-to-oil ratio appears important.

This observation is consistent with sample 22 (45% IP, 30% amp, 5 min^{U}, 12.5 wt%) appearing to be an intermediate between sample 15 (70% IP, 30% amp, 5 min^{U}, 5 wt%) and sample 14 (20% IP, 30% amp, 5 min^{U}, 20 wt%), as well as an intermediate between sample 13 (20% IP, 30% amp, 5 min^{U}, 5 wt%) and sample 16 (70% IP, 30% amp, 5 min^{U}, 20 wt%) as the surfactant-to-oil ratio gradually varied over these samples (**Table 3.8**). This sample also suggested that the alterations in morphology occurred gradually and only

Table 3.8 Surfactant-to-oil ratio for samples 13-16 & 22

Sample	Surfactant-to-oil ratio [a]	Preparation
13	0.20	[20% IP, 30% amp, 5 min^{U}, 5 wt%]
14	0.80	[20% IP, 30% amp, 5 min^{U}, 20 wt%]
15	0.02	[70% IP, 30% amp, 5 min^{U}, 5 wt%]
16	0.09	[70% IP, 30% amp, 5 min^{U}, 20 wt%]
22	0.15	[45% IP, 30% amp, 5 min^{U}, 12.5 wt%]

[a] The ratio of surfactant to the oil present by mass.

once with the variation in the internal phase and surfactant level (i.e. no curvature was observed) when the emulsification energy was fixed.

Unfortunately, the emulsions prepared with 20 vol% internal phase at lower emulsification energies were unstable, presumably due to the reduced droplet contact, meaning any dependency on the morphology from both the internal phase volume and the emulsification energy could not be fully evaluated. It could be assumed, given the droplet contact was expected to be significantly lower, that open cellular materials would not have been obtained. This also highlights that, since the polymerised material does not form instantaneously, the emulsion stability is another factor that must be considered as alterations in the emulsions structure can occur over time due to coalescence and/or Ostwald ripening. The material obtained may therefore not reflect that of the original emulsion [42] and hence the stability studies employed in this work are important.

It is clear from this study that the emulsification energy and the surfactant-to-oil ratio (which is altered by both the internal phase volume and surfactant level relative to the continuous phase) are the most important parameters responsible for the shift observed

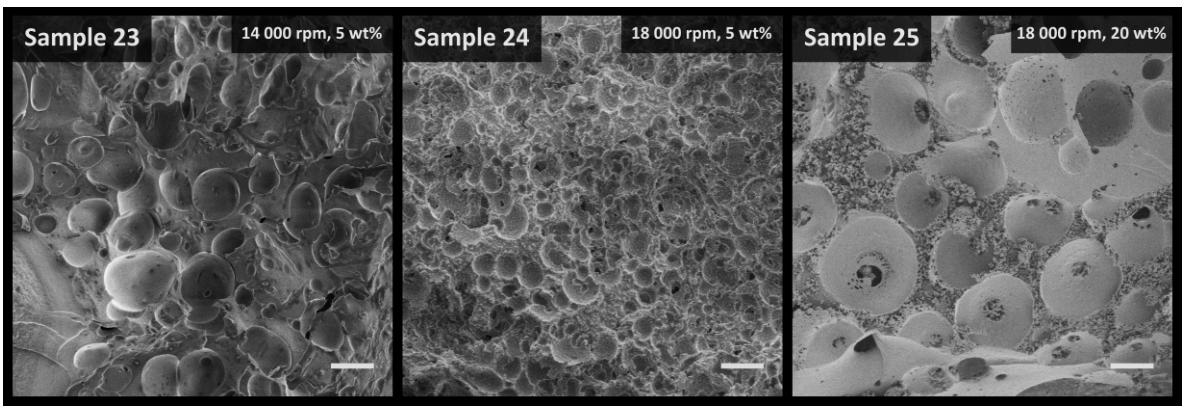

Figure 3.7. SEM images of samples 23-25, prepared with 40 vol% internal phase with various emulsification energies and surfactant levels. Scale bar is 10 µm.

in the materials morphology. Obviously, the internal phase volume is still expected to have an influence over the morphology of these materials as it influences the ability for the droplets to come into contact, which is a prerequisite for window formation, however in this approach it was not varied independently from the surfactant-to-oil ratio. More insight into how this relates to the contributions from the other parameters might be achieved using an additional experimental design approach where the surfactant-to-oil ratio was included as its own parameter.

In terms of the open cellular nature of these materials, the emulsification energy itself appears to be particularly important as three additional samples prepared using a 40 vol% internal phase with the homogeniser (samples 23-25 in **Table 3.5**) were predominantly closed cellular (**Figure 3.7**) in comparison to the open cellular materials obtained when sonication was employed (**Figure 3.4**), even when the surfactant level was increased to 20 wt%. It is worth noting that other parameters, not varied in this work, can also influence the open cellular nature of these materials, including the locus of initiation [51-52], choice of stabiliser [53-54] and the monomers utilised [28, 53].

The dramatic shifts in morphology observed in this work clearly highlight the versatility associated with the emulsion templating approach. The ability to obtain different morphologies is particularly important, as it potentially allows the structure to be better tailored for the intended application. For example, a material possessing predominantly open voids could be more applicable in chromatography, avoiding the potential of mixing associated with the void and window structure of poly(HIPE)s [46]. Closed cellular foams, on the other hand, are also an important class of material with applications in packaging for example [55].

3.3.3 Mechanical properties of the hydrophilic porous polymers

In order to establish if a reduction in the internal phase volume correlated to improved mechanical properties for these materials, cylindrical disks for samples 5, 11, 12 and 14 were investigated under compression. The mechanical properties for sample 13 could not be reliably evaluated, as these disks cracked significantly during purification. This was also

Table 3.9 Mechanical properties under compression for samples 5, 11, 12 and 14

Sample	Average Young's Modulus / MPa	Average Crush Strength / MPa	Average Young's Modulus / MPa [N]	Average Crush Strength / MPa [N]	Preparation
5	180 ± 70	4.7 ± 0.8	5 ± 2	0.13 ± 0.02	[60% IP, 30% amp, 5 min[U], 5 wt%]
11	170 ± 50	6 ± 2	3 ± 1	0.15 ± 0.04	[50% IP, 30% amp, 5 min[U], 5 wt%]
12	490 ± 90	14 ± 2	8 ± 2	0.21 ± 0.03	[40% IP, 30% amp, 5 min[U], 5 wt%]
14	260 ± 60	6 ± 2	4 ± 1	0.10 ± 0.03	[20% IP, 30% amp, 5 min[U], 20 wt%]

[N] Normalised against bulk (%). [U] Emulsification with the digital sonifier®, the amplitude (amp) and sonication time is provided.

the reason that porosity values could not be determined for this sample. Results from the compression studies are shown in **Table 3.9** and the stress-strain curve with the slope closest to the average value for each sample set is shown in **Figure 3.8**, in addition to an expanded region containing the initial elastic region (strain values of 0 to 0.02). The stress-strain curves for the additional replicates are shown in **Figures 3.9 - 3.12**.

Samples 5 and 11 (60 and 50 vol% internal phase respectively) possessed similar Young's moduli of 180 ± 70 and 170 ± 50 MPa, respectively. In addition, they possessed similar crush strength values of 4.7 ± 0.8 and 6 ± 2, respectively. A reduction in the internal phase to 40 vol% (sample 12) resulted in a significant increase in the Young's modulus to 490 ± 90 MPa and an increase in the average crush strength to 14 ± 2 MPa. The Young's moduli

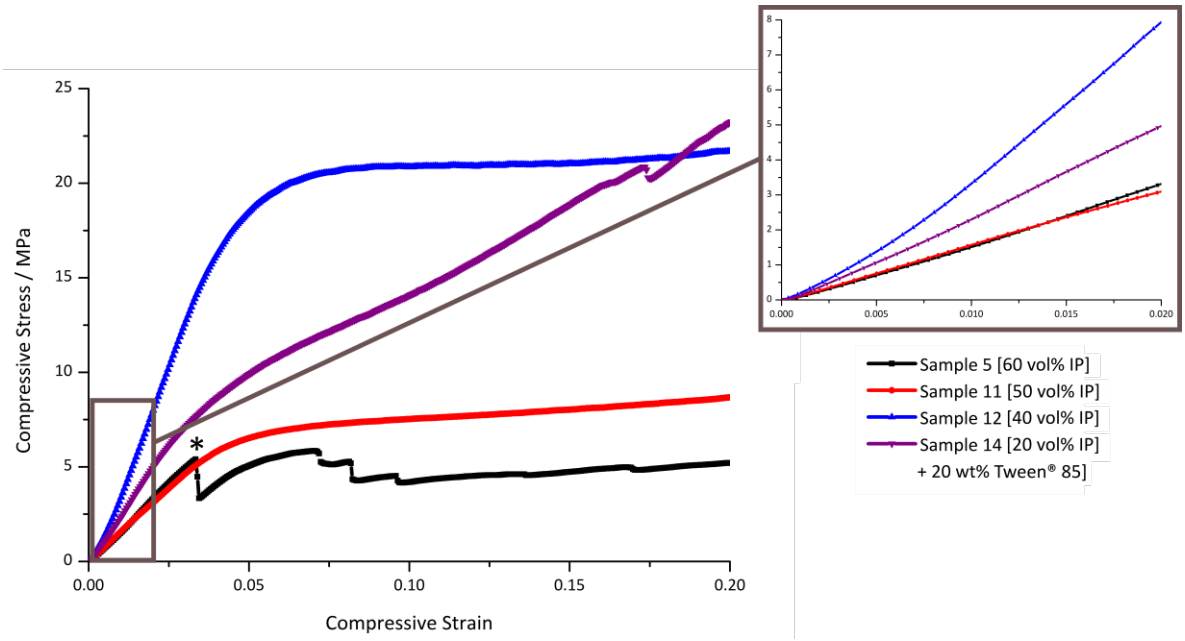

Figure 3.8. Stress-strain curves obtained under a compressive load for samples 12, 14, 11 and 5 (from top to bottom). Magnified area spans from a strain of 0 to 0.02 and contains the initial elastic region. Each sample was prepared with different internal phase volumes with 5 wt% Tween® 85 (samples 5, 11 and 12) or 20 wt% Tween® 85 (sample 14).

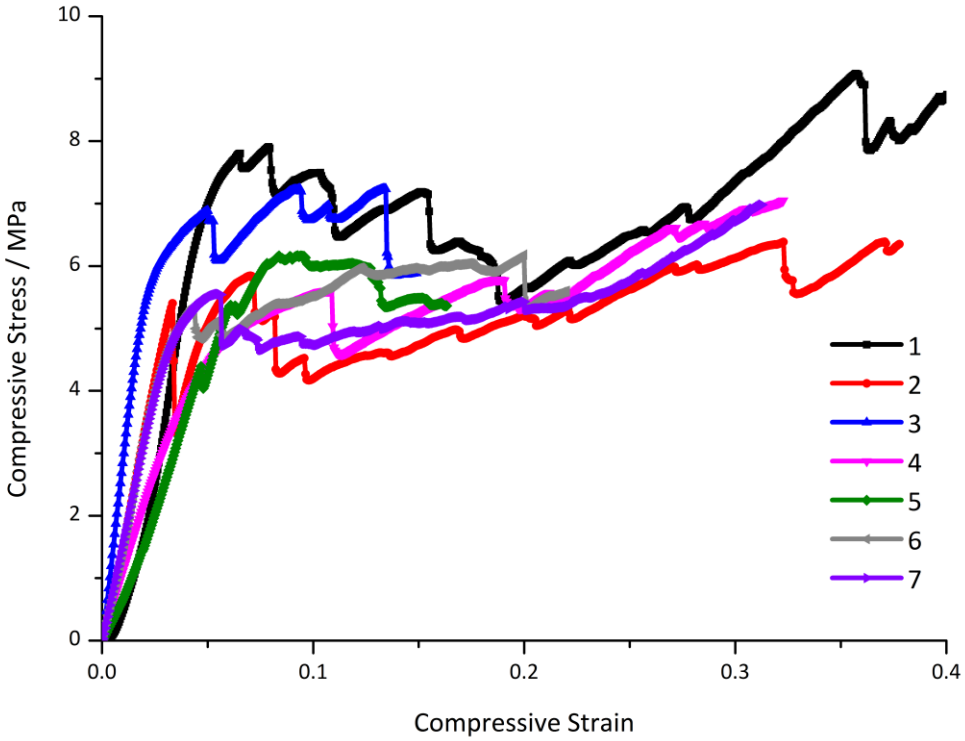

Figure 3.9. Stress-strain curves obtained, under a compressive load, for the replicates for sample 5 (60 vol% internal phase).

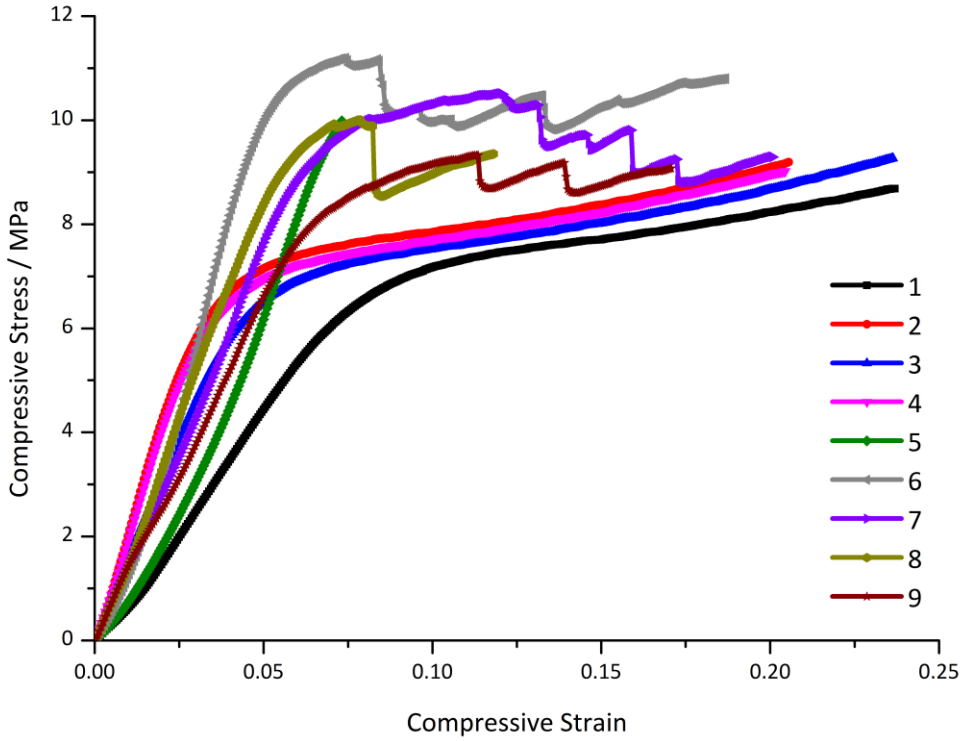

Figure 3.10. Stress-strain curves obtained, under a compressive load, for the replicates for sample 11 (50 vol% internal phase).

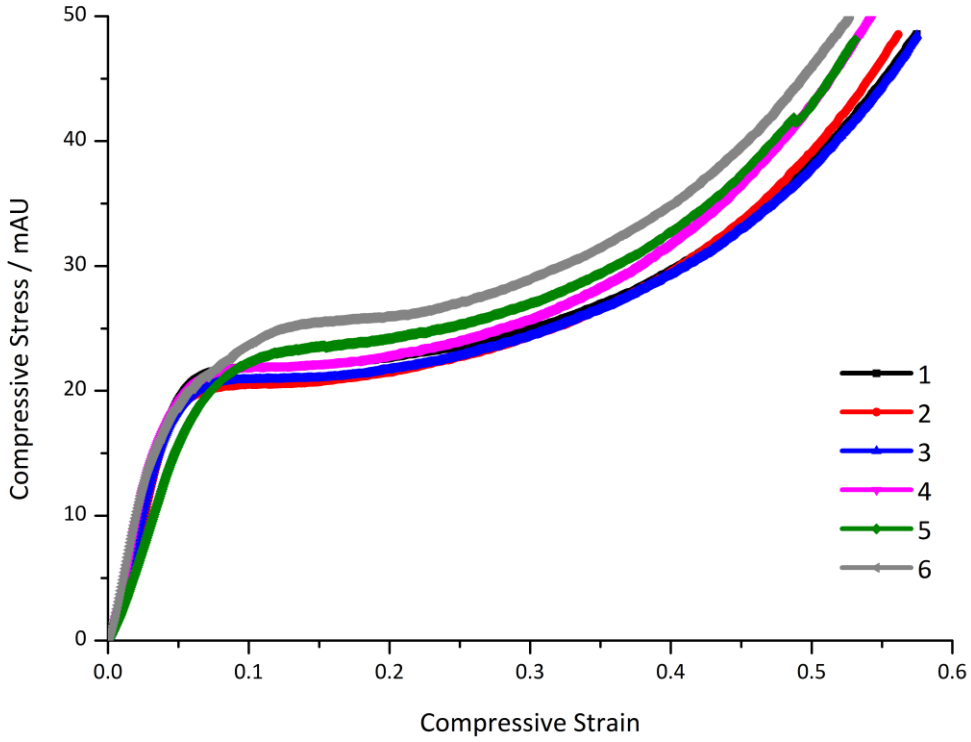

Figure 3.11. Stress-strain curves obtained, under a compressive load, for the replicates for sample 12 (40 vol% internal phase).

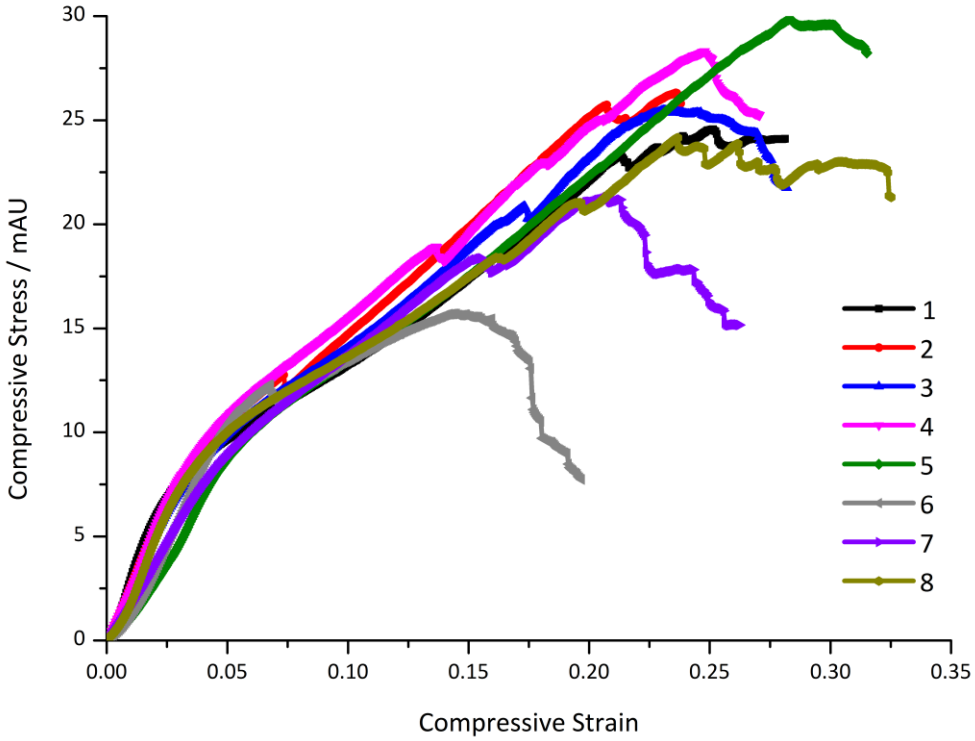

Figure 3.12. Stress-strain curves obtained, under a compressive load, for the replicates for sample 14 (20 vol% internal phase + 20 wt% Tween® 85).

of typical poly(HIPE) materials tend to be much lower in value than those obtained in these experiments [18, 56]. This was also a significant improvement to similar hydrophilic materials prepared by Youssef et al. [25] who achieved a Young's modulus of 70 ± 30 MPa from an 76 vol% dodecane internal phase with 1-vinyl-5-amino [1,2,3,4]tetrazole and MBAm as monomers. The results obtained in these experiments were also comparable to that obtained by Luo et al. [30] for poly(Sty-*co*-DVB) based poly(MIPE)s prepared from a miniemulsion template with a value of 410 ± 10 MPa.

While a reduction in porosity is known to correlate to improvements in mechanical properties, due to the higher proportion of bulk polymer, this is often at the expense of interconnectivity [14, 26, 30]. However sample 12, which possessed the highest Young's modulus and crush strength with a porosity of 36 ± 3 %, still possessed a high degree of interconnectivity (**Figure 3.4**) as a result of the use of sonication. This is extremely important as it potentially affords the possibility of applying this hydrophilic material under higher operating pressures, for example affording the possibility of using higher flow rates for rapid separations for chromatographic applications. The stress-strain curves obtained for this sample were also highly repeatable and very smooth (**Figure 3.11**) and **Figure 3.13** demonstrates the degree of compressibility this material was able to withstand during the compression tests without any visual signs of failure.

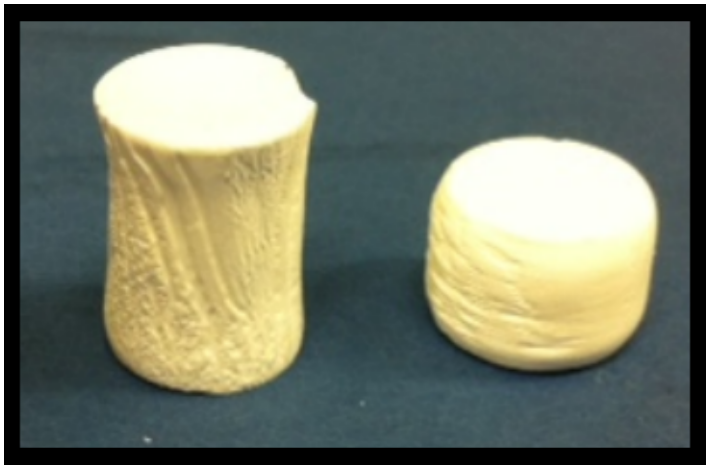

Figure 3.13. Photograph of two replicates of Sample 12 (40 vol% internal phase) used for mechanical testing. One before compression (left) and one after compression (right) with the 5 kN load cell.

When the internal phase was reduced further to 20 vol% (sample 14) a reduction of the Young's modulus and crush strength was observed with values of 260 ± 60 MPa and 6 ± 2 MPa obtained respectively, even though these materials shared similar experimental porosities. However, this was prepared with 20 wt% surfactant and increased levels of surfactant have previously been shown to be detrimental to the mechanical properties of emulsion templated materials [31, 57]. Regardless, the Young's modulus of this sample is still notable.

The stress-strain curves obtained for porous materials under compression typically contain three distinct regions [31, 58-59]. These are the initial elastic region at low deformation values followed by a plateau, where the stress is approximately constant over a range of strain, and then finally a densification region where the stress again begins to rise (these regions are clearly visible in the expanded stress-strain curves for sample 12 in **Figure 3.11**). In the elastic region the stress and strain are proportional and any deformation that occurs is non-permanent and reversible. The Young's modulus is taken as the slope of this region for each sample.

The onset of non-linear behaviour (which is defined here as the crush strength) signifies the change in behaviour from elastic to plastic as permanent deformation starts to occur. The change in curvature and onset of the plateau region signifies where the sample starts to break and lose its porous structure. The material irreversibly deforms through this flat region, which can correspond to buckling or cracking of the polymer walls. If all the pores become compressed, foam densification (increase in the foam density) can be observed as the stress again rises. Deviations from this stress-strain profile can provide additional information about the mechanical behaviour of these porous materials [58].

Only the first region was observed for the replicates of sample 5 (**Figure 3.9**) and the samples fractured shortly after the elastic region, prior to the onset of the plateau region. The noise, or dips, observed after the failure of the material corresponds to rearrangement of the cracked specimen and is typical of an elastic-brittle foam [31, 59]. An asterisk in **Figure 3.8** marks the first occurrence of these dips where fragments were observed to detach from the polymer disk. Some replicates of sample 11 also exhibited

this behaviour (**Figure 3.10**). Sample 12 (as well as some of the replicates from sample 11) exhibited behaviour more representative of poly(HIPE)s [31, 59] and that of an elastomeric foam [58] with all three regions observed for all replicates (**Figure 3.11**), highlighting the excellent mechanical behaviour of this sample. Sample 14 appeared to exhibit failure of the material before a plateau region could be observed, however the increase in stress with increased strain appeared to occur over a wider range for all replicates (**Figure 3.12**) compared to the other samples, with failure occurring much later than sample 5, indicating this sample still possessed good mechanical properties.

The samples compared in this work possess quite different porous morphologies (**Figures 3.1** & **3.4**) and this will also have an influence on the mechanical properties in addition to the differences in porosity. In order to investigate this, the Young's modulus and crush strength were normalised against percentage of bulk polymer (**Table 3.9**). Here, samples 5 (60 vol% internal phase) and 11 (50 vol% internal phase) possessed similar values for the normalised Young's modulus of 5 ± 2 and 3 ± 1 MPa, respectively. This was significantly higher, however, for sample 12 (40 vol% internal phase) with a value of 8 ± 2 MPa.

Sample 5 possessed the void and window structure typical for poly(HIPE)s, while sample 12 possessed predominately open voids. Sample 11 on the other hand appeared to be an intermediate between the two. This could suggest that the predominately open structure of sample 12 might be enhancing the mechanical properties, in contrast to the bimodal structure present for sample 5 and partially present for sample 11. Sample 14 (20 vol% internal phase), which also did not possess the void and window structure, possessed a lower normalised Young's modulus of 4 ± 1 MPa, however, as discussed above, this was prepared with a higher surfactant concentration. The normalised crush strength also followed similar trends.

The mechanical properties of porous materials can, however, depend on a variety of other factors [60] including the homogeneity of the material and the pore geometry, and therefore warrants further investigation. It is clear, however that it is possible to obtain highly interconnected hydrophilic materials with excellent mechanical properties, which is important for increasing the practicality of these materials for several applications [12-18].

In order to improve the mechanical properties further it is also possible to introduce particles into the emulsion templates [14, 22, 56] and/or utilise a different monomer system [25].

3.3.4 Swelling Characteristics

In order to find appropriate applications for these materials it is first important to establish their behaviour in different solvent environments. For example, during the preparation for the samples for mechanical testing it became apparent that these materials exhibited significant shrinkage upon exposure to acetone. Polymer disks for each sample were therefore exposed to three different solvent environments; acetone, MeOH and H_2O. The change in mass, volume and their respective porosities are shown in **Table 3.10** for samples 5, 11, 12 and 14 (the values for other samples prepared in this work can be found in **Table A1** in **Appendix A**).

Differences in the swellability in the different solvents resulted in variations in the porosity values for all samples, with the highest porosity occurring for Milli-Q H_2O (with a volume change between 90 and 120% for the samples shown in **Table 3.10**), the second highest for MeOH (with a volume change between 10 and 16%) and the lowest in acetone (where the volume change was negligible). Such a dramatic change in volume when immersed in H_2O resulted in the porosity approaching 100%, meaning that the pore volume is dominating the total volume of the swollen polymer disk.

This also resulted in quite a significant uptake of H_2O, which was 470 ± 12 % by mass (w.r.t. mass of the dry disk) for sample 5. Sample 12 was capable of taking up less H_2O with a value of 307 ± 8 %, however this is still significant. Given this sample possessed the highest mechanical properties this material might be applicable as a rigid but mechanically strong absorbent [61], especially given that the swelling occurred rapidly within minutes of exposure for all samples. **Figure 3.14** shows a disk of sample 5 before and after being immersed in a beaker of H_2O for 2 min, while **Figure 3.15** shows a disk of sample 5 before and after drops of H_2O (~20 drops, totalling ~1 g) were pipetted onto it.

Table 3.10 Swelling characteristics for samples 5, 11, 12 and 14

Sample	φ_w / % ^{A}	φ_w / % ^{M}	φ_w / % ^{W}	ΔV / % ^{A}	ΔV / % ^{M}	ΔV / % ^{W}	m_s / % ^{A}	m_s / % ^{M}	m_s / % ^{W}
5	63 ± 3	71 ± 4	103 ± 2	0.4 ± 2	16 ± 3	90 ± 10	130 ± 20	160 ± 30	470 ± 12
11	48 ± 5	62 ± 3	97 ± 4	- 2 ± 3	15 ± 4	84 ± 11	80 ± 20	120 ± 20	369 ± 5
12	36 ± 3	49 ± 1	91 ± 2	- 3 ± 2	11 ± 3	120 ± 16	44 ± 8	63 ± 5	307 ± 8
14	39 ± 1	52 ± 1	93 ± 2	- 3 ± 3	10 ± 3	100 ± 10	48 ± 3	70 ± 3	298 ± 7

φ_w signifies the porosity, ΔV the change in volume of the polymer disk relative to the original volume and m_s indicates the mass of solvent present in the disk relative to the mass of the dry disk. ^{A} These values were determined through immersion in acetone. ^{M} These values were determined through immersion in MeOH. ^{W} These values were determined through immersion in H_2O. The preparation conditions for these samples can be found in **Table 3.1**.

It is clear that these materials exhibit contrasting behaviour in different solvent environments and the significant swelling and shrinkage of these polymers when exposed to H_2O and acetone respectively, may also offer opportunities for applications in controlled release [9-10] when these materials are exposed to a solvent gradient. However these alterations in the porous morphology when exposed to solvents of different polarity is concerning for chromatographic applications involving a solvent gradient.

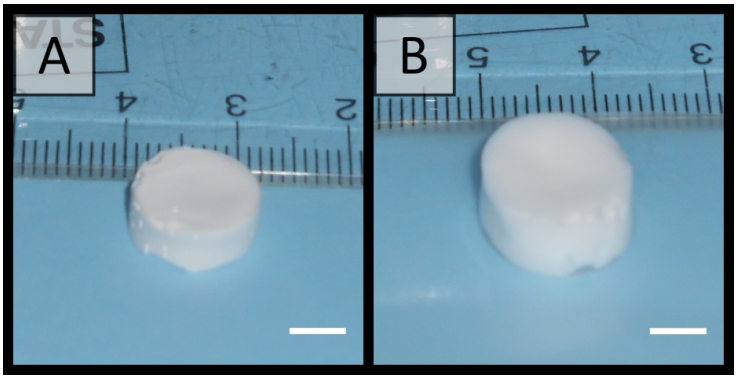

Figure 3.14. Photographs of a disk from sample 5 (40 vol% internal phase) **(A)** prior to immersion in a beaker of Milli-Q H_2O and **(B)** after 2 min of immersion. Scale bar is 0.5 cm.

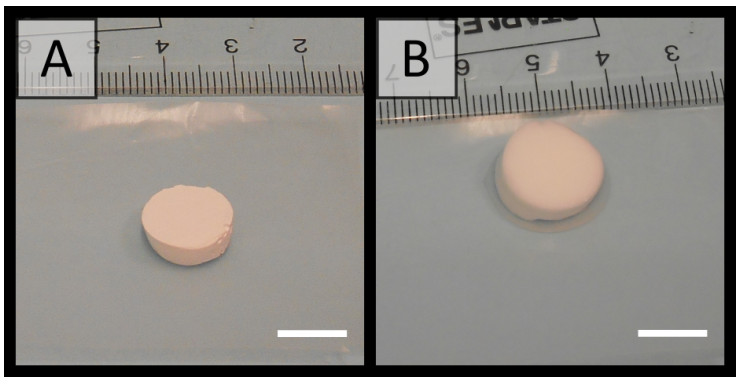

Figure 3.15. Photographs of a disk from sample 5 (40 vol% internal phase) **(A)** prior to addition of ~20 drops of Milli-Q H_2O to the top surface and **(B)** immediately after addition. Scale bar is 1 cm.

This was particularly problematic when these samples were prepared in capillary format where detachment from the capillary wall was observed when acetone was pumped through the column in order to remove the paraffin-oil internal phase. This appeared to be the result of shrinkage, as the material removed from the capillary housing possessed a skin suggesting that the porous material was originally in contact with the capillary wall when formed. This is shown for sample 1 in **Figure 3.16**, however this occurred for all emulsion formulations prepared in this work. The diameter of this particular material was estimated to be 93 ± 2 µm, which was significantly smaller than the i.d. of the capillary, which was 150 µm, indicating significant shrinkage had occurred during purification.

More recent work by another PhD candidate in our research group has shown that the shrinkage of poly(AAm-*co*-MBAm) poly(HIPE)s can be reduced through the use of a macro-RAFT agent as stabiliser, allowing for the stable attachment of the poly(HIPE)s to the capillary wall [62]. This approach may allow these materials to be applied for chromatography.

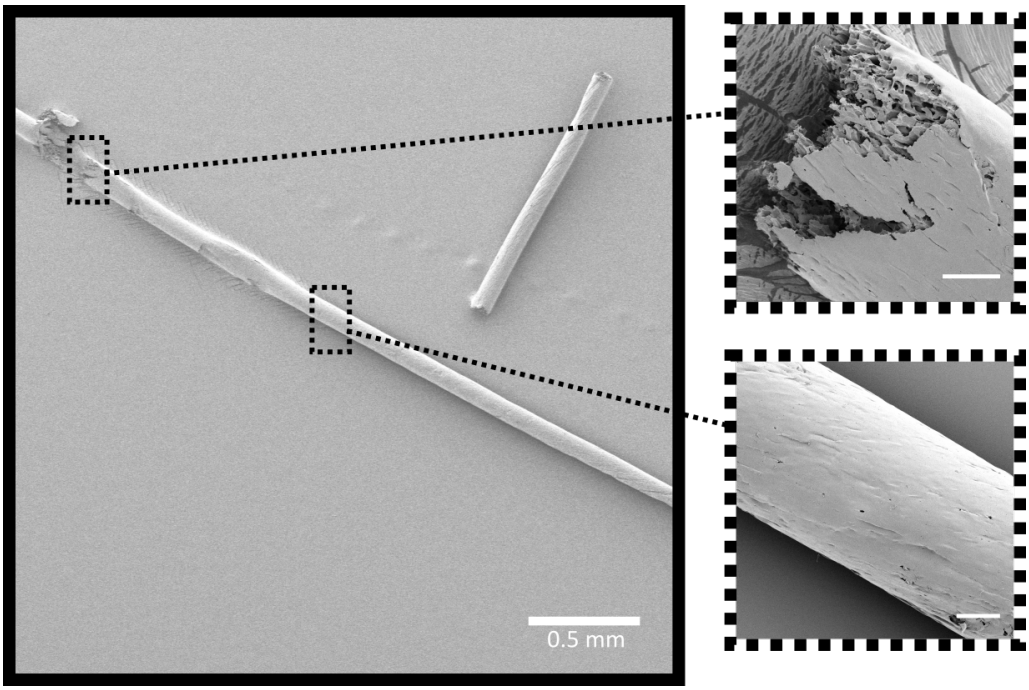

Figure 3.16. SEM images of the porous material (sample 1) that was removed from the capillary housing during purification with acetone. Scale bar is 0.5 mm for the main image and 25 µm for the expanded regions.

3.4 Conclusions

In summary, highly interconnected hydrophilic polymers with excellent mechanical properties were successfully prepared using (paraffin-oil)-in-water emulsion templates using reduced internal phase volumes. Increases in the emulsification energy, which resulted in an increase in the contact between emulsion droplets, ensured that open cellular and highly interconnected materials were obtained. Combining the increase in emulsification energy with a reduction in the internal phase volume allowed for the preparation of hydrophilic materials with significantly improved mechanical properties under compression, with a Young's modulus of 490 ± 90 MPa achieved for a material with 36 ± 3 % porosity. This is important for improving the applicability of these materials for use under higher pressures.

In addition, alterations in the porous morphology of these materials were observed when the emulsification energy, internal phase volume and surfactant level were varied. In some cases, this resulted in a significantly different morphology with an apparent loss of the void/window structure typically associated with emulsion templated materials. It was suggested that in these cases the voids of these materials had become predominately open due to the presence of thinner continuous phase films between adjacent droplets, and the surfactant-to-oil ratio and emulsification energy were suggested to be the most important factors. It also appeared that these structures, in contrast to the void and window structure, might have contributed to the increase in mechanical properties observed. The ability to prepare materials of contrasting morphologies is particularly useful as it offers the opportunity to tailor the structure for the intended application.

Finally, these porous polymers exhibited different swelling/shrinkage behaviour in different solvent environments, and were capable of absorbing relatively large quantities of H_2O, suggesting their potential applicability for use as rigid absorbents or in controlled release. Unfortunately the shrinkage when exposed to acetone resulted in difficulties in preparing these materials in capillary format, rendering them unsuitable for conventional LC applications.

3.5 References

[1] Jiang, Z.; Smith, N. W.; Liu, Z. *J. Chromatogr. A.* **2011**, *1218*, 2350-2361.
[2] Jiang, Z.; Smith, N. W.; Ferguson, P. D.; Taylor, M. R. *J. Sep. Sci.* **2009**, *32*, 2544-2555.
[3] Tegeler, T. J.; Mechref, Y.; Boraas, K.; Reilly, J. P.; Novotny, M. V. *Anal. Chem.* **2004**, *76*, 6698-6706.
[4] Pulko, I.; Krajnc, P. *Macromol. Rapid Commun.* **2012**, *33*, 1731-1746.
[5] Gitli, T.; Silverstein, M. S. *Polymer.* **2011**, *52*, 107-115.
[6] Hua, Y.; Zhang, S.; Zhu, Y.; Chu, Y.; Chen, J. *J. Polym. Sci. A Polym. Chem.* **2013**, *51*, 2181-2187.
[7] Barbetta, A.; Dentini, M.; De Vecchis, M. S.; Filippini, P.; Formisano, G.; Caiazza, S. *Adv. Funct. Mater.* **2005**, *15*, 118-124.
[8] Hayward, A. S.; Sano, N.; Przyborski, S. A.; Cameron, N. R. *Macromol. Rapid. Commun.* **2013**, *34*, 1844-1849.
[9] Zhang, H.; Cooper, A. I. *Adv. Mater.* **2007**, *19*, 2439-2444.
[10] Grant, N. C.; Cooper, A. I.; Zhang, H. *ACS Appl. Mater. Interfaces.* **2010**, *2*, 1400-1406.
[11] Jiang, Q.; Menner, A.; Bismarck, A. *React. Funct. Polym.* **2017**, *114*, 104-109.
[12] Huš, S.; Krajnc, P. *Polymer.* **2014**, *55*, 4420-4424.
[13] Luo, Y.; Wang, A.-N.; Gao, X. *Soft Matter.* **2012**, *8*, 1824-1830.
[14] Ikem, V. O.; Menner, A.; Horozov, T. S.; Bismarck, A. *Adv. Mater.* **2010**, *22*, 3588-3592.
[15] Menner, A.; Bismarck, A. *Macromol. Symp.* **2006**, *242*, 19-24.
[16] Menner, A.; Powell, R.; Bismarck, A. *Macromolecules.* **2006**, *39*, 2034-2035.
[17] Menner, A.; Ikem, V.; Salgueiro, M.; Shaffer, M. S. P.; Bismarck, A. *Chem. Commun.* **2007**, 4274-4276.
[18] Menner, A.; Haibach, K.; Powell, R.; Bismarck, A. *Polymer.* **2006**, *47*, 7628-7635.
[19] Jerenec, S.; Šimić, M.; Savnik, A.; Podgornik, A.; Kolar, M.; Turnšek, M.; Krajnc, P. *React. Funct. Polym.* **2014**, *78*, 32-37.
[20] Yao, C.; Qi, L.; Jia, H.; Xin, P.; Yang, G.; Chen, Y. *J. Mater. Chem.* **2009**, *19*, 767-772.
[21] Choudhury, S.; Fitzhenry, L.; White, B.; Connolly, D. *Materials.* **2016**, *9*, 212-225.
[22] Wu, R.; Menner, A.; Bismarck, A. *J. Polym. Sci. A Polym. Chem.* **2010**, *48*, 1979-1989.
[23] Wong, L. L.; Ikem, V. O.; Menner, A.; Bismarck, A. *Macromol. Rapid. Commun.* **2011**, *32*, 1563-1568.
[24] Cameron, N. R.; Sherrington, D. C. *J. Mater. Chem.* **1997**, *7*, 2209–2212.
[25] Youssef, C.; Backov, R.; Treguer, M.; Birot, M.; Deleuze, H. *J. Polym. Sci. A Polym. Chem.* **2010**, *48*, 2942-2947.
[26] Manley, S. S.; Graeber, N.; Grof, Z.; Menner, A.; Hewitt, G. F.; Stepanek, F.; Bismarck, A. *Soft Matter.* **2009**, *5*, 4780-4787.
[27] Wu, R.; Menner, A.; Bismarck, A. *Polymer.* **2013**, *54*, 5511-5517.
[28] Mathieu, K.; Jérôme, C.; Debuigne, A. *Polymer.* **2016**, *99*, 157-165.
[29] Lissant, K. J. *J Soc Cosmet Chem.* **1970**, *21*, 141-154.
[30] Luo, Y.; Wang, A.-N.; Gao, X. *Soft Matter.* **2012**, *8*, 7547-7551.
[31] Williams, J. M.; Wrobleski, D. A. *Langmuir.* **1988**, *4*, 656-662.
[32] Svec, F.; Fréchet, J. M. J. *Chem. Mater.* **1995**, *7*, 707-715.
[33] Kimmins, S. D.; Cameron, N. R. *Adv. Funct. Mater.* **2011**, *21*, 211-225.
[34] Cameron, N. R.; Sherrington, D. C.; Albiston, L.; Gregory, D. P. *Colloid Polym. Sci.* **1996**, *274*, 592-595.

[35] Kimmins, S. D.; Wyman, P.; Cameron, N. R. *Reactive and Functional Polymers.* **2012**, *72*, 947-954.
[36] Carnachan, R. J.; Bokhari, M.; Przyborski, S. A.; Cameron, N. R. *Soft Matter.* **2006**, *2*, 608-616.
[37] Barkley, S.; Scarfe, S. J.; Weeks, E. R.; Dalnoki-Veress, K. *Soft Matter.* **2016**, *12*, 7398-7404.
[38] Rangharajan, K. K.; Kwak, K. J.; Conlisk, A. T.; Wu, Y.; Prakash, S. *Soft Matter.* **2015**, *11*, 5214-5223.
[39] Cameron, N. R.; Sherrington, D. C. *Adv. Polym. Sci.* **1996**, *126*, 162-214.
[40] Costantini, M.; Colosi, C.; Guzowski, J.; Barbetta, A.; Jaroszewicz, J.; Święszkowski, W.; Dentini, M.; Garstecki, P. *J. Mater. Chem. B.* **2014**, *2*, 2290–2300.
[41] Silverstein, M. S. *Polymer.* **2014**, *55*, 304-320.
[42] Tebboth, M.; Kogelbauer, A.; Bismarck, A. *Chem. Eng. Sci.* **2015**, *137*, 786–795.
[43] Svec, F.; Lv, Y. *Anal. Chem.* **2015**, *87*, 250-273.
[44] Urban, J.; Svec, F.; Fréchet, J. M. *J. Chromatogr. A.* **2010**, *1217*, 8212-8221.
[45] Candish, E.; Wirth, H. J.; Gooley, A. A.; Shellie, R. A.; Hilder, E. F. *J. Chromatogr. A.* **2015**, *1410*, 9-18.
[46] Krajnc, P.; Leber, N.; Štefanec, D.; Kontrec, S.; Podgornik, A. *J. Chromatogr. A.* **2005**, *1065*, 69-73.
[47] Hoegger, D.; Freitag, R. *J. Chromatogr. A.* **2001**, *914*, 211-222.
[48] Zhang, K.; Yan, C.; Yang, J.; Zhang, Z.; Wang, Q.; Gao, R. *J. Sep. Sci.* **2005**, *28*, 217-224.
[49] Cameron, N. R. *Polymer.* **2005**, *46*, 1439–1449.
[50] Morgan, E. *Chemometrics: Experimental Design*. 1st ed. John Wiley & Sons Ltd.: Baffins Lane, Chichester West Sussex PO19 1UD, England, 1997.
[51] Quell, A.; Bergolis, B. d.; Drenckhan, W.; Stubenrauch, C. *Macromolecules.* **2016**, *49*, 5059−5067.
[52] Khodabandeh, A.; Dario Arrua, R.; Desire, C. T.; Rodemann, T.; Bon, S. A. F.; Thickett, S. C.; Hilder, E. F. *Polym. Chem.* **2016**, *7*, 1803-1812.
[53] Xu, H.; Zheng, X.; Huang, Y.; Wang, H.; Du, Q. *Langmuir.* **2016**, *32*, 38-45.
[54] Viswanathan, P.; Johnson, D. W.; Hurley, C.; Cameron, N. R.; Battaglia, G. *Macromolecules.* **2014**, *47*, 7091−7098.
[55] Zhang, T.; Xu, Z.; Guo, Q. *Polym. Chem.* **2016**, *7*, 7469–7476.
[56] Haibach, K.; Menner, A.; Powell, R.; Bismarck, A. *Polymer.* **2006**, *47*, 4513-4519.
[57] Kovačič, S.; Matsko, N. B.; Jerabek, K.; Krajnc, P.; Slugovc, C. *J. Mater. Chem. A.* **2013**, *1*, 487-490.
[58] Gibson, L. J.; Ashby, M. F. *Cellular Solids, Structure and Properties*. NY Pergamon Press: 1988.
[59] Graeber, N., Doctor of Philosophy, Imperial College London 2013.
[60] Nielsen, L. F. *Mater Struct.* **1998**, *31*, 651–661.
[61] Jing, P.; Fang, X.; Yan, J.; Guo, J.; Fang, Y. *J. Mater. Chem. A.* **2013**, *1*, 10135-10141.
[62] Khodabandeh, A.; Arrua, R. D.; Mansour, F. R.; Thickett, S. C.; Hilder, E. F. *Sci. Rep.* **2017**, *7*, 7847.

Appendix A

Preparation of highly interconnected hydrophilic polymers from emulsion templates with improved mechanical properties

A.1 Stability Samples

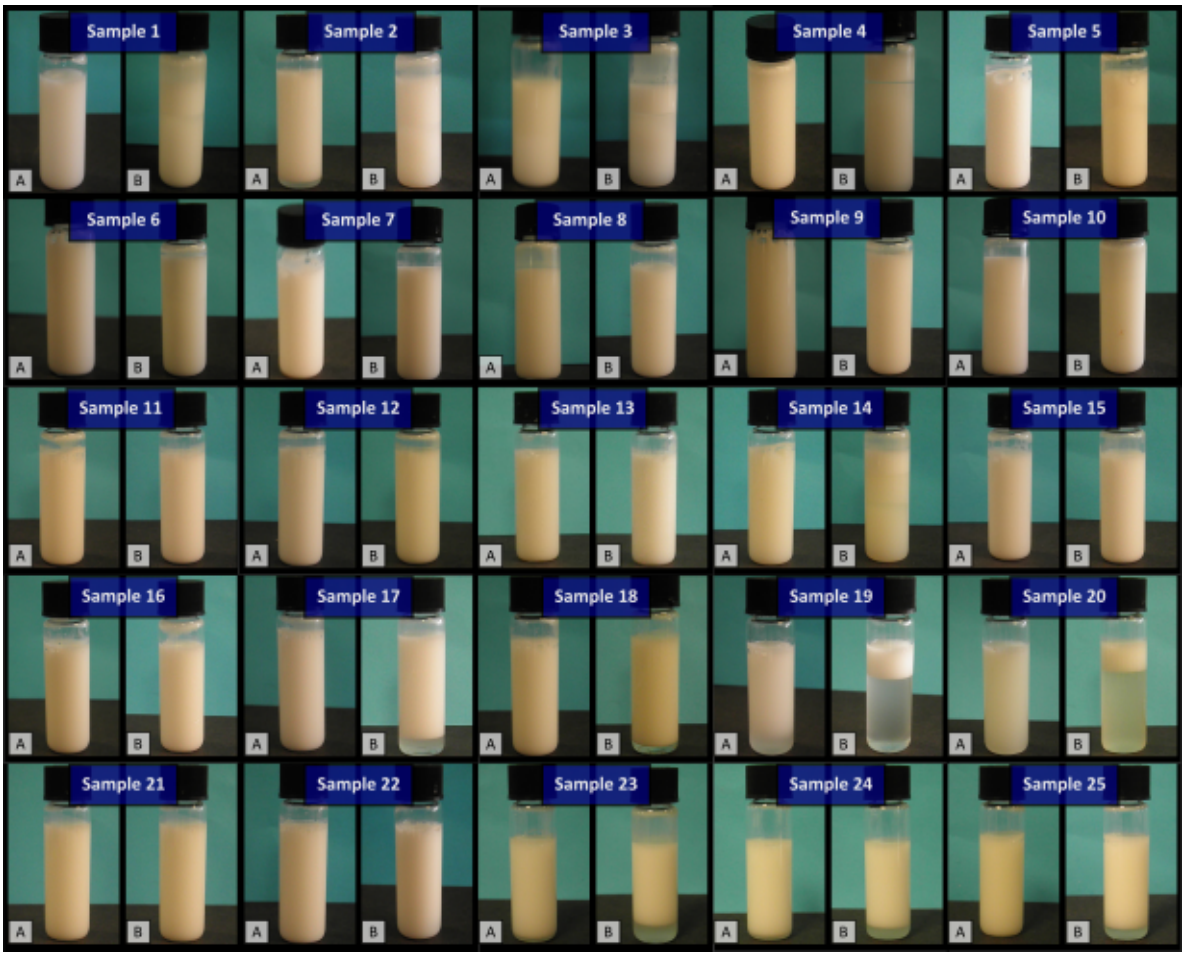

Figure A1. Photographs of the stability samples for samples 1-25 **(A)** immediately after preparation and **(B)** 24 h later for samples 1-18 & 22, ~10 min later for samples 19 & 20 & 23-25 and ~1 h later for sample 21.

A.2 Optical Microscopy

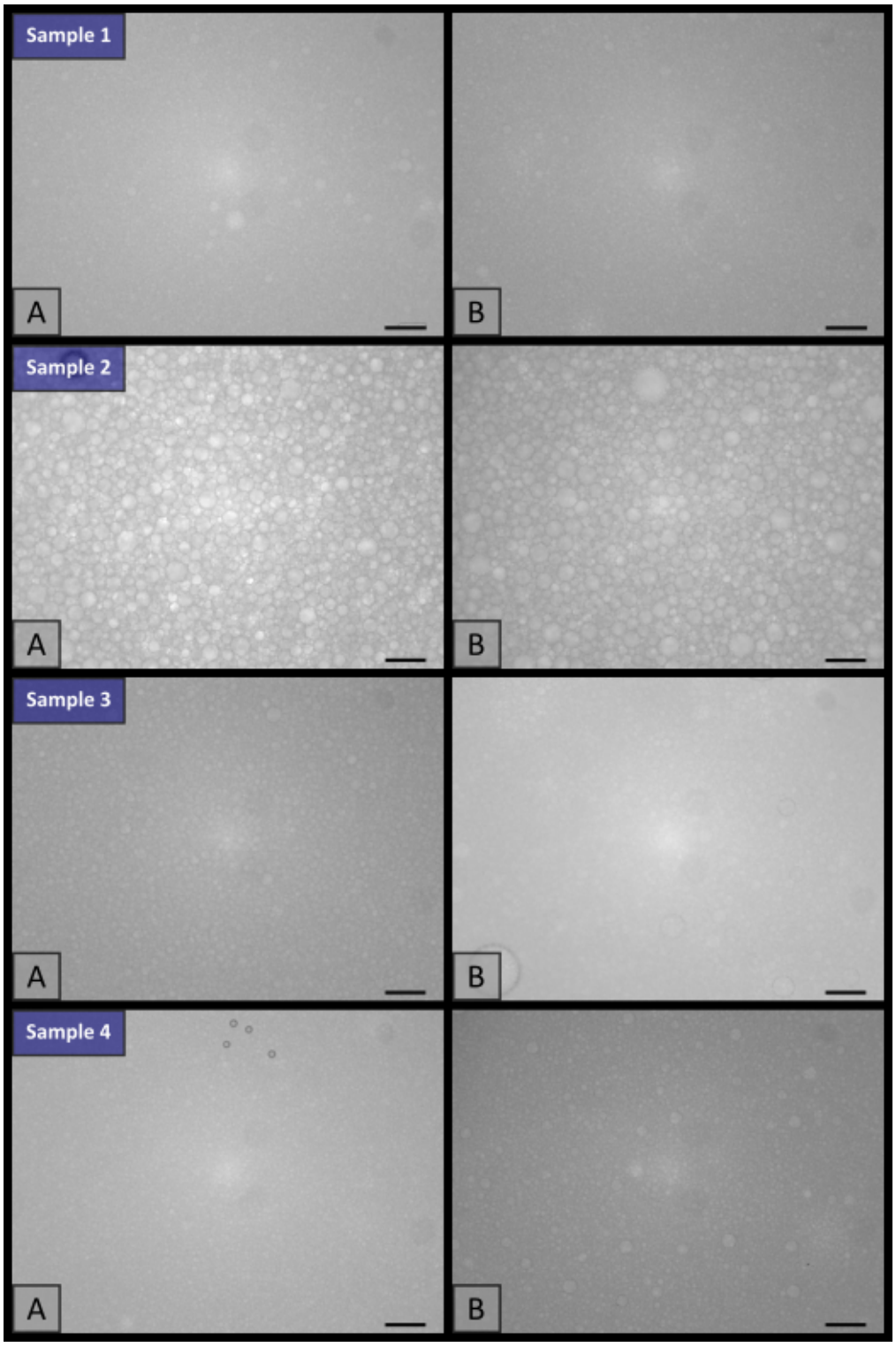

Figure A2. Optical microscopy images of emulsion templates from samples 1-4 **(A)** immediately after preparation and **(B)** 24 h later. Scale bar is 50 µm.

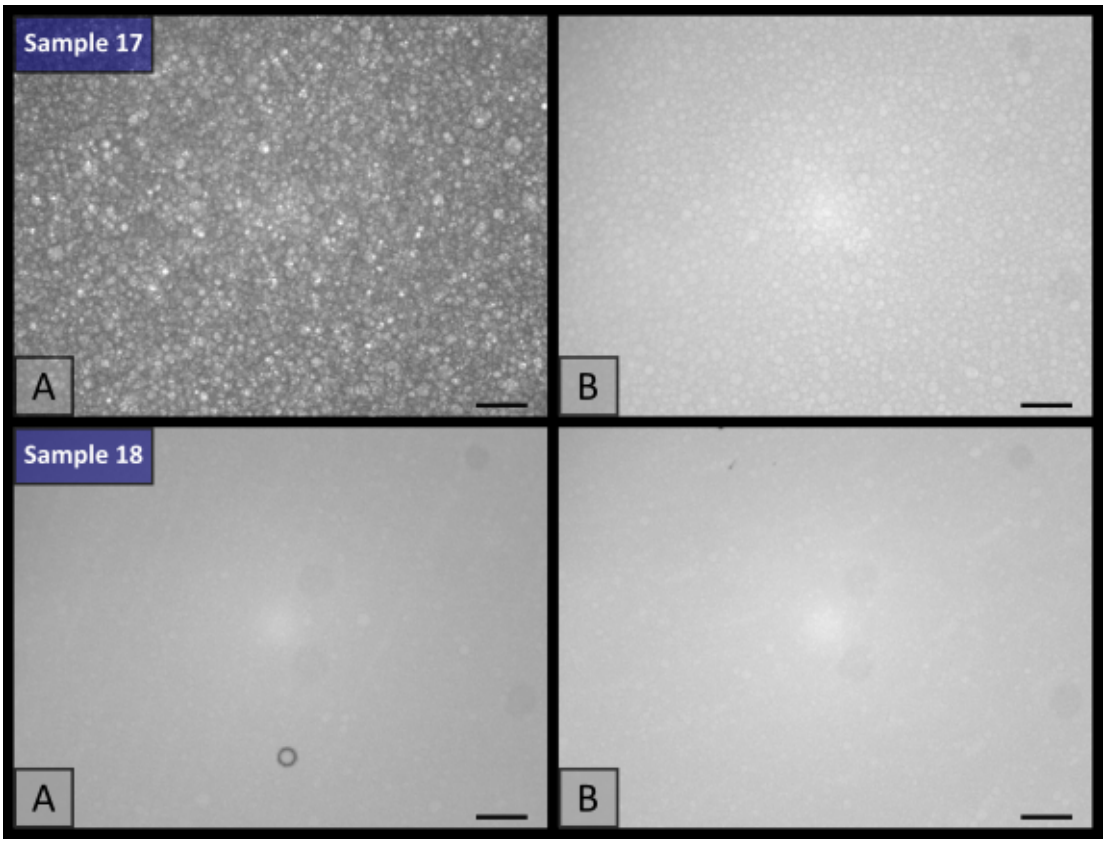

Figure A3. Optical microscopy images of emulsion templates from samples 17 & 18 immediately **(A)** after preparation and **(B)** 24 h later. Scale bar: 50 µm.

A.3 Mercury Instrusion Porosimetry

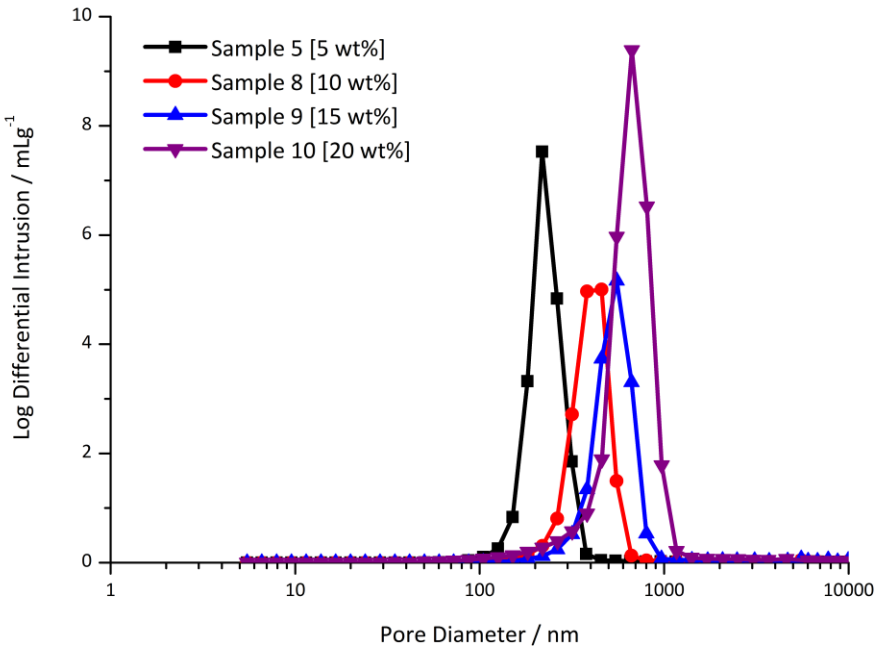

Figure A4. Pore Size distributions obtained from MIP for samples 5 & 8-10, prepared from 60 vol% internal phase emulsions with different surfactant levels.

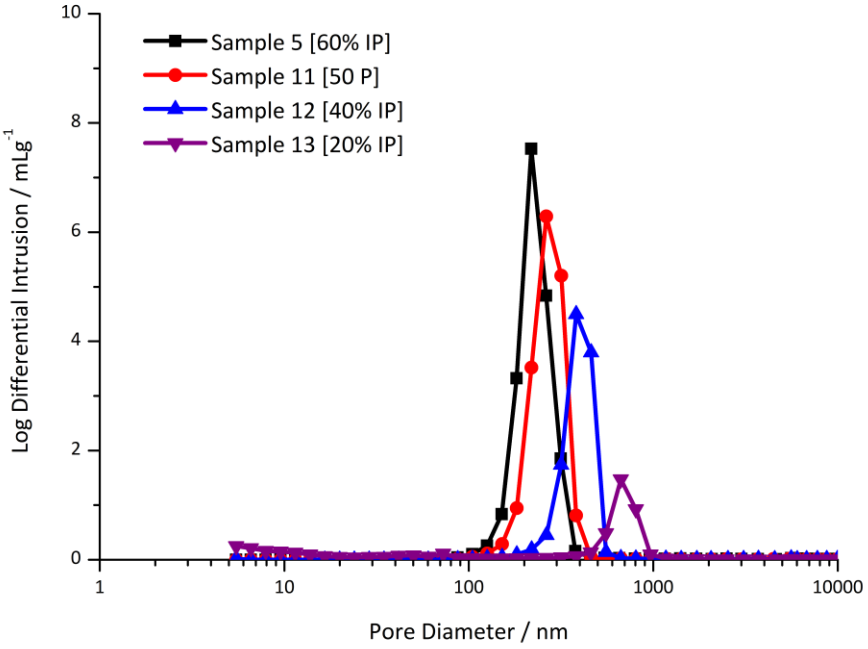

Figure A5. Pore Size distributions obtained from MIP for samples 5 & 11-13, prepared from different internal phase volumes.

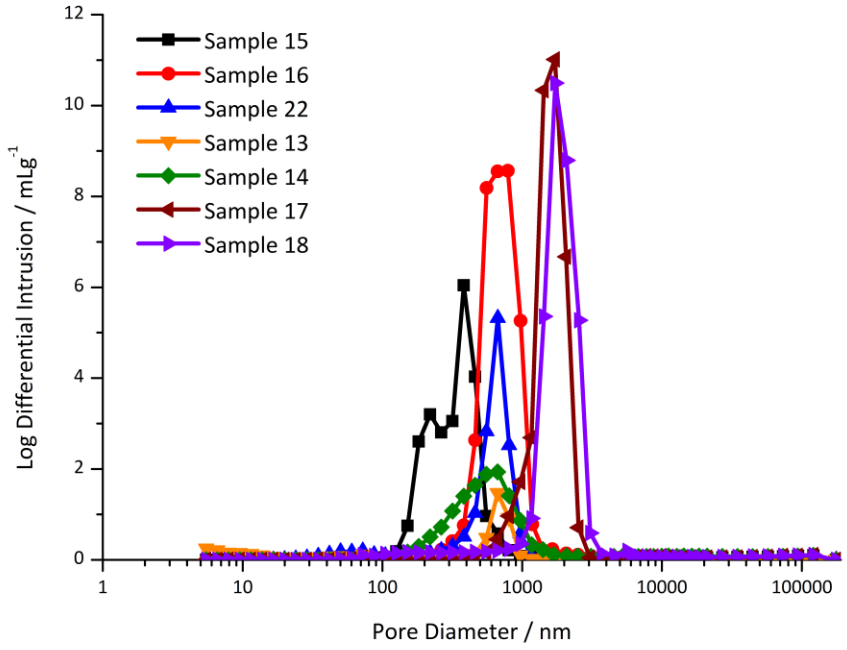

Figure A6. Pore Size distributions obtained from MIP for samples 13-18 & 22.

A.4 Swelling Characteristics

Table A1 Swelling characteristics for samples 1 - 22

Sample	φ_w / % [A]	φ_w / % [M]	φ_w / % [W]	ΔV / % [A]	ΔV / % [M]	ΔV / % [W]	m_s / % [A]	m_s / % [M]	m_s / % [W]
1	69 ± 2	78 ± 5	108 ± 5	- 2 ± 3	15 ± 4	48 ± 5	300 ± 40	120 ± 20	920 ± 20
2	58 ± 3	60 ± 6	96 ± 6	- 2 ± 1	11 ± 1	97 ± 20	123 ± 3	120 ± 30	450 ± 90
3	53 ± 9	60 ± 10	90 ± 5	0 ± 4	14 ± 5	81 ± 30	100 ± 40	110 ± 30	370 ± 70
4	53 ± 3	64 ± 3	98 ± 4	- 4 ± 3	10 ± 1	100 ± 20	100 ± 10	130 ± 20	480 ± 20
5	63 ± 3	71 ± 4	103 ± 2	0.4 ± 2	16 ± 3	90 ± 10	130 ± 20	160 ± 30	470 ± 12
6	59 ± 4	70 ± 3	101 ± 3	- 3 ± 2	12 ± 2	67 ± 6	130 ± 20	170 ± 30	490 ± 20
7	55 ± 5	66 ± 1	100 ± 3	- 3 ± 2	14 ± 2	140 ± 20	100 ± 30	130 ± 20	500 ± 20
8	62 ± 3	69 ± 5	114 ± 7	- 3 ± 3	14 ± 4	70 ± 10	130 ± 20	160 ± 30	510 ± 20
9	59 ± 1	70 ± 6	103 ± 4	- 2 ± 1	10 ± 5	80 ± 20	130 ± 3	150 ± 20	460 ± 30
10	62 ± 2	70 ± 3	118 ± 2	- 2 ± 4	15 ± 3	60 ± 10	131 ± 9	150 ± 30	540 ± 10
11	48 ± 5	62 ± 3	97 ± 4	- 2 ± 3	16 ± 4	80 ± 10	80 ± 20	120 ± 20	369 ± 5
12	36 ± 3	49 ± 1	91 ± 2	- 3 ± 2	12 ± 3	120 ± 20	44 ± 8	63 ± 5	307 ± 8
13	-	-	-	-	-	-	-	-	-
14	39 ± 1	52 ± 1	93 ± 2	- 3 ± 3	10 ± 3	100 ± 10	48 ± 3	70 ± 3	298 ± 7
15	67 ± 2	70 ± 2	102 ± 2	- 3 ± 3	15 ± 3	110 ± 40	180 ± 30	180 ± 30	650 ± 20
14	39 ± 1	52 ± 1	93 ± 2	- 3 ± 3	10 ± 3	100 ± 10	48 ± 3	70 ± 3	298 ± 7
15	67 ± 2	70 ± 2	102 ± 2	- 3 ± 3	15 ± 3	110 ± 40	180 ± 30	180 ± 30	650 ± 20
16	60 ± 10	78 ± 5	110 ± 6	- 4 ± 6	15 ± 7	130 ± 40	130 ± 50	210 ± 50	630 ± 30
17	55 ± 3	68 ± 3	93 ± 4	- 3 ± 1	10 ± 3	80 ± 20	130 ± 20	190 ± 20	410 ± 60
18	67 ± 3	81 ± 3	117 ± 6	- 1 ± 3	9 ± 4	80 ± 20	190 ± 30	250 ± 30	720 ± 20
19	-	-	-	-	-	-	-	-	-
20	-	-	-	-	-	-	-	-	-
21	-	-	-	-	-	-	-	-	-
22	48 ± 1	60 ± 1	102 ± 3	- 2 ± 1	12 ± 2	100 ± 30	67 ± 8	115 ± 5	390 ± 20

φ_w signifies the porosity, ΔV the change in volume of the polymer disk relative to the original volume and m_s indicates the mass of solvent present in the disk relative to the mass of the dry disk. [A] These values were determined through immersion in acetone. [M] These values were determined through immersion in MeOH. [W] These values were determined through immersion in H_2O. The composition of these samples can be found in **Table 3.1** and **Table 3.5**.

Chapter 4

Effect of shearing stress on the radial heterogeneity and chromatographic performance of styrene-based polymerised high internal phase emulsions prepared in capillary format

4.1 Introduction

The porous poly(AAm-*co*-MBAm) emulsion templated materials prepared in **Chapter 3** exhibited a significant degree of shrinkage during purification, which resulted in difficulties for the preparation in capillary format. In contrast, stable attachment to the capillary wall has previously been demonstrated for poly(HIPE)s prepared from water-in-oil emulsions [1-3]. This is potentially related to a lower degree of shrinkage/swelling that occurs for these materials when exposed to different solvent environments. For example, Tunç et al. [1] prepared poly(HIPE)s from isodecylacrylate and DVB in 100 µm i.d. capillaries for the separation of alkylbenzenes by CEC, while Choudhury et al. [3] reported the RPLC separation of alkylbenzenes using graphene oxide modified poly(Sty-*co*-DVB) poly(HIPE)s prepared in 200 µm i.d. capillaries.

However, to the best of my knowledge at the time of writing there exist no examples for the separation of larger molecules, such as proteins, using poly(HIPE)s prepared in capillary format in the literature. This is particularly surprising given polymer monoliths have been demonstrated to be highly suitable for the separation of proteins [4] and the use of capillary format has several advantages, including lower sample and solvent consumption, the reduction of peak broadening as a result of radial diffusion and increased sensitivity for MS detection [5]. In addition, relatively few reports have focused in depth on the influence of the poly(HIPE)s structure on the chromatographic performance [6-7], in particular when prepared in the narrow dimensions of a capillary.

In this chapter the preparation of poly(Sty-*co*-DVB) poly(HIPE)s in capillaries of various internal diameter was investigated and their applicability for the RPLC separation of a common protein mixture was assessed. This system was chosen as it has been extensively studied [8], and the chromatographic behaviour of conventional poly(Sty-*co*-DVB) monoliths under RPLC conditions is well documented [4]. Particular attention was paid to the influence of the poly(HIPE)s structure on the chromatographic performance, as well as any alterations in morphology that occurred as a result of the preparation in capillary format. The influence of emulsification energy on the materials structure and chromatographic performance was also studied, with particular attention to the degree of radial heterogeneity present in each case.

4.2 Experimental

4.2.1 Preparation of poly(Sty-*co*-DVB) poly(HIPE)s

Poly(Sty-*co*-DVB) poly(HIPE)s were prepared from a modified procedure of Hainey et al. [9]. The internal phase was prepared by dissolving 0.04 g of potassium persulfate (KPS) and 0.012 g of calcium chloride dihydrate in 18 mL of H_2O. This was added dropwise at a rate of 0.3 mL/min using a Harvard Apparatus Model 33 twin syringe pump to a continuous phase consisting of 0.594 g of Span® 80, 1.6 mL of Sty and 0.4 mL of DVB in a 100 mL round bottom flask with constant stirring at 300 rpm. After that, the resulting emulsion was passed through 20 cm of either 150, 250 and 540 µm i.d. surface-modified fused silica capillaries by hand using a 250 µL Hamilton® syringe. The syringe was initially filled with emulsion using a 25 G (5/8 in.) needle.

The emulsion emerging from the capillary outlet was collected in 4 mL glass vials. The capillaries were filled multiple times to limit the number of air bubbles or voids present and the ends were sealed with rubber. This was performed for at least three capillaries for each capillary i.d. Optical microscopy images of the emulsions immediately after preparation, and when passed through the capillaries, were collected. These capillaries were then placed horizontally in the water bath at 60 °C and cured for 48 h. The remaining

emulsion was transferred to a 25 mL glass vial as a bulk sample and this was immersed, along with the 4 mL vials, in the water bath at 60 °C for 48 h. Once cured the capillaries and vials were removed from the water bath. The bulk material from the vials was removed, cut into smaller pieces and washed using MeOH with a Soxhlet apparatus for 24 h, in order to remove the internal phase and any impurities, before being left to dry at 25 °C in a vacuum oven for 1 week. The capillaries were flushed with MeOH for 2 h and then with H_2O for 2 h using the capillary LC system at a flow rate of 2 µL/min.

For additional experiments involving the syringe pump to control the filling rate or the use of longer capillaries, the emulsion was prepared as described above. However, for experiments involving increased emulsification energy a modified procedure was adopted, where the internal phase was added dropwise at a rate of 1 drop per second to the continuous phase with constant stirring at 300 rpm, after which the emulsion was blended using an IKA Ultra Turrax T 25 homogeniser equipped with an S 25 N 10 G dispersing element (7.5-mm rotor) at 14 000 rpm for 2 min.

The polymer disks for porosity determination for the different emulsification energies were prepared as described above, except the emulsion was transferred to 10 mL disposable syringes (~1.5 cm in diameter). These were sealed and placed in the water bath at 60°C at an angle of ~45° from the horizontal to ensure any air bubbles migrated to the top of the syringe and polymerised for 48 h. Once cured these were removed from the syringe, cut into 0.5 cm thick pieces and then washed with MeOH using the Soxhlet apparatus for 24 h. These samples were then dried in a vacuum oven at 25 °C for 1 week.

4.3 Results and Discussion

4.3.1 Preparation of poly(Sty-*co*-DVB) poly(HIPE)s in capillary format

Poly(Sty-*co*-DVB) poly(HIPE)s were first prepared under low shear conditions using an emulsification rate of 300 rpm within surface modified fused silica capillaries of 150, 250 and 540 µm i.d. of 20 cm total length. These capillaries were initially surface modified as

this limits the formation of gaps between the monolith and the capillary wall that can result due to shrinkage during polymerisation [10]. This ensures that the mobile phase flows through the pores of the monolith and not between the monolith and the capillary wall.

SEM analysis (**Figure 4.1**) revealed that successful attachment of the monolith to the capillary wall was achieved in all cases. The images in **Figure 4.1** are taken at different magnifications to show the entire cross-section for each column. Images at the same magnification, showing a smaller section for each column, can be found in **Figure B1** in **Appendix B**. When MeOH and H_2O were pumped through these columns at flow rates between 0.5 and 10 µL/min the back pressure varied linearly with flow rate (**Figure 4.2**), indicating no significant compression or mechanical failure of the monolith occurred [10].

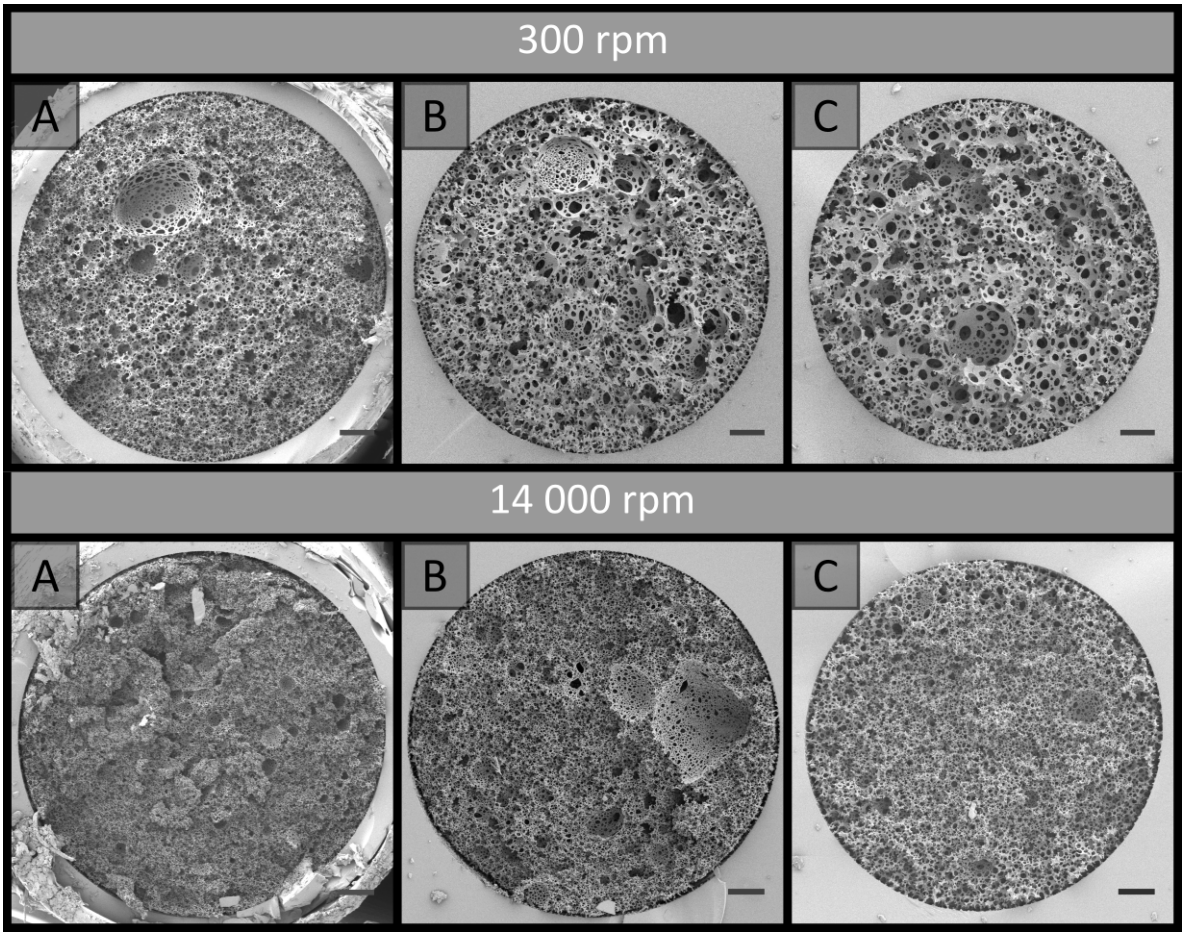

Figure 4.1. SEM images of poly(HIPE)s prepared from emulsions emulsified at 300 rpm or 14 000 rpm in fused silica capillaries of different i.d.: **A)** 540 µm, **B)** 250 µm and **C)** 150 µm. Scale bar is: **A)** 50 µm, **B)** 25 µm and **C)** 15 µm.

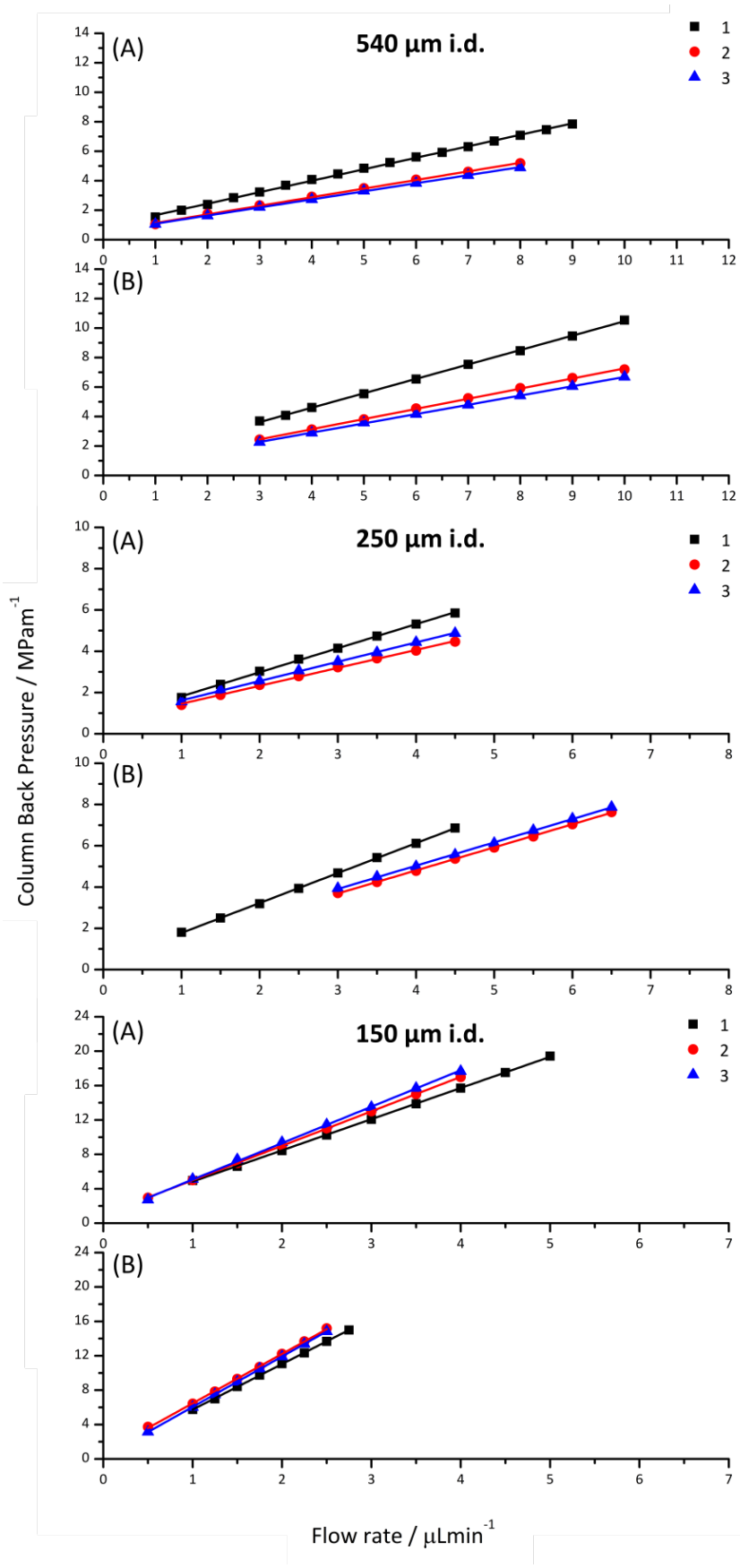

Figure 4.2. Plot of column back pressure (MPa/m) against flow rate (µL/min) for poly(Sty-*co*-DVB) poly(HIPE)s prepared from the same batch in different capillary i.d. using a shear rate of 300 rpm and using **A)** MeOH or **B)** H_2O as the mobile phase. For each capillary i.d. three replicates are shown, labeled 1, 2 & 3.

Table 4.1 Permeabilities (k) of poly(HIPE)s prepared from emulsions emulsified at 300 or 14 000 rpm in capillaries of different i.d. in MeOH and H_2O

	300 rpm		14 000 rpm	
Column i.d. / µm	Average k (MeOH) / × 10^{-13} m^2	Average k (H_2O) / × 10^{-13} m^2	Average k (MeOH) / × 10^{-13} m^2	Average k (H_2O) / × 10^{-13} m^2
540	3.5 ± 0.5	10 ± 6	0.3 ± 0.1	0.3 ± 0.2
250	4 ± 1	5 ± 2	1.6 ± 0.5	1.5 ± 0.3
150	1.6 ± 0.2	1.7 ± 0.2	2.1 ± 0.5	1.6 ± 0.2

This is important as poly(HIPE)s, in general, are considered to possess poor mechanical properties when exposed to compressive forces, as a result of their low foam density, and as discussed in the previous chapter this has been limiting for their application in a variety of areas [11-13]. However, these columns appeared mechanically stable over the range of flow rates utilised.

The back pressure produced by these columns was significantly lower in comparison to that of conventional monoliths, resulting in column permeabilities (**Table 4.1**) at least an order of magnitude larger. For example, monoliths prepared through phase separation from a porogen typically possess permeabilities in the range of (1-10) × 10^{-14} m^2 [5, 10, 14], as compared to the values obtained for these poly(HIPE)s which were in the range of (1-10) × 10^{-13} m^2. The values calculated when MeOH was employed as the mobile phase were (3.5 ± 0.5) × 10^{-13}, (4 ± 1) × 10^{-13} and (1.6 ± 0.2) × 10^{-13} when prepared in 540, 250 and 150 µm i.d. columns, respectively. These values were not statistically different from the values obtained using H_2O of (10 ± 6) × 10^{-13}, (5 ± 2) × 10^{-13} and (1.7 ± 0.2) × 10^{-13} for the 540, 250 and 150 µm i.d. columns, respectively. This suggested that no significant swelling or shrinkage occurred in both solvents. These relatively high permeabilities are due to the large windows these materials possess, which were in excess of 1 µm (**Table 4.2**).

While the permeability values between solvents were not statistically different it can be seen that the values obtained between different internal diameters differed (**Table 4.1**), with the permeability appearing to decrease with decreasing capillary i.d. at this emulsification energy. This indicates that although these poly(HIPE)s were prepared from the same emulsion, they possessed different porous properties [14]. If their porous

Table 4.2 Porous properties of poly(HIPE)s prepared from emulsions emulsified at 300 or 14 000 rpm using capillaries of different i.d.

		300 rpm			14 000 rpm		
#	Sample	V [a] / μm	W [b] / μm	D [c] / μm	V [a] / μm	W [b] / μm	D [c] / μm
1	Bulk	20 ± 10	2 ± 1	7 ± 4	4 ± 2	1.4 ± 0.4	3 ± 1
2	540 μm i.d.	20 ± 10	3 ± 2		6 ± 4	1.5 ± 0.8	-
3	540 μm i.d.[p]	17 ± 9	3 ± 2	7 ± 5	4 ± 2	1.2 ± 0.4	3 ± 2
4	250 μm i.d.	12 ± 7	3 ± 2		6 ± 4	1.4 ± 0.6	-
5	250 μm i.d.[p]	8 ± 3	2 ± 1	5 ± 2	4 ± 2	1.2 ± 0.5	3 ± 1
6	150 μm i.d.	8 ± 5	2 ± 1		4 ± 3	1.1 ± 0.4	-
7	150 μm i.d.[p]	5 ± 2	1.1 ± 0.5	4 ± 2	2.7 ± 0.8	1.6 ± 0.6	3 ± 1

[a] Average void diameter as determined from SEM. [b] Average window diameter as determined from SEM. [c] Average droplet diameter immediately after preparation or after being passed through capillary as determined from optical microscopy. [p] indicates emulsion that has been passed through 20 cm of capillary and cured.

morphologies were equivalent, each column would have the same back pressure for a given flow velocity, and hence the same permeability [10]. Examining the average void size of the poly(HIPE)s within the capillaries (**Table 4.2**) revealed a trend where the average void size appeared to decrease as the capillary i.d. decreased. For example, the average void size went from 20 ± 10 μm to 12 ± 7 μm and then to 8 ± 5 μm when the capillary i.d. was decreased from 540 (entry 2) to 250 (entry 4) and then to 150 μm (entry 6).

While the void size was observed to decrease with decreasing capillary i.d., the void size distribution obtained within the 540 μm i.d. column was identical to that of the bulk material (**Table 4.2** entry 1), suggesting that the shift in void size only occurred for capillary i.d.s less than 540 μm. This trend was more apparent for the emulsions that were cured after being passed through 20 cm of capillary (**Figure 4.3**), with the emulsion passed through the 540 μm i.d. capillary resembling that of the bulk material, while a decrease in the void size was visually apparent for the emulsions passed through the 250 and 150 μm i.d. capillaries (entries 5 & 7, respectively, in **Table 4.2**). In addition, passing the emulsion through the syringe and/or needle used for filling the capillaries did not appear to reduce the droplet and void size relative to the bulk material (**Figure 4.4**, **Table 4.3** & **Figure B2** in **Appendix B**). Decreases in the window size with reduced i.d. were also observed, consistent with the permeability measurements obtained.

The same trend was observed for the emulsion droplets immediately after being passed through the capillaries (**Table 4.2** & **Figure B3** in **Appendix B**). The droplet sizes observed

were consistent with the void sizes obtained after curing when passed through the 250 and 150 µm i.d. capillaries, suggesting these emulsions were stable during this time. However, the void sizes obtained were significantly larger for the bulk material and the emulsion that was passed through the 540 µm i.d. capillary. This indicates that some degree of coalescence occurred for these emulsions [15], and that by passing the emulsion through lower i.d. capillaries the stability of the emulsion was enhanced. The porosity of the bulk material was estimated to be 97.1 ± 0.2 % through immersion in MeOH, which is consistent with the 90 vol% internal phase utilised, but also suggested some degree of creaming may have occurred over time resulting in the slightly higher value [16], in addition to droplet coalescence. Higher experimental porosities are also sometimes observed due to the removal of surfactant during purification [17].

The porosity in acetone was consistent with that obtained in MeOH, with a value of 104 ± 7 %, while the volume change in both solvents was negligible (**Table B1** in **Appendix B**). This is potentially the reason why these poly(HIPE)s possessed stable attachment to the capillary wall in contrast to the hydrophilic materials prepared in **Chapter 3**. When Milli-Q H_2O was used as the solvent the centrifugal force applied was insufficient to force H_2O into the pores of the hydrophobic material, making these porosity measurements unreliable.

A decrease in the droplet size often corresponds to increases in the droplet packing and viscosity of the emulsion, which promotes increased stability [16]. This was also observed for the (paraffin-oil)-in-water emulsions prepared in **Chapter 3**. This is consistent with the observation that the emulsion, which initially exhibited a milky consistency, became more viscous after emerging from the 250 and 150 µm i.d. capillaries, resembling that of shaving cream, which is more representative of a HIPE. These results suggest that a physical alteration of the emulsion is occurring when it either enters and/or is passed through the capillary when the i.d. is below 540 µm.

Additionally, examination of the void size distributions revealed that when confined within the capillaries the void size distributions obtained were broader, even though their average void sizes were not statistically different from the cured emulsions that had been

Table 4.3 Porous properties of cured emulsions which had been passed through the syringe and the syringe and needle

Sample	V [a] / µm	W [b] / µm	D [c] / µm
Bulk	30 ± 10	4 ± 2	20 ± 10
Syringe	30 ± 10	4 ± 2	13 ± 8
Syringe + Needle	20 ± 10	4 ± 2	12 ± 6

[a] Average void diameter as determined from SEM. [b] Average window diameter as determined from SEM. [c] Average droplet diameter immediately after preparation as determined from optical microscopy.

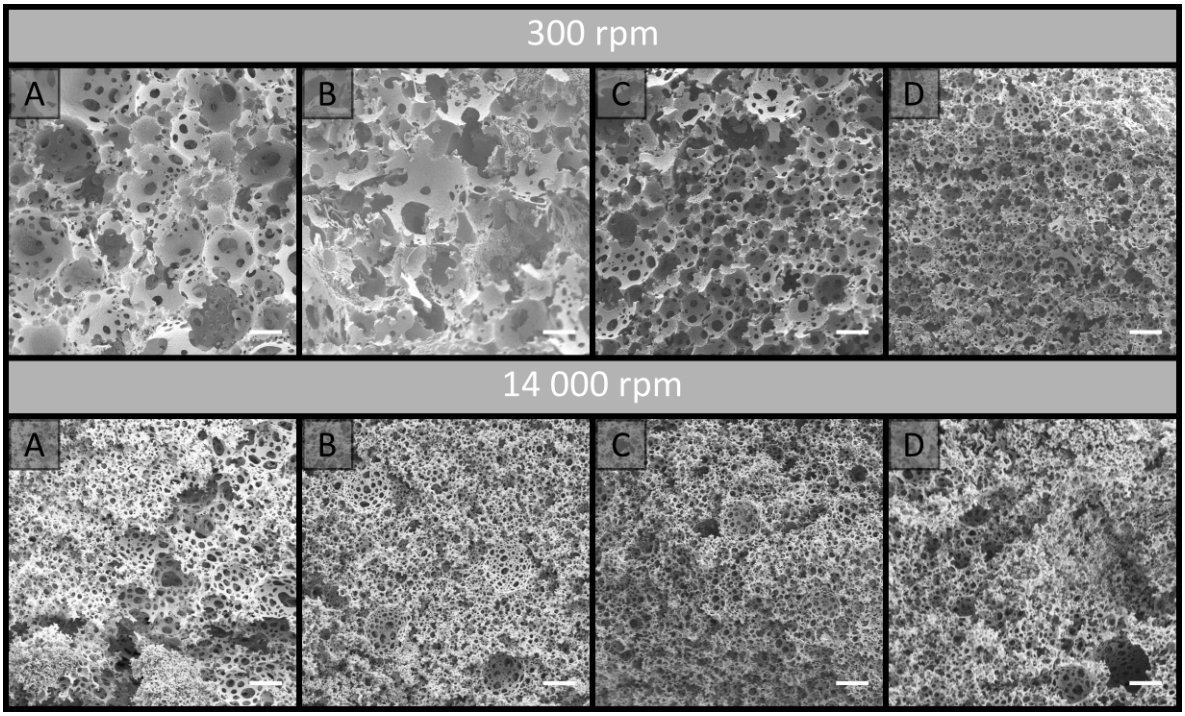

Figure 4.3. SEM images of poly(HIPE)s obtained by curing emulsions which had been emulsified at 300 or 14 000 rpm and passed through 20 cm of various i.d. capillaries at the same magnification. **A)** Bulk, **B**) 540 µm i.d., **C)** 250 µm i.d. and **D)** 150 µm i.d. Scale bar is 10 µm.

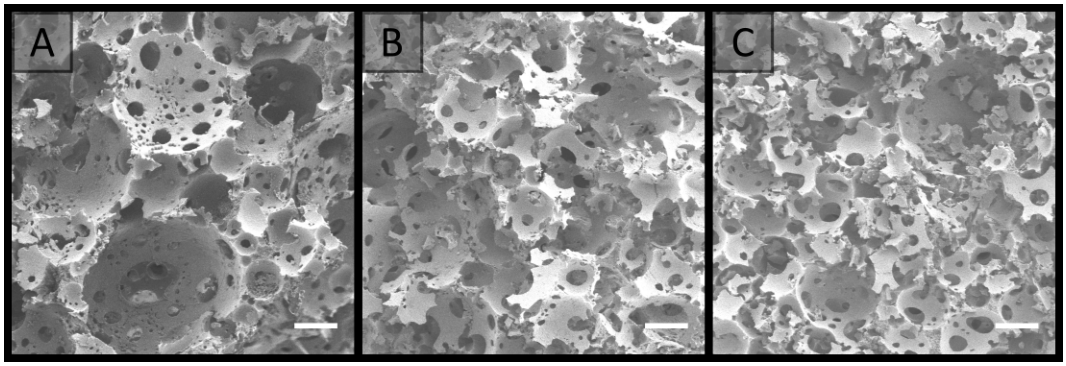

Figure 4.4. SEM images of poly(HIPE)s obtained by curing emulsions which had been emulsified at 300 rpm and passed through the syringe and/or needle. **A)** Bulk, **B)** Syringe and **C)** Syringe and needle. Scale bar is 20 µm.

passed through these capillaries (**Table 4.2**). Closer inspection of the capillary cross-sections (**Figure 4.1**) revealed the presence of radial heterogeneity, with small voids towards the outside of the capillaries and larger voids towards the centre. A plot of the average void size measured within the annulus formed from concentric circles, which differed in radius by 25 µm originating from the capillary wall, clearly demonstrates this trend (**Figure 4.5**). This increase in average void size did not appear to occur linearly with increased distance from the capillary wall.

In comparison, this radial distribution of voids was not obvious for the cured emulsions that had been passed through the respective capillaries (**Figure 4.3**), thus suggesting that the confinement within the capillary is having an additional effect on the resulting material. The presence of radial heterogeneity is particularly concerning from a chromatographic perspective as this can result in deviations from a plug flow profile, resulting in band broadening and compromised chromatographic performance [18].

Differences in the porous properties for polymer monoliths prepared using a porogen has also been observed when confined within capillaries of different internal diameter [10, 19-21]. In these cases the confinement resulted in a non-permeable sheath that forms at the

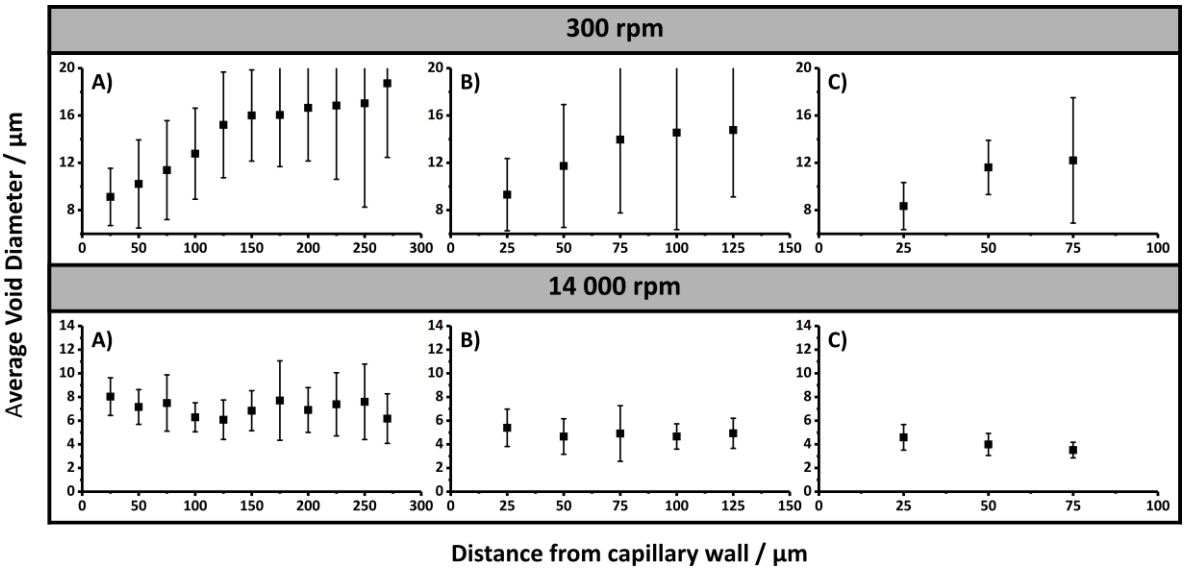

Figure 4.5. Plot of average void diameter with increased distance from capillary wall for poly(HIPE)s prepared with emulsification at 300 or 14 000 rpm within different capillary i.d.s: **A)** 540 µm, **B)** 250 µm and **C)** 150 µm.

capillary wall during curing, as a result of monomer diffusion, however its presence was only significant for internal diameters less than 50 µm where it occupied a significant proportion of the capillary dimensions. No significant wall effect was observed in this work (**Figure 4.1**), and even if present this could not account for the alteration in the emulsions structure itself.

A more likely explanation for the shift in porous properties is the shear associated with the emulsion droplets being forced through the narrow capillary inlet and/or traversing along the capillaries length. A higher degree of shear would be expected for narrower capillary i.d.s, thus resulting in increased fragmentation of the emulsion droplets into much smaller ones, which is consistent with the results obtained (**Table 4.2**). If the shift in the emulsions structure occurred gradually along the capillaries length, this would result in longitudinal heterogeneity.

To investigate this, a new batch of columns were prepared in 20 cm of 540, 250 and 150 µm i.d. capillaries and these were cross-sectioned at a variety of lengths between 2 and 18 cm from the capillary inlet. SEM images of these cross-sections were obtained (**Figures 4.6 - 4.8**). No significant trend was observed for the average void and window size along the columns length, as these were not statistically different (**Table 4.4**) for all columns investigated. This suggests that the shift in the emulsions structure occurs at the capillary inlet and not as the emulsion traverses the capillary, and only becomes significant when the capillary i.d. is less than 540 µm.

While a shift in void size along the capillaries length was not observed, these images revealed an additional concern for these materials with the presence of significantly larger voids that appeared randomly throughout the column. The presence of similar voids has also been observed for other poly(HIPE) systems [6, 22], for example the poly(GMA-*co*-EDMA) poly(HIPE)s discussed in **Chapter 1** (**Figure 1.16**). While coalescence can lead to the presence of larger voids, voids of intermediate size would have also been present if this was the case [17]. Ostwald ripening, on the other hand, could account for the presence of these larger voids, which were embedded in much smaller ones [23-24], however, given the significant difference in size, their origin is most likely from air bubbles [17]. These air

Table 4.4 Porous properties of poly(HIPE)s obtained from emulsions which had been emulsified at 300 rpm and cured in 20 cm of different i.d. capillaries then cut at different lengths from the capillary inlet

540 µm i.d.	**V [a] / µm**	**W [b] / µm**
2 cm	12 ± 5	3 ± 1
5 cm	12 ± 5	3 ± 1
10 cm	14 ± 6	3 ± 2
15 cm	12 ± 4	4 ± 2
18 cm	12 ± 7	2 ± 1
250 µm i.d.	**V [a] / µm**	**W [b] / µm**
2 cm	12 ± 4	3 ± 2
5 cm	9 ± 3	3 ± 2
10 cm	9 ± 4	2 ± 1
15 cm	8 ± 4	2 ± 1
18 cm	9 ± 7	3 ± 1
150 µm i.d.	**V [a] / µm**	**W [b] / µm**
2 cm	9 ± 4	3 ± 1
5 cm	8 ± 6	3 ± 1
10 cm	9 ± 4	2 ± 1
15 cm	9 ± 3	2.3 ± 0.9
18 cm	8 ± 6	2 ± 1

[a] Average void diameter as determined from SEM. [b] Average window diameter as determined from SEM.

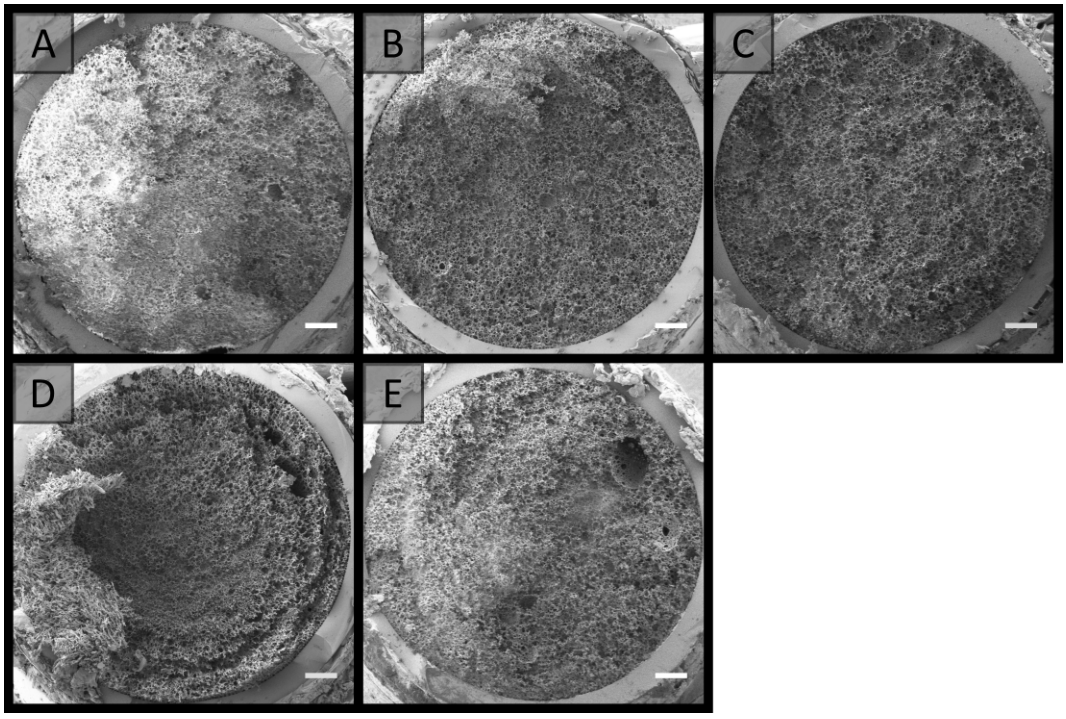

Figure 4.6. SEM images of poly(HIPE)s obtained from emulsions which had been emulsified at 300 rpm and cured in 20 cm of a 540 µm i.d. capillary then cut at different lengths from the capillary inlet. **A)** 2 cm, **B)** 5 cm, **C)** 10 cm, **D)** 15 cm and **E)** 18 cm. Scale bar is 50 µm.

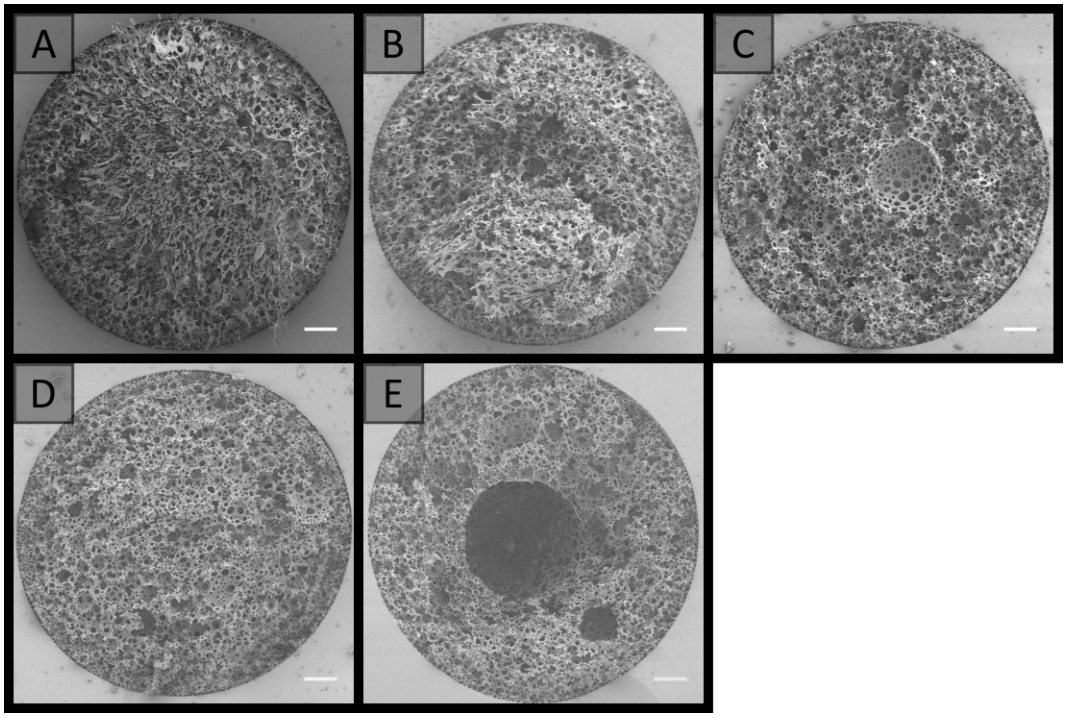

Figure 4.7. SEM images of poly(HIPE)s obtained from emulsions which had been emulsified at 300 rpm and cured in 20 cm of a 250 µm i.d. capillary then cut at different lengths from the capillary inlet. **A)** 2 cm, **B)** 5 cm, **C)** 10 cm, **D)** 15 cm and **E)** 18 cm. Scale bar is 25 µm.

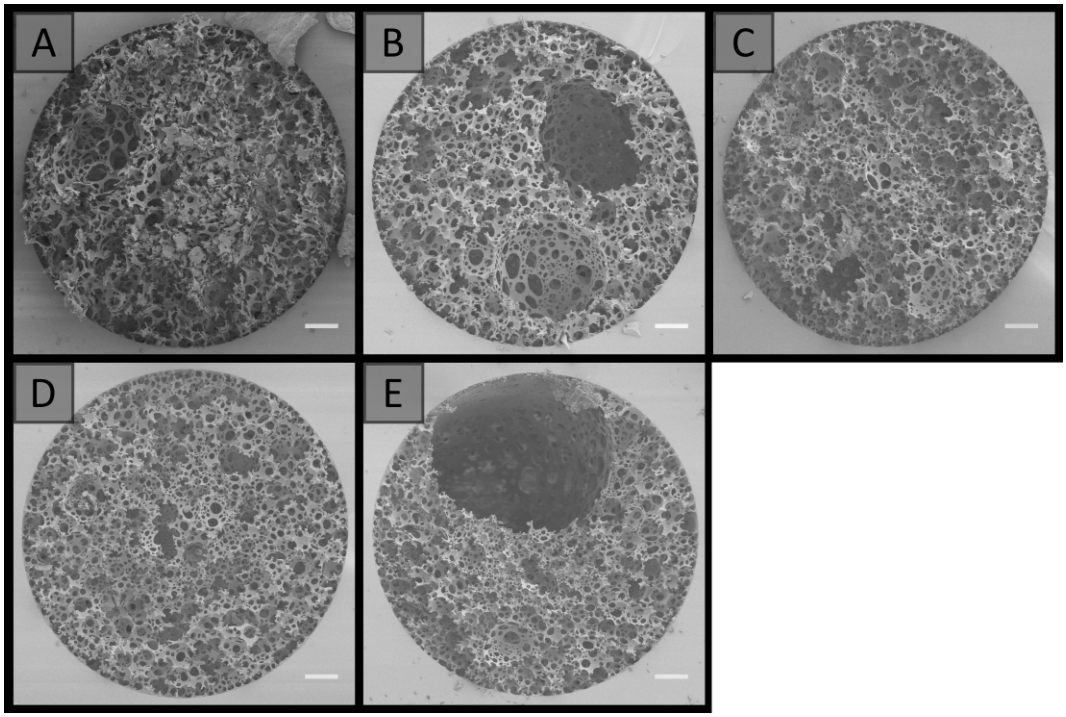

Figure 4.8. SEM images of poly(HIPE)s obtained from emulsions which had been emulsified at 300 rpm and cured in 20 cm of a 150 µm i.d. capillary then cut at different lengths from the capillary inlet. **A)** 2 cm, **B)** 5 cm, **C)** 10 cm, **D)** 15 cm and **E)** 18 cm. Scale bar is 15 µm.

bubbles, in addition to the radial heterogeneity that was also observed throughout the entire capillary length, will contribute to band broadening.

While the additional shear can account for the shift in droplet and void size observed, this does not explain the presence of radial heterogeneity when the emulsion was confined within the capillaries and cured. A plausible mechanism is capillary hydrodynamic fractionation (CHDF), where, assuming a laminar flow profile, larger droplets are excluded from the slower moving outer regions of the capillary [25]. This is in principle the same mechanism responsible for the separation of analytes of different sizes in hydrodynamic chromatography [26]. Instead of separating the larger droplets from the smaller ones over the length of the column, because the emulsion is being replenished at the inlet, this would result in their concentration towards the centre. This effect is typically only significant for small capillary dimensions, and the same void size distribution would be expected when cured outside the capillary as both the large and small droplets ultimately emerge from the capillary.

Another explanation is droplet coalescence as a result of a temperature gradient. Since the polymerisation process is exothermic and heat is easier to dissipate from the outer regions of the column as opposed to the interior, this can result in a thermal gradient across the capillaries diameter [27-28]. Since elevated temperatures are known to promote droplet coalescence [16], the droplets towards the centre of the column are more likely to undergo a higher degree of coalescence, and a radial temperature gradient would therefore account for the radial distribution of voids observed. However, this is typically only observed for larger column diameters for conventional polymer monoliths [27] and is therefore less likely. In addition, a similar temperature gradient would be expected for the emulsions cured outside the capillary, which would result in a similar void size distribution.

While both CHDF and the presence of a temperature gradient could account for the radial distribution of voids observed, neither provides an explanation for why the void size distribution was narrower when the emulsion was cured outside of the capillary. This could be as a result of the random nature in which these poly(HIPE)s were imaged, as it is

Table 4.5 Porous properties of poly(HIPE)s obtained from emulsions which had been emulsified at 300 rpm and passed through 20 cm of 250 or 150 µm i.d. capillaries at different rates

Filling	**250 µm**			**150 µm**		
Rate / µLmin^{-1}	V [a] / µm	W [b] / µm	D [c] / µm	V [a] / µm	W [b] / µm	D [c] / µm
10	30 ± 10	5 ± 3	10 ± 5	21 ± 7	4 ± 2	9 ± 5
25	30 ± 10	4 ± 2	11 ± 6	30 ± 10	5 ± 4	8 ± 4
50	30 ± 10	4 ± 2	8 ± 5	30 ± 10	4 ± 2	9 ± 5
100	21 ± 9	3 ± 2	9 ± 5	19 ± 8	3 ± 1	9 ± 5

[a] Average void diameter as determined from SEM. [b] Average window diameter as determined from SEM.
[c] Average droplet diameter immediately after preparation as determined from optical microscopy.

difficult to know exactly where a section of the bulk material being imaged was located. Alternatively, the introduction of a small number of air bubbles to the capillary during filling, which become large voids after curing, could account for the broader void size distribution.

Regardless of the mechanism responsible for the radial heterogeneity observed within the capillaries, the influence of passing the emulsion through the capillary inlet, as a result of the additional shear, is clear. While the capillary i.d. has already been shown to influence the resulting droplet diameter, the rate at which the emulsion is forced through the inlet is also expected to influence the emulsions structure, with higher rates corresponding to greater shear. This was investigated by filling 20 cm of 250 µm and 150 µm i.d. capillaries at different rates between 10 and 100 µL/min using a syringe pump, instead of filling by hand. No significant difference between the droplet and void size distributions (**Table 4.5**, **Figures 4.9 - 4.10** & **B4 - B5** in **Appendix B**) were observed. However, given the viscous nature of the emulsion emerging from the capillary outlet, this could simply have been a result of the increase in back pressure resulting in difficulties in accurately controlling the flow, particularly if the maximum back pressure of the pump (99.5 PSI or 6.86 bar) was exceeded.

An alternative method was therefore employed which involved filling the capillaries by hand using different lengths, as increases in capillary length correlate to higher back pressures and therefore lower flow velocities. This was performed for both the 250 and 150 µm i.d. capillaries using capillary lengths between 5 and 60 cm. A clear trend was observed with both the droplet and corresponding void size decreasing with decreases in the capillary length for both capillary i.d.s (**Table 4.6**, **Figures 4.11 - 4.12** & **B6 - B7** in

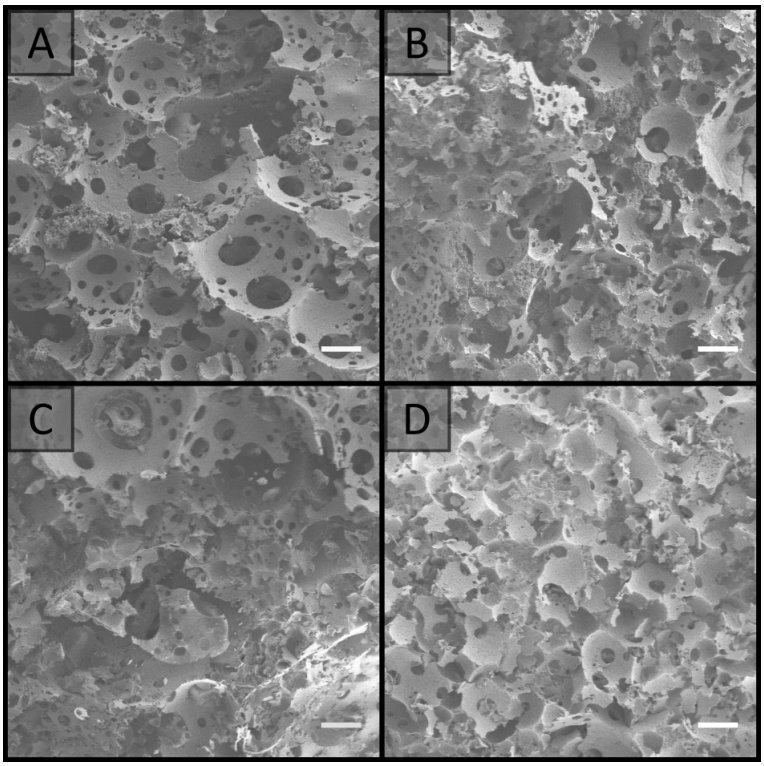

Figure 4.9. SEM images of poly(HIPE)s obtained from emulsions which had been emulsified at 300 rpm, passed through 20 cm of 250 µm i.d. capillary at different rates and cured. **A)** 10 µL/min, **B)** 25 µL/min, **C)** 50 µL/min and **D)** 100 µL/min. Scale bar is 15 µm.

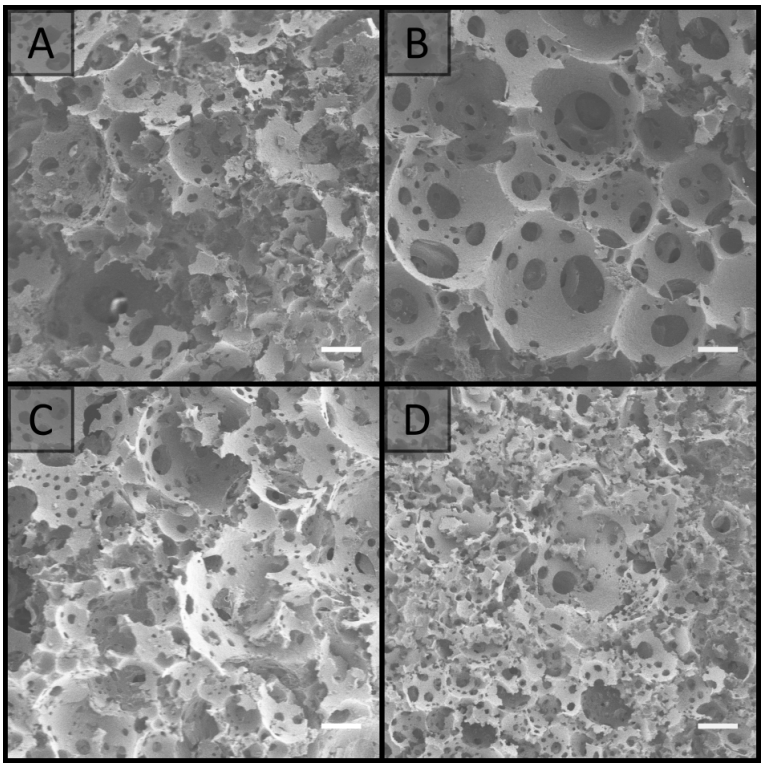

Figure 4.10. SEM images of poly(HIPE)s obtained from emulsions which had been emulsified at 300 rpm, passed through 20 cm of 150 µm i.d. capillary at different rates and cured. **A)** 10 µL/min, **B)** 25 µL/min, **C)** 50 µL/min and **D)** 100 µL/min. Scale bar is 15 µm.

Table 4.6 Porous properties of poly(HIPE)s prepared from emulsions emulsified at 300 rpm and passed through different lengths of 250 or 150 µm i.d. capillaries

Length of		**250 µm**			**150 µm**	
Capillary / cm	V [a] / µm	W [b] / µm	D [c] / µm	V [a] / µm	W [b] / µm	D [c] / µm
5	8 ± 3	1.7 ± 0.7	3 ± 1	6 ± 2	1.9 ± 0.8	3 ± 1
10	9 ± 3	2.0 ± 0.7	4 ± 2	10 ± 4	3 ± 1	4 ± 2
20	10 ± 8	2 ± 1	5 ± 2	9 ± 5	2.3 ± 0.8	6 ± 3
30	10 ± 5	2.0 ± 0.7	6 ± 2	19 ± 9	4 ± 2	6 ± 3
40	10 ± 6	3 ± 2	6 ± 3	20 ± 10	3 ± 2	8 ± 4
50	14 ± 5	3 ± 2	7 ± 3	20 ± 10	4 ± 2	10 ± 5
60	15 ± 6	3 ± 2	11 ± 5	20 ± 10	5 ± 2	10 ± 4

[a] Average void diameter as determined from SEM. [b] Average window diameter as determined from SEM. [c] Average droplet diameter immediately after being passed through capillary as determined from optical microscopy.

Appendix B). This is consistent with the higher shear associated with higher flow velocities, resulting in increased fragmentation of the droplets as they are forced through the inlet. In all cases the droplet size observed was smaller than the void size obtained after curing suggesting a degree of coalescence occurred.

These results are particularly concerning as the use of low shear mixers for the preparation of poly(HIPE)s for separation science is popular, with most reports utilising shear rates in the order of 300 rpm [1, 3, 6-7, 22, 29-30], as this typically affords larger void and window sizes, allowing high permeabilities to be achieved. However, it is apparent that when these materials are prepared using capillaries with internal diameters less than 540 µm significantly different structures are obtained compared to the bulk material, with the capillary i.d. and filling rate having a significant effect. This makes it extremely difficult to predict the behaviour of these materials and in particular control and/or alter their morphology based on the original emulsification conditions, which is the main advantage of using a templating approach.

In contrast, relatively few reports exist where shear rates in excess of 300 rpm are employed for the preparation of poly(HIPE)s for separation applications [31-34], of which most utilise shear rates in the order of 1000 - 3000 rpm using overhead stirrers [31-33]. While the use of high energy mixers with shear rates in excess of 10 000 rpm for the preparation of poly(HIPE)s is not uncommon [34-35], their use in this field is extremely limited [34]. Presumably this is due to the reduced permeability these materials would possess as a result of the smaller voids and windows [11].

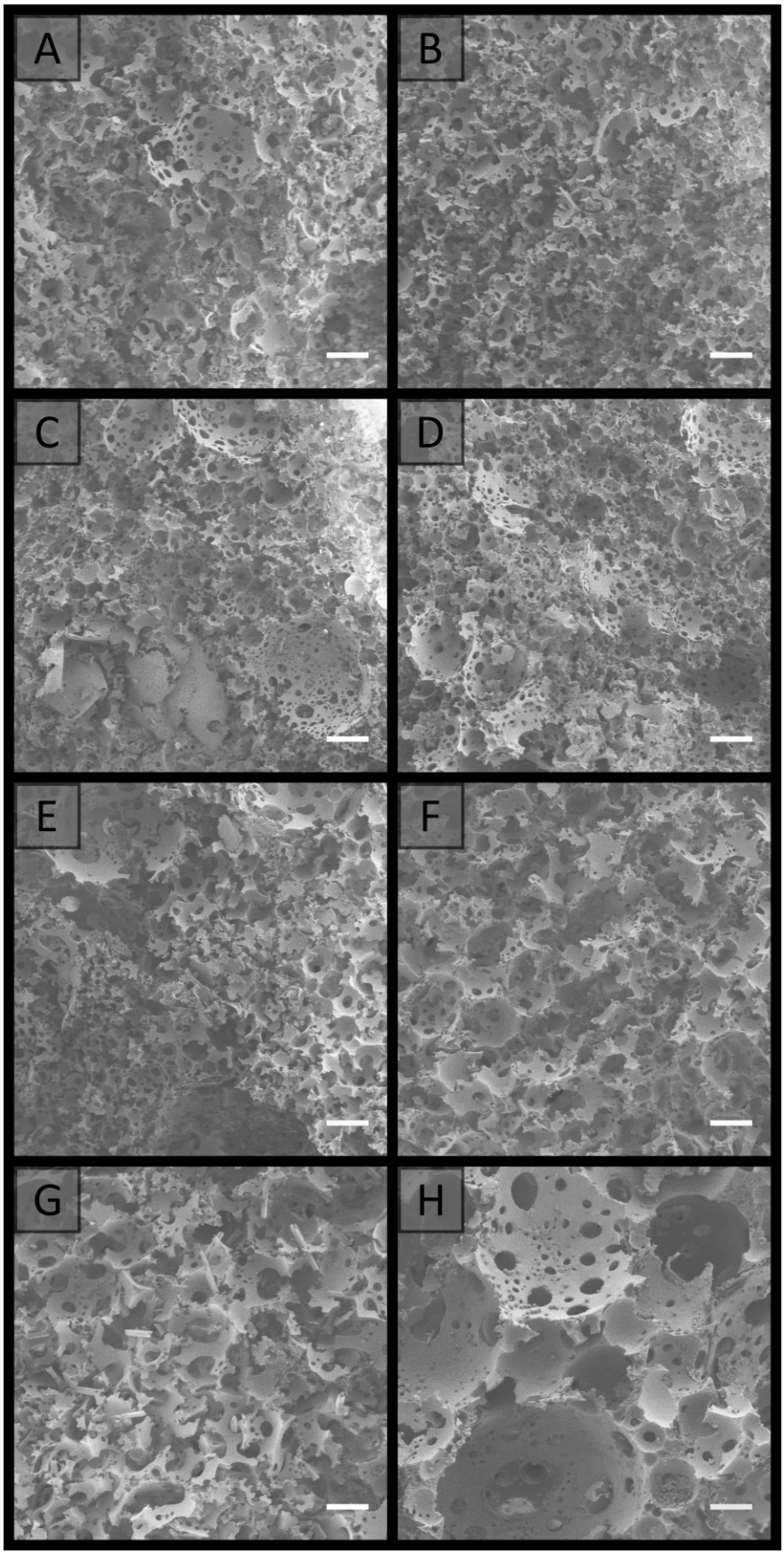

Figure 4.11. SEM images of poly(HIPE)s obtained from emulsions which had been emulsified at 300 rpm and passed through different lengths of 250 µm i.d. capillary and then cured. **A)** 5 cm, **B)** 10 cm, **C)** 20 cm, **D)** 30 cm, **E)** 40 cm, **F)** 50 cm, **G)** 60 cm and **H)** Bulk. Scale bar is 15 µm.

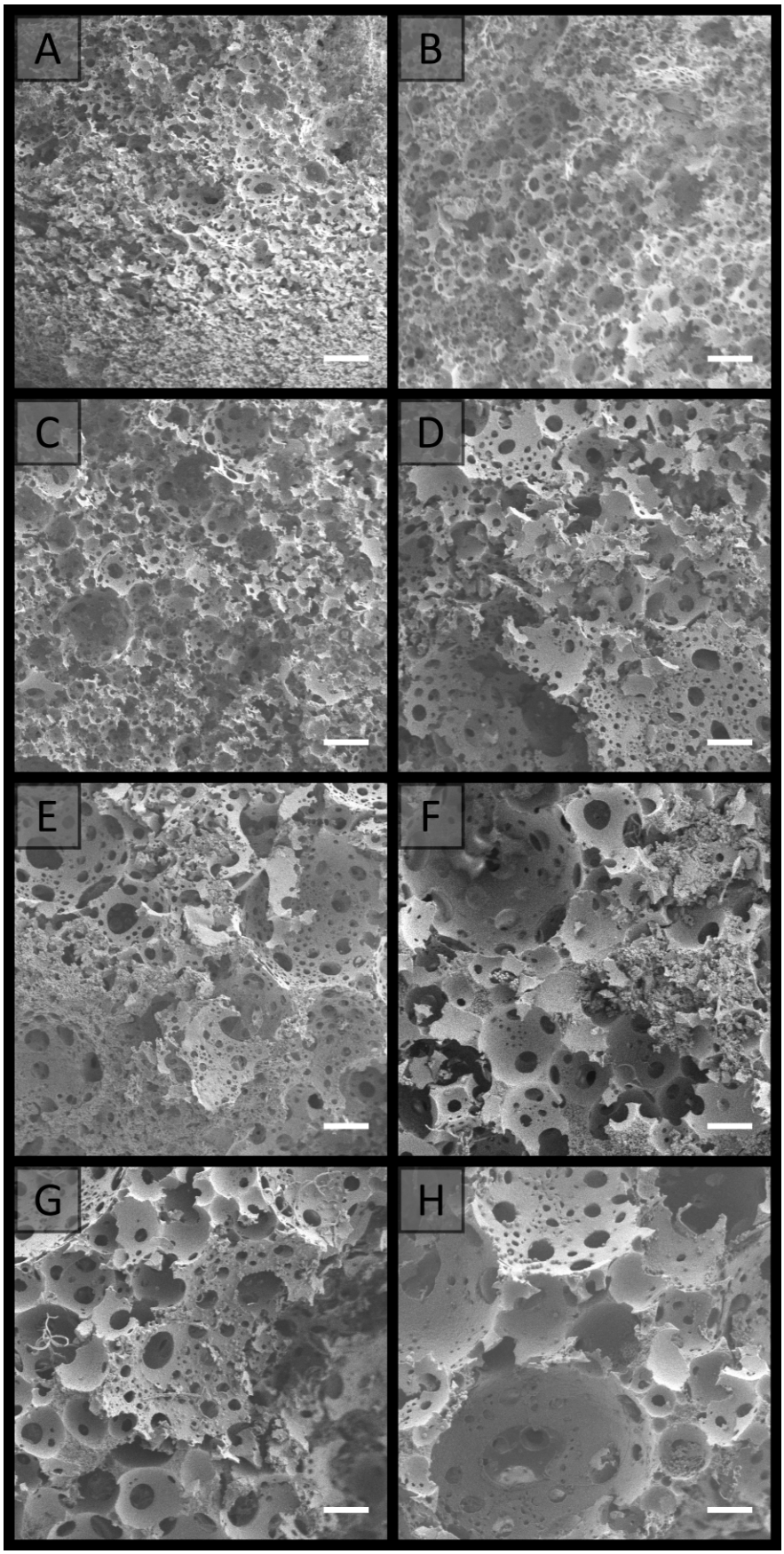

Figure 4.12. SEM images of poly(HIPE)s obtained from emulsions which had been emulsified at 300 rpm and passed through different lengths of 150 µm i.d. capillary and then cured. **A)** 5 cm, **B)** 10 cm, **C)** 20 cm, **D)** 30 cm, **E)** 40 cm, **F)** 50 cm, **G)** 60 cm and **H)** Bulk. Scale bar is 15 µm.

While this is a valid concern, the use of high energy mixers can result in emulsions with increased stability and yield stress, due to the decrease in droplet size and associated increase in droplet packing [11], as well as narrower droplet size distributions [17]. This is potentially beneficial for the preparation in capillary format, as an increase in yield stress reduces the influence of additional shear on the emulsions structure, while the increased stability and/or narrower droplet size distribution may reduce the degree of radial heterogeneity present, depending on the mechanism responsible. This was investigated by employing a homogeniser and utilising a shear rate of 14 000 rpm for emulsification. The emulsion obtained possessed the consistency of shaving cream, in contrast to the milky consistency obtained at the lower shear rate, suggesting this emulsion possessed a higher yield stress. Optical microscopy revealed an average droplet diameter of 3 ± 1 µm (**Table 4.2**), which was lower but not statistically different to the average droplet diameter of 7 ± 4 µm obtained using a shear rate of 300 rpm. However, the droplet size distribution obtained using the higher emulsification energy was narrower.

Upon curing an average void diameter of 4 ± 2 µm was obtained, which was not statistically different to the initial droplet size suggesting minimal coalescence occurred, but this was significantly lower than the average void diameter of 20 ± 10 µm obtained using the lower shear rate, highlighting the enhanced stability of this emulsion. The void size distribution was also narrower. Even though the void size was lower, the average window diameters were not statistically different with a value of 1.4 ± 0.4 µm for emulsification at 14 000 rpm and 2 ± 1 µm for emulsification at 300 rpm. The porosity of the bulk material was also consistent with that obtained with the lower emulsification energy with a value of 97 ± 4 % when immersed in MeOH, compared to 97.1 ± 0.2%, suggesting that the use of increased emulsification energy had only altered the void size and void size distribution of the poly(HIPE) obtained. The specific surface areas were also similar with values of 21.1 ± 0.8 m^2/g and 25.8 ± 0.7 m^2/g for emulsification at 14 000 rpm and 300 rpm, respectively.

When the emulsion was passed through 20 cm of 540, 250 and 150 µm i.d. capillary, no alteration in the droplet size (**Table 4.2** & **Figure B8** in **Appendix B**) or corresponding void and window size (**Table 4.2** & **Figure 4.3**) was apparent, indicating that the emulsion

preserved its structure when forced through the capillary inlet as a result of its increased yield stress. In all cases the void sizes obtained were consistent with the initial droplet size observed by optical microscopy, indicating the emulsions stability was not compromised when it was forced through the capillary. When confined within these capillaries and cured, excellent attachment to the capillary wall was achieved (**Figure 4.1**) and the resulting poly(HIPE)s again possessed similar void and window sizes compared to the bulk material (**Table 4.2**). However, the void size distributions were again slightly broader within the capillaries. Examination of the capillary cross-sections revealed the absence of any obvious radial heterogeneity, and no clear trend in the average void size with distance from the capillary wall was observed (**Figure 4.5**).

In terms of column permeabilities (**Table 4.1**), the values obtained for both the 250 µm and 150 µm i.d. columns were not statistically different, with permeabilities of $1.6 \pm 0.5 \times 10^{-13}$ m^2 and $2.1 \pm 0.5 \times 10^{-13}$ m^2 in MeOH, consistent with their similar porous properties. These values are not statistically different from the value of $1.6 \pm 0.2 \times 10^{-13}$ m^2 obtained for the poly(HIPE) prepared in the 150 µm i.d. capillary using a shear rate of 300 rpm. This is not unexpected as these materials shared similar void and window sizes (**Table 4.2**). This suggests that the use of the higher emulsification energy resulted in a similar overall structure to that achieved when the emulsion was forced through the 150 µm i.d. capillary when emulsified under low shear, albeit with the absence of radial heterogeneity when prepared in capillary format. As such the permeability did not appear to be significantly compromised through the use of a high energy mixer.

In contrast, the permeability obtained for the poly(HIPE) prepared in the 540 µm i.d. capillary was significantly lower with a value of $0.3 \pm 0.1 \times 10^{-13}$ m^2 using MeOH as the mobile phase (**Table 4.1**), despite it possessing similar void and window sizes (**Table 4.2**). The permeability of these materials does not depend solely on average window size, but rather on the smallest window in the flow path [17]. Therefore, even though these materials shared similar average window sizes, in the case of the poly(HIPE) prepared in the 540 µm i.d. capillary it is likely that a small number of smaller windows existed in the flow path resulting in its reduced permeability. For all columns the permeabilities obtained in both MeOH and H_2O were similar (**Table 4.1**), suggesting limited shrinkage

and/or swelling occurred in these solvents, and they appeared mechanically stable with a linear increase in back pressure over the flow rates utilised (**Figure 4.13**).

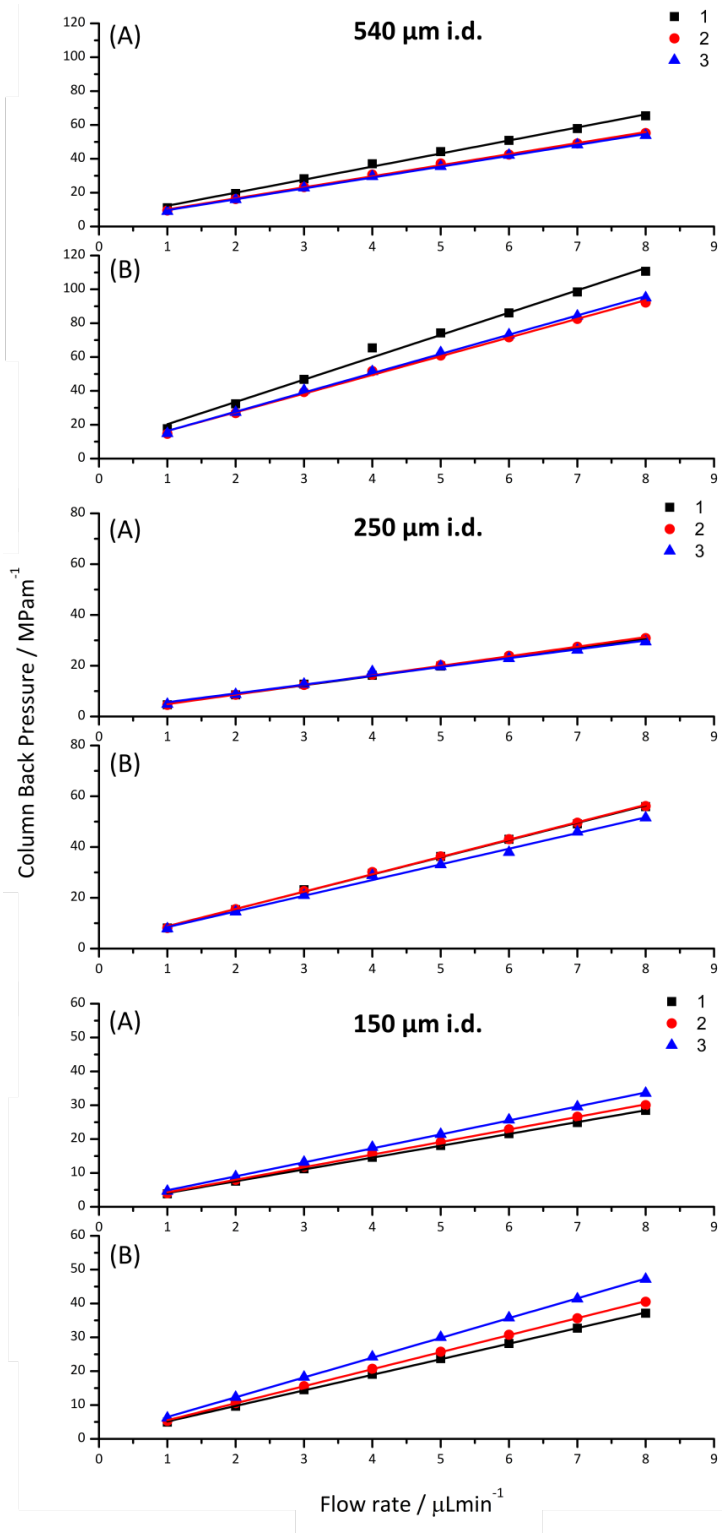

Figure 4.13. Plot of column back pressure (MPa/m) against flow rate (µL/min) for poly(Sty-*co*-DVB) poly(HIPE)s prepared from the same batch in different capillary i.d. using a shear rate of 14 000 rpm and using **A)** MeOH or **B)** H_2O as the mobile phase. For each capillary i.d. three replicates are shown, labeled 1, 2 & 3.

The use of increased emulsification energy appears to correspond to emulsions that are capable of preserving their structure when forced through the narrow capillary inlets as a result of the increased yield stress. While similar porous properties were observed to that obtained by passing the emulsion prepared at low shear through the 150 µm capillary, the increase in emulsion stability and/or the narrower droplet size distribution appears to have eliminated the presence of radial heterogeneity. Thus these poly(HIPE)s appear to be better candidates as stationary phases for chromatography. However, the use of high energy mixers is not without disadvantages as they are known to introduce air bubbles, which can expand non-uniformly during polymerisation resulting in irregular voids [36]. The presence of these voids can clearly be seen in **Figure 4.1B**, and like those observed in the case of the materials prepared under low shear, these will contribute to band broadening.

4.3.2 Chromatographic Performance

While HPLC is an important technique for the separation of a variety of compounds, it is also a good technique for providing insight into the column bed heterogeneity, as the separation resolution is strongly influenced by eddy dispersion [37]. The performance of these poly(HIPE)s for the separation of proteins in liquid chromatography was therefore evaluated by investigating their ability to separate a standard protein mixture consisting of ribonuclease A, lysozyme and α-chymotrypsinogen A, under reversed phase conditions. This particular mixture was chosen as the separation of these compounds using poly(styrene)-based monoliths by RPLC is well documented [4]. The separations obtained for all columns prepared in this work are shown in **Figure 4.14** using identical gradient conditions and the same flow rate.

Higher protein concentrations were utilised for the 540 µm i.d. columns to ensure the peaks could adequately be identified from the baseline and provide similar peak intensities, while the same flow rate was utilised to ensure the front of the gradient reached the inlet of the capillary at the same time and that the separation performance was not influenced by the dwell volume of the LC system [5, 38].

Examination of the chromatograms obtained for the poly(HIPE)s prepared using the homogeniser at 14 000 rpm revealed a significant improvement in separation resolution of the protein mixture as the capillary i.d. was decreased. Significant co-elution was observed for all proteins for the poly(HIPE) in the 540 µm i.d. capillary, while α-chymotrypsinogen A was distinguishable from the peak corresponding to both ribonuclease A and lysozyme for the 250 µm i.d. capillary. In contrast, all proteins along with the impurity peak corresponding to ribonuclease A and lysozyme were distinguishable when the internal diameter was reduced to 150 µm. Decreases in the column i.d. have previously been observed to result in improvements in the chromatographic performance for poly(Sty-*co*-DVB) monoliths [39], however this was as a result of differences in their porous properties as a result of confinement within narrower capillaries. Here, the porous properties of the poly(HIPE)s were similar (**Tables 4.1** & **4.2**) and thus this is the result of a different effect.

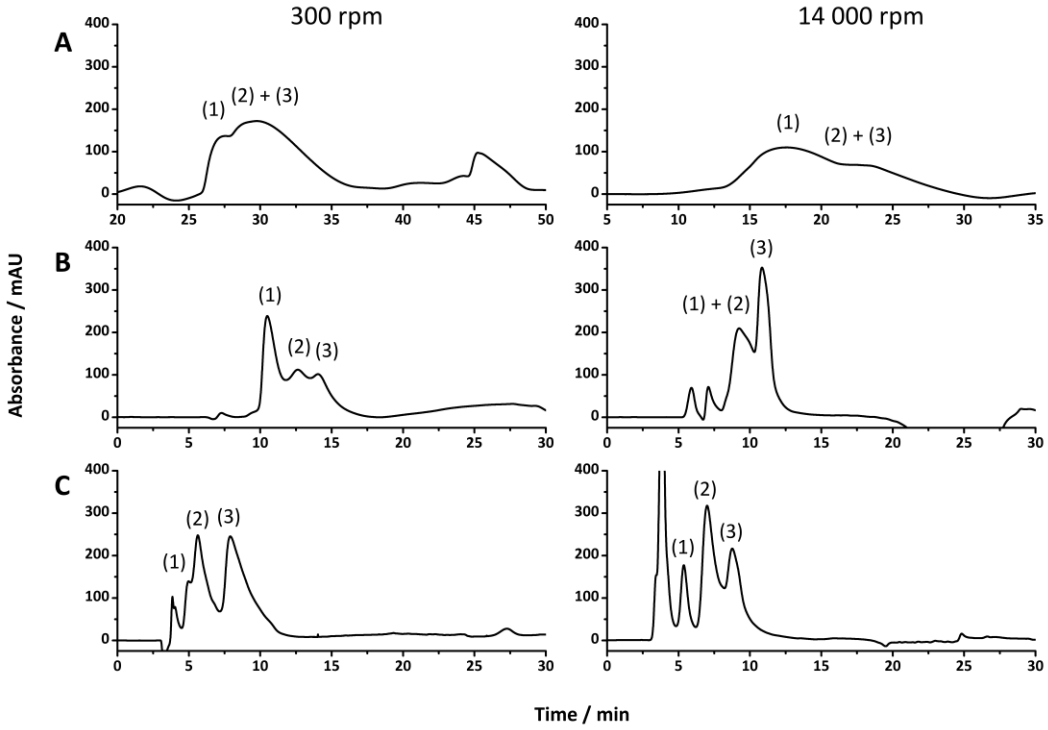

Figure 4.14. The separation of ribonuclease A (1), lysozyme (2) and α-chymotrypsinogen A (3) under reversed-phase conditions. Conditions: 18 cm of different i.d. columns: **(A)** 540 µm i.d., **(B)** 250 µm i.d., **(C)** 150 µm i.d., prepared from emulsions using different emulsification energies. Eluent A was 0.1 vol% formic acid in Milli-Q H_2O, and eluent B was 0.1 vol% formic acid in ACN; injection volume, 1 µL; protein concentration, 0.05 mg/mL for **(B)** and **(C)** and 0.3 mg/mL for **(A)**. Gradient: linear gradient 15 to 90% B in 15 min and then isocratic elution at 90% B for 5 min before returning to 15% B in 5 min; flow rate, 2.0 µL/min. UV detection at 214 nm.

The increase in performance is more likely as a result of the decrease in residence time due to the increased flow velocity, given the flow rate utilised for all columns was identical. For example, when a flow rate of 2 µL/min is utilised the flow velocities for 150 µm, 250 µm and 540 µm i.d. columns are 1.89×10^{-3} ms^{-1}, 0.679×10^{-3} ms^{-1} and 0.146×10^{-3} ms^{-1}, respectively. As such, the residence time within the 540 µm i.d. capillary is significantly longer than that of the 150 µm i.d. capillary, resulting in an increase in band broadening and significant co-elution of the proteins.

In contrast, an increase in chromatographic performance with decreasing capillary i.d. was not observed in all cases for the poly(HIPE)s prepared using an emulsification rate of 300 rpm. While a decrease in capillary i.d. from 540 µm to 250 µm resulted in a significant improvement in chromatographic performance, with the three proteins peaks clearly identifiable, significant co-elution between ribonuclease A and lysozyme was observed upon decreasing the capillary i.d. further to 150 µm. This could suggest that the porous properties of the poly(HIPE) in the 250 µm i.d. column was superior to that in the 150 µm i.d. column for the separation of these proteins, however this could simply have been a result of the increase in flow velocity.

While comparisons made between columns of different internal diameter at the same flow rate are not reliable, comparisons made between poly(HIPE)s prepared within the same capillary i.d. are more representative. In the case of both the 540 µm and 150 µm i.d. capillaries the poly(HIPE)s prepared using an emulsification rate of 14 000 rpm offered improved chromatographic performance. In contrast, for the separations obtained using the 250 µm i.d. capillaries the performance of the poly(HIPE)s obtained under low shear was superior, as significant co-elution was observed for ribonuclease A and lysozyme for the poly(HIPE)s prepared under high shear. As suggested, this could indicate that the morphology achieved by passing the emulsion prepared under low shear through the 250 µm i.d. capillary was better suited for this application, given the similar porous properties obtained for all columns prepared under high shear (**Table 4.2**).

In order to achieve a more reliable comparison an additional separation was performed for this column using the same flow velocity as that for the 150 µm i.d. columns and the

same protein concentration relative to column volume, to ensure a similar column load [10]. **Figure 4.15** shows the comparison between this separation and that obtained using the poly(HIPE) prepared under high shear in the 150 µm i.d. column. From this it appears that the poly(HIPE) prepared using high shear, in the 150 µm i.d. capillary, actually offered significantly improved chromatographic performance and the best separation achieved overall, as the increase in flow velocity and protein loading resulted in significant co-elution between ribonuclease A and lysozyme for the poly(HIPE) prepared under low shear in the 250 µm i.d. column. This co-elution was not as significant as that of the poly(HIPE) prepared under low shear in the 150 µm i.d. column (**Figure 4.14**), suggesting that it offered the best separation performance for the poly(HIPE)s obtained using low shear emulsification.

The increase in performance observed for the poly(HIPE)s prepared under high shear is most likely due to the absence of radial heterogeneity and narrower void size distributions, which resulted in a significant reduction in band broadening, as indicated by narrower peaks that appeared more Gaussian in nature. While the poly(HIPE) prepared in

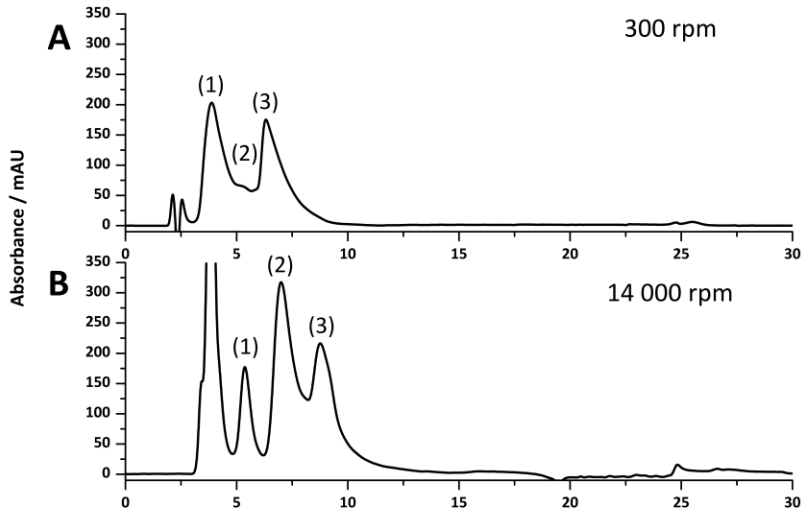

Figure 4.15. The separation of ribonuclease A (1), lysozyme (2) and α-chymotrypsinogen A (3) under reversed-phase conditions. Conditions: 18 cm of different i.d. columns: **(A)** 250 µm i.d. and **(B)** 150 µm i.d. prepared with different emulsification energies. Eluent A was 0.1 vol% formic acid in Milli-Q H_2O, and eluent B was 0.1 vol% formic acid in ACN; injection volume, 1 µL; protein concentration, 0.14 mg/mL for **(A)** and 0.05 mg/mL for **(B)**. Gradient: linear gradient 15 to 90% B in 15 min and then isocratic elution at 90% B for 5 min before returning to 15% B in 5 min; flow rate, 11 µL/min for **(A)** and 2.0 µL/min for **(B)**. Superficial velocity for both columns was 1.89 x 10^{-3} ms^{-1}. UV detection at 214 nm.

the 250 µm i.d. column appeared to offer reduced separation performance in comparison to its low shear counterpart, this was likely to have been as a result of increased band broadening associated with the presence of the large irregular voids observed in its structure (**Figure 4.1B**), highlighting an inherent disadvantage associated with their preparation. These larger voids are difficult to eliminate due to the emulsification process and ultimately limit the chromatographic performance of these materials. However, the use of shallower gradients, coupled with an increase in the flow rate, can result in almost baseline resolution for these proteins (**Figures 4.16** & **4.17**).

These columns also appeared stable, with one column being used extensively over a 4-month period, after which the silica capillary wall cracked preventing further use, suggesting excellent stability of these monoliths. In terms of repeatability, an additional poly(HIPE) was prepared in a 150 µm i.d. capillary using high shear emulsification and applied for the same protein separation. This is shown in **Figure 4.18** where a similar separation profile was obtained, except for co-elution between ribonuclease A and the impurity peak that occurred for the poly(HIPE) from the second batch.

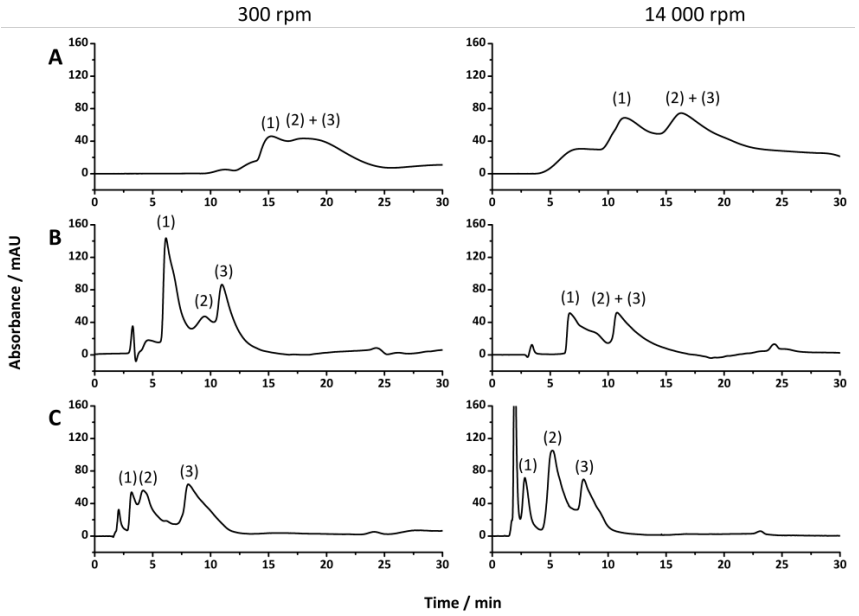

Figure 4.16. The separation of ribonuclease A (1), lysozyme (2) and α-chymotrypsinogen A (3) under reversed-phase conditions. Conditions: 18 cm of different i.d. columns: **(A)** 540 µm i.d., **(B)** 250 µm i.d. and **(C)** 150 µm i.d., prepared with different emulsification energies. Eluent A was 0.1 vol% formic acid in Milli-Q H_2O, and eluent B was 0.1 vol% formic acid in ACN; injection volume, 1 µL; protein concentration, 0.05 mg/mL for **(B)** and **(C)** and 0.3 mg/mL for **(A)**. Gradient: linear gradient 15 to 70% B in 15 min and then isocratic elution at 70% B for 5 min before returning to 15% B in 5 min; flow rate, 4.0 µL/min. UV detection at 214 nm.

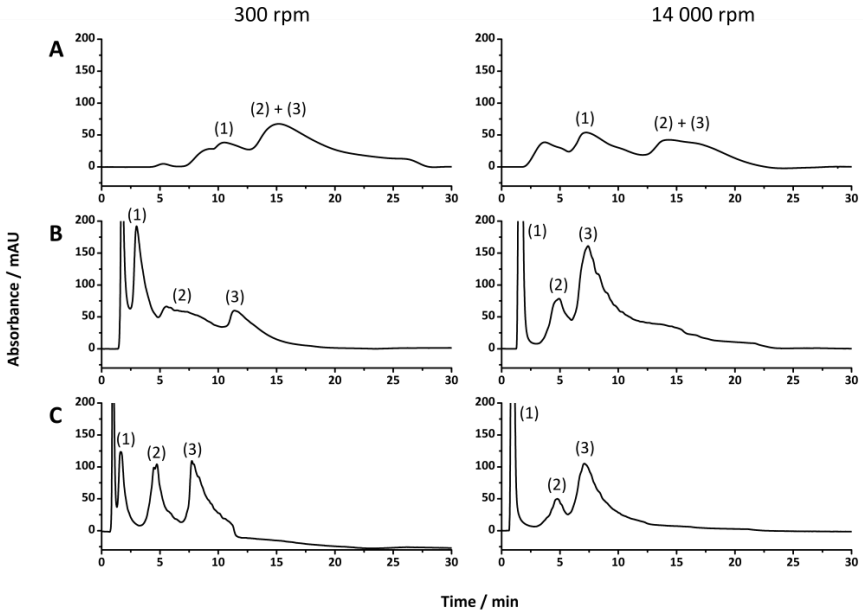

Figure 4.17. The separation of ribonuclease A (1), lysozyme (2) and α-chymotrypsinogen A (3) under reversed-phase conditions. Conditions: 18 cm of different i.d. columns: **(A)** 540 µm i.d., **(B)** 250 µm i.d. and **(C)** 150 µm i.d., prepared with different emulsification energies. Eluent A was 0.1 vol% formic acid in Milli-Q H_2O, and eluent B was 0.1 vol% formic acid in ACN; injection volume, 1 µL; protein concentration, 0.3 mg/mL. Gradient: linear gradient 15 to 50% B in 15 min and then isocratic elution at 50% B for 5 min before returning to 15% B in 5 min; flow rate, 8.0 µL/min. UV detection at 214 nm.

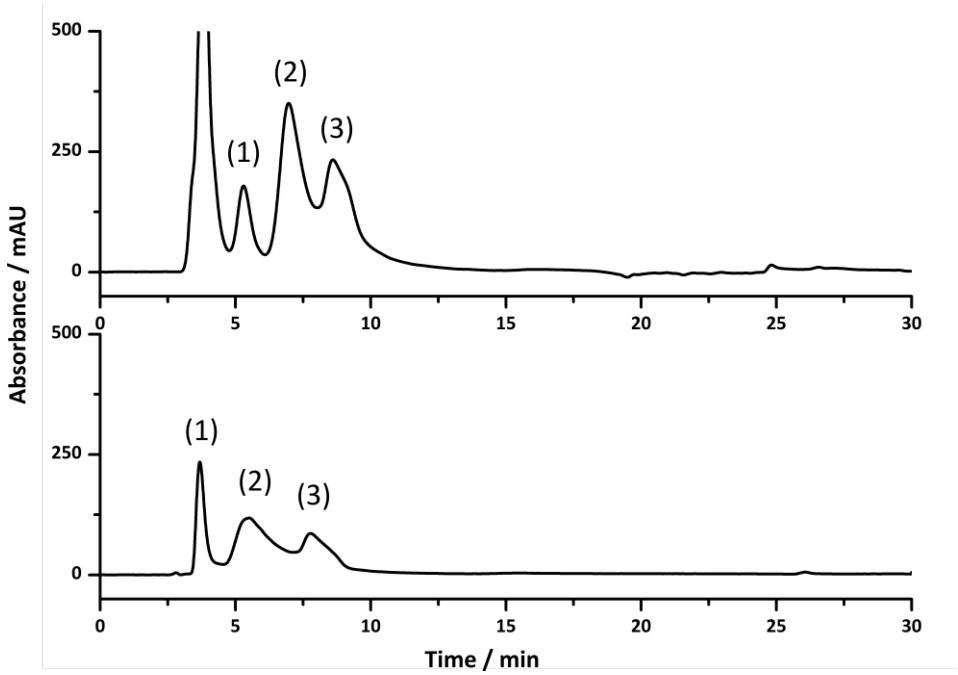

Figure 4.18. The separation of ribonuclease A (1), lysozyme (2) and α-chymotrypsinogen A (3) under reversed-phase conditions. Conditions: 18 cm of 150 µm i.d. columns from different batches prepared at 14 000 rpm; eluent A was 0.1 vol% formic acid in Milli-Q H_2O, and eluent B was 0.1 vol% formic acid in ACN, injection volume, 1 µL; protein concentration, 0.05 mg/mL. Gradient: linear gradient 15 to 90% B in 15 min and then isocratic elution at 90% B for 5 min before returning to 15% B in 5 min; flow rate, 2.0 µL/min. UV detection at 214 nm.

The presence of larger voids has also been observed for other templating techniques used to prepare polymer monoliths for chromatography, resulting in reduced separation performance [37]. Therefore in order to further improve the chromatographic performance of these materials more focus on the emulsification process itself is required. For example, poly(HIPE)s can be prepared from relatively monodisperse HIPEs obtained using microfluidics [40-41], avoiding the use of a high energy mixer, and this approach may offer a more viable route for the preparation of poly(HIPE)s for chromatography.

If the presence of these larger voids can be reduced or eliminated, the chromatographic performance of these materials could approach that of conventional polymer monoliths, where baseline resolution of similar protein mixtures is readily achieved [42-43]. However, their significantly higher permeabilities may allow for rapid analysis for applications requiring high sample throughput, particularly if the pressure of the LC system is limited, for example for miniaturised platforms. This was demonstrated for the separation of ribonuclease A and α-chymotrypsinogen (**Figure 4.19**), where baseline resolution was achieved in less than 2.5 min using a flow rate of 8 µL/min.

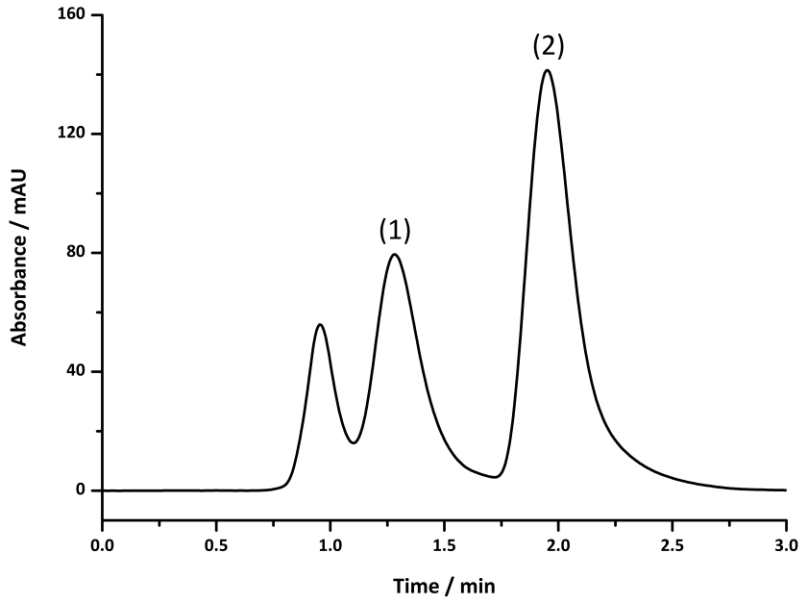

Figure 4.19. The separation of ribonuclease A (1) and α-chymotrypsinogen A (2) under reversed-phase conditions. Conditions: 18 cm of 150 µm i.d. columns prepared using a shear rate of 14 000 rpm. Eluent A was 0.1 vol% formic acid in Milli-Q H_2O, and eluent B was 0.1 vol% formic acid in ACN; injection volume, 1 µL; protein concentration, 0.05 mg/mL. Gradient: linear gradient 15 to 50% B in 1.5 min and then isocratic elution at 90% B for 5 min before returning to 15% B in 5 min; flow rate, 8.0 µL/min. UV detection at 214 nm.

4.4 Conclusions

In summary a series of poly(Sty-*co*-DVB) poly(HIPE)s were prepared in capillary format using high and low shear emulsification. The emulsions prepared under low shear exhibited significant structural change when passed through and confined within capillaries with internal diameters less than 540 μm and all columns prepared possessed significant radial heterogeniety. The use of high shear emulsification, on the other hand, resulted in emulsions that preserved their structure when prepared in capillary format, thus reflecting that of the original emulsification conditions.

In addition, these materials possessed narrower void size distributions and no radial heterogeneity was present. This resulted in significantly improved chromatographic performance for the separation of a standard protein mixture, but their chromatographic performance was ultimately limited by the presence of larger voids, presumably due to the introduction of air bubbles. These materials, however, possessed permeabilities at least an order of magnitude larger than conventional polymer monoliths, which afforded the possibility of achieving rapid separations utilising high flow rates with minimal back pressure.

4.5 References

[1] Tunç, Y.; Gölgelioğlu, Ç.; Hasirci, N.; Ulubayram, K.; Tuncel, A. *J. Chromatogr. A.* **2010**, *1217*, 1654-1659.
[2] Choudhury, S.; Connolly, D.; White, B. *J. Appl. Polym. Sci.* **2016**, *133*, 44237.
[3] Choudhury, S.; Duffy, E.; Connolly, D.; Paull, B.; White, B. n. *Separations.* **2017**, *4*, 5.
[4] Svec, F. *J. Sep. Sci.* **2004**, *27*, 1419-1430.
[5] Nischang, I.; Svec, F.; Fréchet, J. M. *J. Chromatogr. A.* **2009**, *1216*, 2355-2361.
[6] Krajnc, P.; Leber, N.; Štefanec, D.; Kontrec, S.; Podgornik, A. *J. Chromatogr. A.* **2005**, *1065*, 69-73.
[7] Yao, C.; Qi, L.; Yang, G.; Wang, F. *J. Sep. Sci.* **2010**, *33*, 475-483.
[8] Kimmins, S. D.; Cameron, N. R. *Adv. Funct. Mater.* **2011**, *21*, 211-225.
[9] Hainey, P.; M.Huxham, I.; Rowatt, B.; C.Sherrington, D.; L.Tetley. *Macromolecules.* **1991**, *24*, 117-121.
[10] Nischang, I.; Svec, F.; Fréchet, J. M. J. *Anal. Chem.* **2009**, *81*, 7390-7396.
[11] Luo, Y.; Wang, A.-N.; Gao, X. *Soft Matter.* **2012**, *8*, 7547-7551.

[12] Menner, A.; Ikem, V.; Salgueiro, M.; Shaffer, M. S. P.; Bismarck, A. *Chem. Commun.* **2007**, 4274-4276.
[13] Menner, A.; Haibach, K.; Powell, R.; Bismarck, A. *Polymer.* **2006**, *47*, 7628-7635.
[14] Trojer, L.; Lubbad, S. H.; Bisjak, C. P.; Wieder, W.; Bonn, G. K. *J. Chromatogr. A.* **2007**, *1146*, 216-224.
[15] Kovačič, S.; Štefanec, D.; Krajnc, P. *Macromolecules.* **2007**, *40*, 8056-8060.
[16] Cameron, N. R.; Sherrington, D. C. *Adv. Polym. Sci.* **1996**, *126*, 162-214.
[17] Tebboth, M.; Kogelbauer, A.; Bismarck, A. *Chem. Eng. Sci.* **2015**, *137*, 786–795.
[18] Guiochon, G. *J. Chromatogr. A.* **2007**, *1168*, 101-168.
[19] Nischang, I.; Brueggemann, O.; Svec, F. *Anal Bioanal Chem.* **2010**, *397*, 953-960.
[20] He, M.; Zeng, Y.; Sun, X.; Harrison, D. J. *Electrophoresis.* **2008**, *29*, 2980-2986.
[21] Gibson, G. T. T.; Mugo, S. M.; Oleschuk, R. D. *Polymer.* **2008**, *49*, 3084-3090.
[22] Choudhury, S.; Fitzhenry, L.; White, B.; Connolly, D. *Materials.* **2016**, *9*, 212-225.
[23] Wong, L. L.; Ikem, V. O.; Menner, A.; Bismarck, A. *Macromol. Rapid. Commun.* **2011**, *32*, 1563-1568.
[24] Wong, L. L.; Villafranca, P. M.; Menner, A.; Bismarck, A. *Langmuir.* **2013**, *29*, 5952-5961.
[25] Miller, C. M.; Venkatesan, J.; Silebi, C. A.; Sudol, E. D.; El-Aasser, M. S. *J. Colloid Interface Sci.* **1994**, *162*, 11-18.
[26] Small, H. *J. Colloid Interface Sci.* **1974**, *48*, 147-161.
[27] Svec, F.; Fréchet, J. M. J. *Ind. Eng. Chem. Res.* **1999**, *38*, 34-48.
[28] Peters, E. C.; Svec, F.; Fréchet, J. M. J. *Chem. Mater.* **1997**, *9*, 1898-1902.
[29] Yao, C.; Qi, L.; Jia, H.; Xin, P.; Yang, G.; Chen, Y. *J. Mater. Chem.* **2009**, *19*, 767-772.
[30] Jerenec, S.; Šimić, M.; Savnik, A.; Podgornik, A.; Kolar, M.; Turnšek, M.; Krajnc, P. *React. Funct. Polym.* **2014**, *78*, 32-37.
[31] Du, F.; Sun, L.; Zhen, X.; Nie, H.; Zheng, Y.; Ruan, G.; Li, J. *Anal. Bioanal. Chem.* **2015**, *407*, 6071–6079.
[32] Yin, D.; Guan, Y.; Gu, H.; Jia, Y.; zhang, Q. *RSC Adv.* **2017**, *7*, 7303-7309.
[33] Hughes, J. M.; Budd, P. M.; Tiede, K.; Lewis, J. *J. Appl. Polym. Sci.* **2015**, *132*, 41229.
[34] Hus, S.; Kolar, M.; Krajnc, P. *J. Chromatogr. A.* **2016**, *1437*, 168-175.
[35] Hua, Y.; Zhang, S.; Zhu, Y.; Chu, Y.; Chen, J. *J. Polym. Sci. A Polym. Chem.* **2013**, *51*, 2181-2187.
[36] Lau, T. H. M.; Wong, L. L. C.; Lee, K.-Y.; Bismarck, A. *Green Chem.* **2014**, *16*, 1931-1940.
[37] Dario Arrua, R.; Hilder, E. F. *RSC Adv.* **2015**, *5*, 71131-71138.
[38] Geiser, L.; Eeltink, S.; Svec, F.; Fréchet, J. M. *J. Chromatogr. A.* **2007**, *1140*, 140-146.
[39] Gu, C.; Lin, L.; Chen, X.; Jia, J.; Ren, J.; Fang, N. *J. Chromatogr. A.* **2007**, *1170*, 15-22.
[40] Costantini, M.; Colosi, C.; Guzowski, J.; Barbetta, A.; Jaroszewicz, J.; Święszkowski, W.; Dentini, M.; Garstecki, P. *J. Mater. Chem. B.* **2014**, *2*, 2290–2300.
[41] Quell, A.; Bergolis, B. d.; Drenckhan, W.; Stubenrauch, C. *Macromolecules.* **2016**, *49*, 5059−5067.
[42] Wang, Q. C.; Svec, F.; Fréchet, J. M. J. *Anal. Chem.* **1993**, *65*, 2243-2248.
[43] Xie, S.; Allington, R. W.; Svec, F.; Fréchet, J. M. J. *J. Chromatogr. A.* **1999**, *865*, 169-174.

Appendix B

Effect of shearing stress on the radial heterogeneity and chromatographic performance of styrene-based polymerised high internal phase emulsions prepared in capillary format

B.1 Preparation of poly(Sty-*co*-DVB) poly(HIPE)s in capillary format

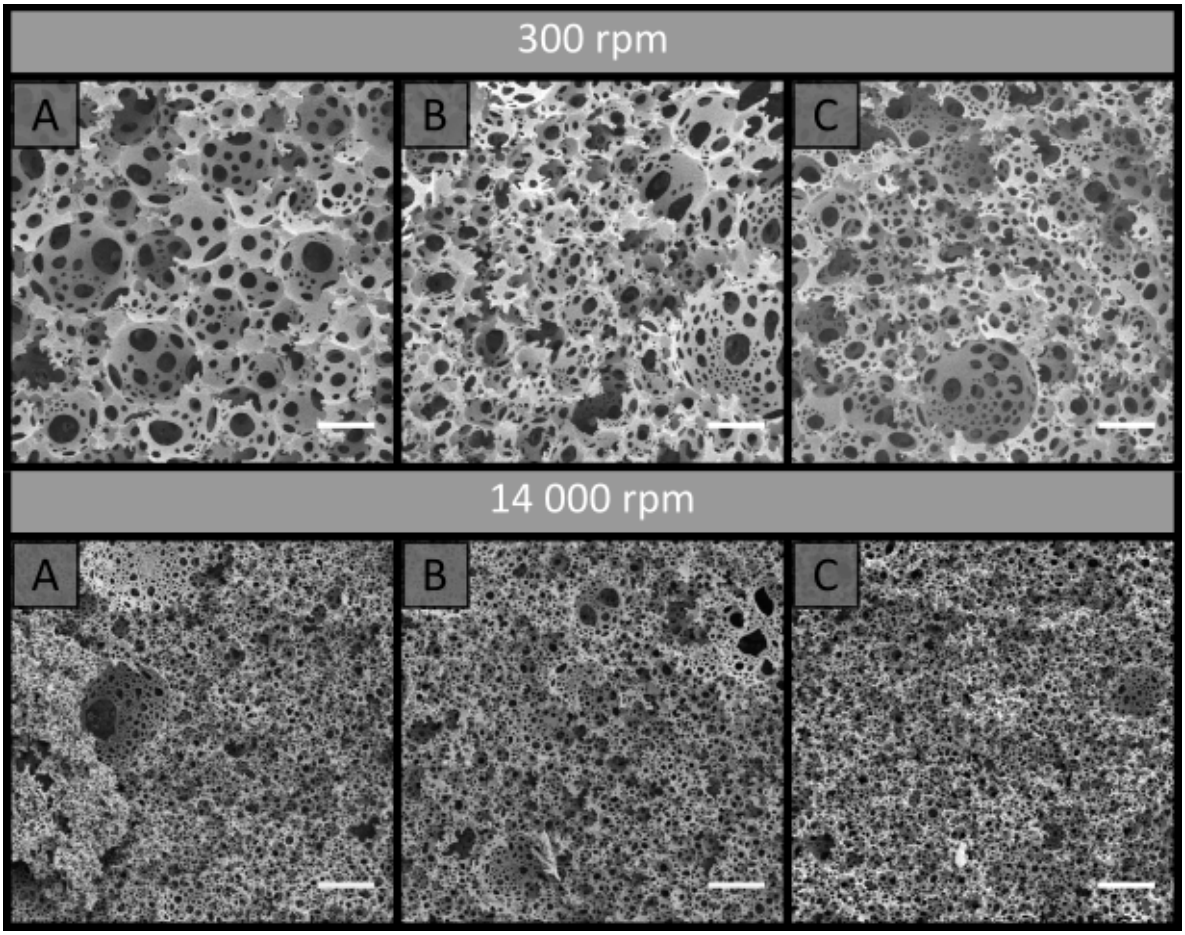

Figure B1. SEM images of poly(HIPE)s prepared from emulsions emulsified at 300 rpm or 14 000 rpm in fused silica capillaries of different i.d.: **A)** 540 µm, **B)** 250 µm and **C)** 150 µm. Scale bar is 15 µm.

B.2 Optical Microscopy

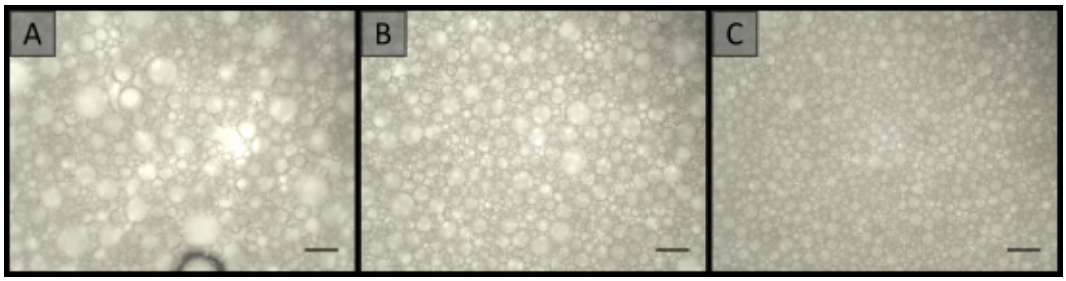

Figure B2. Optical microscopy images of emulsions which had been emulsified at 300 rpm and passed through the syringe and/or needle. **A)** Bulk, **B)** Syringe and **C)** Syringe and needle. Scale bar is 50 µm.

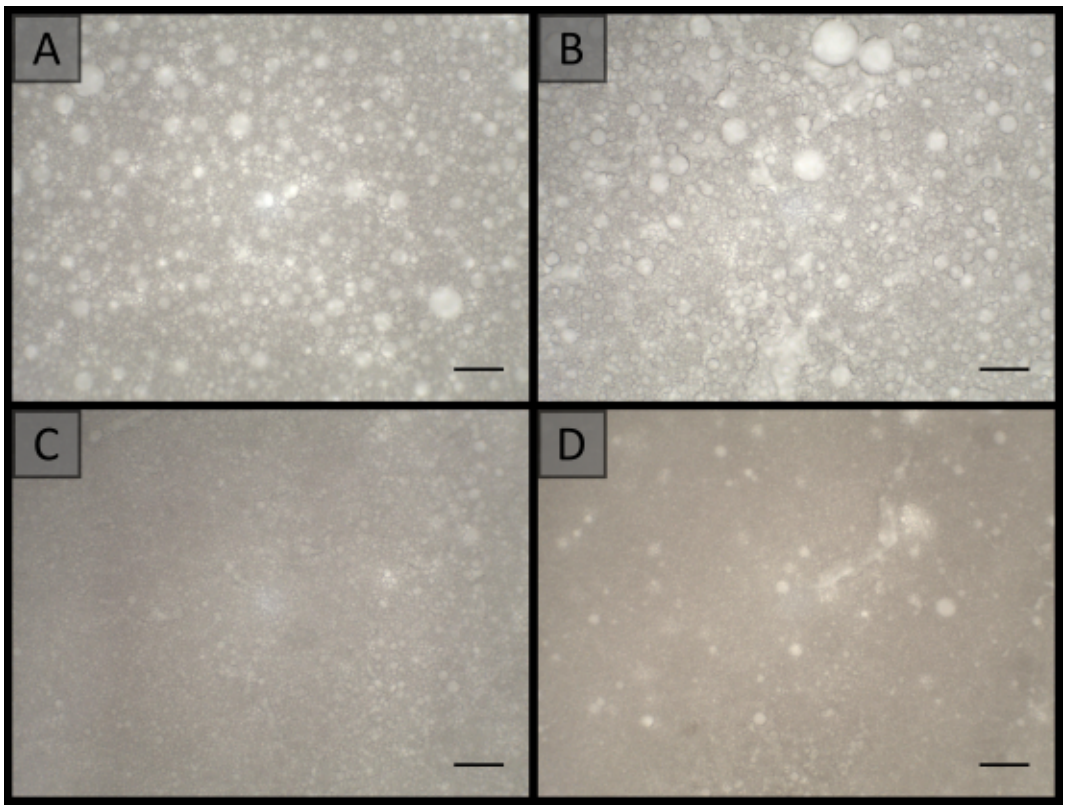

Figure B3. Optical microscopy images of emulsions which had been emulsified at 300 rpm and passed through 20 cm of various i.d. capillary columns: **A)** Bulk, **B)** 540 µm i.d., **C)** 250 µm i.d. and **D)** 150 µm i.d. Scale bar is 50 µm.

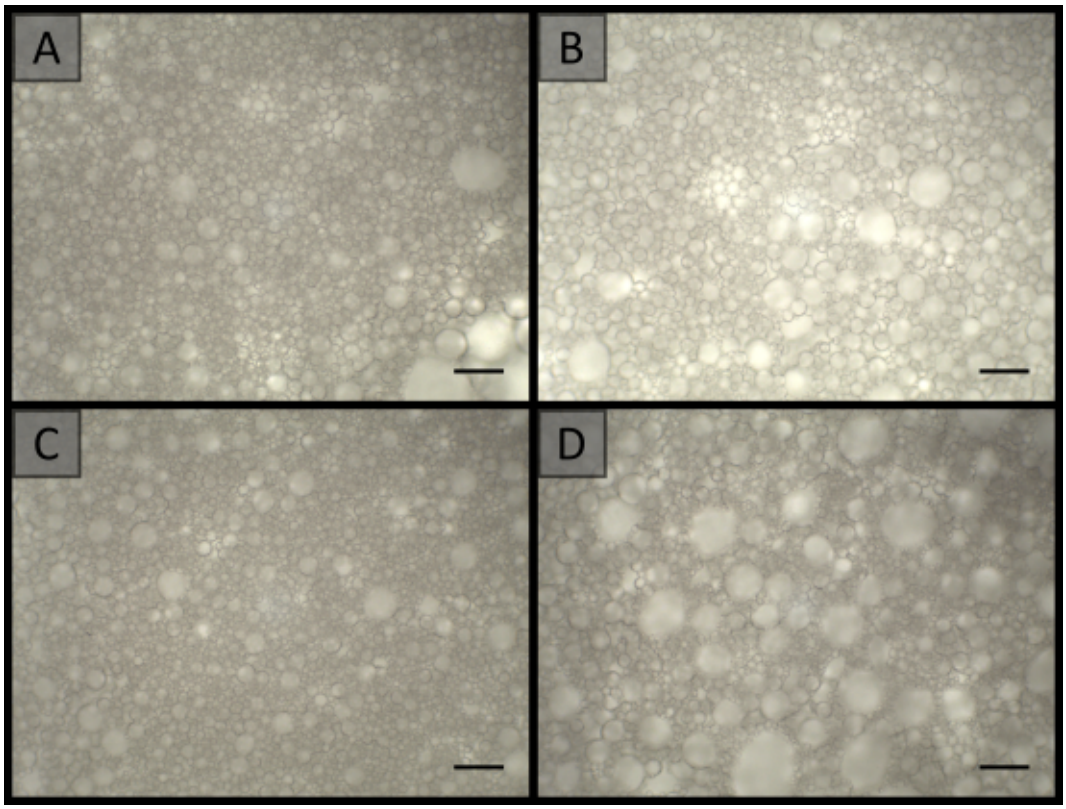

Figure B4. Optical microscopy of emulsions which had been emulsified at 300 rpm and passed through 20 cm of 250 µm i.d. capillary at different rates. **A)** 10 µL/min, **B)** 25 µL/min, **C)** 50 µL/min and **D)** 100 µL/min. Scale bar is 50 µm.

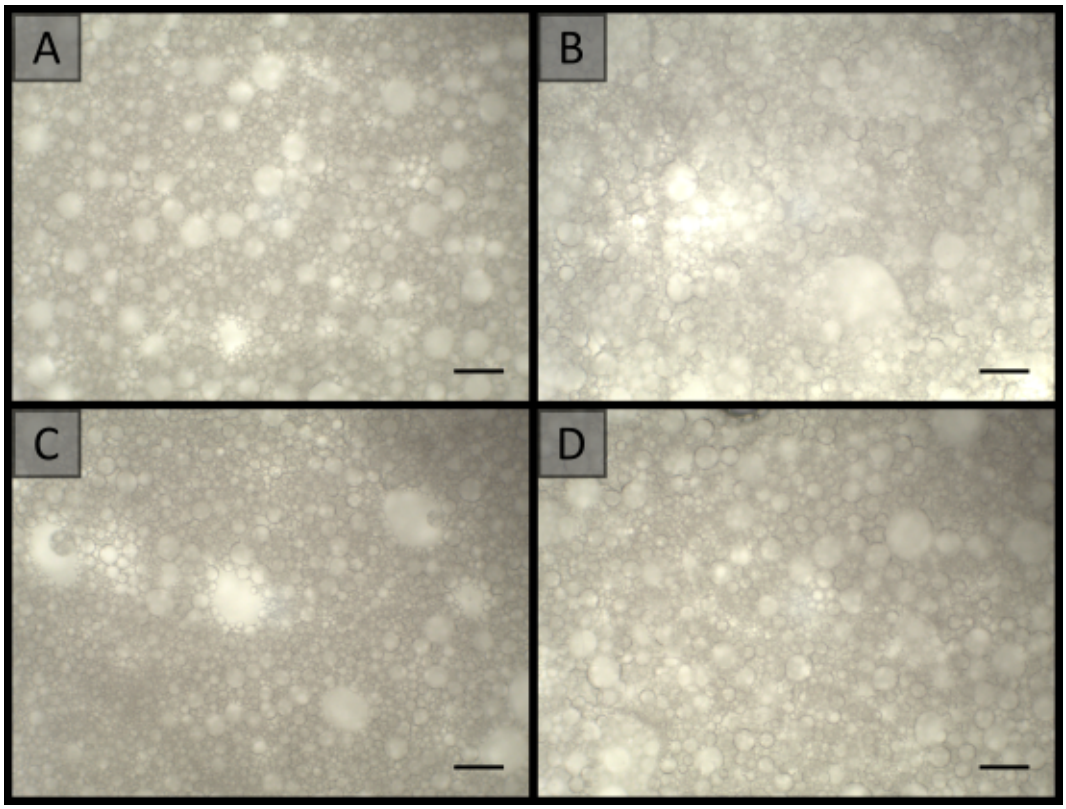

Figure B5. Optical microscopy of emulsions which had been emulsified at 300 rpm and passed through 20 cm of 150 µm i.d. capillary at different rates. **A)** 10 µL/min, **B)** 25 µL/min, **C)** 50 µL/min and **D)** 100 µL/min. Scale bar is 50 µm.

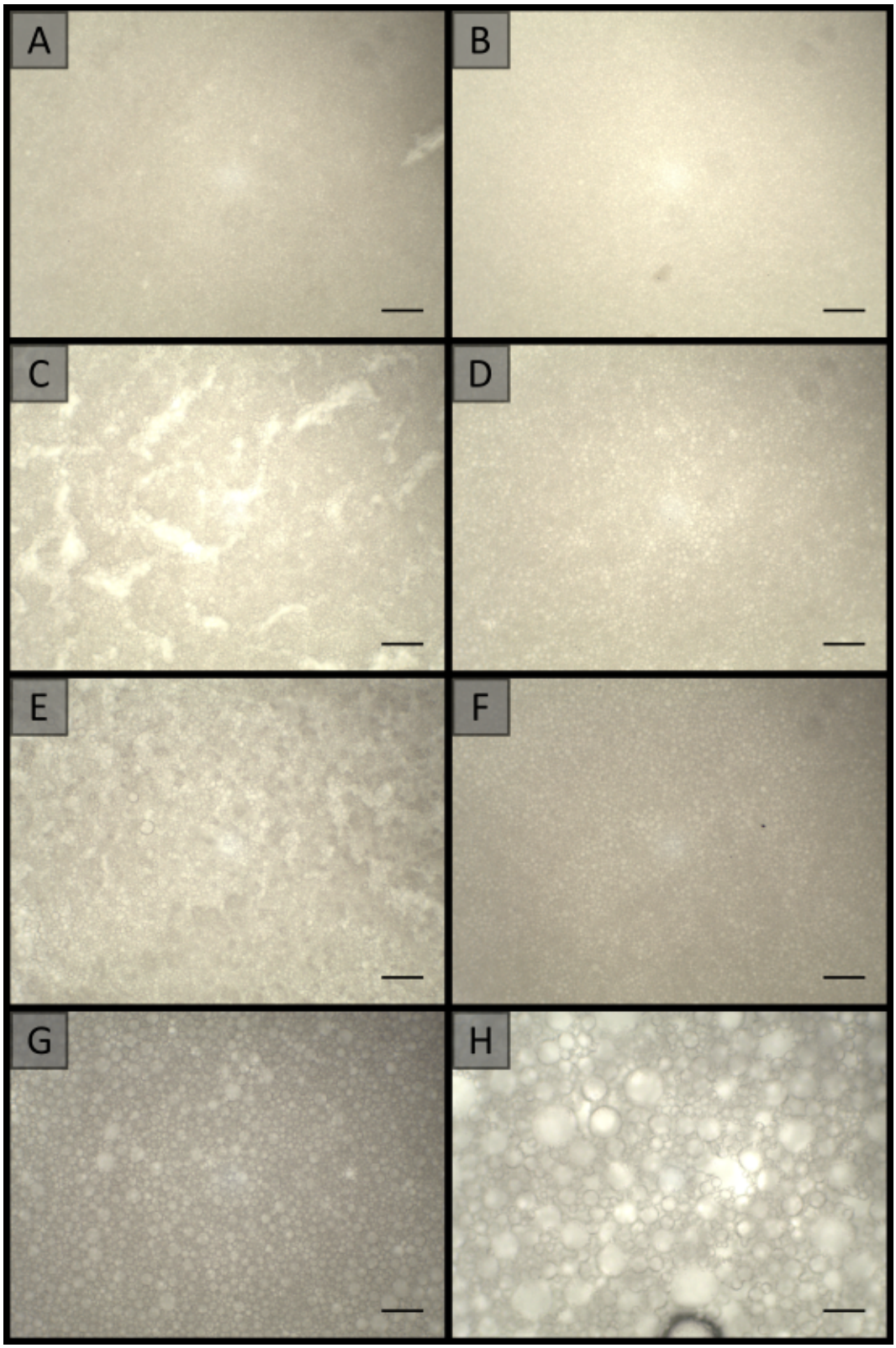

Figure B6. Optical microscopy images of emulsions which had been emulsified at 300 rpm and passed through different lengths of 250 µm i.d. capillary. **A)** 5 cm, **B)** 10 cm, **C)** 20 cm, **D)** 30 cm, **E)** 40 cm, **F)** 50 cm, **G)** 60 cm and **H)** Bulk. Scale bar is 50 µm.

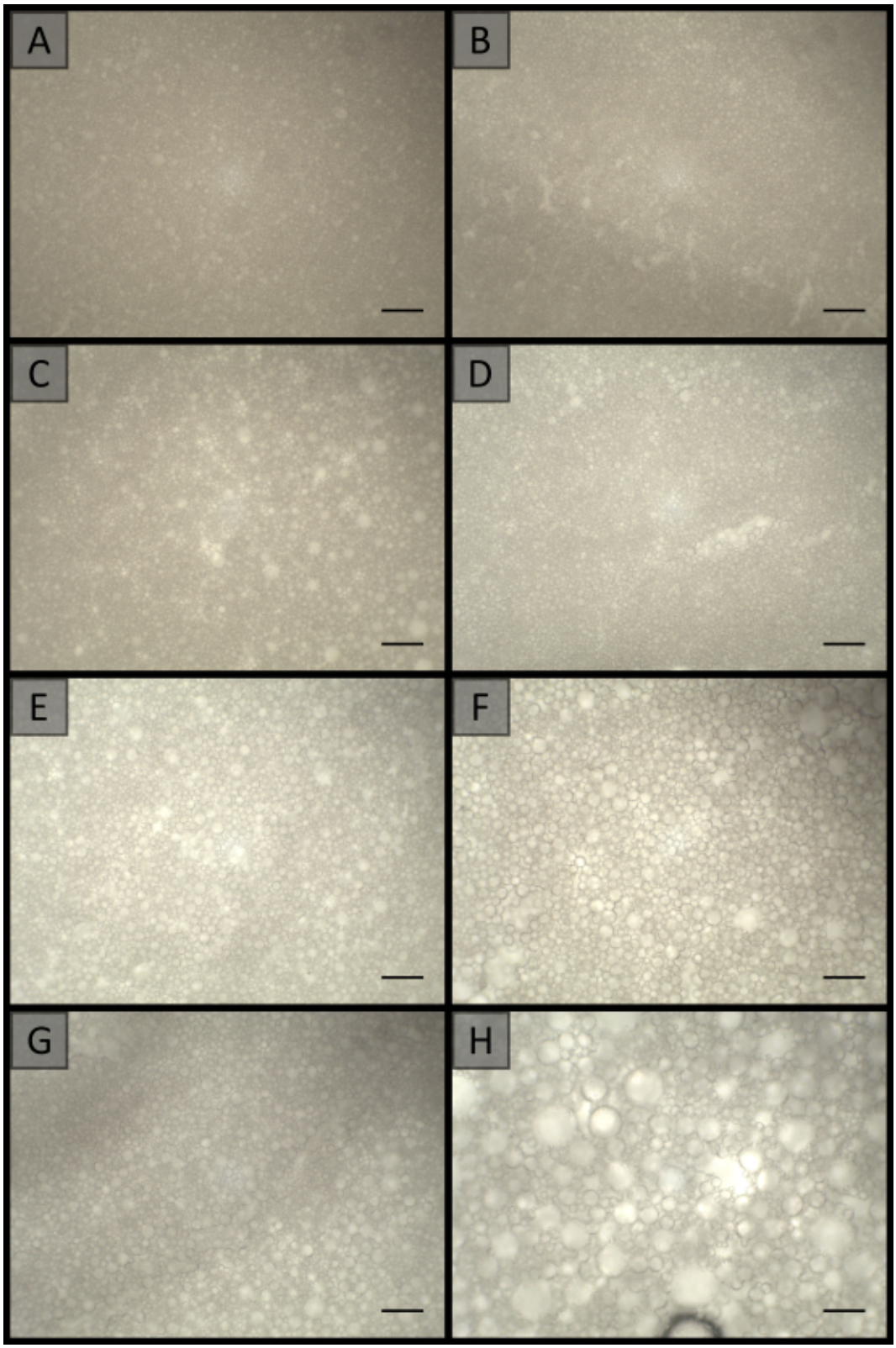

Figure B7. Optical microscopy images of emulsions which had been emulsified at 300 rpm and passed through different lengths of 150 µm i.d. capillary. **A)** 5 cm, **B)** 10 cm, **C)** 20 cm, **D)** 30 cm, **E)** 40 cm, **F)** 50 cm, **G)** 60 cm and **H)** Bulk. Scale bar is 50 µm.

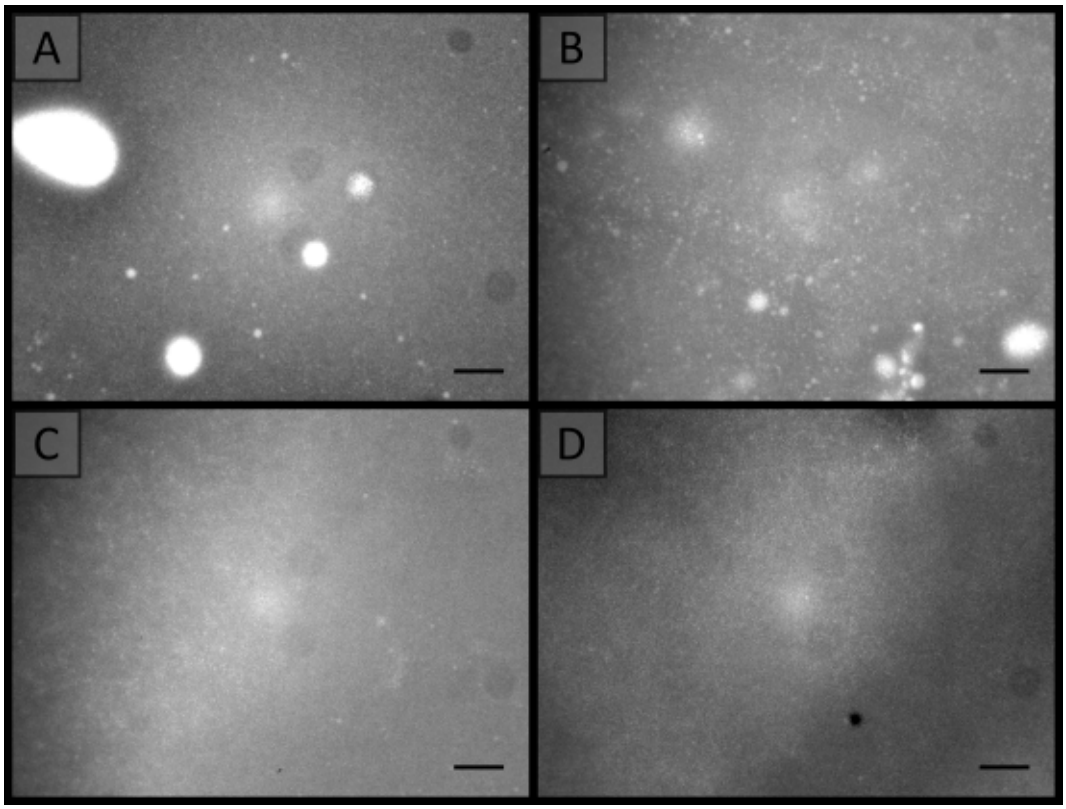

Figure B8. Optical microscopy images of emulsions which had been emulsified at 14 000 rpm and passed through 20 cm of various i.d. capillary columns: **A)** Bulk, **B)** 540 µm i.d., **C)** 250 µm i.d. and **D)** 150 µm i.d. Scale bar is 50 µm.

B.3 Swelling Characteristics

Table B1 Swelling characteristics for bulk poly(HIPE)s prepared from emulsions emulsified at 300 or 14 000 rpm

Sample	ΔV / % [A]	ΔV / % [M]	m_s / % [A]	m_s / % [M]
Bulk (300 rpm)	0 ± 10	1 ± 4	1130 ± 50	1030 ± 80
Bulk (14 000 rpm)	- 8 ± 2	- 10 ± 9	970 ± 20	900 ± 20

ΔV signifies the change in volume of the polymer disk relative to the original volume and m_S indicates the mass of solvent present in the disk relative to the mass of the dry disk. [A] These values were determined through immersion in acetone. [M] These values were determined through immersion in MeOH.

Chapter 5

The preparation of styrene-based polymerised high internal phase emulsions functionalised with monomers from the internal phase for liquid chromatography

5.1 Introduction

In **Chapter 4** it was demonstrated that poly(Sty-*co*-DVB) poly(HIPE)s with increased homogeneity could be obtained in capillary format through the use of a high energy mixer, which resulted in significantly improved chromatographic performance for the separation of a standard protein mixture using RPLC. However, the strong hydrophobic nature of the poly(Sty-*co*-DVB) surface limits their application to RPLC. In order to allow these materials to be utilised for the separation of analytes using alternative chromatographic modes, their surface chemistry must be modified. For example, conventional polymer monoliths with hydrophilic character have previously been utilised for the separation of peptides [1], nucleotides [2], nucleosides [3] and benzoic acid derivatives [4] using HILIC. Hydrophilic materials are particularly important for extending the range of analytes that can be analysed and are often applied for life science applications such as metabolomics [5].

While hydrophilic poly(HIPE)s can be prepared from oil-in-water emulsions [6-7], these are typically more difficult to stabilise and removal of the oil phase can be problematic [8]. In addition for the poly(AAm-*co*-MBAm) poly(HIPE)s and poly(MIPE)s prepared in **Chapter 3** detachment from the capillary wall was observed during purification due to shrinkage. In accordance efforts have been made to modify the surface chemistry of poly(HIPE)s prepared from water-in-oil templates, with chemical modification post curing being the most preferred method, as it avoids modifying the physical properties of the underlying scaffold [9-10]. However, in the case of poly(Sty-*co*-DVB) monoliths this is problematic due

to their low reactivity. Strategies do exist but these often require aggressive reaction conditions [11-12].

Another strategy involves the incorporation of functional monomers into the organic phase [13-14], but this is limited to co-monomers that are sufficiently hydrophobic so as not to destabilise the emulsion [15-16], and can require re-optimisation of the stabilising system [14]. Using this approach a significant proportion of the functional groups are also often buried within the scaffold and are unavailable at the surface for chromatography [9]. The incorporation of hydrophilic monomers into the internal phase, on the other hand, has been demonstrated to be an attractive alternative. Here poly(HIPE)s grafted with polymer chains [16] or gels [8, 16-19], have been obtained in a much simpler approach. Their incorporation into HIPEs actually dates back to the work of Ruckenstein and co-workers [20-22], who prepared membranes for the separation of water-ethanol mixtures by including sodium acrylate and MBAm into the internal phase with a continuous phase consisting of styrene, butyl acrylate and hexane [20]. This particular approach affords a high density of functionality primarily located on the surface, with the type of material being grafted, i.e. polymer chains or a gel, governed by the location of initiation [16, 19] and/or by including cross-linking monomers into the internal phase [8, 17, 19]. For example this approach has been utilised to prepare poly(styrene)-based poly(HIPE)s with voids that were filled with a pH or thermal responsive gel by incorporating MBAm and AA or N-isopropyl acrylamide (NIPAM) in the internal phase [17]. Poly(styrene)-based poly(HIPE)s have also been prepared that were grafted with either polymer chains or a hydrogel for cell culture by simply including AA in the internal phase and varying the monomer content and the initiator utilised [16].

The incorporation of monomers into the internal phase therefore offers an interesting alternative for obtaining chromatographic stationary phases with varied functionalities and behaviour. Additionally, the monomers included in the internal phase can act as co-stabilisers [19], resulting in poly(HIPE)s with increased homogeneity, which may also prove advantageous for their chromatographic performance.

In this chapter the possibility of preparing poly(Sty-*co*-DVB) poly(HIPE)s in capillary format with varied surface chemistry and improved column homogeneity was investigated by including monomers in the internal phase and emulsifying with high shear. The same system as in **Chapter 4** was utilised consisting of a 90 vol% aqueous internal phase with a continuous phase consisting of Sty and DVB. Initial experiments focused on the inclusion of the hydrophilic monomer AAm (at either 0.1 wt% or 1 wt% w.r.t. the internal phase), where both the monomer content and initiator were varied to establish the influence this had on the morphology and resulting chromatographic performance for a standard protein mixture using RPLC. The surface hydrophilicity was also evaluated by accessing their applicability to be used as stationary phases for HILIC. The inclusion of the less hydrophilic poly(ethylene glycol) diacrylate (PEGDA) (M_w 258) in the internal phase was also investigated and its influence on the chromatographic performance evaluated.

5.2 Experimental

5.2.1 Preparation of poly(Sty-*co*-DVB) poly(HIPE)s

The poly(Sty-*co*-DVB)-based poly(HIPE)s were prepared based on the conditions utilised in **Chapter 4**. Briefly, the internal phase was prepared by dissolving 0.006 g of calcium chloride dihydrate and internal phase monomer in 9 mL of H_2O. This was then added dropwise at a rate of 1 drop per second to a continuous phase consisting of 0.2970 g of Span® 80, 0.8 mL of Sty and 0.2 mL of DVB with constant stirring at 300 rpm. 0.02 g (0.074 mmol) of potassium persulfate (KPS) or 0.012 g (0.074 mmol) of 2,2'-azobis(2-methylpropionitrile (AIBN) were also dissolved in the internal or continuous phase, respectively, before addition of the internal phase. The emulsion was then blended using an IKA Ultra Turrax T 25 homogeniser equipped with an S 25 N 10 G dispersing element (7.5-mm rotor) at 14 000 rpm for 2 min.

This was then passed through 20 cm of 150 µm i.d. surface-modified fused silica capillaries by hand using a 250 µL Hamilton® syringe. The emulsion emerging from the outlet was collected in 4 mL glass vials. At least three capillaries were filled for each emulsion

prepared and they were each filled multiple times to limit the number of air bubbles or voids present before the ends were sealed with rubber. Optical microscopy images of the emulsions immediately after preparation, and when passed through the capillaries, were collected. The capillaries were then placed horizontally in the water bath at 60°C and cured for 48 h.

The remaining emulsion was transferred to 25 mL glass vials as bulk samples and, along with the 4 mL vials, also immersed in the water bath. Once cured the bulk material from the vials was removed, cut into smaller pieces and washed using MeOH with a Soxhlet apparatus for 24 h to remove the internal phase and any impurities. These were then left to dry at 25 °C in a vacuum oven for 1 week. The capillaries were flushed with MeOH for 2 h and then H_2O for 2 h using the capillary LC system with a flow rate of 2 µL/min. The samples in this chapter were referred to as follows: [wt% of monomer (w.r.t. internal phase), monomer, (initiator)].

Polymer disks for porosity measurements were prepared as described above, except the emulsion was transferred to 10 mL disposable syringes (~1.5 cm in diameter). These were then sealed and placed in the water bath at 60°C at an angle of ~45° from the horizontal to ensure any air bubbles migrated to the top of the syringe and then cured for 48 h. Once cured they were removed and cut into 0.5 cm thick pieces and then washed with MeOH using the Soxhlet apparatus for 24 h. They were dried in a vacuum at 25°C for 1 week before use.

5.3 Results and Discussion

5.3.1 Preparation of poly(HIPE)s grafted with AAm

Poly(Sty-*co*-DVB)-based poly(HIPE)s were first prepared by including AAm in the internal phase at two different concentrations, 0.1 and 1 wt% (w.r.t. internal phase), in order to investigate the influence of its inclusion on the morphology and surface chemistry of the resulting poly(HIPE)s. In addition the initiation location was also varied, by employing KPS

Table 5.1 Porous properties of poly(HIPE)s prepared with different amounts of AAm or PEGDA (w.r.t. internal phase) in the internal phase and using different initiators

#	Sample	V_B [a] / µm	W_B [b] / µm	D_B [c] / µm	Porosity [d] / %	Surface Area [e] / m^2g^{-1}	V_C [a] / µm	W_C [b] / µm
1	0 wt% (KPS)	3.4 ± 0.7	0.8 ± 0.3	3 ± 1	97 ± 4	19.7 ± 0.8	4 ± 2	1.1 ± 0.4
2	0.1 wt% AAm (KPS)	2.3 ± 0.7	0.6 ± 0.2	2 ± 1	86 ± 5	43.7 ± 0.4	5 ± 2	1.2 ± 0.5
3	1 wt% AAm (KPS)	2.5 ± 0.9	0.5 ± 0.2	3 ± 1	83 ± 7	30.2 ± 0.3	3 ± 2	0.6 ± 0.2
4	0.4 wt% PEGDA	1.9 ± 0.5	0.5 ± 0.2	2 ± 1	98 ± 7	37.7 ± 0.5	2 ± 1	0.6 ± 0.2
5	4 wt% PEGDA (KPS)	4 ± 3	0.7 ± 0.3	5 ± 2	97.5 ± 0.3	29 ± 1	4 ± 4	0.8 ± 0.3
6	0 wt% (AIBN)	7 ± 2	1.6 ± 0.7	7 ± 3	96 ± 8	14.1 ± 0.4	7 ± 2	1.8 ± 0.6
7	0.1 wt% AAm	4 ± 1	1.2 ± 0.4	3 ± 2	108 ± 8	13.4 ± 0.3	7 ± 4	0.9 ± 0.4
8	1 wt% AAm (AIBN)	2.9 ± 0.6	0.7 ± 0.2	3 ± 1	89 ± 7	17.5 ± 0.8	6 ± 4	1.9 ± 0.8
9	0.4 wt% PEGDA	4 ± 2	1.2 ± 0.5	4 ± 2	98 ± 5	15 ± 1	5 ± 2	1.5 ± 0.5
10	4 wt% PEGDA	4 ± 1	1.3 ± 0.4	4 ± 2	105 ± 5	13.1 ± 0.8	3 ± 3	1.7 ± 0.5

[B] indicates the bulk material. [C] indicates the material in capillary. [a] Average void diameter for the poly(HIPE)s as determined from SEM. [b] Average window diameter for the poly(HIPE)s as determined from SEM. [c] Average droplet diameter immediately after preparation for the emulsions. [d] Porosity of bulk poly(HIPE)s determined by immersion in MeOH. [e] Specific surface area of bulk poly(HIPE) determined from BET.

as a water-soluble initiator or AIBN as an oil-soluble initiator. Two control samples without monomer in the internal phase, but using the different initiators, were also prepared for comparison. While it is also possible to simply graft AAm to the surface post curing, this often reduces the extent of co-polymerisation, which correlates to a lower density of functional groups, and can result in poor interconnectivity [8].

SEM analysis (**Figure 5.1** & **Table 5.1**) of the resulting poly(HIPE)s revealed an apparent reduction in the average void diameter upon the inclusion of AAm for both initiators. For example, this was reduced from 3.4 ± 0.7 (entry 1) to 2.3 ± 0.7 µm for KPS (entry 2) and

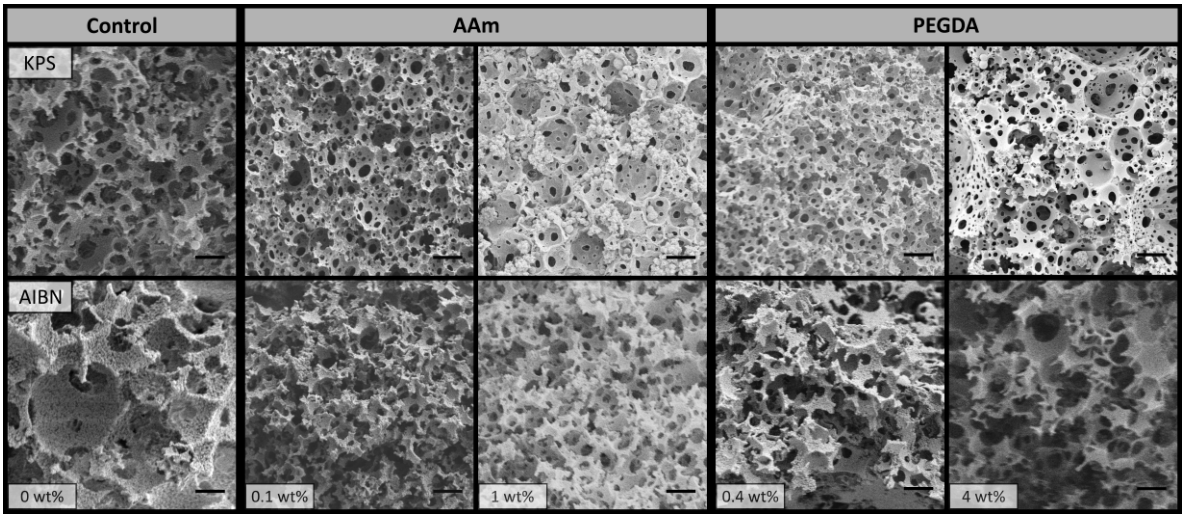

Figure 5.1. SEM images of poly(HIPE)s prepared with different amounts of AAm or PEGDA (w.r.t. internal phase) in the internal phase and using different initiators. Scale bar is 3 µm.

from 7 ± 2 (entry 6) to 4 ± 1 µm (entry 7) for AIBN with the inclusion of 0.1 wt% AAm into the internal phase. This suggests that either AAm, poly(AAm) and/or its copolymers, are acting as a co-stabiliser resulting in a reduction in the droplet and resulting void size, as previously observed by Gitli and Silverstein [19]. Increasing the AAm content further to 1 wt% resulted in an additional reduction in the void size to 2.9 ± 0.6 µm (entry 8) for AIBN, however the value obtained for KPS of 2.5 ± 0.9 µm (entry 3) was not statistically different to that of 0.1 wt% AAm. The same trend was also observed for the window size (**Table 5.1**).

In all cases the poly(HIPE)s prepared using AIBN as initiator possessed larger void sizes and therefore lower surface areas (**Table 5.1**) than the equivalent materials prepared using KPS as initiator. This is well documented for poly(styrene)-based systems [23-24] and is due to the reduced salt concentration when AIBN is used as initiator. The addition of salt, such as KPS, can have a stabilising effect on the oil-water interface and therefore can reduce the droplet size and aid in emulsion stability [23-25]. As such KPS is commonly used as the initiator in the preparation of poly(HIPE)s from water-in-oil emulsions [23].

This enhanced stability could also explain why the influence of increasing the AAm content on the resulting void size was less pronounced for KPS in comparison to AIBN. Regardless, the droplet sizes observed immediately after preparation (**Table 5.1** & **Figure C1** in

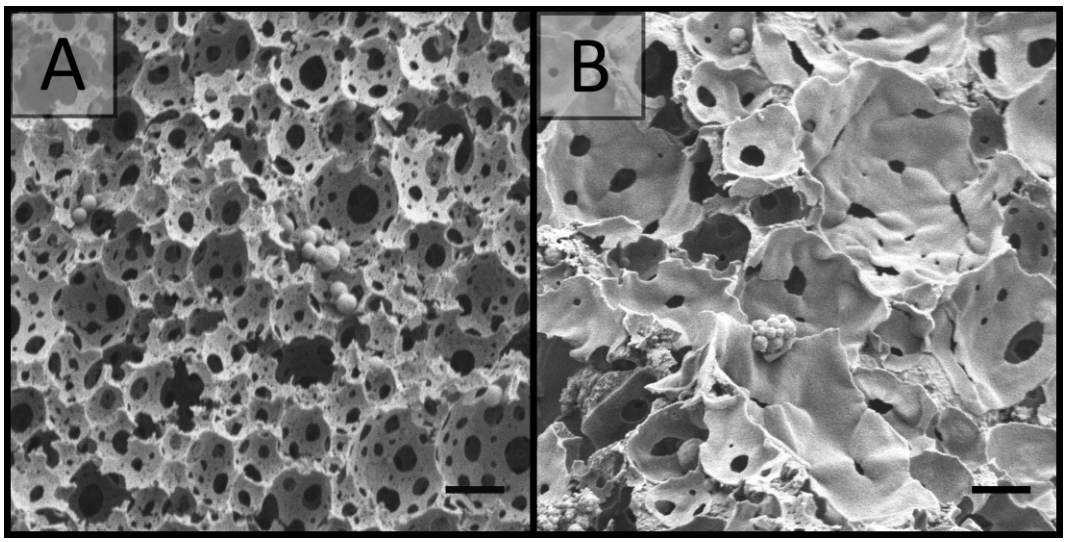

Figure 5.2. SEM images of poly(HIPE)s prepared with different amounts of AAm (w.r.t. internal phase) in the internal phase using KPS as initiator. **A)** 0.1 wt% and **B)** 1 wt%. Scale bar is 2 µm.

Appendix C) for all emulsions were consistent with the void sizes obtained, suggesting that no significant coalescence occurred during curing, even when AIBN was used as the initiator. Given the droplet sizes immediately obtained after the preparation of the emulsion also appear to mirror the trends observed upon the inclusion of AAm for the void size, this suggests that AAm is indeed acting as a co-stabiliser as previously reported [19, 26], rather than poly(AAm) and/or its copolymers formed during curing. It should be noted that the formation of these polymers, however, might also aid in stability later in the curing process.

In terms of the porosity of these materials, the values calculated through immersion in MeOH (**Table 5.1**) were also consistent with the 90 vol% internal phase utilised, which suggests that no or limited creaming of these emulsions occurred [25]. These values were also consistent with those obtained through immersion in acetone, and the change in volume was negligible for both solvents (**Table C1** in **Appendix C**). Even though the increase in AAm content from 0.1 to 1 wt% did not result in a shift in the void size in the case of KPS, a significantly different void surface was obtained (**Figure 5.1**).

In the case of 0.1 wt% AAm (KPS) a smooth void surface was observed, however for 1 wt% AAm (KPS) the resulting void surface appeared wrinkled and crumpled regions were present on the void walls. This texturing is indicative of the presence of a collapsed hydrogel [27]. A comparison of these two contrasting materials at a higher magnification

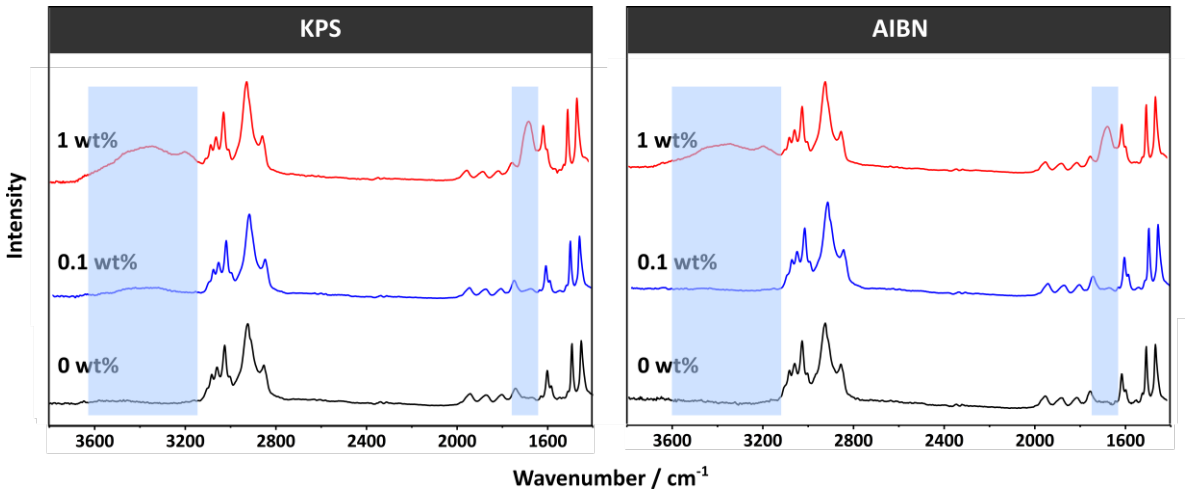

Figure 5.3. ATR-IR of poly(HIPE)s prepared with different amounts of AAm (w.r.t. internal phase) in the internal phase and using different initiators.

Table 5.2 Elemental analysis for the poly(HIPE)s prepared with different amounts of AAm (w.r.t. internal phase) in the internal phase and using different initiators

#	Sample	N / %	C / %	H / %	S / %	AAm [a] / %
1	0 wt% AAm (KPS)	0.03	90.34	8.16	0.10	0
2	0.1 wt% AAm (KPS)	0.06	89.49	8.13	0.10	17
3	1 wt% AAm (KPS)	1.05	86.30	7.86	0.11	58
4	0 wt% AAm (AIBN)	0.04	90.97	8.14	0.00	0
5	0.1 wt% AAm (AIBN)	0.06	91.26	8.15	<0.01	11
6	1 wt% AAm (AIBN)	1.63	86.14	7.99	<0.01	90

[a] Estimate of AAm incorporated into the poly(HIPE)s based on nitrogen content w.r.t. AAm in the internal phase. This was calculated assuming full conversion of monomers and subtracting the nitrogen content in the blank samples (0 wt% AAm).

can be found in **Figure 5.2**. The presence of a hydrogel that filled the voids of this poly(HIPE) was also supported by the decrease in porosity observed from 97 ± 4 % for 0.1 wt% AAm to 83 ± 7 % for 1 wt% AAm.

This hydrogel appeared to be AAm-based with elemental analysis (**Table 5.2**) indicating a significant increase in nitrogen content from 0.03 wt% for 0 wt% AAm (entry 1) in the internal phase to 1.05 wt% for 1 wt% AAm (entry 3) in the internal phase, with AAm the only plausible source. This corresponded to an estimated incorporation of 58 % of the internal phase monomer into the resulting poly(HIPE). In addition, the characteristic amide bands at 3402 (NH_2 stretch), 3192 (NH_2 stretch) and 1672 cm^{-1} (C=O stretch) were clearly observed by FTIR (**Figure 5.3**), indicating the presence of polymerised AAm at the surface [19]. In addition to the presence of a hydrogel, particles of ~500 nm in diameter were also observed for 1 wt% AAm (KPS). These were also present for 0.1 wt% AAm (KPS), but in smaller number. This suggests that some degree of phase inversion occurred [28], which was also associated with the increase in AAm content.

This was in contrast to that of AIBN where the increase in AAm content simply resulted in a decrease in the void size, with no alteration in the texture of the void surface, suggesting no hydrogel was formed in this case. However, elemental analysis (**Table 5.2**) also revealed the presence of a significant level of nitrogen with a value of 1.63 wt for 1 wt% AAm (AIBN) (entry 6), which corresponded to an estimated incorporation of 90% of the internal phase monomer. In addition, the characteristic amide bands were also observed by FTIR (**Figure 5.3**). This clearly indicates that although a hydrogel was not observed in the case of AIBN, AAm was still incorporated into the resulting structure.

To understand the reason for the presence or absence of an AAm-based hydrogel in the case of KPS and AIBN, respectively, it is important to consider the mechanism responsible for the incorporation of AAm into the material. Given the partition co-efficient for AAm between toluene and H_2O is expected to be relatively low [19, 29] (the log P value for the partitioning of AAm between octanol and water is -0.78 [30]), the amount of AAm located in the continuous phase is not considered to be significant [19]. The incorporation of AAm into the resulting poly(HIPE) therefore occurs through the co-polymerisation of AAm from the internal phase and external phase monomers at the oil-water interface [19, 27].

Given AAm is acting as a co-stabiliser a proportion of AAm is expected to be located at the interface, where it is available to undergo co-polymerisation. During this process, however, the AAm in the internal phase is also undergoing a degree of polymerisation, the extent of which is determined by both the radical and AAm concentration in the internal phase. In regards to the degree of co-polymerisation between AAm and the external phase monomers, this also depends on their relative reactivity ratios. For the co-polymerisation of styrene and AAm, r_1 (styrene) is typically greater than 1, while r_2 (AAm) is typically less than 1 [31]. This suggests that styrene radicals are more likely to undergo homopolymerisation, while the AAm radicals are more likely to undergo co-polymerisation with styrene at the interface. This also indicates that in a simplified system the styrene monomer will be consumed faster.

When AIBN is used as initiator, the radicals are generated in the external phase, and the polymerisation of this phase is predominant. This results in the grafting of AAm-chains rather than a gel to the surface [16, 19]. This was also previously observed by Gitli and Silverstein [19], who incorporated AAm and MBAm into the internal phase, when using the oil-soluble benzoyl peroxide initiator. In addition, based on the reactivity ratios, the styrene radicals generated undergo a higher degree of homopolymerisation relative to the degree of co-polymerisation occurring with the internal phase AAm.

In contrast when KPS is utilised as initiator the radicals are generated in the internal phase and the polymerisation of the external phase is initiated at the interface [19]. Given the higher concentration of radicals in the internal phase the AAm present can undergo a

higher degree of polymerisation. If AAm is present at a sufficient concentration a hydrogel can form which is grafted to the surface without the presence of an additional cross-linker. Hayward et al. [16] observed a similar result upon increasing the concentration of AA in the internal phase when using KPS as initiator. The tendency for the AAm radicals to undergo co-polymerisation with styrene would also suggest that a higher degree of AAm would be incorporated onto the surface in comparison to when AIBN was utilised. However, when 1 wt% AAm was included in the internal phase the estimated incorporation was 58 and 90% (**Table 5.2**), respectively.

The lower degree of AAm incorporated in the case of KPS is potentially related to the higher concentration of AAm radicals relative to the amount of styrene present at the interface. In this case a higher degree of homopolymerisation can occur in the internal phase, resulting in the formation of the observed hydrogel. It is therefore plausible that a larger proportion of AAm was preferentially bound to other AAm chains and not the surface, resulting in its removal during purification. This is in contrast to AIBN where the amount of AAm radicals generated in the internal phase is significantly lower and thus homopolymerisation of AAm is limited. This results primarily in its co-polymerisation with styrene at the interface and subsequent incorporation onto the surface.

In terms of the lower concentration of AAm, both 0.1 wt% AAm (KPS) and 0.1 wt% AAm (AIBN) showed a negligible increase in nitrogen content (**Table 5.2**) and no obvious amide signals were observed (**Figure 5.3**). It is likely that the low AAm content resulted in significantly less co-polymerisation at the oil-water interface, as the likelihood for a growing AAm chain to be captured by the surface is significantly lower when the concentration is low, regardless of the initiator utilised. As a result a significant proportion of the AAm in the internal phase was unbound and simply removed during the purification process, resulting in an estimated incorporation of internal phase monomer of only 17 and 11 %, respectively. In this case the incorporation of AAm was slightly higher when KPS was utilised, in comparison to AIBN, which was consistent with the information obtained from the relative reactivity ratios, with the co-polymerisation of AAm radicals with styrene at the interface being preferred. This difference in behaviour, between the two AAm concentrations, could be related to the lower amount of AAm radicals present in this case,

in comparison to when 1 wt% AAm was included in the internal phase, relative to the amount of styrene at the interface. Alternatively this could be due to the increased polymerisation rate in the case of increased AAm concentrations.

5.3.2 Preparation of poly(HIPE)s grafted with AAm in capillary format

In order to evaluate the chromatographic performance of these materials, they were first prepared in capillary format using 150 µm i.d. fused silica capillaries. In most cases the average void and window size obtained within the capillaries was consistent with that obtained with the bulk materials (**Figure 5.4** & **Table 5.1**). In addition, the average droplet and resulting void and window sizes for the emulsions that were passed through these capillaries and then cured were also consistent with that of the bulk materials (**Table 5.3**, **Figure 5.5** & **Figure C2** in **Appendix C**) in most cases. This suggested that passing these particular emulsions through the capillary inlet and/or confining them within the capillary itself did not compromise their structure or stability. However, the void size distributions within the capillaries were again broader (**Table 5.1**), and this was potentially related to the presence of a small number of larger voids, for example one can clearly be seen in the cross-section for 0.1 wt% AAm (KPS) in **Figure 5.4**.

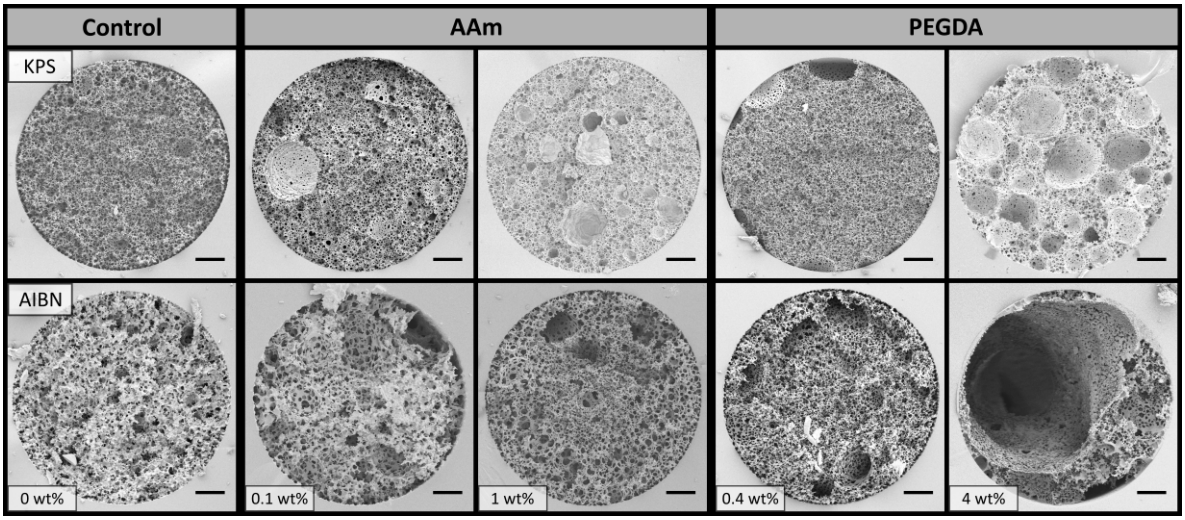

Figure 5.4. SEM images of poly(HIPE)s prepared with different amounts of AAm or PEGDA (w.r.t. internal phase) in the internal phase in 150 µm i.d. capillaries using different initiators. Scale bar is 20 µm.

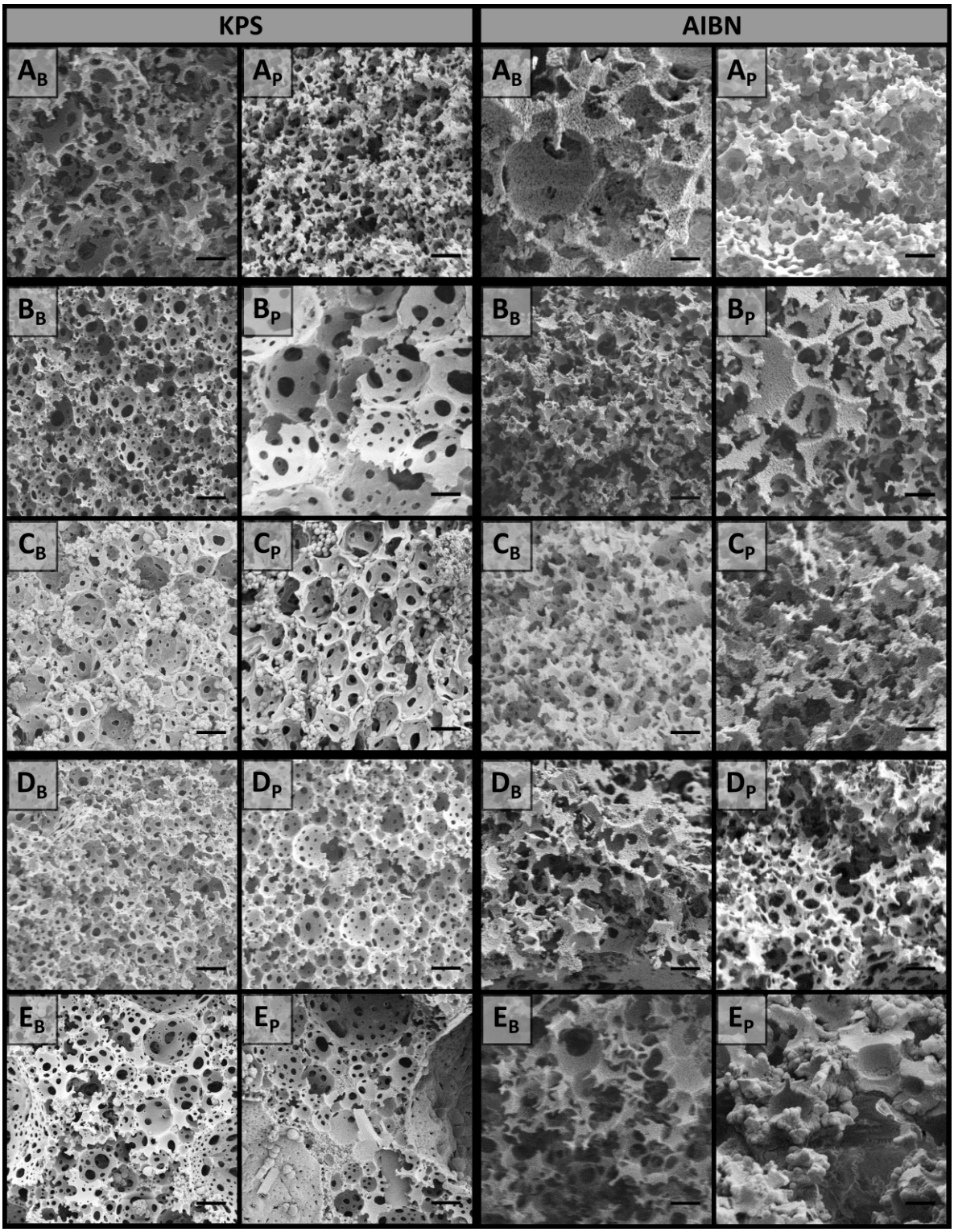

Figure 5.5. SEM images of poly(HIPE)s prepared with different amounts of monomer (w.r.t. internal phase) in the internal phase and using different initiators. **A)** 0 wt%, **B)** 0.1 wt% AAm, **C)** 1 wt% AAm, **D)** 0.4 wt% PEGDA and **E)** 4 wt% PEGDA. ^{B} indicates poly(HIPE)s obtained by curing the bulk emulsions, ^{P} indicates poly(HIPE)s obtained after curing the emulsions which that had been passed through 20 cm of capillary. Scale bar is 3 µm.

Table 5.3 Comparison between the porous properties of poly(HIPE)s prepared in bulk and passed through capillary with different amounts of AAm or PEGDA (w.r.t. internal phase) in the internal phase and using different initiators

#	Sample	V_B [a] / µm	W_B [b] / µm	D_B [c] / µm	V_P [a] / µm	W_P [b] / µm	D_P [c] / µm
1	0 wt% (KPS)	3.4 ± 0.7	0.8 ± 0.3	3 ± 1	3.4 ± 0.7	0.7 ± 0.3	3 ± 1
2	0.1 wt% AAm (KPS)	2.3 ± 0.7	0.6 ± 0.2	2 ± 1	8 ± 2	1.8 ± 0.7	4 ± 2
3	1 wt% AAm (KPS)	2.5 ± 0.9	0.5 ± 0.2	3 ± 1	2.9 ± 0.7	0.8 ± 0.3	1.9 ± 0.9
4	0.4 wt% PEGDA (KPS)	1.9 ± 0.5	0.5 ± 0.2	2 ± 1	1.9 ± 0.7	0.4 ± 0.2	1.8 ± 0.9
5	4 wt% PEGDA (KPS)	4 ± 3	0.7 ± 0.3	5 ± 2	3 ± 2	0.4 ± 0.2	5 ± 2
6	0 wt% AAm (AIBN)	7 ± 2	1.6 ± 0.7	7 ± 3	5 ± 2	1.0 ± 0.5	5 ± 3
7	0.1 wt% AAm (AIBN)	4 ± 1	1.2 ± 0.4	3 ± 2	4.3 ± 0.7	0.9 ± 0.3	3 ± 1
8	1 wt% AAm (AIBN)	2.9 ± 0.6	0.7 ± 0.2	3 ± 1	6 ± 2	1.4 ± 0.5	2.2 ± 0.9
9	0.4 wt% PEGDA (AIBN)	4 ± 2	1.2 ± 0.5	4 ± 2	3 ± 2	0.8 ± 0.3	5 ± 2
10	4 wt% PEGDA (AIBN)	4 ± 1	1.3 ± 0.4	4 ± 2	4 ± 2	1.6 ± 0.6	3 ± 1

[B] indicates the bulk material. [P] indicates the material passed through 20 cm of capillary. [a] Average void diameter for the poly(HIPE)s as determined from SEM. [b] Average window diameter for the poly(HIPE)s as determined from SEM. [c] Average droplet diameter immediately after preparation, or after being passed through the capillary, for the emulsions as determined from optical microscopy.

As discussed in **Chapter 4**, the origin of these larger voids is most likely from the introduction of air bubbles associated with the use of a high energy mixer and/or the capillary filling process, and their presence will contribute towards band broadening. However the use of high energy mixers was also shown to result in emulsions that better preserved their structure when passed through narrow capillaries, in comparison to low energy emulsification. In addition their use has also resulted in capillaries with minimal radial heterogeneity, which significantly reduces band broadening. It is also important to

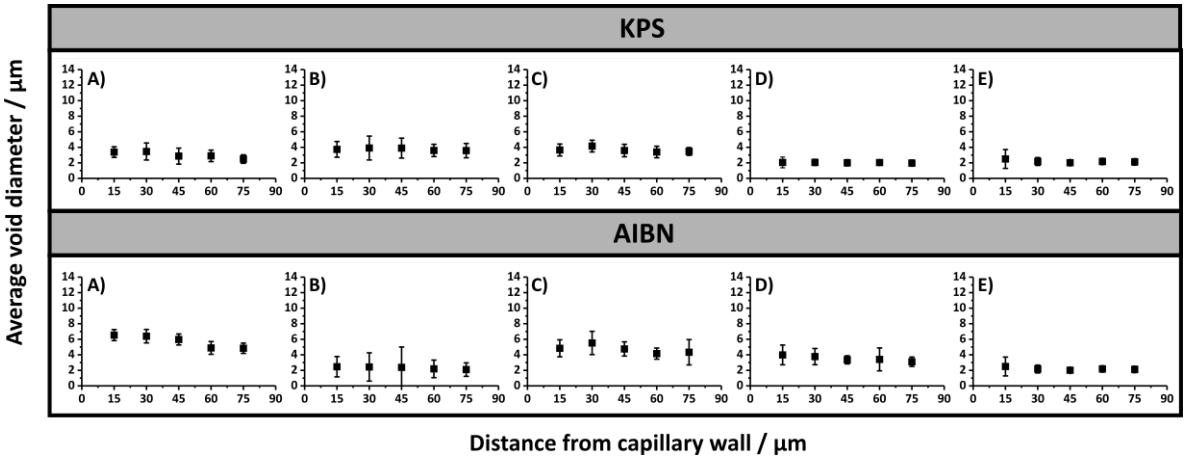

Figure 5.6. Plot of average void diameter with increased distance from capillary wall for poly(HIPE)s prepared with different amounts of monomer (w.r.t. internal phase) in the internal phase in 150 µm i.d. capillaries using different initiators. **A)** 0 wt%, **B)** 0.1 wt% AAm, **C)** 1 wt% AAm, **D)** 0.4 wt% PEGDA and **E)** 4 wt% PEGDA.

note that the formation of nitrogen gas during the decomposition of AIBN could also result in the formation of these larger voids.

While all the columns prepared in this work exhibited no significant radial heterogeneity (**Figure. 5.6**), not all the materials prepared in capillary format reflected that of their bulk counterparts. Both 0.1 wt% AAm (KPS) and 1 wt% AAm (AIBN) possessed larger void and window sizes when confined within the capillaries in comparison to when cured in glass vials (**Table 5.1**, entries 2 & 8, respectively). For example, the void and window size increased from 2.3 ± 0.7 and 0.6 ± 0.2 μm, respectively, to 5 ± 2 and 1.2 ± 0.5 μm for 0.1 wt% AAm (KPS), while the void and window size increased from 2.9 ± 0.6 and 0.7 ± 0.2 μm, respectively, to 6 ± 4 and 1.9 ± 0.8 μm for 1 wt% AAm (AIBN), when confined within the capillary.

The emulsions that were passed through these capillaries actually had similar droplet sizes to that of the original emulsion (**Table 5.3**, entries 2 & 8, respectively), suggesting no initial alteration in the emulsions structure occurred. However after curing these emulsions, larger void and window sizes were also obtained. This suggests that a degree of coalescence occurred during the curing process, and suggests that passing the emulsion through the narrow capillary inlet has resulted in a reduction in the stability of these particular emulsions. However, the stability of all other emulsions did not appear to be compromised (**Table 5.3**).

SEM analysis (**Figure 5.4**) revealed good attachment of the monoliths to the capillary wall and the presence of a wrinkled surface in the case of 1 wt% AAm (KPS) was again observed, indicating the presence of a hydrogel that filled the voids of this poly(HIPE), even when prepared within the capillary format. The back pressure for these columns was found to vary linearly with flow rate when both MeOH and H_2O were pumped through these columns using flow rates between 0.5 and 2.5 μL/min (**Figures 5.7** & **5.8**), which indicated no mechanical failure or compression of these monoliths occurred [32]. The column permeabilities (**Table 5.4**) also reflected that of the porous properties observed. For example a reduction in permeability from $1.3 \pm 0.1 \times 10^{-13}$ m^2 to $0.6 \pm 0.3 \times 10^{-13}$ m^2 in MeOH was observed with an increase in AAm content from 0 to 0.1 wt% when KPS was

used as initiator (entries 1 & 2, respectively), consistent with the apparent reduction in void and window size observed (**Table 5.1**).

Unfortunately the columns obtained using AIBN without AAm were not permeable, even though windows with an average size of 1.8 ± 0.6 μm (**Table 5.1**) were present (**Figure 5.4**). This is in contrast to the bulk material, which had a porosity reflective of the internal phase volume utilised (**Table 5.1**), suggesting that it was permeable (as liquid had to fill the voids for the porosity measurement). It is likely that there exist a number of non-permeable voids located along the columns length restricting the flow (as cutting the column at different lengths did not allow for liquid to flow).

The use of different initiators is known to influence window formation [33], and it is possible that the use of AIBN (without monomer in the internal phase) resulted in reduced window formation. This could simply have been a result of the larger droplets this emulsion possessed [34-35], and this only appeared to be significant when confined within the narrower dimensions of the capillary. This is consistent with a closer inspection of the capillary cross-sections (**Figure 5.4**), which revealed a larger proportion of voids with no windows in the case of AIBN, in contrast to the control column prepared with KPS. In fact, the average number of windows per void was estimated to be 1 ± 1 and 6 ± 4, respectively.

The inclusion of a co-stabiliser such as AAm, which may lower the interfacial tension and reduce the droplet size, is expected to promote window formation [36]. In accordance, the inclusion of 0.1 wt% AAm resulted in an increase in the average number of windows per void to 3 ± 3. This was consistent with the columns prepared with AAm present in the internal phase being permeable when AIBN was used as the initiator, in contrast to without AAm.

The column permeability for 1 wt% AAm (KPS) was significantly lower than that of 0.1 wt% AAm (KPS) with a value of 0.08 ± 0.01 × 10^{-13} m^2 in MeOH, even though their average void

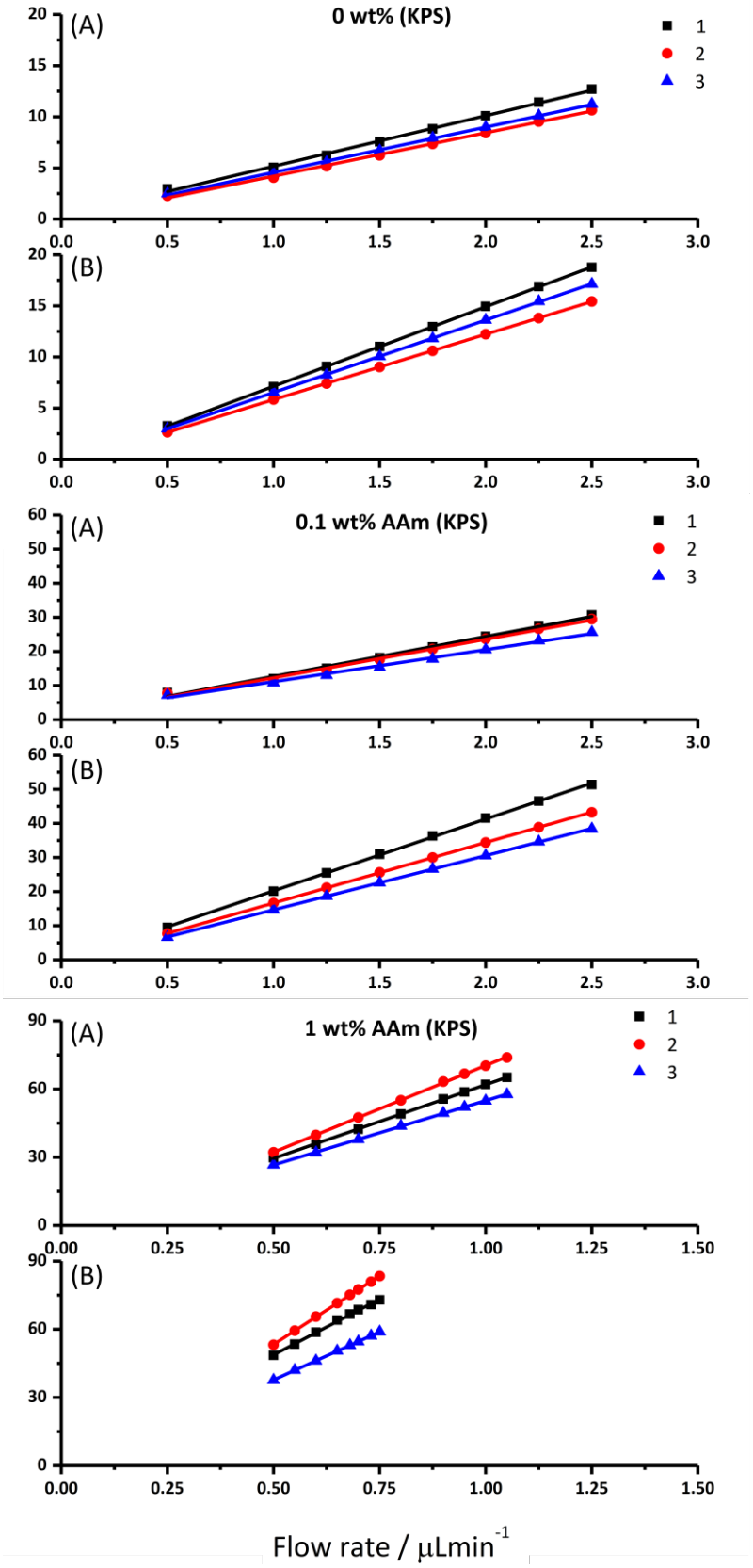

Figure 5.7. Plot of column back pressure (MPa/m) against flow rate (µL/min) for poly(Sty-*co*-DVB) poly(HIPE)s prepared in 150 µm i.d. silica capillaries from the same batch with different amounts of AAm (w.r.t. internal phase) in the internal phase using KPS as initiator and using **A)** MeOH or **B)** H_2O as the mobile phase. For each AAm concentration three replicates are shown, labeled 1, 2 & 3.

Table 5.4. Permeabilities of poly(HIPE)s prepared with different amounts of AAm or PEGDA (w.r.t. internal phase) in the internal phase in 150 µm i.d. capillaries

#	Column i.d. / µm	k_{avg} [a] (MeOH) / × 10^{-13} m^2	k_{avg} [a] (H_2O) / × 10^{-13} m^2
1	0 wt% AAm (KPS)	1.3 ± 0.1	1.4 ± 0.2
2	0.1 wt% AAm (KPS)	0.6 ± 0.3	0.7 ± 0.3
3	1 wt% AAm (KPS)	0.08 ± 0.01	0.08 ± 0.01
4	0.4 wt% PEGDA (KPS)	2.6 ± 0.5	4 ± 1
5	4 wt% PEGDA (KPS)	3.4 ± 0.2	3.9 ± 0.2
6	0 wt% AAm (AIBN)	NP *	NP *
7	0.1 wt% AAm (AIBN)	0.3 ± 0.1	0.3 ± 0.1
8	1 wt% AAm (AIBN)	2.3 ± 0.3	2.3 ± 0.3
9	0.4 wt% PEGDA (AIBN)	21 ± 3	23 ± 3
10	4 wt% PEGDA (AIBN)	200 ± 200	300 ± 300

[a] Average permeability calculated from at least three columns from the same batch of emulsion. * NP indicates the column was non-permeable.

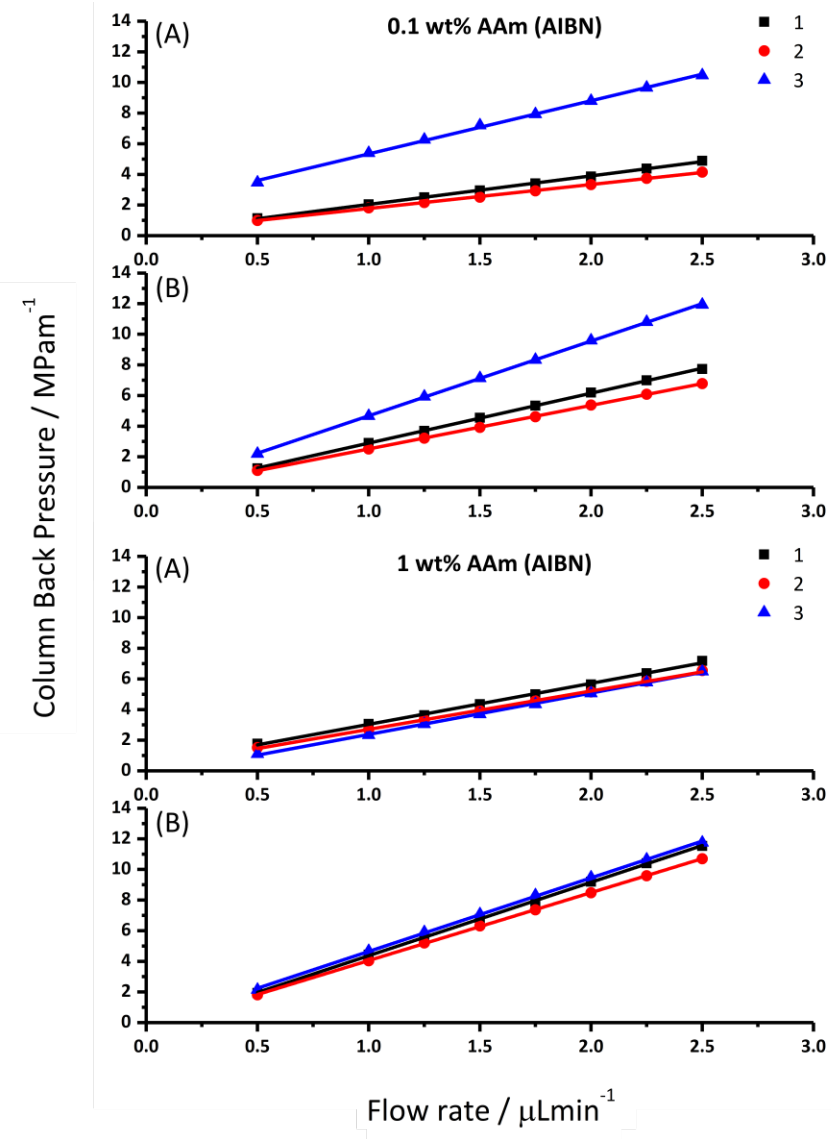

Figure 5.8. Plot of column back pressure (MPa/m) against flow rate (µL/min) for poly(Sty-*co*-DVB) poly(HIPE)s prepared in 150 µm i.d. silica capillaries from the same batch with different amounts of AAm (w.r.t. internal phase) in the internal phase using AIBN as initiator and using **A)** MeOH or **B)** H_2O as the mobile phase. For each AAm concentration three replicates are shown, labeled 1, 2 & 3.

and window sizes were not statisically different. It is important to consider that these values for the void and window size are obtained in the dry state, and may not be reflective of the solvated morphology. In particular in the case of a hydrogel, with the reduction in permeability consistent with the presence of a hydrogel that filled the voids of this poly(HIPE) and potentially reduced the window size in the solvated state.

The permeability when H_2O was used as the mobile phase was identical, suggesting that any difference in the swelling of this gel between MeOH and H_2O was not significant enough to further restrict the window size or the flow path. In contrast, when the AAm content was increased from 0.1 to 1 wt% using AIBN as initiator, the permeability in MeOH also increased from $0.3 \pm 0.1 \times 10^{-13}$ m^2 to $2.3 \pm 0.3 \times 10^{-13}$ m^2, consistent with the larger than expected voids and windows in the case of 1 wt% AAm (AIBN).

In addition to 1 wt% AAm (KPS), all other columns exhibited similar permeabilities in H_2O, suggesting that negligible shrinkage or swelling occured in these solvents. This is particularly important for their suitability to be utilised as stationary phases for liquid chromatography using a solvent gradient. It is important to note that the permeability values obtained for these poly(HIPE)s, except for 1 wt% AAm (KPS), are significantly larger than that of conventional polymer monoliths prepared using a porogen, which typically have permeabilities in the range of $(1\text{-}10) \times 10^{-14}$ [37-38]. This potentially allows these materials to be used for rapid separations with minimal increase in back pressure as previously discussed in **Chapter 4**.

5.3.3 Chromatographic performance of poly(HIPE)s grafted with AAm

As discussed, the separation performance of poly(Sty-*co*-DVB) monoliths for the separation of proteins is well documented [39]. In particular, in **Chapter 4** the applicability of the 0 wt% AAm (KPS) poly(HIPE) for the separation of a standard protein mixture consisting of ribonuclease A, lysozyme and α-chymotrypsinogen A was demonstrated by RPLC. The chromatographic performance of these poly(HIPE)s was therefore first evaluated for the separation of this mixture using this chromatographic mode and the chromatograms obtained are shown in **Figure 5.9**.

As previously demonstrated, almost baseline resolution was achieved for the 0 wt% AAm (KPS) column. However, as the AAm content was increased the co-elution between these proteins also increased. For example, significant co-elution was observed between ribonuclease A and lysozyme for 0.1 wt% AAm (KPS), while significant co-elution between all three proteins was observed for 1 wt% AAm (KPS). In all cases the peaks corresponding to lysozyme and α-chymotrypsinogen A exhibited significant rear tailing, while both the retention time and peak width increased for all proteins as the AAm content was increased. While a reduction in resolution between these proteins could simply be the result of an increase in surface hydrophilicity due to the increase in AAm content, given these analytes are separated based on hydrophobic interactions, this is inconsistent with the longer retention time observed.

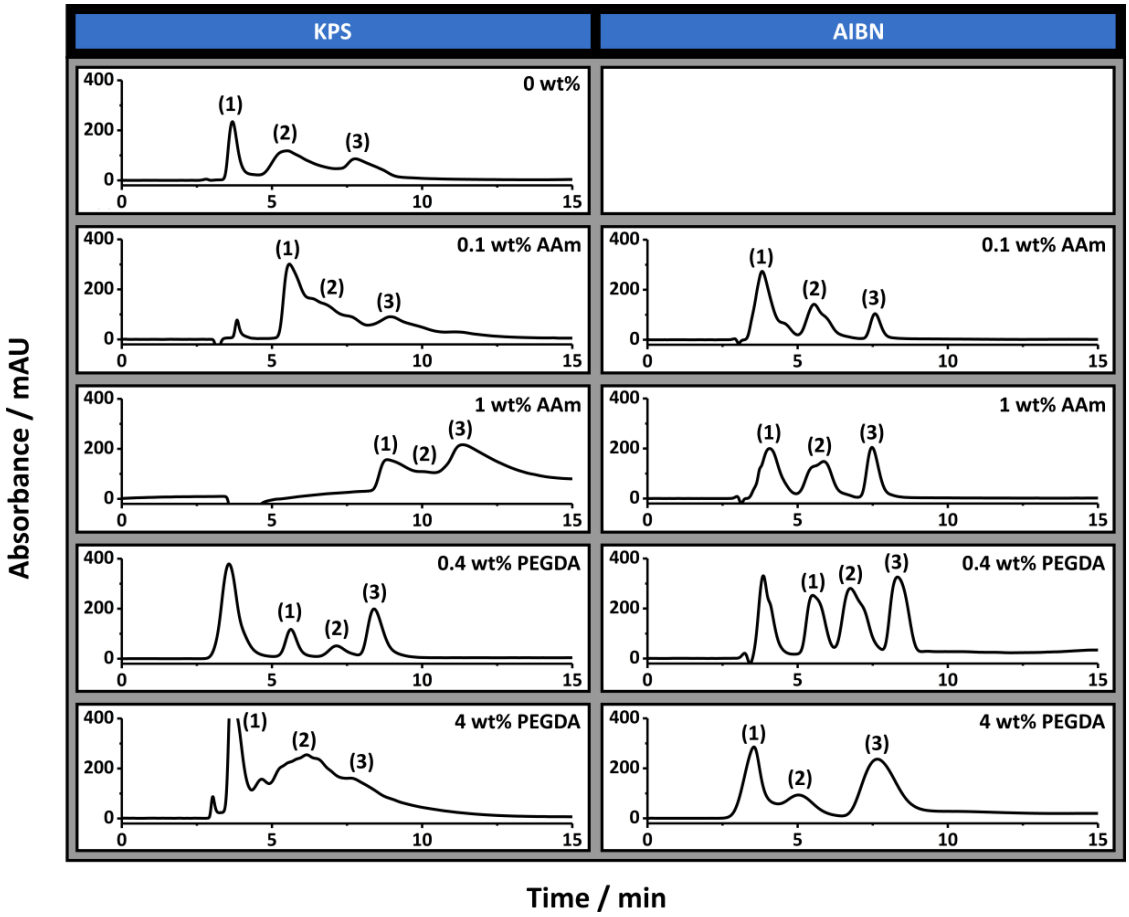

Figure 5.9. The separation of ribonuclease A (1), lysozyme (2) and α-chymotrypsinogen A (3) under reversed-phase conditions using columns prepared with different amounts of monomer in the internal phase using different initiators. Conditions: 18 cm × 150 µm i.d. columns; eluent A was 0.1 vol% formic acid in Milli-Q H_2O, and eluent B was 0.1 vol% formic acid in ACN; linear gradient 15 to 90% B in 15 min and then isocratic elution at 90% B for 5 min before returning to 15% B in 5 min; flow rate, 2.0 µL/min; injection volume, 1 µL; protein concentration, 0.05 mg/mL except for 0.1 wt% AAm (KPS) and 4 wt% PEGDA (KPS) which was 0.1 mg/mL; UV detection at 214 nm.

The increase in retention time could be related to a decrease in void and window size observed for these poly(HIPE)s when the AAm content was increased from 0 wt% to 0.1 wt%. Smaller voids and windows often correlate to increased surface areas and therefore a potentially greater interaction of the analytes with the column surface. This could also explain the broader nature of these peaks, as analytes that spend more time within the column naturally have broader peaks. However, when prepared in capillary format the broader nature of the voids and windows resulted in the difference between them not being as significant as when prepared in bulk (**Table 5.1**). Another more plausible explanation is column bed heterogeneity.

While the rear tailed nature of these peaks can be indicative of non-specific interactions [40], it can also be an indication of column bed heterogeneity [41]. It is therefore probable that the large irregular voids observed for both 0.1 wt% AAm (KPS) and 1 wt% AAm (KPS) (**Figure 5.4**) are responsible for the broad and tailed nature of these peaks and ultimately the decrease in their chromatographic performance. In addition, for 1 wt% AAm (KPS) it is also possible that the presence of the hydrogel within the voids has contributed to the heterogeneity of the flow through the column and/or a secondary interaction, resulting in its inferior performance.

As mentioned the 0 wt% AAm (AIBN) poly(HIPE) was not permeable under the pressures investigated and so its chromatographic performance could not be evaluated. However, both 0.1 wt% AAm (AIBN) and 1 wt% AAm (AIBN) exhibited a significantly improved chromatographic separation in contrast to that achieved with 0 wt% AAm (KPS). For these columns baseline resolution of these proteins was readily achieved, in particular when using a shallower solvent gradient (**Figure 5.10**). The peaks corresponding to lysozyme and α-chymotrypsinogen A also appeared narrower and more Guassian in nature, consistent with columns that possessed greater homogeneity. Of these, 1 wt% AAm (AIBN) appeared to have the most symmetrical peaks.

The reduction in rear tailing of these peaks could also have been related to the incorporation of AAm onto the surface of these poly(HIPE)s, which reduced non-specific interactions as a result of a potential increase in surface hydrophilicity. However the

retention times were identical to that of the 0 wt% AAm (KPS) column suggesting they possessed similar surface hydrophobicities. This could also have been a result of the different porous morphologies observed for these columns, but if this were the case different retention times would also have been expected. It therefore appears that the inclusion of AAm, which is acting as a co-stabiliser, has resulted in poly(HIPE)s with increased column bed homogeneity, in the case of the columns prepared with AIBN, which has resulted in a significantly improved separation of these proteins.

5.3.4 Preparation of poly(HIPE)s grafted with PEGDA

Given the improvement in chromatographic performance observed for the separation of proteins by RPLC upon the inclusion of AAm, the inclusion of the weakly hydrophilic PEGDA (M_w 258) into the emulsion formulation was also investigated. This divinyl

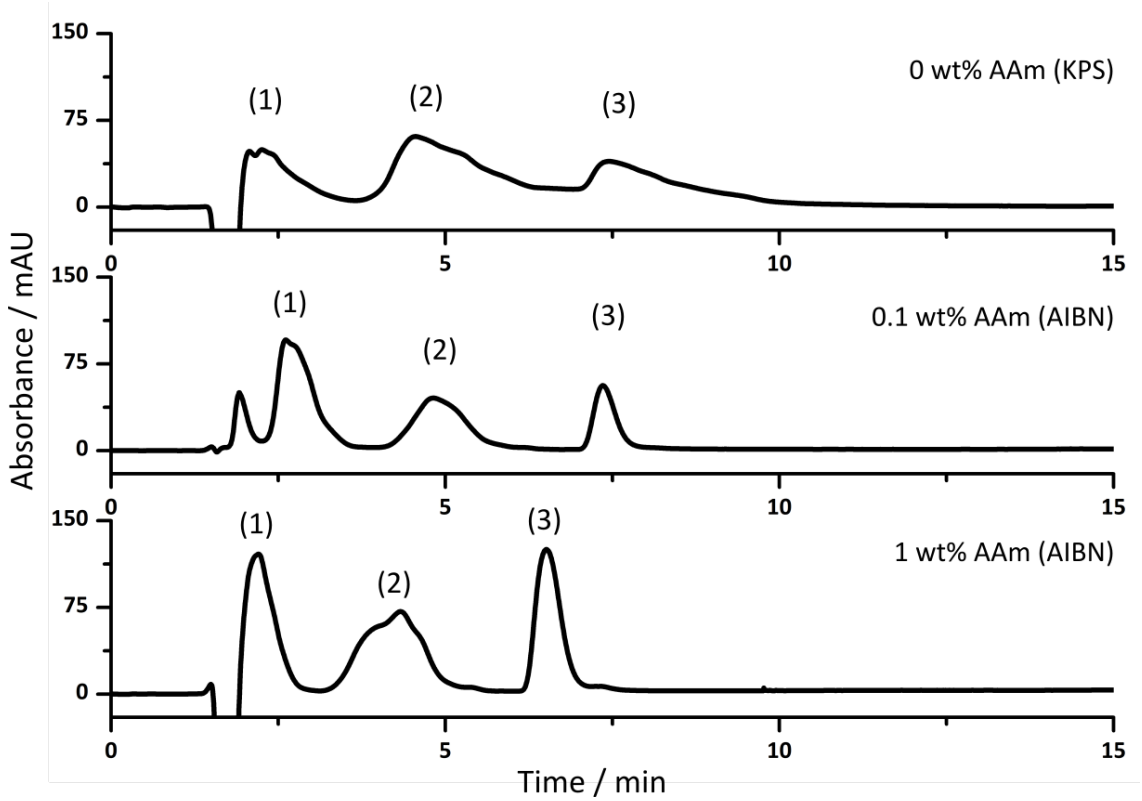

Figure 5.10. The separation of ribonuclease A (1), lysozyme (2) and α-chymotrypsinogen A (3) under reversed-phase conditions using columns prepared with different amounts of AAm in the internal phase and different initiators. Conditions: 18 cm × 150 µm i.d. columns; eluent A was 0.1 vol% formic acid in Milli-Q H_2O, and eluent B was 0.1 vol% formic acid in ACN; linear gradient 15 to 70% B in 15 min and then isocratic elution at 70% B for 5 min before returning to 15% B in 5 min; flow rate, 4.0 µL/min; injection volume, 1 µL; protein concentration, 0.05 mg/mL; UV detection at 214 nm.

monomer is expected to partition more strongly between the internal and external phase and therefore may be a better co-stabiliser than AAm, which could further improve the homogeneity of the resulting columns. In addition, this particular monomer has previously been used to obtain monoliths capable of separating proteins with high efficiency [42-43]. This was included at the same mol% as AAm, to allow representative comparisons to be achieved, though the rate of polymerisation will differ due to the divinyl nature of this monomer, and **Figure 5.1** shows the resulting bulk materials.

Similar trends were observed to that of the inclusion of AAm, with an initial reduction in void size upon the inclusion of 0.4 wt% PEGDA (**Table 5.1**) for both initiators. This decrease in void size was consistent with PEGDA also acting as a co-stabiliser. Again the material prepared with AIBN possessed a larger void size with a value of 4 ± 2 μm compared to 1.9 ± 0.5 μm for KPS. No significant alteration in the void size was observed upon increasing the PEGDA content to 4 wt% in the case of AIBN, with an average void size of 4 ± 1 μm. However the void size increased from 1.9 ± 0.5 to 4 ± 3 μm for KPS. In all cases the void size obtained was consistent with the average droplet size measured immediately after preparation (**Table 5.1** & **Figure C1** in **Appendix C**), suggesting that minimal coalescence occurred. This also indicated that coalescence was unlikely to have been the origin of the increase in void size observed for 4 wt% PEGDA (KPS).

While the inclusion of PEGDA initially appears to reduce the droplet size, it is possible that an increase in its concentration in the internal phase has resulted in migration of the Span® 80 emulsifier into the external phase [44] as it competes with PEGDA at the interface. Alternatively, the inclusion of water-soluble organics, such as PEGDA and AAm, is known to enhance the solubility of Span® 80 in the aqueous phase [26]. Both explanations would result in a reduction in the amount of Span® 80 at the interface and result in droplets of larger size with a broader distribution, which was reflected in the void structure of the resulting poly(HIPE) for 4 wt% PEGDA (KPS). This was also observed by Gitli and Silverstein [19] for their poly(HIPE) system with an initial reduction in void size upon the addition of small amounts of AAm, however as the AAm content was increased the void size also increased.

The same effect was not observed for AAm in this work but the percentage of AAm was not increased above 1 wt% (w.r.t. internal phase). The reason why this was observed for PEGDA, even though it was present at the same mol% as AAm, is potentially related to its weakly hydrophilic nature. For example, a higher proportion of PEGDA is expected to be located at the interface, in comparison to the highly hydrophilic AAm, which is primarily located in the internal phase. It is not clear though why an increase in the void size was not also observed for 4 wt% PEGDA (AIBN). In light of this discussion, it is also important to consider that the weakly hydrophilic nature of PEGDA would also result in a greater proportion partitioning into the external phase. This would result in a poly(Sty-*co*-DVB-*co*-PEGDA) poly(HIPE) as the base material. As such a proportion of the PEGDA initially incorporated into the internal phase may be buried within the backbone of the monolith and not grafted to the surface [9].

The window sizes observed (**Table 5.1**) also followed the same trends as the void size, and the porosities (**Table 5.1** & **Table C1** in **Appendix C**) were again consistent with the internal phase volume utilised for most samples. In addition negligible change in volume in both MeOH and acetone were also observed. In the case of 4 wt% PEGDA (KPS) and 4 wt% PEGDA (AIBN) the porosity values were slightly higher than expected (**Table 5.1**) suggesting some degree of creaming may have occurred. The surface areas were again also higher when KPS was utilised, in comparison to AIBN (**Table 5.1**). In terms of the surface morphology, particles were observed for both 4 wt% PEGDA (KPS) and 4 wt% PEGDA (AIBN) suggesting a degree of phase inversion occurred for these samples. This could be related to the possible migration of Span® 80 to the internal phase, which potentially stabilises (in conjunction with PEGDA) droplets of external phase monomer within the internal phase, resulting in particle formation.

Apart from the presence of these particles, both 4 wt% PEGDA (KPS) and 4 wt% PEGDA (AIBN) possessed a smooth void surface (**Figure 5.1**), suggesting the absence of a hydrogel even when KPS was used as initiator. This may suggest that the incorporation of PEGDA occurred primarily in the external phase, however FTIR (**Figure 5.11**) clearly showed the characteristic carbonyl stretch at 1732 cm^{-1} and ether stretch at 1161 cm^{-1}, suggesting the incorporation of PEGDA did occur to some degree at the surface. It is important to note

that these bonds are also present in the emulsifier Span® 80, however these signals were noticeably absent in the case of 0 wt% PEGDA (KPS) and 0 wt% PEGDA (AIBN), suggesting their origin was indeed from PEGDA. Similarly to AAm, these signals were also absent for the lower concentration of PEGDA (0.4 wt%) for both initiators, consistent with a lower incorporation of PEGDA onto the surface of the resulting poly(HIPE).

The lack of textured surface (**Figure 5.1**) coupled with the presence of these characteristic IR signals suggests that PEGDA was primarily incorporated into the resulting poly(HIPE)s by the grafting of PEGDA chains to the surface for both 4 wt% PEGDA (KPS) and 4 wt% PEGDA (AIBN) rather than forming a hydrogel, even when KPS was used as initiator. Since PEGDA itself is a cross-linker, as it possesses two vinyl groups, a higher degree of cross-linking might be expected to occur in the internal phase, however this did not appear to be the case. It is more likely that the increased partitioning of PEGDA into the external phase resulted in a reduction in the concentration of PEGDA in the internal phase that was sufficient enough to reduce the degree of polymerisation to a point where the formation of a hydrogel was avoided. The extent of homopolymerisation and the degree of co-polymerisation between the internal phase and external phase monomers also depends on their relative reactivity ratios. These values could also potentially account for the different behaviour observed, in comparison to when AAm was included in the internal phase, however these particular values were not readily available in the literature.

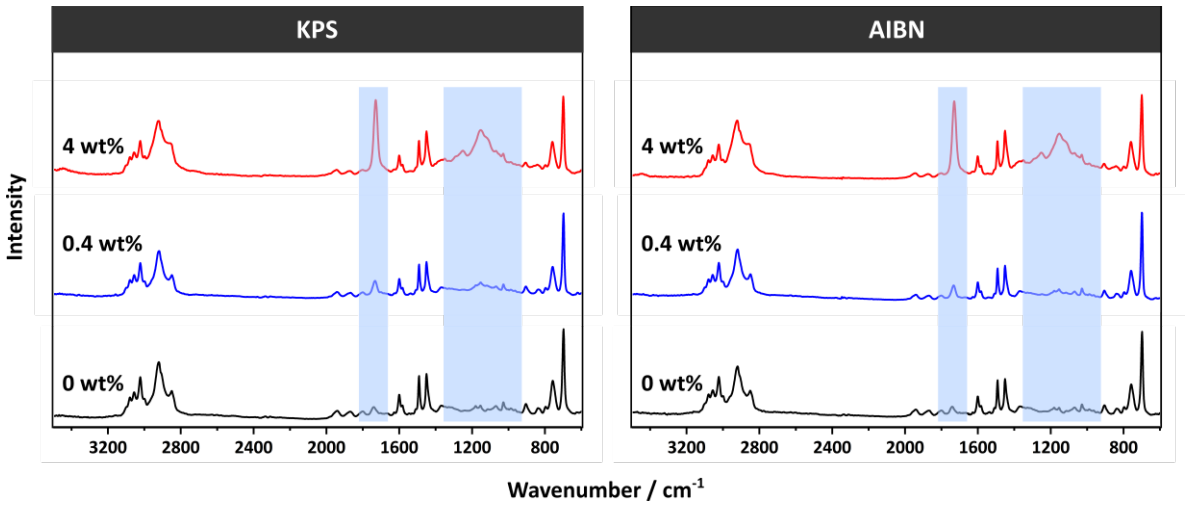

Figure 5.11. ATR-IR of poly(HIPE)s prepared with different amounts of PEGDA (w.r.t. internal phase) in the internal phase and using different initiators.

When these emulsions were confined within (**Figure 5.4** & **Table 5.1**) or passed through the 150 µm i.d. capillaries (**Figure 5.5**, **Table 5.3** & **Figure C2** in **Appendix C**) no significant alteration in the average droplet and/or resulting average void and window size was observed. Additionally, no radial heterogeneity in terms of void size was observed within the capillaries (**Figure 5.6**). In terms of homogeneity, 0.4 wt% PEGDA (KPS) appeared to have the narrowest void size distribution of these materials with an average void size of 2 ± 1 µm. However, some larger voids were again observed in its structure, in particular near the capillary wall (**Figure 5.4**). Similar voids were also observed for 0.4 wt% PEGDA (AIBN) and as discussed previously are most likely from the introduction of air bubbles. Large voids were also observed for 4 wt% PEGDA (KPS), but unlike the other materials, voids of intermediate size were observed in this case. This suggests that a degree of coalescence occurred for this material, resulting in the void size distribution observed.

While most of the poly(HIPE)s prepared in capillary format, when PEGDA was included, resembled that of their bulk counterparts, a large crater was observed for 4 wt% PEGDA (AIBN), which persisted throughout a large proportion of the column (**Figure 5.4**). This capillary actually resembled that of a wall coated open-tubular column [45]. Interestingly, the poly(HIPE) present within the capillary still had voids and windows consistent with

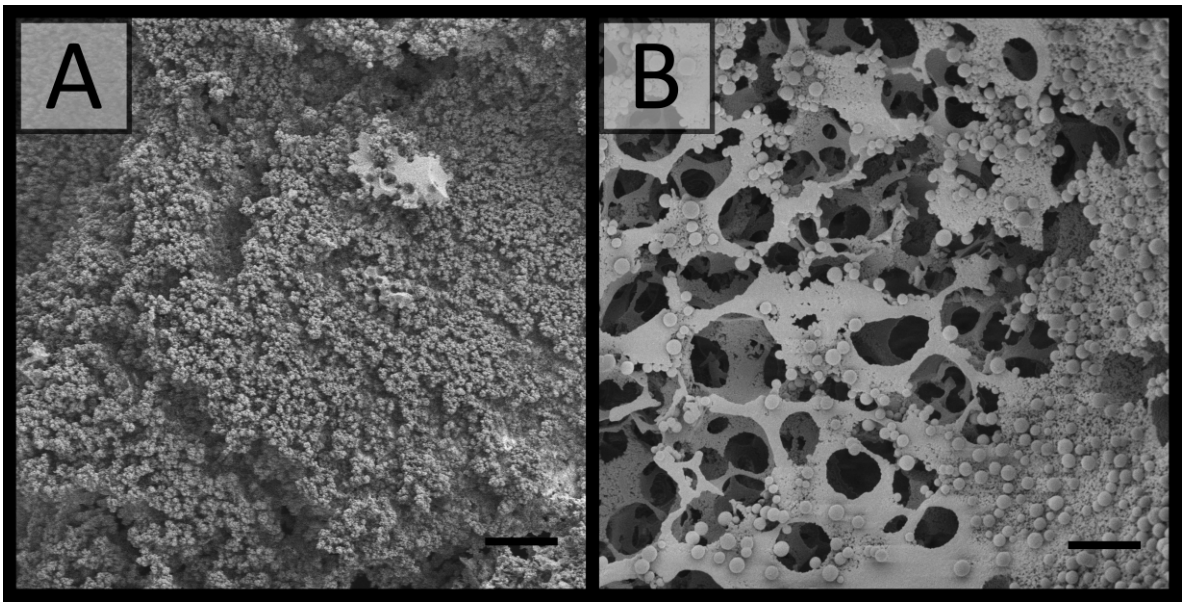

Figure 5.12. SEM images of poly(HIPE)s obtained with 4 wt% PEGDA (w.r.t. internal phase) in the internal phase using KPS as initiator. **A)** Poly(HIPE) obtained by passing the emulsion through 20 cm of capillary and **B)** Poly(HIPE) obtained by curing emulsion within capillary. Scale bar is **A)** 20 µm and **B)** 4 µm.

those present in the bulk material, suggesting that coalescence and phase separation was not responsible for this craters presence. Upon inspection of the emulsion that was passed through the capillary and cured, a significantly large proportion of particles (~500 nm in diameter) were observed in some regions (**Figure 5.12A**). These particles were also observed to be attached to the poly(HIPE) that was present within the capillary (**Figure 5.12B**).

This indicates that a degree of phase inversion has occurred, and the sheer number of particles present for the material obtained after being passed through the capillary

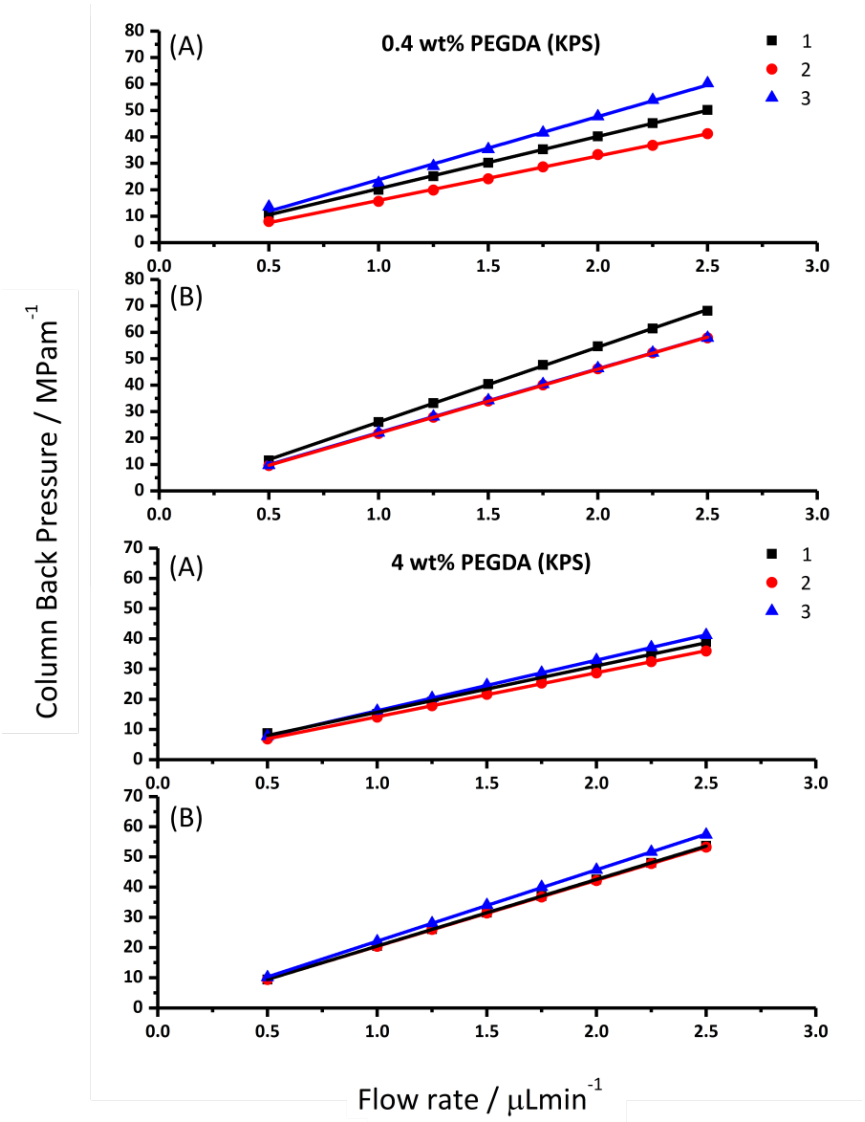

Figure 5.13. Plot of column back pressure (MPa/m) against flow rate (µL/min) for poly(Sty-*co*-DVB) poly(HIPE)s prepared in 150 µm i.d. silica capillaries from the same batch with different amounts of PEGDA (w.r.t. internal phase) in the internal phase using KPS as initiator and using **A)** MeOH or **B)** H_2O as the mobile phase. For each PEGDA concentration three replicates are shown, labeled 1, 2 & 3.

suggests this was quite significant. It is likely that this also occurred within the capillary, resulting in the generation of a large number of particles which were unbound to the poly(HIPE)s surface. As a result a significant proportion of these particles were simply removed during the purification process, resulting in the large crater observed. As discussed, this phase inversion could have been promoted by the migration of Span® 80 to the internal phase as a result of the increased PEGDA content. However, this did not occur in the case of the emulsion that was prepared and cured without being passed through the capillary. This suggests that this phase inversion was promoted by passing this

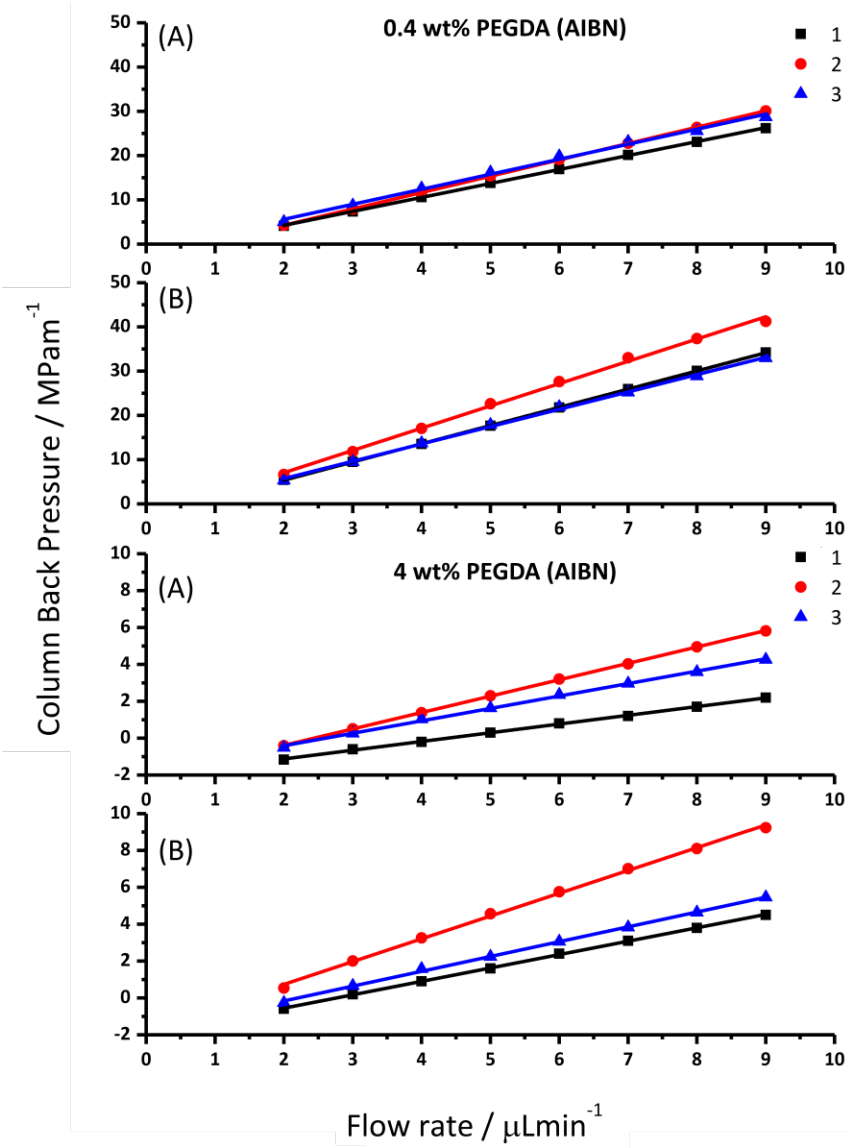

Figure 5.14. Plot of column back pressure (MPa/m) against flow rate (µL/min) for poly(Sty-*co*-DVB) poly(HIPE)s prepared in 150 µm i.d. silica capillaries from the same batch with different amounts of PEGDA (w.r.t. internal phase) in the internal phase using AIBN as initiator and using **A)** MeOH or **B)** H_2O as the mobile phase. For each PEGDA concentration three replicates are shown, labeled 1, 2 & 3.

emulsion through the narrow capillary inlet. The reason for this and why this did not occur in the case of 4 wt% PEGDA (KPS) is not clear.

Apart from 4 wt% PEGDA (AIBN) all other poly(HIPE)s had good attachment to the capillary wall (**Figure 5.4**). In addition the back pressure was observed to vary linearly with flow rate (**Figures 5.13** & **5.14**) again suggesting that no mechanical failure or compression occurred. The permeabilities (**Table 5.4**) were also consistent with the trends observed with the void and window size (**Table 5.1**), however the back pressure for 4 wt% PEGDA (AIBN) was very similar to the back pressure of the system. This was a result of its open-tubular nature, which made it difficult to accurately determine its permeability.

5.3.5 Chromatographic performance of poly(HIPE)s grafted with PEGDA

These columns were also evaluated for the RPLC separation of the same protein mixture and the chromatograms obtained are also shown in **Figure 5.9**. Both 0.4 wt% PEGDA (KPS) and 0.4 wt% PEGDA (AIBN) offered a significantly improved chromatographic separation for these proteins in comparison to the control column prepared with no PEGDA. These separations had significantly improved peak shape, suggesting the inclusion of PEGDA had also improved the column bed homogeneity. The separation achieved with these columns was similar to that achieved with 1 wt% AAm (AIBN), except both 0.4 wt% PEGDA (KPS) and 0.4 wt% PEGDA (AIBN) were capable of separating these proteins from the peak corresponding to impurities from ribonuclease A and lysozyme (the first peak in the corresponding chromatograms in **Figure 5.9**). Interestingly both these columns had very similar chromatographic separations, even though their porous properties were significantly different (**Table 5.1**). This clearly highlights the importance of column homogeneity on the separation performance.

Significant co-elution of these proteins was observed in the case of 4 wt% PEGDA (KPS), which was consistent with the broader void size distribution observed (**Figure 5.4** & **Table 5.1**). Surprisingly the separation obtained with 4 wt% PEGDA (AIBN) was good, with only slight co-elution between ribonuclease A and lysozyme, which suggests the applicability of

these materials for open-tubular liquid chromatography [45]. The use of a shallower gradient again resulted in improvements in these separations, which is demonstrated for some of these columns in **Figure 5.15**.

The improvement in chromatographic performance under RPLC conditions for the separation of proteins upon the inclusion of PEGDA in the emulsion formulation was further demonstrated with the separation of a more complex protein mixture using the 0.4 wt% PEGDA (KPS) column (**Figure 5.16**). Here a reasonable separation was obtained where seven components of the mixture were clearly identifiable. This was in contrast to that of the column without PEGDA where significant co-elution between these components was observed.

5.3.6 Application of poly(HIPE)s grafted with AAm for HILIC

While the inclusion of the weakly hydrophilic PEGDA into the emulsion formulation resulted in a significant improvement in the separation of proteins by RPLC, the inclusion

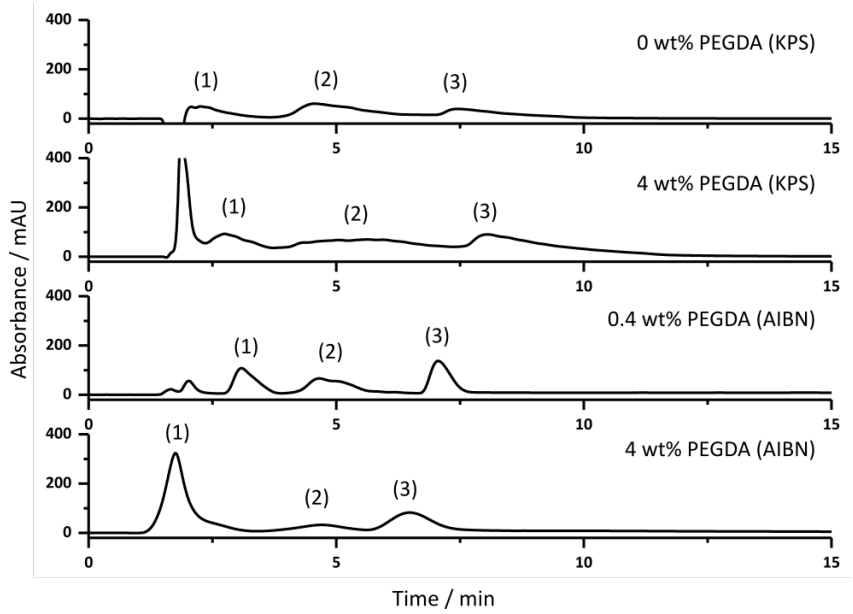

Figure 5.15. The separation of ribonuclease A (1), lysozyme (2) and α-chymotrypsinogen A (3) under reversed-phase conditions using columns prepared with different amounts of PEGDA in the internal phase and different initiators. Conditions: 18 cm × 150 µm i.d. columns; eluent A was 0.1 vol% formic acid in Milli-Q H_2O, and eluent B was 0.1 vol% formic acid in ACN; linear gradient 15 to 70% B in 15 min and then isocratic elution at 70% B for 5 min before returning to 15% B in 5 min; flow rate, 4.0 µL/min; injection volume, 1 µL; protein concentration, 0.05 mg/mL, except for 4 wt% PEGDA (KPS) which was 0.1 mg/mL; UV detection at 214 nm.

of the hydrophilic AAm monomer is expected to impart a degree of hydrophilicity to the poly(HIPE) surface [19]. This might allow for the use of these poly(HIPE)s for other chromatographic modes, such as HILIC. For example, AAm-based monoliths have previously been utilised for the separation of polar compounds making use of the hydrophilic interactions between the analytes and the monolithic surface [46-47]. In addition, silica monoliths coated with poly(AAm) have also been reported for the separation of polar compounds such as nucleosides, under HILIC conditions [48]. As such the retention of several analytes, AAm, thiourea, the nucleosides cytidine and guanosine, and a commercially available mixture of peptides (angiotensin II, Gly-Tyr, Leu encephalin, Met encephalin and Val-Tyr-Val) were investigated under isocratic conditions for the poly(HIPE)s prepared with AAm.

In HILIC polar analytes are retained more strongly in high percentages of organic solvent and are eluted more easily when the H_2O content is increased [5]. In accordance with this a mobile phase consisting of 99 vol% ACN was employed to investigate the HILIC character of these columns. No retention was observed for these analytes using 0 wt% AAm (KPS),

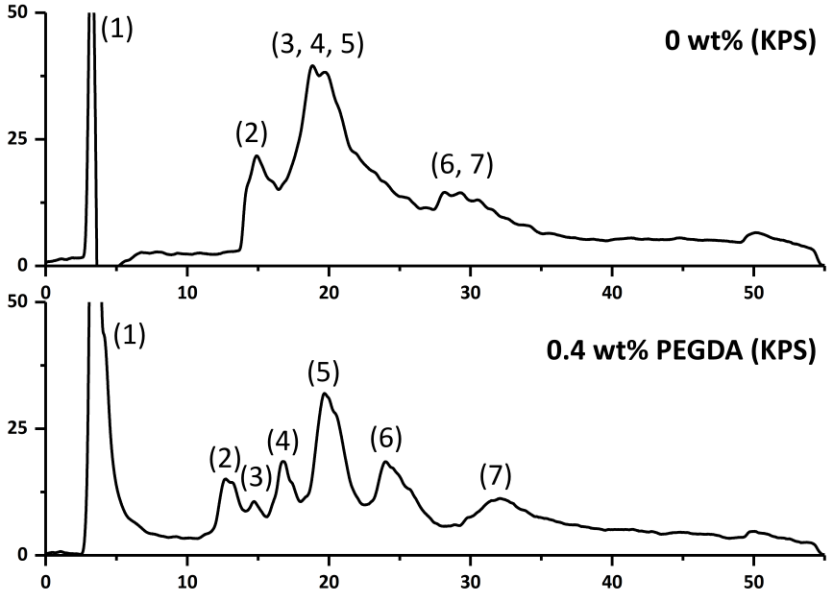

Figure 5.16. The separation of impurities from ribonuclease A and lysozyme (1), ribonuclease A (2) impurity from ovalbumin (3), cytochrome *c* (4), lysozyme (5), myoglobin (6) and ovalbumin (7) using columns prepared with different amounts of PEGDA. Conditions: 18 cm × 150 µm i.d. columns; eluent A was 0.1 vol% formic acid in Milli-Q H_2O, and eluent B was 0.1 vol% formic acid in ACN; linear gradient 5 to 50% B in 40 min and then isocratic elution at 50% B for 5 min before returning to 5% B in 5 min; flow rate, 2.0 µL/min; injection volume, 1 µL; protein concentration, 0.025 mg/mL except for ovalbumin which was 0.05 mg/mL; UV detection at 214 nm.

which is consistent with its hydrophobic nature. Additionally, no retention was observed for both 0.1 wt% AAm (KPS) and 0.1 wt% AAm (AIBN), consistent with their low AAm content (**Table 5.2**). No retention was also observed in the case of 1 wt% AAm (AIBN), even though this material had the highest AAm content (**Table 5.2**). This suggested that the hydrophilic character of this column was limited, which is consistent with the identical retention times observed for the proteins separated in RPLC for this column to that of the column prepared without AAm (**Figure 5.9**), which suggested these columns possessed similar surface hydrophobicities.

In contrast, 1 wt% AAm (KPS) was able to retain guanosine and separate two of the five peptides at this ACN content (**Figure 5.17**). The ability to retain these analytes is potentially related to the presence of the AAm-based hydrogel that filled the voids of this poly(HIPE) (**Figure 5.4**). Reducing the ACN content in the mobile phase resulted in a decrease in retention, and this evident in **Figure 5.17** when the ACN content was reduced to 95 and 90 vol% ACN. The decreased retention with a decrease in ACN content is also

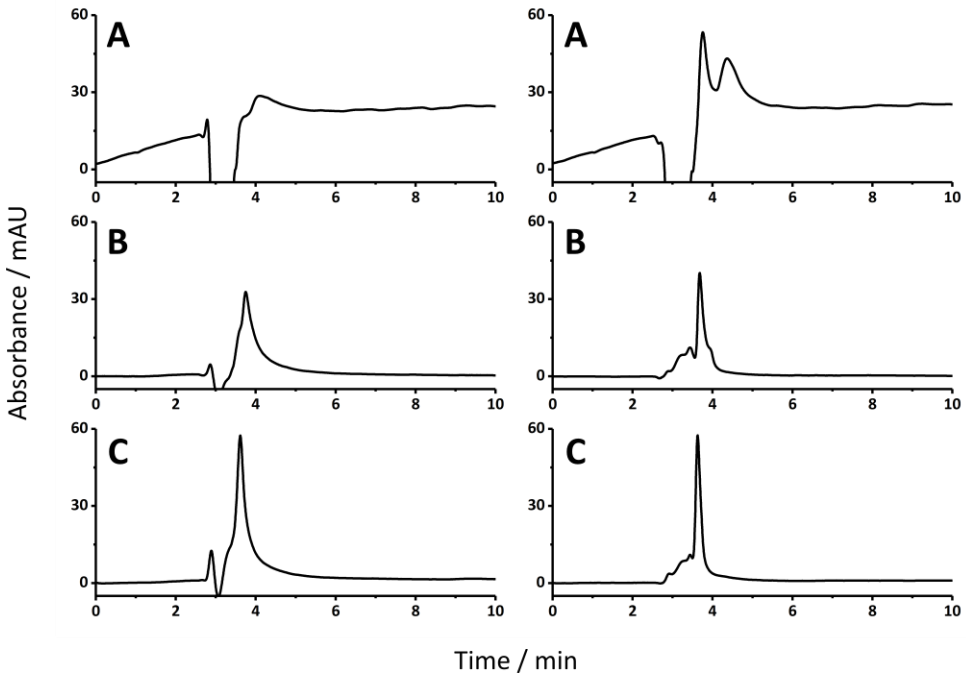

Figure 5.17. The retention of guanosine (left) and the separation of a peptide mixture containing angiotensin II, Gly-Tyr, Leu encephalin, Met encephalin and Val-Tyr- Val (right) under isocratic conditions with different ACN content on the 1 wt% AAm (KPS) column. Conditions: 18 cm × 150 µm i.d. column; eluent A was ACN, and eluent B was Milli-Q H_2O; isocratic conditions for 10 min total duration; flow rate, 2.0 µL/min; injection volume, 1 µL; guanosine concentration, 0.05 mg/mL and the peptide mix was 0.0025 mg/mL; UV detection at 214 nm. **(A)** 99% ACN, **(B)** 95% ACN and **(C)** 90% ACN.

clear from plotting the average retention time taken from three consecutive injections of guanosine against ACN content, which was varied between 99 and 40 vol% (**Figure 5.18**). This behaviour is characteristic of a hydrophilic interaction [5], which is promoted at higher ACN contents and then subsequently reduced as the ACN decreases, resulting in reduced retention. Ultimately this reaches a critical value where the reversed-phase properties of the column become more apparent and the retention again increases.

The lack of retention for 1 wt% AAm (AIBN) in contrast to that of 1 wt% AAm (KPS) could be the result of the significantly larger windows this material possessed, which could limit the interactions with the analytes. However the retention of analytes in RPLC did not appear to be significantly influenced by the presence of these larger windows, with very similar retention to both 0 wt% AAm (KPS) and 0.1 wt% AAm (AIBN), which had much smaller windows, albeit this is a different chromatographic mode using different analytes. The lack of retention is likely to be related to the presence of AAm chains on the surface, rather than an AAm-based hydrogel that filled the voids. Even though the AAm content was lower in the case of 1 wt% AAm (KPS), the formation of this hydrogel appears to have been advantageous for this particular application, in contrast to its inferior performance under RPLC conditions.

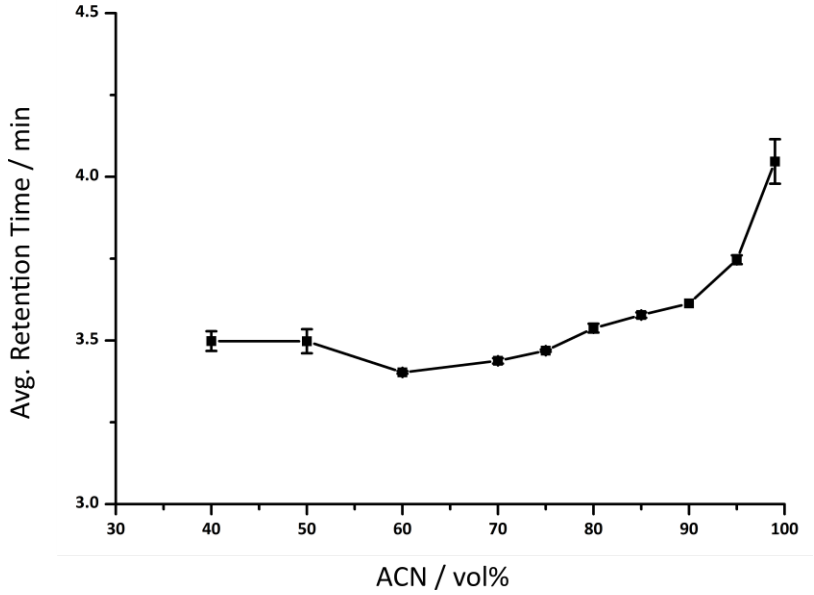

Figure 5.18. The effect of ACN content on the retention of guanosine for the 1 wt% AAm (KPS) column. Conditions: 18 cm × 150 µm i.d. column; eluent A was ACN, and eluent B was Milli-Q H_2O; isocratic conditions for 10 min total duration; flow rate, 2.0 µL/min; injection volume, 1 µL; guanosine concentration, 0.05 mg/mL; UV detection at 214 nm.

While the complete separation of the peptide mixture or significantly enhanced retention for the analytes investigated was not demonstrated with this column, it appears that the grafting approach used in this work can be beneficial for obtaining materials with hydrophilic character. The use of poly(Sty-*co*-DVB) as the backbone may also have been detrimental for this particular application as very few styrene-based monoliths have been reported for use in HILIC due to their strong hydrophobic character [5]. However, it has been shown that the surface hydrophilicity can be increased sufficiently to retain some analytes through the incorporation of an AAm-based hydrogel.

Further optimisation and modification of the structure may yet yield improved chromatographic separations using HILIC. However, these particular materials may also find applications elsewhere, for example hydrophilic poly(2-ethylhexyl acrylate-*co*-DVB) poly(HIPE)s have recently been announced for use in sanitary napkins by P&G [27]. Additionally, the poly(HIPE)s grafted with PEG chains could be useful as biocompatible materials capable of resisting the non-specific adsorption of proteins [49], or for stationary phases for HIC [43, 50], which is a chromatographic mode that better preserves the proteins native conformation in contrast to RPLC and relies on the presence of both hydrophobic and hydrophilic patches on the surface [49].

5.4 Conclusions

In summary a series of poly(Sty-*co*-DVB)-based poly(HIPE)s were prepared by including the monomers AAm or PEGDA into the internal phase and emulsifying under high shear. It was found that both AAm and PEGDA acted as co-stabilisers resulting in significantly improved column bed homogeneity when these poly(HIPE)s were prepared in capillary format. This resulted in significantly improved chromatographic performance for the separation of proteins by RPLC, where a poly(HIPE) grafted with PEGDA was capable of separating a more complex protein mixture, consisting of seven components. This highlights the benefit of including co-stabilisers in the emulsion formulation for obtaining columns with enhanced homogeneity.

In addition, a poly(HIPE) grafted with an AAm-hydrogel was found to be suitable for the separation of two components of a peptide mixture by HILIC. The formation of this hydrogel was promoted by an increase in the AAm content and the use of the water-soluble initiator KPS. This demonstrated that the inclusion of monomers in the internal phase was also an appropriate method for the surface functionalisation of these materials. This route potentially allows for the preparation of poly(HIPE)s with improved homogeneity and tailored surface chemistry for various applications, simply by including monomers in the internal phase and optimising the monomer content and initiation location based on the intended application.

5.5 References

[1] Chen, M. L.; Li, L. M.; Yuan, B. F.; Ma, Q.; Feng, Y. Q. *J. Chromatogr. A.* **2012**, *1230*, 54-60.
[2] Holdšvendová, P.; Suchánková, J.; Bunček, M.; Bačkovská, V.; Coufal, P. *J. Biochem. Biophys. Methods.* **2007**, *70*, 23-29.
[3] Lin, J.; Lin, J.; Lin, X.; Xie, Z. *J. Chromatogr. A.* **2009**, *1216*, 801-806.
[4] Lin, J.; Lin, J.; Lin, X.; Xie, Z. *J. Chromatogr. A.* **2009**, *1216*, 7728-7731.
[5] Jiang, Z.; Smith, N. W.; Liu, Z. *J. Chromatogr. A.* **2011**, *1218*, 2350-2361.
[6] Krajnc, P.; Štefanec, D.; Pulko, I. *Macromol. Rapid Commun.* **2005**, *26*, 1289-1293.
[7] Hua, Y.; Zhang, S.; Zhu, Y.; Chu, Y.; Chen, J. *J. Polym. Sci. A Polym. Chem.* **2013**, *51*, 2181-2187.
[8] Gitli, T.; Silverstein, M. S. *Polymer.* **2011**, *52*, 107-115.
[9] Svec, F. *J. Chromatogr. A.* **2010**, *1217*, 902-924.
[10] Desire, C. T.; Hilder, E. F.; Arrua, R. D. in *Monolithic High-Performance Liquid Chromatography Columns*, *Vol.* 2017; pp. 1-37.
[11] Mercier, A.; Deleuze, H.; Mondain-Monval, O. *React. Funct. Polym.* **2000**, *46*, 67-79.
[12] Cameron, N. R.; Sherrington, D. C.; Ando, I.; Kurosu, H. *J. Mater. Chem.* **1996**, *6*, 719-726.
[13] Benicewicz, B. C.; Jarvinen, G. D.; Kathios, D. J.; Jorgensen, B. S. *J. Radioanal. Nucl. Chem.* **1998**, *235*, 31-35.
[14] Sevšek, U.; Krajnc, P. *React. Funct. Polym.* **2012**, *72*, 221-226.
[15] Audouin, F.; Fox, M.; Larragy, R.; Clarke, P.; Huang, J.; O'Connor, B.; Heise, A. *Macromolecules.* **2012**, *45*, 6127-6135.
[16] Hayward, A. S.; Sano, N.; Przyborski, S. A.; Cameron, N. R. *Macromol. Rapid. Commun.* **2013**, *34*, 1844-1849.
[17] Kovačič, S.; Jeřabek, K.; Krajnc, P. *Macromol. Chem. Phys.* **2011**, *212*, 2151-2158.
[18] Jiang, Q.; Menner, A.; Bismarck, A. *Pure Appl. Chem.* **2014**, *86*, 203-213.
[19] Gitli, T.; Silverstein, M. S. *Soft Matter.* **2008**, *4*, 2475–2485.
[20] Sun, F.; Ruckenstein, E. *J. Memb. Sci.* **1993**, *85*, 59-69.
[21] Park, J. S.; Ruckenstein, E. *J. Appl. Polym. Sci.* **1989**, *38*, 453–461.

[22] Ruckenstein, E.; Park, J. S. *J. Appl. Polym. Sci.* **1990**, *40*, 213–220.
[23] Viswanathan, P.; Johnson, D. W.; Hurley, C.; Cameron, N. R.; Battaglia, G. *Macromolecules.* **2014**, *47*, 7091−7098.
[24] Williams, J. M.; Gray, A. J.; Wilkerson, M. H. *Langmuir.* **1990**, *6*, 437–444.
[25] Cameron, N. R.; Sherrington, D. C. *Adv. Polym. Sci.* **1996**, *126*, 162-214.
[26] Zhu, J.-H.; Shao, F.; Zhan, Y.-H.; Yan, X.-L.; Zhang, B. *Colloids Surf., A.* **2006**, *290*, 19-24.
[27] Jiang, Q.; Menner, A.; Bismarck, A. *React. Funct. Polym.* **2017**, *114*, 104-109.
[28] Cohen, N.; Samoocha, D. C.; David, D.; Silverstein, M. S. *J. Polym. Sci. A Polym. Chem.* **2013**, *51*, 4369-4377.
[29] Graillat, C.; Pichot, C.; Guyot, A.; Aasser, M. S. E. *J. Polym. Sci. A Polym. Chem.* **1986**, *24*, 427–449.
[30] Sangster, J. *J. Phys. Chem. Ref. Data.* **1989**, *18*, 1111-1227.
[31] Brandrup, J.; Immergut, E. H.; Grulke, E. A. *Polymer Handbook*. 4th. John Wiley & Sons, Inc: Hoboken, N.J, 1999.
[32] Nischang, I.; Svec, F.; Fréchet, J. M. J. *Anal. Chem.* **2009**, *81*, 7390-7396.
[33] Quell, A.; Bergolis, B. d.; Drenckhan, W.; Stubenrauch, C. *Macromolecules.* **2016**, *49*, 5059−5067.
[34] Luo, Y.; Wang, A.-N.; Gao, X. *Soft Matter.* **2012**, *8*, 7547-7551.
[35] Mathieu, K.; Jérôme, C.; Debuigne, A. *Polymer.* **2016**, *99*, 157-165.
[36] Williams, J. M.; Wrobleski, D. A. *Langmuir.* **1988**, *4*, 656-662.
[37] Nischang, I.; Svec, F.; Fréchet, J. M. *J. Chromatogr. A.* **2009**, *1216*, 2355-2361.
[38] Trojer, L.; Lubbad, S. H.; Bisjak, C. P.; Wieder, W.; Bonn, G. K. *J. Chromatogr. A.* **2007**, *1146*, 216-224.
[39] Svec, F. *J. Sep. Sci.* **2004**, *27*, 1419-1430.
[40] Guiochon, G. *J. Chromatogr. A.* **2007**, *1168*, 101-168.
[41] Miyabe, K.; Guiochon, G. *J. Chromatogr. A.* **1999**, *830*, 29–39.
[42] Desire, C. T.; Arrua, R. D.; Talebi, M.; Lacher, N. A.; Hilder, E. F. *J. Sep. Sci.* **2013**, *36*, 2782-2792.
[43] Li, Y.; Tolley, H. D.; Lee, M. L. *Anal. Chem.* **2009**, *81*, 9416-9424.
[44] Carnachan, R. J.; Bokhari, M.; Przyborski, S. A.; Cameron, N. R. *Soft Matter.* **2006**, *2*, 608-616.
[45] Choudhury, S.; Connolly, D.; White, B. *J. Appl. Polym. Sci.* **2016**, *133*, 44237.
[46] Freitag, R. *J. Chromatogr. A.* **2004**, *1033*, 267-273.
[47] Jiang, Z.; Smith, N. W.; Ferguson, P. D.; Taylor, M. R. *J. Sep. Sci.* **2009**, *32*, 2544-2555.
[48] Ikegami, T.; Fujita, H.; Horie, K.; Hosoya, K.; Tanaka, N. *Anal. Bioanal. Chem.* **2006**, *386*, 578-585.
[49] Li, Y.; Lee, M. L. *J. Sep. Sci.* **2009**, *32*, 3369-3378.
[50] Li, Y.; Tolley, H. D.; Lee, M. L. *J. Chromatogr. A.* **2010**, *1217*, 4934-4945.

Appendix C

The preparation of styrene-based polymerised high internal phase emulsions functionalised with monomers from the internal phase for liquid chromatography

C.1 Optical Microscopy

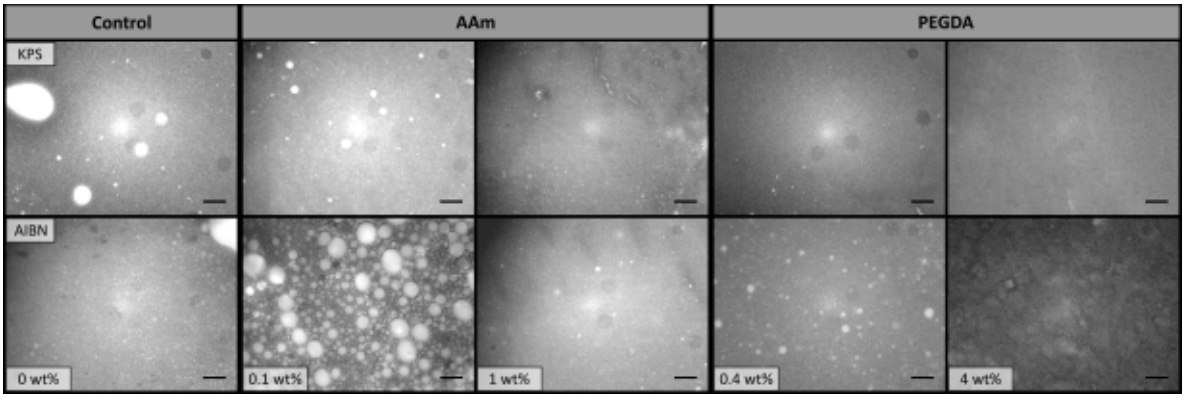

Figure C1. Optical microscopy images of emulsions prepared with different amounts of monomer (w.r.t. internal phase) in the internal phase immediately after preparation. Scale bar is 50 µm.

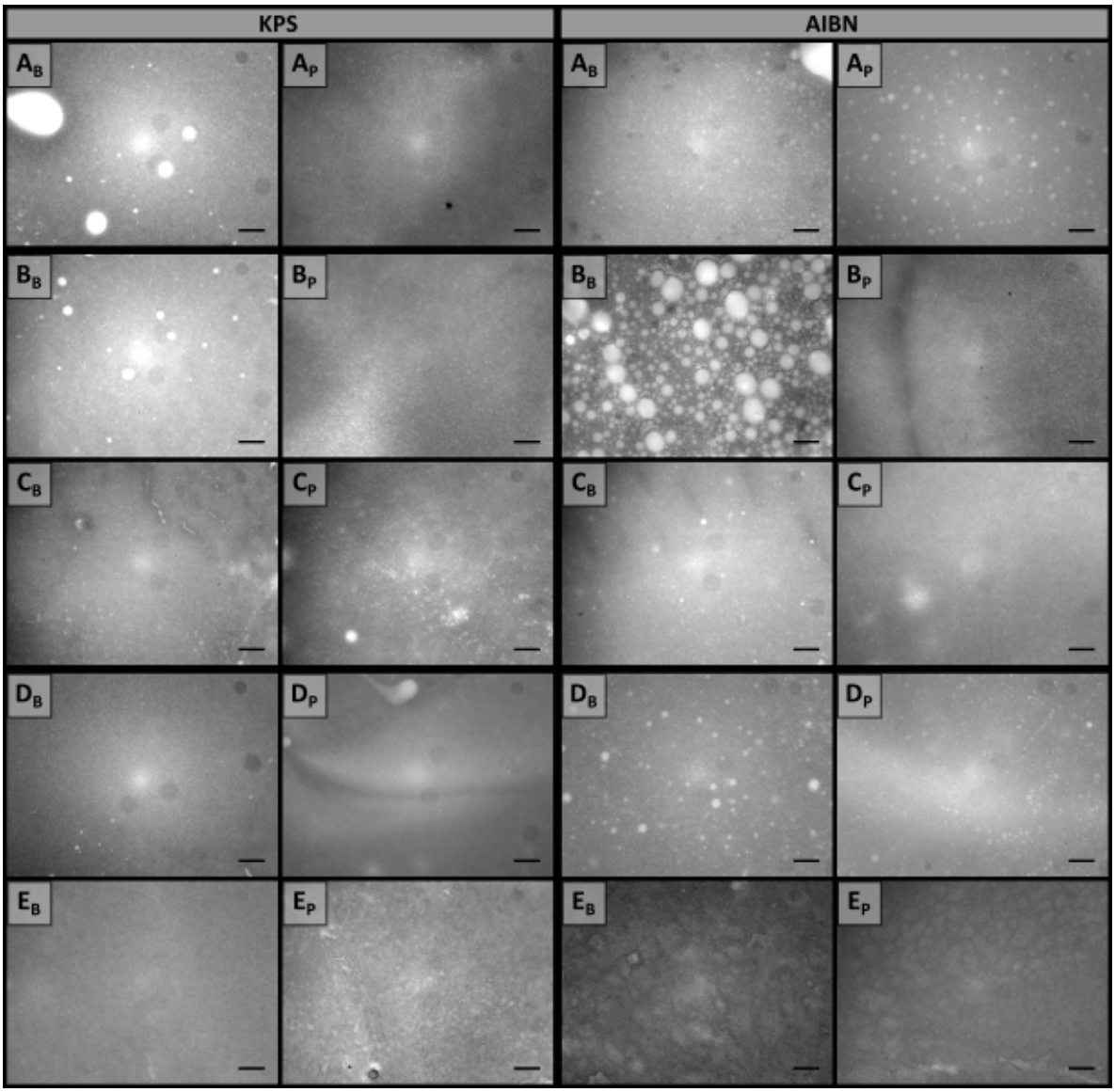

Figure C2. Optical microscopy images of emulsions prepared with different amounts of monomer (w.r.t. internal phase) in the internal phase and using different initiators. **A)** 0 wt%, **B)** 0.1 wt% AAm, **C)** 1 wt% AAm, **D)** 0.4 wt% PEGDA and **E)** 4 wt% PEGDA. ^{B} indicates the bulk emulsions immediately after preparation, ^{P} indicates emulsions after being passed through 20 cm of capillary. Scale bar is 50 µm.

C.2 Swelling Characteristics

Table C1 Swelling characteristics of poly(HIPE)s prepared with different amounts of AAm or PEGDA (w.r.t. internal phase) in the internal phase and using different initiators

Sample	φ^{M} / %	ΔV^{M} / %	$m_s{}^{M}$ / %	φ^{A} / %	ΔV^{A} / %	$m_s{}^{A}$ / %
0 wt% (KPS)	97 ± 4	- 10 ± 9	900 ± 20	110 ± 3	- 8 ± 2	970 ± 20
0.1 wt% AAm (KPS)	86 ± 5	12 ± 9	910 ± 30	97 ± 4	- 6 ± 7	1013 ± 9
1 wt% AAm (KPS)	83 ± 7	10 ± 10	930 ± 30	91 ± 4	10 ± 10	980 ± 20
0.4 wt% PEGDA (KPS)	98 ± 7	10 ± 10	890 ± 50	88 ± 4	0 ± 10	940 ± 40
4 wt% PEGDA (KPS)	97.5 ± 0.3	2 ± 3	650 ± 30	93 ± 1	14 ± 3	700 ± 20
0 wt% (AIBN)	96 ± 8	- 10 ± 20	880 ± 60	103 ± 6	- 10 ± 20	970 ± 80
0.1 wt% AAm (KPS)	108 ± 8	- 5 ± 1	850 ± 20	110 ± 10	0 ± 40	970 ± 30
1 wt% AAm (AIBN)	89 ± 7	10 ± 10	760 ± 20	100 ± 10	3 ± 6	840 ± 30
0.4 wt% PEGDA (AIBN)	98 ± 5	4 ± 9	820 ± 20	116 ± 5	4 ± 4	930 ± 20
4 wt% PEGDA (AIBN)	105 ± 5	- 8 ± 4	690 ± 10	104 ± 6	2 ± 8	750 ± 20

φ signifies the porosity of the disk, ΔV signifies the change in the volume of polymer disk relative to the original volume and m_s indicates the mass of solvent present in the disk relative to the mass of the dry disk. ^{A} These values were determined through immersion in acetone. ^{M} These values were determined through immersion in MeOH.

Chapter 6

Preparation of polymer monoliths from colloidal gels formed using latexes prepared from the soap-free emulsion polymerisation of styrene

6.1 Introduction

Since their development in the 1990s [1-2] polymer monoliths have attracted significant attention, in particular as materials for solid phase chemistry [3], as catalytic supports [4-8], metal chelating agents [9], tissue engineering scaffolds [10-11], controlled release devices [12], absorbents [13], chromatography [2-3, 14-16] and for extraction and sample preparation [9, 17-19]. As discussed in **Chapter 1** polymer monoliths have several advantages over conventional formats such as packed-beds, owing to their high permeability, enhanced mass transfer as a result of convective flow, ease of miniaturisation, and the associated lower solvent/sample consumption. These properties therefore allow for higher-throughput and greater process efficiency [14]. In accordance polymer monoliths have been identified as greener alternatives to these other formats [4-7, 10, 14].

Polymer monoliths are most commonly prepared by phase separation from a binary solvent mixture, referred to as the porogen [3, 20], where the monomers (usually a functional and cross-linking monomer) and a suitable free-radical initiator are dissolved. During polymerisation the growing polymer chains undergo phase separation and precipitate as a continuous cross-linked porous material, with the porogen composition influencing the porous properties [21]. The choice of porogen itself is more historical than based on a set of rigid scientific criteria; with most groups opting for previously published solvent mixtures [22]. A wide variety of monomers have been utilised for this approach, including acrylates [23-24], methacrylates [25-26], styrene/divinylbenzene [27-29] and acrylamides [30-31].

In particular poly(styrene)-based monoliths have been demonstrated to be green alternatives for catalysis [4-7], as absorbents [13] and for chromatography [14]. However, the porogen utilised in their preparation, in most cases, consists of a mixture of toluene and dodecanol, and the monolith is often purified using THF [4-7, 29]. The use of toluene and THF is concerning from an industrial and environmental perspective, as both have been classed as problematic for implementation at the production scale, based on a set of safety, health and environmental criteria [32]. It is therefore desirable to utilise greener alternatives. However replacement of the porogenic solvent is not a straightforward process, requiring re-optimisation of its composition and the polymerisation conditions, with no guarantee that suitable porous properties will be obtained [22, 33]. Water, in particular, is problematic for this approach, given the low water-solubility of styrene.

Other approaches, such as the use of emulsion templates (for example those in **Chapters 4** & **5**), do allow for the use of water [13, 34-35], however this typically requires the presence of relatively large amounts of surfactant, which introduces additional purification requirements and can be difficult to completely remove [10]. In general, the toxicity and environmental impact of surfactant waste is unclear, requiring an in-depth investigation for individual cases [36-39]. In addition, surfactants can also act as plasticisers for polymer-based materials reducing their mechanical properties [40-41]. Ionic liquids have also been employed in the preparation of poly(styrene)-based monoliths [14], however much debate about their green credentials exist [42-46], in particular relating to their synthesis, environmental impact and intrinsic properties. Alternatives for the preparation of these materials should be explored to alleviate these concerns.

The use of particles as building blocks has also emerged as an alternative for the preparation of porous materials, in particular the coagulation of oppositely charged particles to form so called *colloidal gels* [47-50]. For example, Wang et al. [48] prepared a porous network from the coagulation of oppositely charged poly(D,L-lactic-*co*-glycolic acid) (PLGA)-based nanoparticles, with potential for use as a tissue engineering scaffold. Hydrogels prepared from the combination of oppositely charged dextran microspheres have also been prepared and their potential as injectable and biodegradable tissue engineering scaffolds demonstrated [51-53]. This approach could potentially be applied to

the preparation of styrene-based porous materials as styrene-based particles of opposite charge can easily be prepared by soap-free emulsion polymerisation [54-57]. Emulsion polymerisation is an attractive technique owing to its simplicity, low cost, high yield, and use of water as a non-toxic and environmentally friendly solvent. The use of water is also advantageous for its excellent heat dissipation during the course of polymerisation, and this technique has been widely utilised in industry for the preparation of large quantities of latex for surface coatings, such as paints and adhesives [58]. The soap-free emulsion polymerisation approach is therefore particularly attractive due to the absence of surfactant [54-57], which in addition to the concerns raised above, can result in destabilisation of the latex upon removal [55, 57].

However, the poor mechanical rigidity of colloidal gels, due to the absence of covalent bonds between particles, makes physical handling and the application of pressure for flow-through applications challenging. It would therefore be desirable to improve their rigidity, which can be achieved by introducing cross-linking points through chemical cross-linking [2, 59]. A similar process has previously been applied for poly(styrene)-based

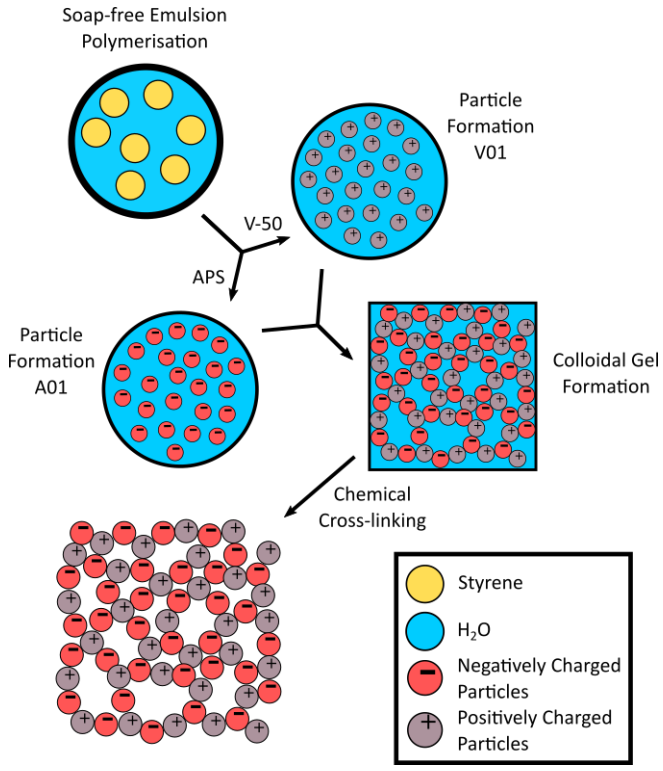

Figure 6.1. Schematic representation for the formation of cross-linked colloidal gels from oppositely charged latex particles prepared from the soap-free emulsion polymerisation of styrene using different initiators.

particles prepared from emulsion polymerisation for the preparation of macroporous materials [59]. In this case the addition of salt (NaCl) to the swollen latex resulted in aggregation of the particles, which were then cross-linked using residual monomer. However, these particles were prepared using the surfactant sodium dodecyl sulfate.

In this chapter the use of styrene-based latexes of opposite charge, prepared from soap-free emulsion polymerisation, for the preparation of porous colloidal gels was investigated. Chemical cross-linking of these colloidal gels was employed to obtain rigid porous materials. This is presented as a greener alternative for the preparation of styrene-based polymer monoliths, with the use of water as an industrially and environmentally friendly solvent, absence of surfactant, and limited purification the main advantages. The synthetic strategy employed in this work is shown in **Figure 6.1**. The possibility of using a single latex was also investigated as a simpler approach.

6.2 Experimental

6.2.1 Synthesis of the cationic co-monomer

The triethyl(4-vinylbenzyl)ammonium chloride (TEVBAC) cationic co-monomer was synthesised using the Menschutkin reaction with 4-vinylbenzyl chloride and triethylamine as reagents based on a method for the synthesis of trimethyl(vinylbenzyl)ammonium chloride (TMVBAC) [54]. Briefly, 4-vinylbenzyl chloride (1.00 g, 6.55×10^{-3} mol) and triethylamine (1.99 g, 19.7×10^{-3} mol) were added to a 50 mL round bottom flask containing acetone (5 mL). This was sealed with a rubber septa and the contents shaken vigorously. This was removed from light for 24 h, before the white needle-like crystals were collected under vacuum, washing with cold acetone, in 40% yield. The crystals were kept under nitrogen prior to use.

The product was characterised by ^{1}H NMR (**Figure D1** in **Appendix D**) and ^{13}C NMR spectroscopies (**Figure D2** in **Appendix D**). ^{1}H-NMR (300 MHz, DMSO-d_6) δ 1.10-1.53 (t, 9H, J = 6.9 Hz, $(CH_3)_3$-CH_2-N^+), δ 3.02-3.42 (q, 6H, J = 7.2 Hz, CH_3-$(CH_2)_3$-N^+), δ 4.56 (s, 2H,

Ar-CH+-N^+), δ 5.27-5.65 (d, 1H, J_{cis} = 11.0 Hz, CH=C-Ar), δ 5.83-6.05 (d, 1H, J_{trans} = 17.6 Hz, CH=C-Ar), δ 6.69-7.06 (dd, 1H, CH_2=CH-Ar), δ 7.48-7.66 (m, 4H, Ar).^{13}C-NMR (300 MHz, DMSO-d_6) δ 8.1, δ 52.5, δ 59.8, δ 116.7, δ 127.0, δ 127.9, δ 133.4, δ 136.3, δ 139.2. In addition the crystal structure was determined (**Figure D3**, **Tables D1** - **D3** in **Appendix D**). All of which were consistent with the formation of TEVBAC.

6.2.2 General procedure for the soap-free emulsion polymerisation of styrene

A typical soap-free emulsion polymerisation process was adopted and is summarised as follows: Styrene (9.9 g) was added to a continuous phase consisting of co-monomer (0.1 g) and H_2O (90 g) in a 250 mL round bottom flask. A stirrer bar was added, the flask sealed with a rubber septa, and the contents purged with N_2 for 20 min. The system was kept under N_2 for the duration of the polymerisation with constant stirring. The reaction vessel was heated to 70°C using an oil bath and after 15 min the initiator solution (0.01 g of initiator dissolved in 1 mL of deoxygenated H_2O) was injected through the septa. This was left at 70°C for 12 h to ensure reaction completion. The concentration of the latex was determined by gravimetry.

Particles of larger size were synthesised without ionic co-monomer under semi-batch conditions [54] in a similar procedure to that above, except the continuous phase consisted of H_2O (109.2 g) and MeOH (43.2 g), the initiator solution contained 0.3640 g of 2,2-azobis(2-methylpropanimidamide) dihydrochloride (V-50) dissolved in 2 g of deoxygenated H_2O. Styrene (18.2 g), which had been purged with N_2, was added at a rate of 5 mL/h over a period of 4 h using a syringe pump. MeOH was removed by dialysing the latex against H_2O for 1 week, replacing the water twice daily.

6.2.3 General procedure for the preparation of colloidal gels

The latexes were initially concentrated under reduced pressure (to ~30 wt%, the exact concentration was determined gravimetrically). These solutions were then diluted with H_2O to obtain the desired concentration (in the range 5-25 wt%). A mixture consisting of oppositely charged latexes was then prepared in a glass vial by mixing equal amounts of

the positively charged latex and the negatively charged latex. Coagulation was promoted by sonication using an Elma Elmasonic P sonicator bath (80 kHz, 5 mins, 100% power). The gel was left to settle at room temperature for at least 2 h prior to characterisation. Inversion of the vial was performed to evaluate the cohesiveness of the gel [47, 60-61], with photographs taken after 20 min equilibration time.

6.2.4 Preparation of cross-linked colloidal gels

A series of colloidal gels were prepared at 20 wt% as described above, except one latex was diluted with different amounts of Di(ethylene glycol) diacrylate (DEGDA) (containing 1 wt% AIBN w.r.t latex solids) in the range 10-30 wt% (w.r.t. total solid content of the resulting gel) and the amount of H_2O added was adjusted accordingly. After equilibration these colloidal gels were placed in an oil bath at 60°C for 24 h. The resulting materials were then washed in H_2O with gentle agitation and characterised once the washings remained visually clear.

A series of cross-linked colloidal gels were also obtained using a single latex in a similar procedure. Here, the positively charged latex was diluted with H_2O and various amounts of DEGDA in the range 15-65 wt% (w.r.t. solids). However instead of AIBN, APS was added at a concentration of 1 wt% (w.r.t. solids) using a 0.04 mg/mL solution of APS, to promote coagulation before equilibration and curing. The amount of H_2O added to the latex was varied so that upon addition of DEGDA and APS solution, an overall latex concentration of 20 wt% was obtained. The colloidal gels were then cured thermally, or by the addition of N,N,N',N'-tetramethylethylenediamine (TEMED) at room temperature.

6.2.5 Preparation in different formats

Colloidal gels (2 g each) were prepared in 10 mL glass vials using the approaches described above, where DEGDA was incorporated at 30 wt% (w.r.t. solids). Cylindrical formats were obtained simply by using glass vials as the mould and curing. The resulting materials were removed by carefully breaking the glass vials. Flat sheets were prepared by sandwiching the gel between two glass slides (76 mm x 26 mm, 1.0-1.2 mm thick, Academy Science

Limited) and curing. Removal of the top slide resulted in the obtainment of a continuous flat sheet. Other formats (such as a pyramid) were also prepared by moulding the gel using a spatula into the desired shape and then curing. The resulting materials were all gently washed with H_2O using a wash bottle, air-dried, and then photographed.

The polymer disks for porosity measurements were prepared by cross-linking 1 g of the colloidal gels using either 20 or 30 wt% DEGDA (w.r.t. solids) in 4 mL glass vials. After curing the vials were smashed and the resulting disks were removed and rinsed with H_2O. These were then dried in a vacuum oven at 25°C for 1 week prior to analysis.

6.3 Results and Discussion

6.3.1 The preparation of oppositely charged latexes

Two latexes of opposite charge were prepared from the soap-free emulsion polymerisation of styrene using APS and V-50 as water-soluble initiators, and were denoted as A01 and V01, respectively. These initiators provide a surface charge to the latex through their fragmentation, with a negative charge provided by APS [62] and a positive charge provided by V-50 [54, 63], thus promoting latex stability through electrostatic stabilisation [62]. Ionic co-monomers of similar charge, sodium styrene sulfonate in the case of APS and TEVBAC in the case of V-50 (1 wt% for each system), were also included to enhance the stability of these latexes.

Both A01 and V01 were obtained in relatively high yield (>90%), possessed low polydispersities, and possessed an average particle diameter in the order of 100 nm (**Table 6.1**), with A01 having an average diameter of 80 ± 10 nm by SEM and 109 ± 1 nm by Dynamic Light Scattering (DLS), while V01 had an average diameter of 130 ± 20 nm by SEM and 172.5 ± 0.4 by DLS. This was consistent with previous reports [54, 62, 64-65]. In addition, for both A01 and V01 the sign of their zeta potentials were consistent with their expected charge (**Table 6.1**). Both latexes also appeared stable with no obvious sign of

Table 6.1 Characterisation of latexes

Sample [a]	Z-Ave / nm [b]	Average PDI [c]	Z / nm [d]	wt% [e]	Conversion / % [f]	ζ / mV [g]
A01	109 ± 1	0.010 ± 0.009	80 ± 10	9.79 ± 0.03	92	- 53 ± 3
V01	172.5 ± 0.4	0.02 ± 0.02	130 ± 20	7.62 ± 0.05	92	34 ± 1
V02	560 ± 10	0.05 ± 0.04	470 ± 50	9.4 ± 0.2	93*	41.2 ± 0.5

[a] The following nomenclature is used, samples prepared with APS start with an A, while those prepared with V-50 start with a V. [b] Average particle diameter determined from DLS measurements using dilute samples. [c] Average polydispersity index obtained from the DLS measurements. [d] Average particle diameter measured directly from SEM images of dilute samples with at least 300 particles measured. [e] Average wt% determined from gravimetry after synthesis. [f] Conversion determined from mass of monomer added and the mass of latex obtained. [g] Average zeta potential determined from dilute latex samples. [*] Estimate of conversion before dialysis.

coagulation, and their SEM images (**Figure 6.2**) showed no evidence of secondary nucleation, which is the generation of a new smaller batch of particles.

The reason for the difference in average particle diameters as determined by SEM and DLS is related to the way that DLS works. DLS measurements tend to be an overestimate, as the scattering intensity is more pronounced for larger particle sizes (the intensity is proportional to the sixth power of particle diameter). No purification of these latexes was performed in order to keep the synthetic strategy as simple as possible, and to demonstrate the versatility of this approach. It should also be noted that large quantities of latex can easily be prepared using this methodology [54, 62, 64-65], with the size of the reactor or flask the main limiting factor, which is an important consideration for preparation at the production scale.

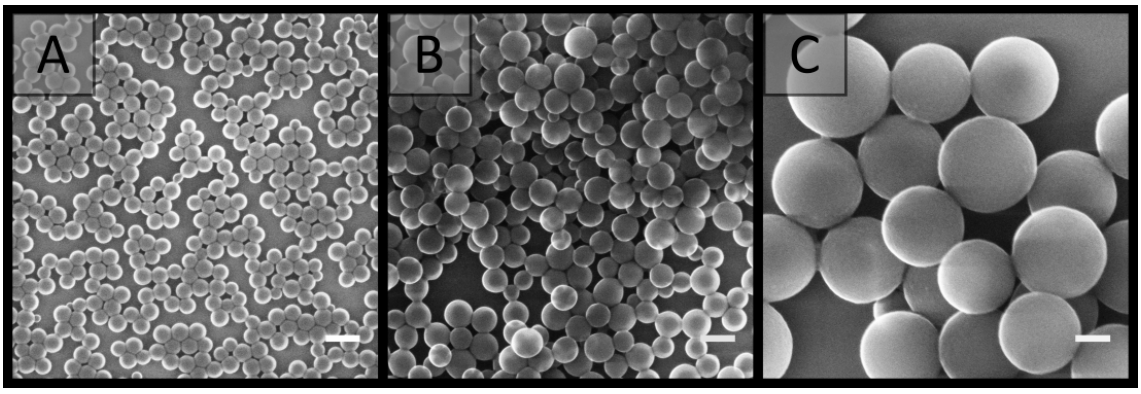

Figure 6.2. SEM images of latexes taken from dilute samples **A)** A01, **B)** V01 and **C)** V02. Scale bar is 200 nm.

6.3.2 Formation of colloidal gels

The possibility of preparing colloidal gels was explored by combining A01 and V01 at equal weight percent at a variety of concentrations in the range 5 to 25 wt%. Since these latexes were originally synthesised at ~10 wt%, in order to obtain latexes of different concentration, both latexes were concentrated under reduced pressure to ~30 wt% and then diluted. It is possible to prepare latexes with higher concentrations using the soap-free emulsion polymerisation approach [63], in a more energy efficient process, however alterations in the monomer concentration during synthesis is known to influence both the particle size and the number of particles present in the resulting latex [63-64]. This was avoided so that any differences between these gels could be attributed solely to the particle concentration. No significant changes in the properties of these latexes (particle size, particle size distribution, and the sign of their zeta potential) were observed upon concentration (**Table 6.2**). To promote gel formation the vials containing both latexes were sonicated to ensure the same energy input in all cases, as this is likely to be variable when shaking these vials by hand.

Upon inspection, clumps were observed, rather than a continuous gel, for the lower concentrations of 5 and 10 wt%, and these exhibited significant flow upon inversion (**Figure 6.3**). This is a result of the particles being too distant from each other, due to the high water content [52]. Cohesive gels were only obtained for particle concentrations greater than 10 wt%, with 15, 20 and 25 wt% resulting in a single plug of material, which exhibited greater resistance to flow (**Figure 6.3**). Physical manipulation of these gels revealed that more viscous structures were obtained for latex concentrations of 20 and 25 wt%, when compared to 15 wt%. In comparison, individual latexes exhibited a high degree of flow (**Figure 6.3**).

The cohesive nature of these gels is therefore predominately provided by the electrostatic interactions between the oppositely charged particles, although it does also depend on van der Waals interactions and steric hindrance [48, 66]. An increase in the number of particles per unit volume therefore results in an increase in the number of these interactions, with increases in particle concentration corresponding to gels with greater

Table 6.2 Characterisation of concentrated latexes

Sample [a]	Batch [b]	wt% [c]	Z-Ave initial / nm [d]	Z-Ave final / nm [e]	Z initial / nm [f]	Z final / nm [g]	ζ / mV [h]
A01	1	16.3 ± 0.1	109 ± 1	105.2 ± 0.2	80 ± 10	80 ± 10	- 46.3 ± 0.8
	2	25.90 ± 0.09	109 ± 1	104.2 ± 0.9	80 ± 10	81 ± 8	- 44.2 ± 0.8
	3	30.2 ± 0.5	109 ± 1	106 ± 1	80 ± 10	80 ± 10	- 41.5 ± 0.4
	4	32 ± 1	109 ± 1	100 ± 1	80 ± 10	80 ± 10	- 43.5 ± 0.6
V01	1	20.8 ± 0.3	172.5 ± 0.4	164 ± 2	130 ± 20	130 ± 20	36 ± 2
	2	28.2 ± 0.5	172.5 ± 0.4	169 ± 1	130 ± 20	130 ± 20	45.7 ± 0.3
	3	30.8 ± 0.2	172.5 ± 0.4	157 ± 4	130 ± 20	130 ± 20	42.2 ± 0.8
	4	28 ± 1	172.5 ± 0.4	163 ± 2	130 ± 20	140 ± 30	51.1 ± 0.5
V02	1	31.4 ± 0.9	560 ± 10	530 ± 10	470 ± 50	480 ± 40	40.7 ± 0.6
	2	40.9 ± 0.8	560 ± 10	584 ± 7	470 ± 50	480 ± 50	43.9 ± 0.9
	3	26.6 ± 0.8	560 ± 10	530 ± 10	470 ± 50	520 ± 60	45.2 ± 0.5
	4	28.6 ± 0.9	560 ± 10	562 ± 8	470 ± 50	490 ± 60	31.9 ± 0.4

[a] The following nomenclature is used, samples prepared with APS start with an A, while those prepared with V-50 start with a V. [b] Multiple batches were prepared by concentrating different amounts of the original latex. [c] Average wt% determined from gravimetry after concentration under reduced pressure. [d] Average particle diameter determined from DLS measurements using dilute samples before concentration. [e] Average particle diameter determined from DLS measurements using dilute samples after concentration. [f] Average particle diameter measured directly from SEM images of dilute samples before concentration with at least 300 particles measured. [g] Average particle diameter measured directly from SEM images of dilute samples after concentration with at least 300 particles measured. [h] Average zeta potential determined from dilute latex samples after concentration.

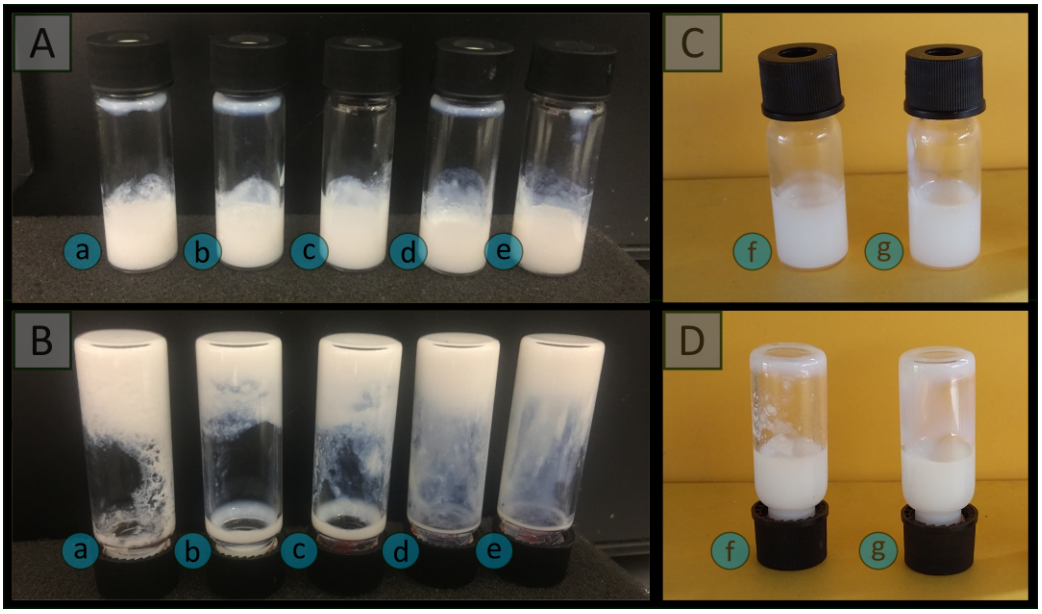

Figure 6.3. Photographs of colloidal gels obtained by combining A01 and V01 at equal weight percent. **A)** taken with vials upright 2 h after preparation, **B)** taken 20 min after inversion. Particle concentration: **a)** 5 wt%, **b)** 10 wt%, **c)** 15 wt%, **d)** 20 wt% and **c)** 25 wt%. Also shown are individual latex solutions at 25 wt%: **f)** A01 and **g)** V01. **C)** upright and **D)** taken 20 min after inversion.

viscosity and elastic moduli [47]. In addition, these gels appeared to be highly mouldable and capable of retaining their shape, which makes them excellent candidates for polymer monolith precursors, as the ability to easily prepare a variety of formats is one of the advantages polymer monoliths possess over conventional formats such as packed-beds [67].

SEM analysis (**Figure 6.4**) revealed that the materials prepared at particle concentrations of 15, 20 and 25 wt%, as well as the clumps obtained at 5 and 10 wt% (**Figure D4** in **Appendix D**), possessed a porous morphology. No significant difference in morphology was observed with the particle concentrations utilised, and their porous nature appeared to be the result of interstitial space between closely packed particles in a cluster, coupled with the presence of voids, presumably resulting from multiple clusters intersecting

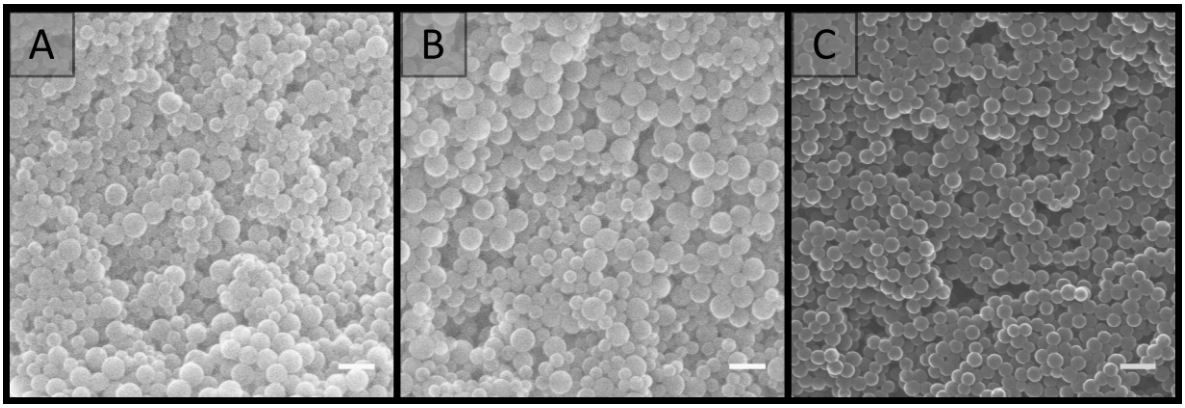

Figure 6.4. SEM images of colloidal gels obtained by combining A01 and V01 at equal weight percent. Particle concentration: **A)** 15 wt%, **B)** 20 wt% and **C)** 25 wt%. Scale bar is 250 nm.

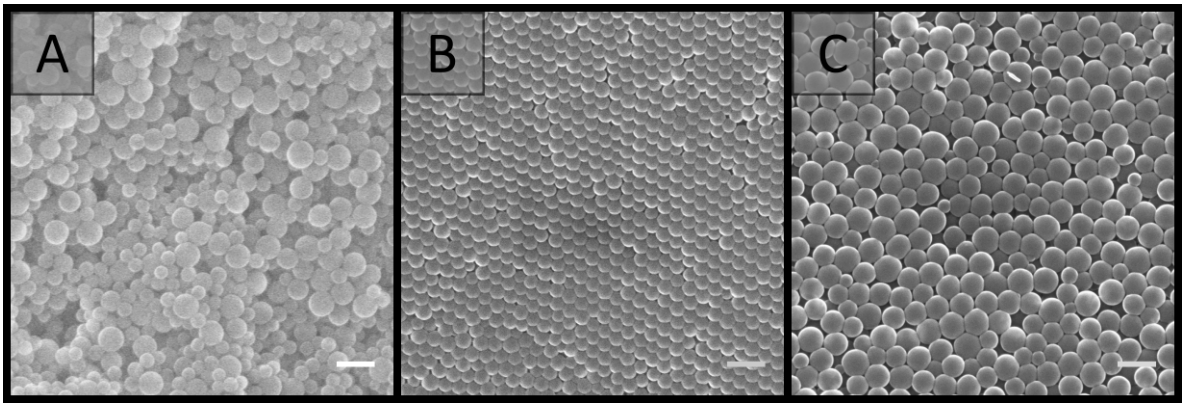

Figure 6.5. SEM images comparing **A)** the colloidal gel obtained from the combination of A01 and V01 at 20 wt%, with individual dried latexes at 20 wt%: **B)** A01 and **C)** V01. Scale bar is 250 nm.

imperfectly. This resulted in an average pore size of 100 ± 50 nm for the particle concentration of 20 wt%. This is in comparison to the large cellular domains sometimes observed with other systems [48-50].

This porous structure did not appear to be related to the removal of H_2O during the imaging process, as individual latexes, which were dried and then imaged, appeared to be more densely packed with a higher degree of order, and no particle clusters were observed (**Figure 6.5**). However it is important to consider that these SEM images may not be representative of the structure of the colloidal gel in solution, as any shrinkage, as a result of their non-rigid nature, could have altered their morphology. Regardless, the particle arrangement observed resulted in pore sizes in the order of the particle dimensions, with pores less than 300 nm present.

6.3.3 Formation of cross-linked colloidal gels

Chemical cross-linking was employed to improve the rigidity of these materials by including divinyl monomers into the 20 wt% gel formulation. This particle concentration was chosen given it was sufficiently cohesive (**Figure 6.3**) while still maintaining a high water content and therefore porosity. Chemical cross-linking was utilised as increases in the cross-linking density are known to improve the mechanical properties of polymer monoliths, while also restricting the degree to which the network can shrink or swell in different solvent environments [2, 68]. The increase in mechanical properties is due to the introduction of covalent bonds, during the chemical cross-linking process, and these are stronger than the ionic interactions responsible for the cohesive nature of the gels [52]. As such, it is common for 20-30 wt% cross-linking monomer to be utilised in the preparation of polymer monoliths.

Initial experiments focused on the incorporation of DVB, which is commonly used in the preparation of poly(styrene)-based monoliths [15, 29, 67, 69], however this resulted in significant coagulation of the individual latexes, even for DVB contents as low as 10 wt% (w.r.t. solids) (**Table D4** in **Appendix D**). This was due to the swelling of the particles, which occurs in the presence of hydrophobic monomers, which reduced their overall

stability and promoted coagulation. A less hydrophobic cross-linker, which results in less swelling of the particles may therefore be more appropriate. As such DEGDA was incorporated in the range of 10-30 wt% (w.r.t. solids). DEGDA is a monomer with low water solubility, so any swelling that occurs is less than with DVB. In addition its low water solubility should encourage its phase separation onto the hydrophobic particle network, rather than gelling of the aqueous phase, which would reduce the porosity and permeability of the resulting material. The incorporation of DEGDA in this range did not appear to compromise the stability of the individual latexes, nor the ability to obtain cohesive gels.

The resulting gels were therefore cured thermally using AIBN as initiator by dissolving this initially in the DEGDA cross-linker. When 10 wt% DEGDA (w.r.t. total solid content of the gel) was utilised, this resulted in a material with the same consistency as the original colloidal gel. However when DEGDA concentrations of 15 wt% and above were utilised rigid cylinders were obtained. Washing these materials with H_2O or MeOH did not appear

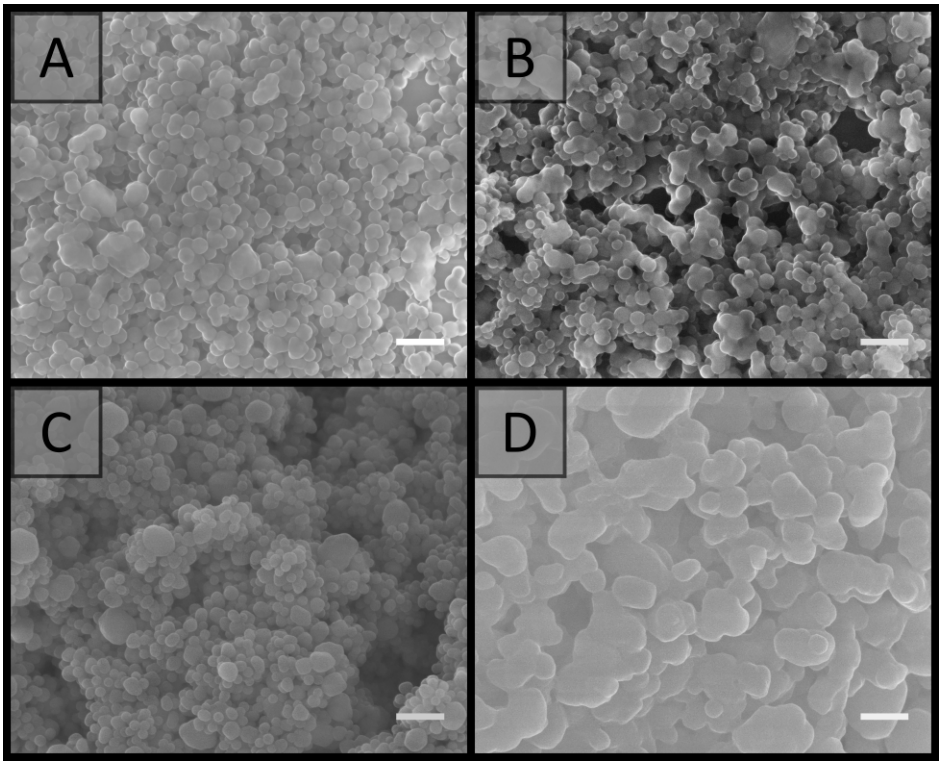

Figure 6.6. SEM images of cross-linked colloidal gels obtained by combining 20 wt% of A01 and V01 and cured with different concentrations of DEGDA. DEGDA concentration (w.r.t. total solid content of the gel): **A)** 15 wt%, **B)** 20 wt%, **C)** 25 wt% and **D)** 30 wt%. Scale bar is 500 nm.

to compromise their integrity and the washings remained clear, suggesting the latex particles were incorporated into the continuous network.

SEM analysis (**Figure 6.6**) revealed that the material prepared with 15 wt% DEGDA possessed a very similar morphology to that of the non-cross-linked colloidal gels (**Figure 6.4**). However, closer inspection revealed there were regions where multiple particles were fused together, with what appeared to be a smooth polymer coating. This coating is consistent with previous reports, where DEGDA was used to encapsulate calcium carbonate particles [70]. As the DEGDA content was increased this fused morphology became more predominant. This is clearer at higher magnification (**Figure D5** in **Appendix D**).

Thicker coatings were present for 25 wt%, however this material appeared more heterogeneous, with large variations in thickness of the coating observed. In terms of the porous morphology, the presence of this polymer coating resulted in a reduction in the interstitial space between the particles in a single cluster, however this did not appear to compromise the voids present between adjacent clusters, with an average void size of 140 ± 80 nm for the material prepared with 20 wt% DEGDA. This was not statistically different to that of the original colloidal gels, however the slightly higher value could be related to reduced shrinkage upon drying, associated with increased cross-linking density [2, 68]. This material also possessed a specific surface area of 38 ± 4 m^2/g, which was similar to the poly(styrene)-based monoliths prepared in **Chapters 4** & **5**, with a type II isotherm which is consistent with the obtainment of a macroporous material (**Figure D9** in **Appendix D**). As expected, the thickest polymer coatings were achieved for 30 wt% DEGDA, and this did appear to compromise its porous nature. As such the use of 20 wt% DEGDA appeared to be optimal for these materials, as this resulted in a reasonably homogenous porous material with good rigidity.

6.3.4 Formation of porous materials using a single latex

Curing of the colloidal gels was performed using AIBN as thermal initiator, as the addition of APS to the individual latexes resulted in their coagulation, with small clumps initially

observed which became larger over time. This occurred due to the increase in ionic strength, which depresses the electrostatic double-layer, allowing for greater contact between the particles [55, 57, 63, 71-72]. If APS was present at 1 wt% (w.r.t solids), or higher, full coagulation of the latex was observed over a period of 2 h for V01. The volume or concentration of the APS solution did not appear to influence the ability to obtain full coagulation, provided APS was present at 1 wt% (w.r.t. solids) (**Figure D6** in **Appendix D**).

While coagulation of A01 and V01 prevented their combination, SEM analysis (**Figure 6.7A**) revealed that the gel obtained for V01 also possessed a porous structure similar to the previous colloidal gels obtained (**Figure 6.4**). This potentially allows for the preparation of rigid porous materials using only one latex, where the initiator not only promotes the cross-linking process, but also the formation of the colloidal gel itself. The addition of salt to particle suspensions has previously been used to induce their aggregation allowing for the obtainment of macroporous materials [59, 73-74]. However, the ability to use the thermal initiator, which itself is a salt, to initiate this process further simplifies this process. DEGDA was therefore included in the range 15-65 wt% (w.r.t. solids) before the addition of APS. Again the presence of DEGDA did not compromise the ability to obtain cohesive gels and thermal curing resulted in the obtainment of rigid cylinders in all cases.

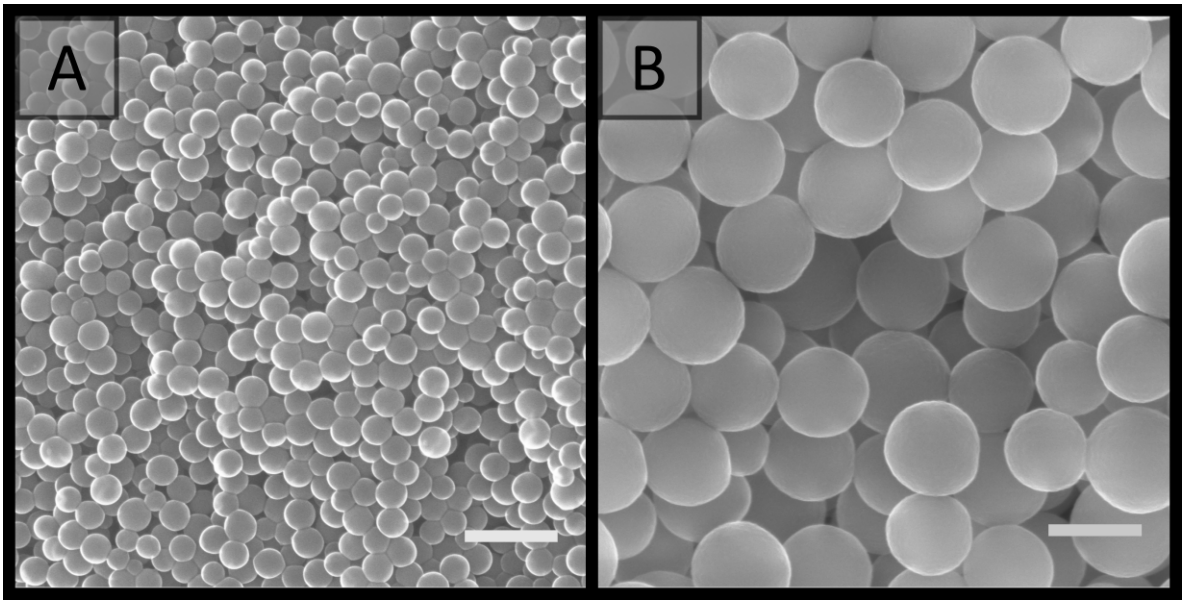

Figure 6.7. SEM images of colloidal gels obtained from the addition of APS at 1 wt% (w.r.t. solids) to 20 wt% **A)** V01 and **B)** V02. Scale bar is 500 nm.

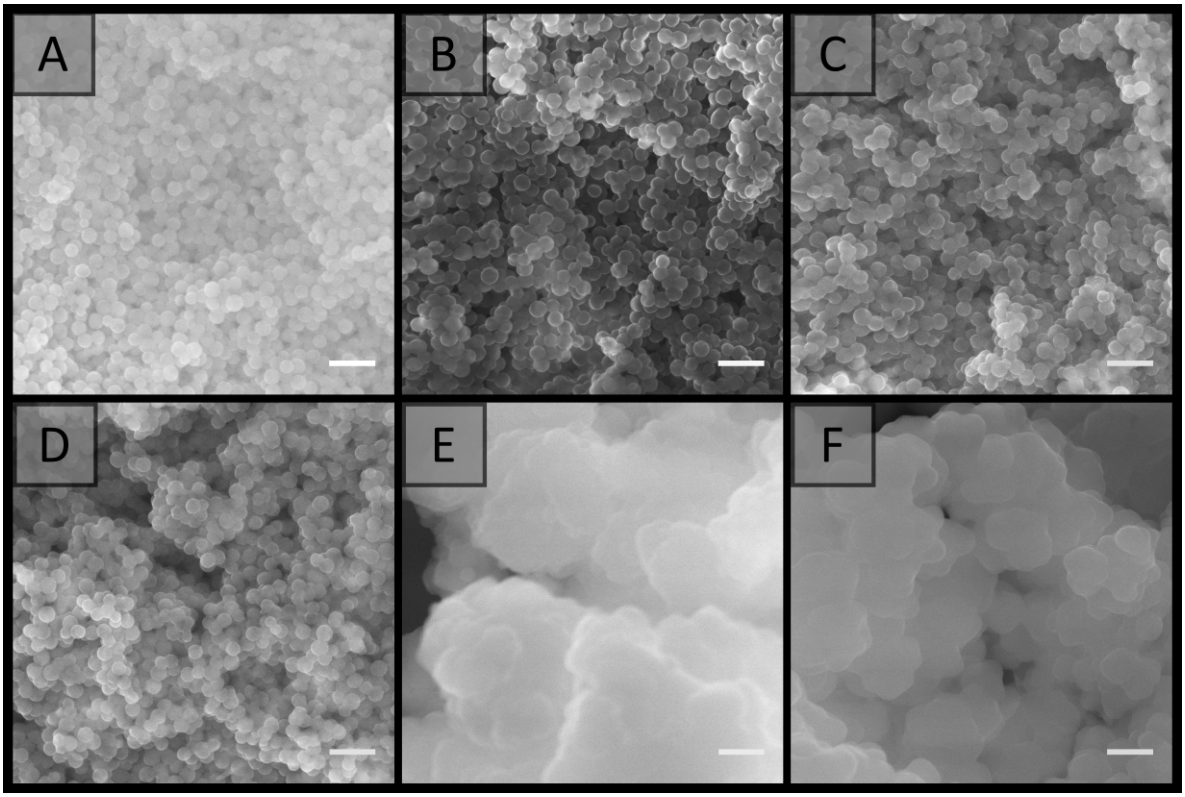

Figure 6.8. SEM images of cross-linked colloidal gels obtained from the addition of APS at 1 wt% (w.r.t. solids) to 20 wt% V01 and cured with different concentrations of DEGDA. DEGDA concentration (w.r.t. solids): **A)** 15 wt%, **B)** 20 wt%, **C)** 25 wt%, **D)** 30 wt%, **E)** 40 wt% and **F)** 65 wt%. Scale bar is 500 nm.

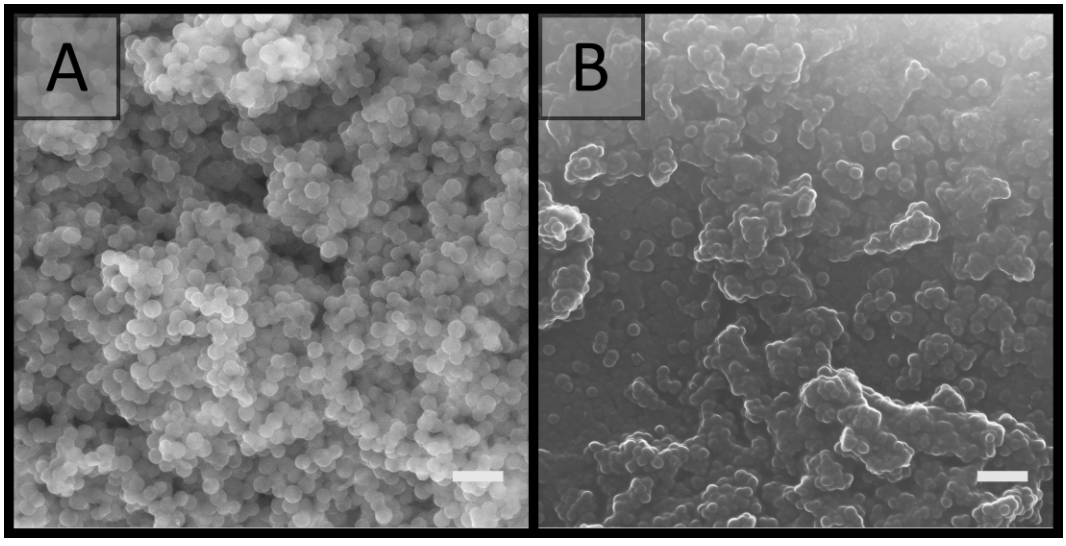

Figure 6.9. SEM image of cured 20 wt% V01 prepared with 30 wt% DEGDA (w.r.t. solids). **A)** Latex was coagulated by the addition of APS at 1 wt% (w.r.t. solids) prior to curing. **B)** No coagulation prior to curing where AIBN was incorporated at the same mol% as APS. Scale bar is 500 nm.

SEM analysis (**Figure 6.8**) revealed similar results to that obtained above with 15 wt% DEGDA resembling that of the non-cross-linked colloidal gels, and as the DEGDA content was increased a fused morphology became more predominant up to 30 wt% DEGDA. The average pore size for these materials was also similar with a value of 170 ± 60 nm in the case of 30 wt% DEGDA. This material possessed a specific surface area of 25 ± 3 m^2/g, which was consistent with a slightly higher average pore size. Coagulation, prior to curing, appeared to be a requirement for the obtainment of these porous materials, as simply curing the latex, using AIBN instead of APS, resulted in a non-porous material consisting of particles trapped within bulk polymer (**Figure 6.9**).

Increasing the DEGDA content above 30 wt% resulted in significantly thicker coatings, and in contrast to the smooth coatings obtained previously, a cauliflower type morphology was observed. This was present for both 40 and 65 wt% DEGDA. It is likely that the increased DEGDA content is simply resulting in the formation of uneven polymer layers. Alternatively this could be resulting in the formation of a secondary batch of particles, which are fusing with the existing particle network, however this is less likely. Regardless, the thicker coatings significantly reduced the porous nature of these materials and it is clear that the preparation of porous materials is possible using this approach. In addition to offering a simpler process for the preparation of these porous materials the use of APS as initiator also has an additional advantage, that is it can be coupled with TEMED to allow for the rapid polymerisation of these materials at room temperature [75-77] (**Figure D7** in **Appendix D**).

Given the pore sizes observed appear to be in the order of the particle dimensions, the use of larger particles would be expected to result in the production of larger pores, which is an important consideration for obtaining materials with greater permeability and lower resistance to mass transfer [14, 76, 78]. A positively charged latex with larger particle diameter was therefore synthesised using V-50 as initiator and a continuous phase consisting of a 5:2 mixture of H_2O and MeOH as outlined by Bon et al. [54]. This was synthesised without co-monomer, and these particles were denoted as V02 (**Table 6.1**). The resulting latex possessed an average particle diameter of 470 ± 50 nm by SEM and 560 ± 10 nm by DLS and a positive zeta potential. This was consistent with previous

reports where an ionic co-monomer was absent [54, 62, 64]. In addition, no secondary nucleation was apparent (**Figure 6.2**). Dialysis of this latex against H_2O was performed to remove this co-solvent, allowing for fair comparisons to the materials prepared with H_2O only.

The addition of APS at 1 wt% (w.r.t. solids) to 20 wt% V02 also resulted in full coagulation of this latex and this gel was porous in nature (**Figure 6.7B**). Thermally curing these gels with DEGDA concentrations in the range 20-65 wt% (w.r.t. solids) produced rigid cylinders and SEM analysis (**Figure 6.10**) revealed similar trends to those above, with 20 wt% DEGDA resembling that of the colloidal gel, while DEGDA contents of 30 and 40 wt% resulted in predominately fused structures with thicker coatings. **Figure 6.11** clearly demonstrates that this fused morphology is directly related to the presence of the water-soluble cross-linker, and not as a result of coagulation, or drying of these latexes.

In terms of the porous morphology, larger pore sizes were observed compared to the materials prepared with the smaller V01 particles (**Figure 6.8**), with an average pore size of 0.8 ± 0.6 µm for the material prepared with 30 wt% DEGDA. Voids of this size are

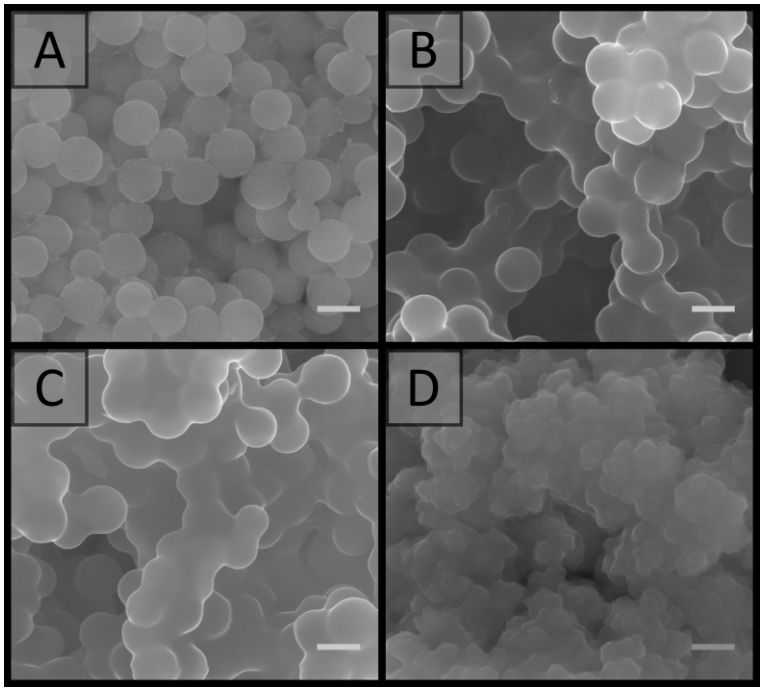

Figure 6.10. SEM images of cross-linked colloidal gels obtained from the addition of APS at 1 wt% (w.r.t. solids) to 20 wt% V02 and cured with different concentrations of DEGDA. DEGDA concentration (w.r.t. solids): **A)** 20 wt%, **B)** 30 wt%, **C)** 40 wt% and **D)** 65 wt%. Scale bar is 500 nm.

important for applications requiring high permeability such as chromatography [79], as flow-through catalytic reactors [5], or for the transport of nutrients in tissue engineering [80]. This increase in pore size was also supported by a significantly lower average specific surface area of 5.6 ± 0.2 m^2/g. Lower magnification images (**Figure 6.12**) demonstrate the porous morphologies of these materials more clearly. In the case of 65 wt% DEGDA a material with cauliflower type morphology was again observed with (**Figure 6.10**), as a result of the thicker coating, significantly reduced void size.

Provided the DEGDA content was below that required for the onset of this morphology, the pore sizes obtained for these materials appear to be directly correlated to particle size, with voids present in the order of the particle dimensions. This is clear when comparing the pore size distributions obtained from the 20 wt% gels (**Figure 6.13**). This potentially allows the porous properties of these materials to be easily predicted, allowing for the preparation of materials specifically designed for particular applications, without

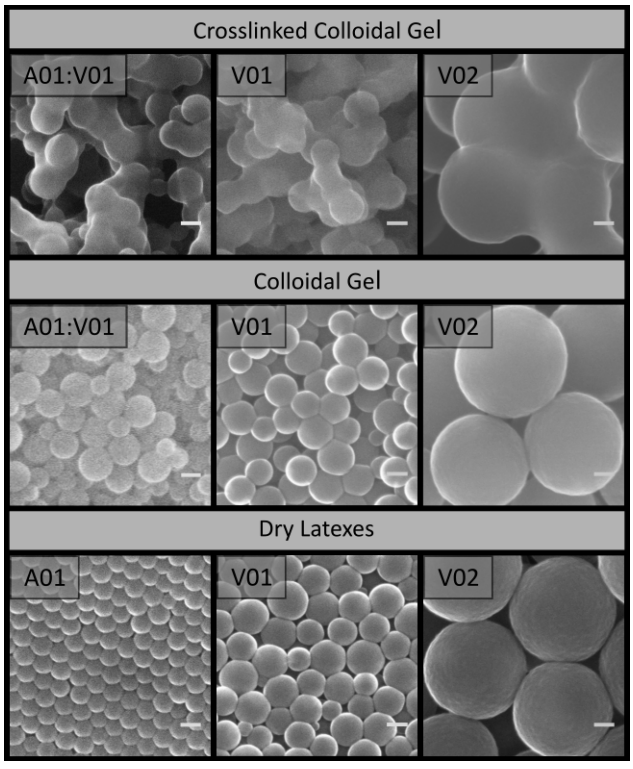

Figure 6.11. SEM images comparing the cross-linked colloidal gels obtained from: A01 and V01 using AIBN as thermal initiator, V01 using APS for coagulation and curing and V02 using APS for coagulation and curing, to the colloidal gels obtained from the addition of: A01 to V01, APS to V01 and APS to V02, and dried latexes. The latex concentration was 20 wt% in all cases and DEGDA was included for the cross-linked colloidal gels at a concentration (w.r.t. solids) of: 20 wt% for A01:V01 and 30 wt% for V01 & V02. Scale bar is 100 nm.

an extensive optimisation process, as is the case when using a new porogenic solvent or monomer system [22].

For example, materials with small pore sizes and higher surface areas are useful for bulk catalysis, adsorbents, and for gas storage, whereas larger pore sizes are important for applications such as flow-through reactors, biochromatography and tissue engineering. In addition, the particle size and particle size distribution can easily be varied in the soap-

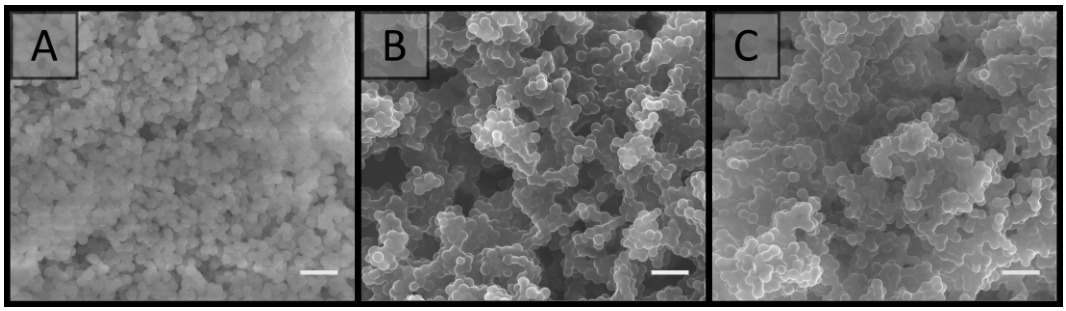

Figure 6.12. SEM images of cross-linked colloidal gels obtained from the addition of APS at 1 wt% (w.r.t. solids) to 20 wt% V02 and cured with different concentrations of DEGDA. DEGDA concentration (w.r.t. solids): **A)** 20 wt%, **B)** 30 wt% and **C)** 40 wt%. Scale bar is 2 µm.

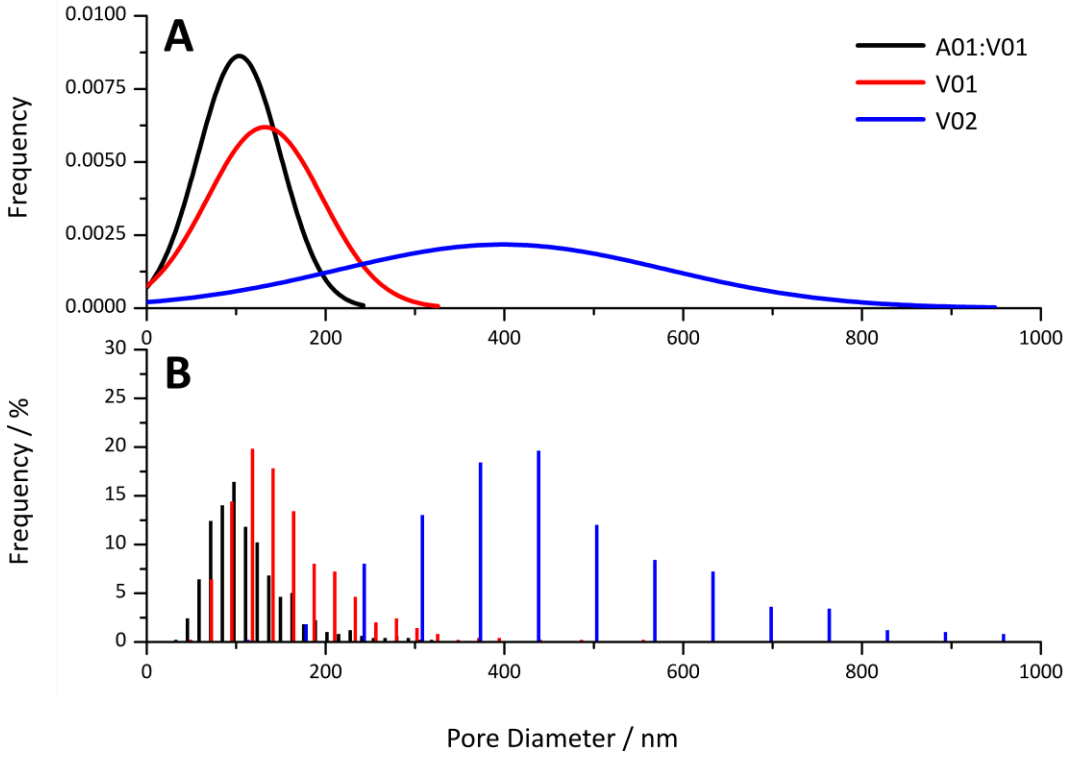

Figure 6.13. (A) Theoretical normal distribution and **(B)** Histograms obtained for pore diameter of the A01:V01, V01 and V02 gels at 20 wt% obtained from the SEM images.

free emulsion polymerisation approach, through changes in a variety of parameters, which include the reaction temperature, monomer concentration, initiator and co-monomer concentration, and the ionic strength [58].

6.3.5 Preparation of cross-linked colloidal gels with different shapes

All gels prepared in this work, including those prepared using a single latex, were highly mouldable, which potentially allows for the preparation of these materials in a variety of formats. The use of vials has already been demonstrated to result in the formation of rigid cylinders (**Figure 6.14A**), however a range of other formats can also easily be prepared as demonstrated in **Figure 6.14** for the colloidal gels obtained using V02. A flat sheet (**Figure 6.14B**) was prepared simply by sandwiching the gel between two glass slides, while a pyramid (**Figure 6.14C&D**) was prepared by moulding the gel with a spatula into the desired shape on a glass slide. This was possible as these gels are capable of maintaining their shape in the absence of an external force, and both became rigid after

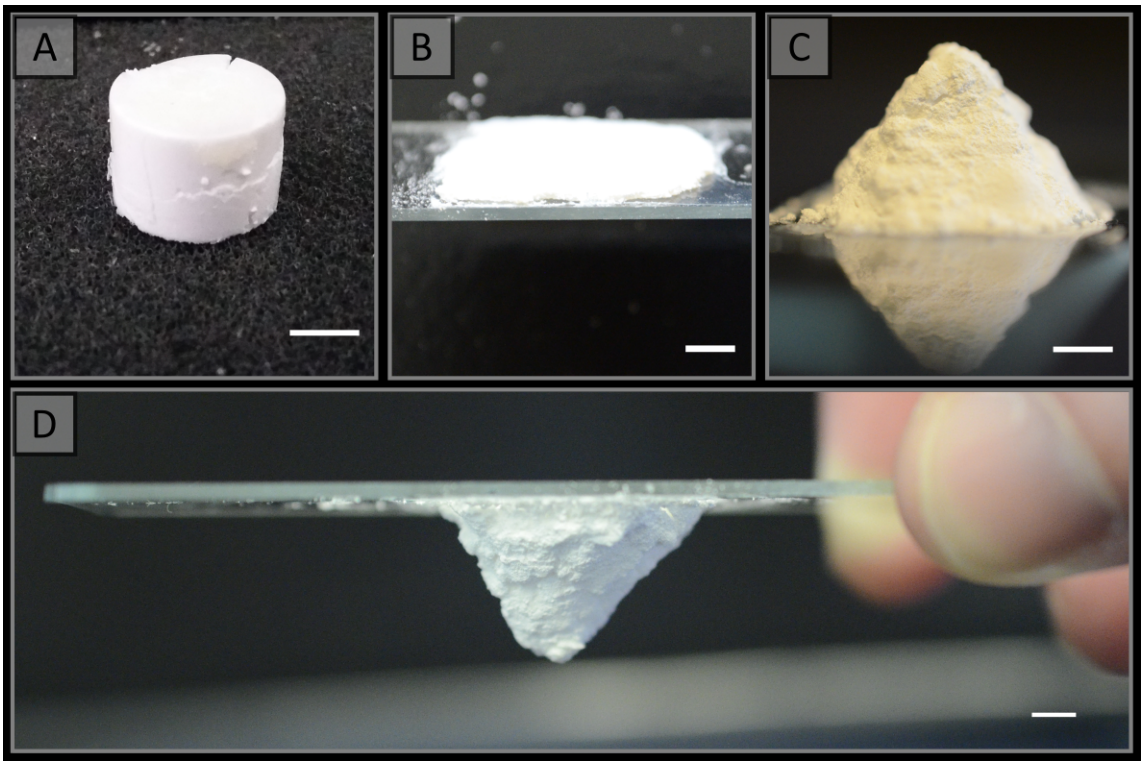

Figure 6.14. Photographs of rigid porous materials obtained in a variety of formats from the addition of APS to V02 with 30 wt% DEGDA (w.r.t. solids). **A)** Cylinder, **B)** Flat sheet and **C)** & **D)** Pyramid. Scale bar is 5 mm.

curing. The other gels used in this work could also easily be prepared in these formats (for example the materials obtained using V01 is shown in **Figure 6.15**).

This demonstrates that a wide variety of formats can readily be prepared, which is important for enabling their use in a wide variety of applications. For example, pumping the gels into column housing could enable their use for chromatography [14], or as catalytic supports [4-7], while the flat sheet format could be useful for the manufacture of plates for thin-layer chromatography (TLC) [16]. The freestanding nature of these gels is particularly advantageous as it provides the possibility of preparing these materials without a mould (**Figure 6.14C&D**), which is not possible when using a porogenic solvent [22].

Attempts were made to prepare these gels in 150 µm i.d. fused-silica capillaries, by loading them into a glass syringe and applying pressure to force the gel to pass through the narrow capillary internal diameter, however this resulted in compression of the gel and expulsion of water was observed. This effect has also previously been observed for hydrogels prepared from oppositely charged dextran microspheres when attempting to pass them through 25 G (5/8 in.) needles using glass syringes [53]. Here the dextran-based gels possessing higher gel strength were mainly affected, with those possessing a less cohesive structure passing through more readily. Therefore alterations in the cohesive nature of the gel may afford gels suitable for preparation in capillary formats but requires additional synthetic optimisation in terms of particle concentration, surface charge, and

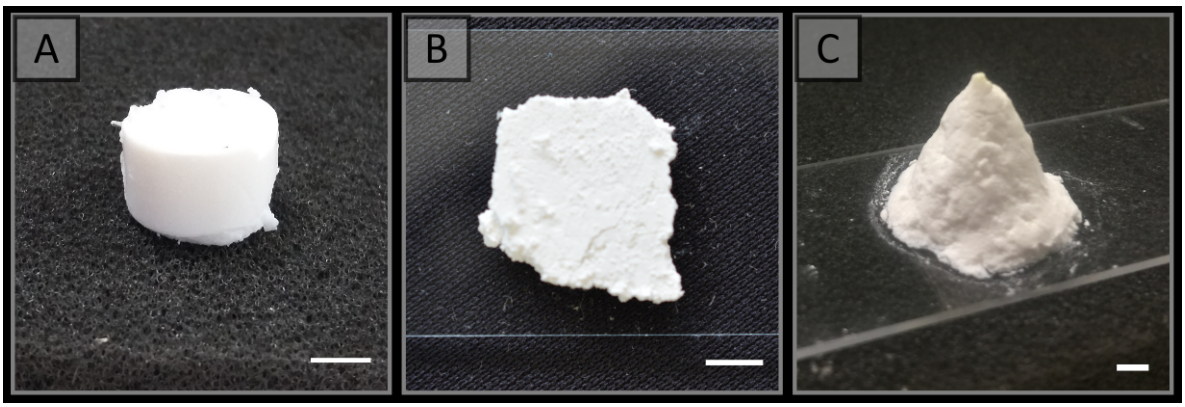

Figure 6.15. Photographs of rigid porous materials obtained in a variety of formats from the addition of APS to V01 with 30 wt% DEGDA (w.r.t. solids). **A)** Cylinder, **B)** Flat sheet and **C)** & **D)** Pyramid. Scale bar is 5 mm.

size. It may, however, be possible to utilise larger column formats, such as conventional chromatographic columns with internal diameters in excess of 2 mm [2, 81].

6.3.6 Solvent Behaviour

In order to access the suitability of these materials for different applications polymer disks prepared from the combination of A01 and V01 or using V01 and V02 only were immersed in solvents of varying polarity. For the gels obtained from A01 and V01 20 wt% DEGDA (w.r.t. solids) was utilised in the cross-linking process, while 30 wt% DEGDA (w.r.t. solids) was utilised for the V01 and V02 gels. The solvents investigated included Milli-Q H_2O, MeOH, EtOH, ACN, hexadecane and sunflower oil. The porosity values calculated for these disks by immersion in these solvents are shown in **Table 6.3**, as well as the theoretical porosity which was calculated from the H_2O content, assuming full conversion and incorporation of the cross-linker into the resulting material.

In most cases the values obtained were in agreement with the theoretical porosities, which were 76% and 74% when 20 and 30 wt% DEGDA were utilised for cross-linking, respectively. These values are higher than that of conventional polymer monoliths, which are often prepared with a porosity of 60%, but similar to that of poly(HIPE)s which have porosities in excess of 74%. The change in volume observed for these disks was also negligible for all solvents (**Table 6.4**), excluding acetonitrile, suggesting these values were reflective of the porosity in the dry state. Given these disks were simply immersed in these solvents, without any applied pressure, this also suggested that the liquid was being drawn into the pores of the polymer disk by capillary action, rather than the swelling of the polymer. This was also observed to occur rapidly with negligible change in mass of the disks after 30 min of immersion, even when sunflower oil was utilised as the solvent.

This behaviour is particularly important for several applications and suggests the potential for these materials to be utilised in TLC or for extraction, where greener solvents such as ethanol or even aqueous solutions could be utilised. The uptake of H_2O was of particular interest given the strong hydrophobic character typically associated with poly(styrene) monoliths [82]. It appeared that the inclusion of DEGDA resulted in an increase in the

Table 6.3 Porosity values obtained using polymer disks prepared from the cross-linked colloidal gels

Sample	[DEGDA] / wt% [a]	ϕ_w / % (H_2O)	ϕ_w / % (MeOH)	ϕ_w / % (EtOH)	ϕ_w / % (ACN)	ϕ_w / % (Hexadecane)	ϕ_w / % (Sunflower oil)	ϕ_T / %
A01:V01	20	50 ± 10	75 ± 3	69 ± 6	72 ± 7	67 ± 4	77 ± 4	76
V01	30	67 ± 7	69 ± 7	70 ± 8	68 ± 7	74 ± 1	76 ± 4	74
V02	30	72 ± 6	71 ± 5	73 ± 4	79 ± 2	67 ± 4	77 ± 5	74

[a] Concentration of DEGDA used w.r.t. solids. ϕ_w signifies the porosity, while ϕ_T indicates the theoretical porosity.

Table 6.4 Change in volume of polymer disks immersed in different solvents

Sample	[DEGDA] / wt% [a]	ΔV / % (H_2O)	ΔV / % (MeOH)	ΔV / % (EtOH)	ΔV / % (ACN)	ΔV / % (Hexadecane)	ΔV / % (Sunflower oil)
A01:V01	20	- 5 ± 9	0 ± 10	- 3 ± 3	22 ± 8	- 3 ± 3	- 14 ± 9
V01	30	- 3 ± 2	- 2 ± 4	- 3 ± 7	21 ± 4	- 10 ± 10	- 10 ± 10
V02	30	1 ± 2	- 2 ± 3	1 ± 4	20 ± 10	0 ± 10	0 ± 10

[a] Concentration of DEGDA used w.r.t. solids. ΔV indicates the change in volume of the polymer disk relative to the original volume.

Table 6.5 Mass of solvent absorbed by the polymer disks when immersed in different solvents

Sample	[DEGDA] / wt% [a]	m_s / % (H_2O)	m_s / % (MeOH)	m_s / % (EtOH)	m_s / % (ACN)	m_s / % (Hexadecane)	m_s / % (Sunflower oil)
A01:V01	20	110 ± 30	150 ± 20	140 ± 20	140 ± 20	120 ± 10	155 ± 3
V01	30	210 ± 30	180 ± 40	180 ± 30	180 ± 50	120 ± 30	180 ± 20
V02	30	217 ± 7	160 ± 20	183 ± 3	210 ± 40	150 ± 30	220 ± 10

[a] Concentration of DEGDA used w.r.t. solids. m_s indicates the mass of solvent present in the disk relative to the mass of the dry disk.

hydrophilicity of the material allowing for H_2O uptake by capillary action, which was not possible for the poly(styrene) monoliths prepared in **Chapter 4**. In fact the amount of DEGDA present appeared to directly correlate to amount of H_2O absorbed, with the disks prepared with 20 wt% DEGDA absorbing significantly lower amounts of H_2O by mass (**Table 6.5** & **Figure D8** in **Appendix D**), resulting in a lower than expected porosity of 50 ± 10 %. This is in comparison to the disks prepared with 30 wt% DEGDA, which had porosities consistent with those obtained using the other solvents (**Table 6.3**). For all other solvents the amount absorbed correlated to the pore volume of these disks, with the mass of solvent entering the disks ranging from 110 to 220 % by mass relative to the mass of the dry disks (**Table 6.5** & **Figure D8** in **Appendix D**), thus resulting in porosity values of ~ 70 % (**Table 6.3**).

The inclusion of DEGDA has therefore resulted in the ability of these disks to absorb solvents of varying polarities, through capillary action, ranging from H_2O to hexadecane. In addition, no incompatibility with these solvents was observed with minimal

swelling/shrinkage of these disks as a result of the cross-linking process utilised. These disks did however swell to a small degree in acetonitrile, with a change in volume of ~ 20 % compared to the original volume observed (**Table 6.4**). However, no shrinkage or swelling was observed for the other solvents.

6.4 Conclusions

The ability to prepare polymer monoliths from latexes synthesised from the soap-free emulsion polymerisation of styrene has been demonstrated in this work. This approach potentially offers a greener alternative in comparison to the use of a porogenic solvent or an emulsion template, with the use of only H_2O and/or MeOH as solvents, the absence of surfactant, and minimal purification the main advantages. Chemical cross-linking was employed through the introduction of DEGDA, which provided these materials with enhanced rigidity. The phase separation of the cross-linker during curing resulted in the presence of a polymer coating, with increases in the DEGDA content resulting in thicker coatings and ultimately a predominately fused morphology. It is expected that the presence of this coating would have modified the surface chemistry, and may offer an alternative method for surface functionalisation through the incorporation of additional water-soluble cross-linkers.

Initial experiments focused on the preparation of these materials using two latexes, however it was found that similar materials could be obtained through the addition of APS to a single latex, where it both promoted the formation of the colloidal gel and initiated the cross-linking process. The use of APS as initiator also allowed for the rapid curing of these materials at room temperature through the addition of TEMED. In conjunction to the greener advantages, this approach also offered some unique advantages over conventional synthetic strategies. For example, the pore size of these materials was found to be in the order of the particle dimensions, with the use of larger particles resulting in materials with larger pore size. Given particles of different size can easily be prepared using the soap-free emulsion polymerisation approach, this offers the ability to easily prepare materials with desired porous properties for particular applications.

Additionally, the high mouldability of all gels prepared in this work afforded the possibility to prepare these materials in a variety of formats and more importantly without the use of a mould. This approach is therefore expected to be applicable for the preparation of polymer monoliths for a wide variety of applications, including but not limited to, tissue engineering, catalysis, chromatography, extraction, sample preparation, and as absorbents. In particular these monoliths were found to possess relatively high porosities and were capable of rapidly absorbing solvents of varying polarity by capillary action, which suggested their applicability for TLC and extraction.

6.5 References

[1] Hjertén, S.; Liao, J.-L.; Zhang, R. *J. Chromatogr. A.* **1989**, *473*, 273-275.
[2] Svec, F.; Fréchet, J. M. J. *Anal. Chem.* **1992**, *64*, 820-822.
[3] Viklund, C.; Svec, F.; Fréchet, J. M. J. *Chem. Mater.* **1996**, *8*, 744-750.
[4] Burguete, M. I.; Cornejo, A.; García-Verdugo, E.; García, J.; Gil, M. J.; Luis, S. V.; Martínez-Merino, V.; Mayoral, J. A.; Sokolova, M. *Green Chem.* **2007**, *9*, 1091-1096.
[5] Altava, B.; Burguete, M. I.; García-Verdugo, E.; Luis, S. V.; Vicent, M. J. *Green Chem.* **2006**, *8*, 717-726.
[6] Chiroli, V.; Benaglia, M.; Puglisi, A.; Porta, R.; Jumde, R. P.; Mandoli, A. *Green Chem.* **2014**, *16*, 2798-2806.
[7] Bortolini, O.; Cavazzini, A.; Dambruoso, P.; Giovannini, P. P.; Caciolli, L.; Massi, A.; Pacifico, S.; Ragno, D. *Green Chem.* **2013**, *15*, 2981-2992.
[8] Xie, S.; Svec, F.; Fréchet, J. M. J. *Biotechnol. Bioeng.* **1999**, *62*, 30-35.
[9] Wang, H.; Zhang, H.; Lv, Y.; Svec, F.; Tan, T. *J. Chromatogr. A.* **2014**, *1343*, 128-134.
[10] Zhang, S.; Luo, W.; Yan, W.; Tan, B. *Green Chem.* **2014**, *16*, 4408-4416.
[11] Christenson, E. M.; Soofi, W.; Holm, J. L.; Cameron, N. R.; Mikos, A. G. *Biomacromolecules.* **2007**, *8*, 3806–3814.
[12] Zhang, H.; Cooper, A. I. *Adv. Mater.* **2007**, *19*, 2439-2444.
[13] Jing, P.; Fang, X.; Yan, J.; Guo, J.; Fang, Y. *J. Mater. Chem. A.* **2013**, *1*, 10135-10141.
[14] Shih, Y.-H.; Singco, B.; Liu, W.-L.; Hsu, C.-H.; Huang, H.-Y. *Green Chem.* **2011**, *13*, 296-299.
[15] Svec, F.; Lv, Y. *Anal. Chem.* **2015**, *87*, 250-273.
[16] Yin, D.; Guan, Y.; Gu, H.; Jia, Y.; zhang, Q. *RSC Adv.* **2017**, *7*, 7303-7309.
[17] Candish, E.; Wirth, H. J.; Gooley, A. A.; Shellie, R. A.; Hilder, E. F. *J. Chromatogr. A.* **2015**, *1410*, 9-18.
[18] Krenkova, J.; Foret, F. *J. Sep. Sci.* **2011**, *34*, 2106-2112.
[19] Candish, E.; Khodabandeh, A.; Gaborieau, M.; Rodemann, T.; Shellie, R. A.; Gooley, A. A.; Hilder, E. F. **2017**.
[20] Svec, F.; Fréchet, J. M. J. *Chem. Mater.* **1995**, *7*, 707-715.
[21] Viklund, C.; Pontén, E.; Glad, B.; Irgum, K. *Chem. Mater.* **1997**, *9*, 463-471.
[22] Svec, F. *J. Chromatogr. A.* **2010**, *1217*, 902-924.

[23] Bedair, M.; El Rassi, Z. *J. Chromatogr. A.* **2003**, *1013*, 35-45.
[24] Gu, B.; Armenta, J. M.; Lee, M. L. *J. Chromatogr. A.* **2005**, *1079*, 382-391.
[25] Huang, X.; Wang, Q.; Yan, H.; Huang, Y.; Huang, B. *J. Chromatogr. A.* **2005**, *1062*, 183-188.
[26] Peters, E. C.; Petro, M.; Svec, F.; Fréchet, J. M. J. *Anal. Chem.* **1998**, *70*, 2296-2302.
[27] Jin, W.; Fu, H.; Huang, X.; Xiao, H.; Zou, H. *Electrophoresis.* **2003**, *24*, 3172-3180.
[28] Oberacher, H.; Premstaller, A.; Huber, C. G. *J. Chromatogr. A.* **2004**, *1030*, 201-208.
[29] Wang, Q. C.; Svec, F.; Fréchet, J. M. J. *J. Chromatogr. A.* **1994**, *669*, 230-235.
[30] Zhang, K.; Yan, C.; Yang, J.; Zhang, Z.; Wang, Q.; Gao, R. *J. Sep. Sci.* **2005**, *28*, 217-224.
[31] Hoegger, D.; Freitag, R. *J. Chromatogr. A.* **2001**, *914*, 211-222.
[32] Prat, D.; Wells, A.; Hayler, J.; Sneddon, H.; McElroy, C. R.; Abou-Shehada, S.; Dunn, P. J. *Green Chem.* **2016**, *18*, 288-296.
[33] Santora, B. P.; Gagné, M. R.; Moloy, K. G.; Radu, N. S. *Macromolecules.* **2001**, *34*, 658-661.
[34] Kimmins, S. D.; Cameron, N. R. *Adv. Funct. Mater.* **2011**, *21*, 211-225.
[35] Cameron, N. R.; Sherrington, D. C. *Adv. Polym. Sci.* **1996**, *126*, 162-214.
[36] Cserháti, T.; Forgács, E.; Oros, G. *Environ. Int.* **2002**, *28*, 337–348.
[37] Guilbot, J.; Kerverdo, S.; Milius, A.; Escola, R.; Pomrehn, F. *Green Chem.* **2013**, *15*, 3337-3354.
[38] Morán, M. C.; Pinazo, A.; Pérez, L.; Clapés, P.; Angelet, M.; García, M. T.; Vinardell, M. P.; Infante, M. R. *Green Chem.* **2004**, *6*, 233-240.
[39] Verdia, P.; Gunaratne, H. Q. N.; Goh, T. Y.; Jacquemin, J.; Blesic, M. *Green Chem.* **2016**, *18*, 1234-1239.
[40] Ghebremeskel, A. N.; Vemavarapu, C.; Lodaya, M. *Int. J. Pharm.* **2007**, *328*, 119–129.
[41] Kovačič, S.; Matsko, N. B.; Jerabek, K.; Krajnc, P.; Slugovc, C. *J. Mater. Chem. A.* **2013**, *1*, 487-490.
[42] Jordan, A.; Gathergood, N. *Chem. Soc. Rev.* **2015**, *44*, 8200-8237.
[43] Coleman, D.; Gathergood, N. *Chem. Soc. Rev.* **2010**, *39*, 600-637.
[44] Smiglak, M.; Reichert, W. M.; Holbrey, J. D.; Wilkes, J. S.; Sun, L.; Thrasher, J. S.; Kirichenko, K.; Singh, S.; Katritzky, A. R.; Rogers, R. D. *Chem. Commun.* **2006**, 2554-2556.
[45] Earle, M. J.; Esperanca, J. M.; Gilea, M. A.; Lopes, J. N.; Rebelo, L. P.; Magee, J. W.; Seddon, K. R.; Widegren, J. A. *Nature.* **2006**, *439*, 831-834.
[46] Welton, T. *Green Chem.* **2011**, *13*, 225.
[47] Wang, H.; Hansen, M. B.; Lowik, D. W.; van Hest, J. C.; Li, Y.; Jansen, J. A.; Leeuwenburgh, S. C. *Adv. Mater.* **2011**, *23*, H119-H124.
[48] Wang, Q.; Wang, L.; Detamore, M. S.; Berkland, C. *Adv. Mater.* **2008**, *20*, 236-239.
[49] Wang, Q.; Jamal, S.; Detamore, M. S.; Berkland, C. *J Biomed Mater Res A.* **2011**, *96*, 520-527.
[50] Wang, Q.; Gu, Z.; Jamal, S.; Detamore, M. S.; Berkland, C. *Tissue Eng Part A.* **2013**, *19*, 2586-2593.
[51] Van Tomme, S. R.; van Nostrum, C. F.; de Smedt, S. C.; Hennink, W. E. *Biomaterials.* **2006**, *27*, 4141-4148.
[52] Tomme, S. R. V.; Steenbergen, M. J. v.; Smedt, S. C. D.; Nostrum, C. F. v.; Hennink, W. E. *Biomaterials.* **2005**, *26*, 2129-2135.
[53] Tomme, S. R. V.; Nostrum, C. F. v.; Dijkstra, M.; Smedt, S. C. D.; Hennink, W. E. *Eur. J. Pharm. Biopharm.* **2008**, *70*, 522-530.
[54] Bon, S. A. F.; Beek, H. V.; Piet, P.; German, A. L. *J. Appl. Polym. Sci.* **1995**, *58*, 19–29.

[55] Chonde, Y.; Krieger, I. M. *J. Appl. Polym. Sci.* **1981** *26*, 1819–1827.
[56] McCracken, J. R.; Datyner, A. *J. Appl. Polym. Sci.* **1974**, *18*, 3365–3372.
[57] Goodwin, J. W.; Hearn, J.; Ho, C. C.; Ottewill, R. H. *Br. Polym. J.* **1973**, *5*, 341-362.
[58] Thickett, S. C.; Gilbert, R. G. *Polymer.* **2007**, *48*, 6965-6991.
[59] Marti, N.; Quattrini, F.; Butté, A.; Morbidelli, M. *Macromol. Mater. Eng.* **2005**, *290*, 221-229.
[60] Yu, L.; Zhang, Z.; Zhang, H.; Ding, J. *Biomacromolecules.* **2009**, *10*, 547–1553.
[61] Yu, L.; Chang, G.; Zhang, H.; Ding, J. *J. Polym. Sci. A Polym. Chem.* **2007**, *45*, 1122-1133.
[62] Kim, J. H.; Chainey, M.; El‐Aasser, M. S.; Vanderhoff, J. W. *J. Polym. Sci. A Polym. Chem.* **1992**, *30*, 171-183.
[63] Liu, L.-J.; Krieger, I. M. *J. Polym. Sci. A Polym. Chem.* **1981**, *19*, 3013–3026.
[64] Juang, M. S.-D.; Krieger, I. M. *J. Polym. Sci. A Polym. Chem.* **1976**, *14*, 2089–2107.
[65] Turner, S. R.; Weiss, R. A.; Lundberg, R. D. *J. Polym. Sci. A Polym. Chem.* **1985**, *23*, 535–548.
[66] Tohver, V.; Chan, A.; Sakurada, O.; Lewis, J. e. A. *Langmuir.* **2001**, *17*, 8414-8421.
[67] Arrua, R. D.; Causon, T. J.; Hilder, E. F. *Analyst.* **2012**, *137*, 5179–5189.
[68] Svec, F.; Fréchet, J. M. J. *Ind. Eng. Chem. Res.* **1999**, *38*, 34-48.
[69] Wang, Q. C.; Svec, F.; Fréchet, J. M. J. *Anal. Chem.* **1993**, *65*, 2243-2248.
[70] McKenzie, H., Doctor of Philosophy, University of Warwick, 2014.
[71] Liu, Z.; Xiao, H. **2000**, *41*, 7023–7031.
[72] Kang, K.; Kan, C. Y.; Du, Y.; Liu, D. S. *J. Appl. Polym. Sci.* **2004**, *92*, 433–438.
[73] Mittal, V.; Matsko, N. B.; Butté, A.; Morbidelli, M. *Macromol. Mater. Eng.* **2008**, *2*, 215-221.
[74] Bechtle, M.; Butte, A.; Storti, G.; Morbidelli, M. *J. Chromatogr. A.* **2010**, *1217*, 4675-4681.
[75] Arrua, R. D.; Nordborg, A.; Haddad, P. R.; Hilder, E. F. *J. Chromatogr. A.* **2013**, *1273*, 26-33.
[76] Arrua, R. D.; Haddad, P. R.; Hilder, E. F. *J. Chromatogr. A.* **2013**, *1311*, 121-126.
[77] Khodabandeh, A.; Dario Arrua, R.; Desire, C. T.; Rodemann, T.; Bon, S. A. F.; Thickett, S. C.; Hilder, E. F. *Polym. Chem.* **2016**, *7*, 1803-1812.
[78] Svec, F. *J. Sep. Sci.* **2004**, *27*, 1419-1430.
[79] Svec, F. *J. Sep. Sci.* **2004**, *27*, 747-766.
[80] Plieva, F. M.; Galaev, I. Y.; Mattiasson, B. *J. Sep. Sci.* **2007**, *30*, 1657-1671.
[81] Xie, S.; Allington, R. W.; Svec, F.; Fréchet, J. M. J. *J. Chromatogr. A.* **1999**, *865*, 169-174.
[82] Jiang, Z.; Smith, N. W.; Liu, Z. *J. Chromatogr. A.* **2011**, *1218*, 2350-2361.

Appendix D

Preparation of polymer monoliths from colloidal gels formed using latexes prepared from the soap-free emulsion polymerisation of styrene

D.1 Synthesis of the cationic co-monomer

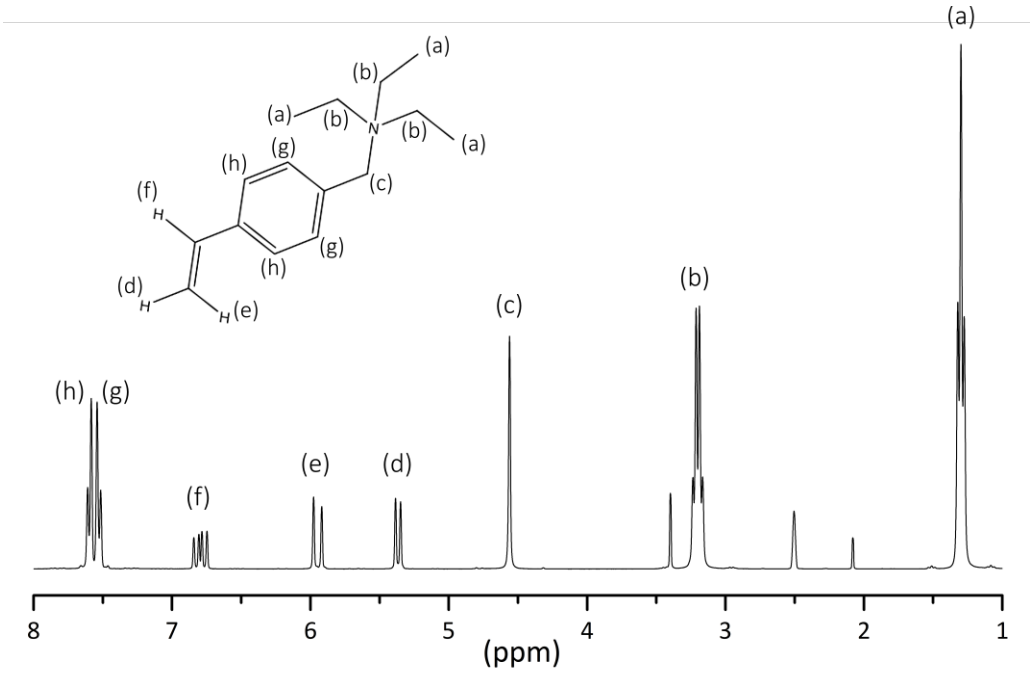

Figure D1. ^{1}H NMR analysis of the product obtained. The peaks at 2.1, 2.5 and 3.4 ppm correspond to acetone, DMSO, and H_2O respectively.

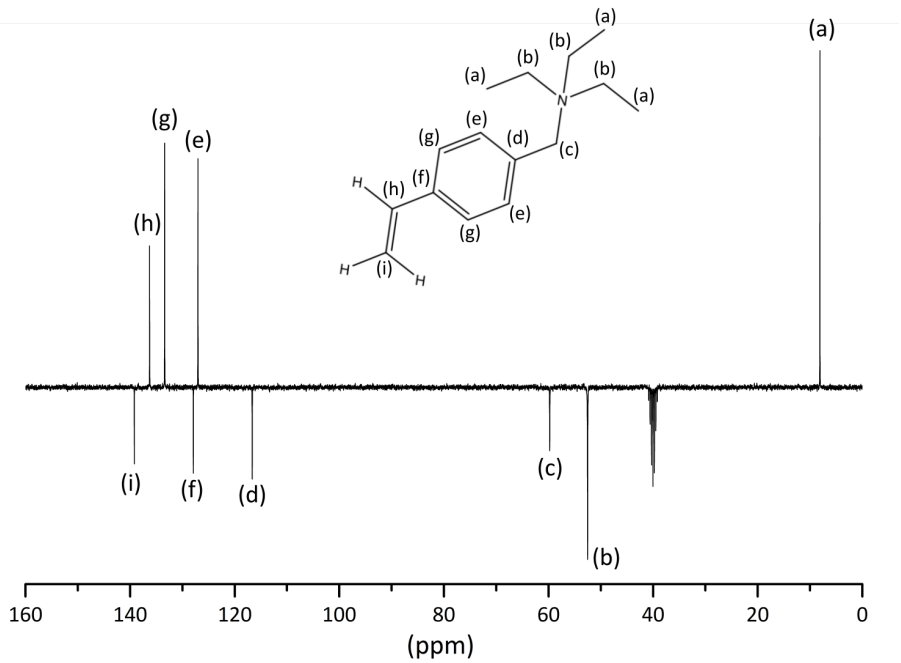

Figure D2. ^{13}C NMR (*J*-modulated) analysis of the product obtained. CH_3 and CH are positive, while CH_2 and C are negative.

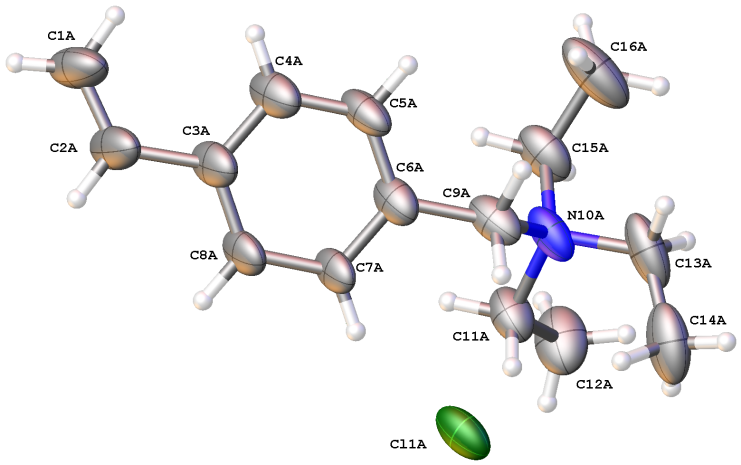

Figure D3. Solid state structure of the product with atom numbering and thermal ellipsoids drawn at 50% probability level. The minor disordered component has been removed for clarity.

Table D1 Crystal data and structure refinement for TEVBAC ($C_{15}H_{24}ClN$)

Empirical formula	$C_{15}H_{24}ClN$
Formula weight	253.80
Temperature/ K	150(2)
Crystal system	orthorhombic
Space group	$P2_12_12_1$
a [Å]	7.97174(17)
b [Å]	12.7398(3)
c [Å]	14.0754(5)
α [deg]	90
β[deg]	90
γ [deg]	90
Volume [Å3]	1429.47(7)
Z	4
ρ_{calc} [g cm^{-3}]	1.179
μ [mm^{-1}]	2.176
F(000)	552.0
Crystal size/mm^3	0.2 × 0.16 × 0.1 colourless block
Radiation	CuKα (λ = 1.54184)
2Θ range for data collection/°	9.364 to 155.902
Tmax. and Tmin.	-9 ≤ h ≤ 9, -15 ≤ k ≤ 16, -17 ≤ l ≤ 17
Reflections collected	15587
Independent reflections	2999 [R_{int} = 0.0324, R_{sigma} = 0.0204]
Data/restraints/parameters	2999/102/290
Goodness-of-fit on F^2	1.033
Final R indexes [I>=2σ (I)]	R_1 = 0.0367, wR_2 = 0.0974
Final R indexes [all data]	R_1 = 0.0426, wR_2 = 0.1032
Largest diff. peak/hole / e $Å^{-3}$	0.14/-0.12
Flack parameter	-0.008(10)

Table D2 Bond Lengths for TEVBAC ($C_{15}H_{24}ClN$)

Atom	Atom	Length / Å
C1	C2	1.244(16)
C2	C3	1.519(11)
C6	C5	1.3900
C6	C7	1.3900
C6	C9	1.480(11)
C5	C4	1.3900
C4	C3	1.3900
C3	C8	1.3900
C8	C7	1.3900
C9	N10	1.518(16)
N10	C11	1.498(11)
N10	C13	1.524(11)
N10	C15	1.520(12)
C11	C12	1.530(8)
C13	C14	1.525(11)
C15	C16	1.515(14)
C14A	C13A	1.526(11)
N10A	C15A	1.517(10)
N10A	C11A	1.531(8)
N10A	C13A	1.515(8)
N10A	C9A	1.569(11)
C1A	C2A	1.334(9)
C2A	C3A	1.517(8)
C15A	C16A	1.487(8)
C11A	C12A	1.529(6)
C6A	C5A	1.3900
C6A	C7A	1.3900
C6A	C9A	1.514(8)
C5A	C4A	1.3900
C4A	C3A	1.3900
C3A	C8A	1.3900
C8A	C7A	1.3900

Table D3 Bond Angles for TEVBAC ($C_{15}H_{24}ClN$)

Atom	Atom	Atom	Angle / °
C1	C2	C3	127.0(13)
C5	C6	C7	120.0
C5	C6	C9	121.3(6)
C7	C6	C9	118.6(6)
C4	C5	C6	120.0
C5	C4	C3	120.0
C4	C3	C2	124.2(7)
C4	C3	C8	120.0
C8	C3	C2	115.7(7)
C7	C8	C3	120.0
C8	C7	C6	120.0
C6	C9	N10	119.2(11)
C9	N10	C13	105.4(8)
C9	N10	C15	111.1(7)
C11	N10	C9	109.4(9)
C11	N10	C13	113.4(6)
C11	N10	C15	111.6(8)
C15	N10	C13	105.8(8)
N10	C11	C12	112.3(6)
N10	C13	C14	114.7(6)
C16	C15	N10	118.2(8)
C15A	N10A	C11A	107.8(5)
C15A	N10A	C9A	111.8(6)
C11A	N10A	C9A	107.7(6)
C13A	N10A	C15A	110.6(6)
C13A	N10A	C11A	111.1(6)
C13A	N10A	C9A	107.9(5)
C1A	C2A	C3A	124.8(7)
C16A	C15A	N10A	115.5(6)
C12A	C11A	N10A	114.7(5)
C5A	C6A	C7A	120.0
C5A	C6A	C9A	119.6(4)
C7A	C6A	C9A	120.4(4)
C6A	C5A	C4A	120.0
C3A	C4A	C5A	120.0
C4A	C3A	C2A	122.1(4)
C4A	C3A	C8A	120.0
C8A	C3A	C2A	117.8(4)
C3A	C8A	C7A	120.0
C8A	C7A	C6A	120.0
N10A	C13A	C14A	116.3(5)
C6A	C9A	N10A	116.7(6)

D.2 Formation of colloidal gels

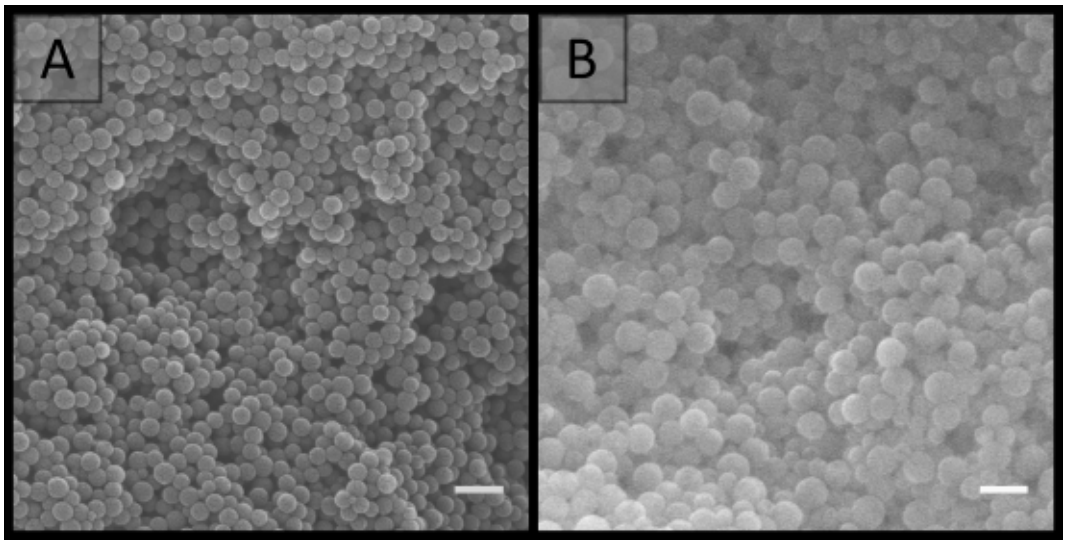

Figure D4. SEM images of colloidal gels obtained by combining A01 and V01 at equal weight percent. Particle concentration: **A)** 5 wt% and **B)** 15 wt%. Scale bar is 250 nm.

D.3 Formation of cross-linked colloidal gels

Table D4 Observations for the addition of DVB to 20 wt% A01 or V01

Sample [a]	Ratio of latex solids to DVB [b] / wt/wt	Result [c]
A01	1:1.5	Significant coagulation
A01	1:0.5	Significant coagulation
A01	1:0.2	Significant coagulation
A01	1:0.1	Significant coagulation
V01	1:1.5	Significant coagulation
V01	1:0.5	Significant coagulation
V01	1:0.2	Significant coagulation
V01	1:0.1	Significant coagulation

[a] The following nomenclature is used, samples prepared with APS start with an A, while those prepared with V-50 start with a V. [b] Mass ratio of solid latex to monomer.
[c] Visual result 2 h after addition of DVB to individual latexes.

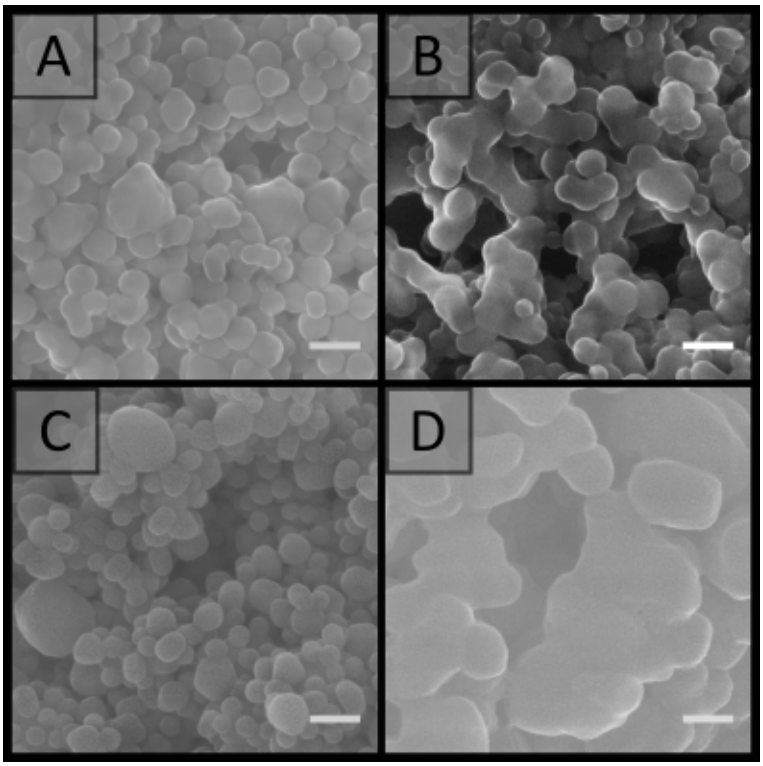

Figure D5. SEM images of cross-linked colloidal gels obtained by combining 20 wt% A01 and V01 and cured with different concentrations of DEGDA. DEGDA concentration (w.r.t. total solid content of the gel): **A)** 15 wt%, **B)** 20 wt%, **C)** 25 wt% and **D)** 30 wt%. Scale bar is 250 nm.

D.4 Formation of porous materials using a single latex

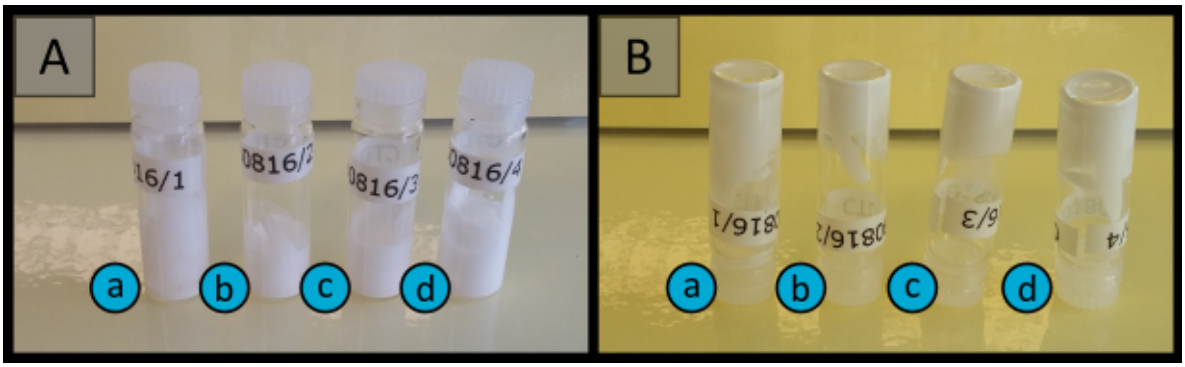

Figure D6. Photographs of colloidal gels obtained from the addition of APS at 1 wt% (w.r.t. solids) to 20 wt% V01. **A)** taken with the vials upright 2 h after the addition of the APS solution and **B)** taken 20 min after inversion. Volume and concentration of APS solution used for 0.2 g of colloidal gel: **a)** 10 µL of 0.04 g/mL, **b)** 20 µL of 0.02 g/mL, **c)** 50 µL of 0.008 g/mL and **d)** 72.8 µL of 0.005 g/mL.

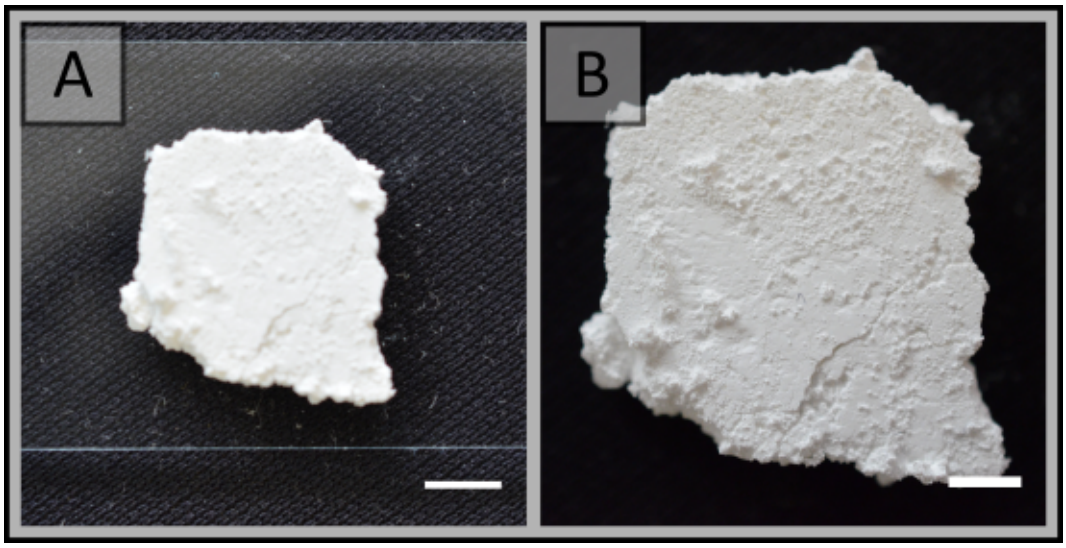

Figure D7. Photographs of a cross-linked colloidal gel obtained from the addition of APS at 1 wt% (w.r.t. solids) to 20 wt% V01 containing 30 wt% DEGDA (w.r.t. solids) and cured by the addition of TEMED at room temperature. Scale bar is **A)** 5 mm and **B)** 3 mm.

D.5 Solvent Behaviour

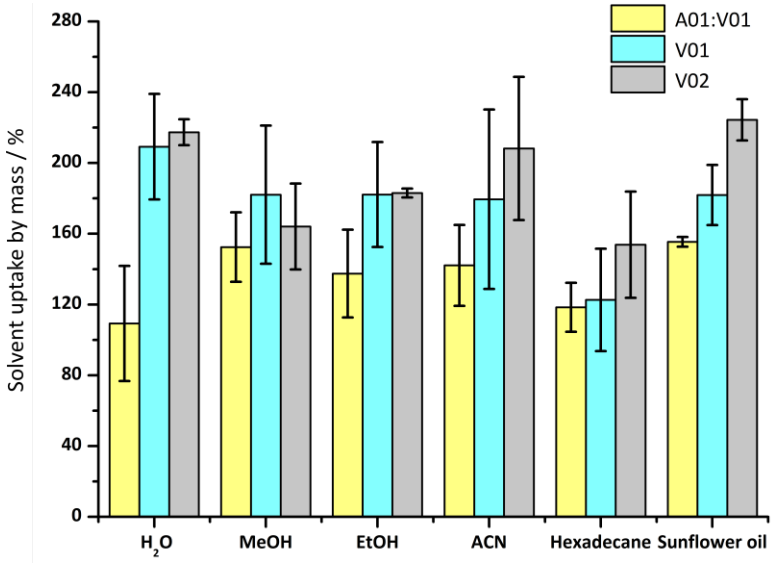

Figure D8. Mass of solvent absorbed by polymer disks of different cross-linked colloidal gels relative to the mass of the dry disks. A01:V01 was cross-linked using 20 wt% DEGDA (w.r.t. solids), while V01 & V02 were cross-linked using 30 wt% DEGDA (w.r.t. solids).

D.6 Surface Area Analysis

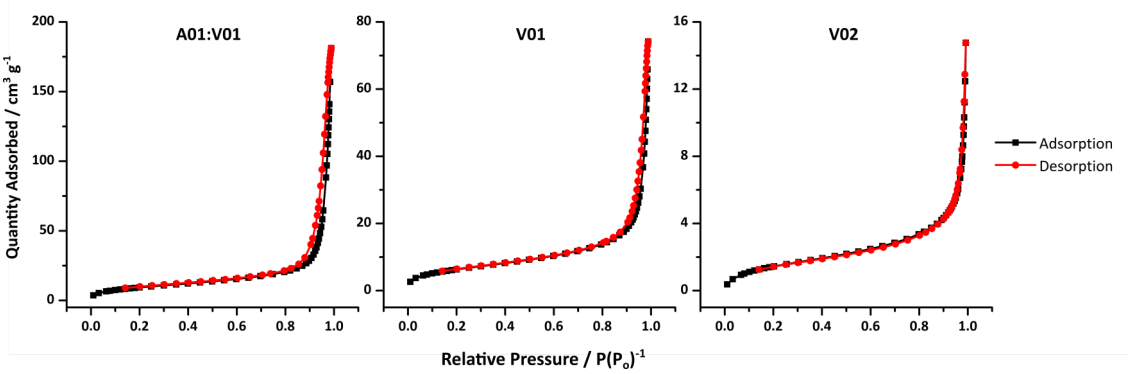

Figure D9. Nitrogen adsorption/desorption isotherms for the cross-linked colloidal gels. A01:V01 was cross-linked using 20 wt% DEGDA (w.r.t. solids), while V01 & V02 were cross-linked using 30 wt% DEGDA (w.r.t. solids).

Chapter 7

General Conclusions and Future Directions

The use of emulsion templates, in particular high internal phase emulsions, for the preparation of polymer monoliths has been widely reported in the literature. However, the chromatographic performance of these materials in LC has so far been limited as a result of dispersion, and relatively few reports have focused in depth on the influence of the materials structure on performance [1]. In addition, only a handful of reports have investigated their preparation in capillary format, which is a format that can result in a reduction in peak broadening [2]. These reports all focused on the separation of small molecules such as alkylbenzenes and not on the separation of larger molecules such as proteins, which polymer monoliths are better suited for. The preparation of these materials for LC has also mainly utilised water-in-oil emulsions, resulting in relatively hydrophobic scaffolds, which limits the applicability of these materials for different chromatographic modes without further chemical modification. To the best of my knowledge there exist no reports in the literature involving the use of oil-in-water emulsions to obtain hydrophilic materials for LC.

Poly(AAm-*co*-MBAm) monoliths were therefore prepared using (paraffin-oil)-in-water emulsions, with Tween® 85 as stabiliser, based on a recipe by Hua et al. [3]. However, in this case the internal phase volume was varied in order to prepare polymer monoliths with improved mechanical properties under compression, as poor mechanical properties as a result of high porosities are known to be problematic for chromatographic applications [4]. For example, when an internal phase of 40 vol% was utilised a Young's modulus of 490 ± 90 MPa was obtained in comparison to a value of 180 ± 70 MPa for a material prepared using an internal phase of 60 vol%.

Reductions in the internal phase volume are known to result in a reduction in the interconnectivity of the resulting materials [5], which is a disadvantage of this approach.

However window formation can be promoted through manipulation of a variety of parameters including the emulsification energy and surfactant level. A systematic study was therefore employed involving the variation of the internal phase volume, emulsification energy and surfactant level. It was found that polymer monoliths with improved mechanical properties could be obtained with a high level of interconnectivity through the use of an appropriate combination of these parameters.

In addition, significantly different porous morphologies were observed through variations in these parameters. For example, an increase in the surfactant-to-oil ratio and emulsification energy was observed to result in a shift in morphology away from the traditional void and window structure of emulsion templated materials to that of materials possessing what appeared to be predominately open voids. It was suggested that this was a result of increased thinning of the continuous phase films between adjacent droplets. This structure also appeared to aid in the mechanical properties of these materials with a normalised Young's modulus of 13 ± 3 MPa for a material possessing this structure compared to a value of 3 ± 1 MPa for a material possessing the typical void and window structure.

These poly(AAm-*co*-MBAm) monoliths were also found to be responsive to different solvent environments with significant variations in volume. For example, the porosity of these materials approached 100% when immersed in H_2O, and they were observed to shrink when exposed to acetone. This suggested their potential application as absorbents or in controlled release. However, these variations in volume are potentially problematic for LC applications involving a solvent gradient. In fact when prepared in capillary format, these monoliths were observed to detach from the capillary wall as a result of shrinkage during purification. If stable attachment could be achieved these materials may be applicable for the separation of compounds of varying hydrophilicity in HILIC, however these particular materials were deemed unsuitable given these inherent characteristics.

The preparation of poly(Sty-co-DVB) poly(HIPE)s, from water-in-oil emulsions, in capillary format for the separation of proteins was therefore investigated, as stable attachment of similar poly(HIPE)s had been demonstrated previously [6]. Stable attachment to the

capillary wall was also observed for these poly(HIPE)s and this was attributed to the negligible change in volume observed when exposed to different solvent environments. These columns were also mechanically stable over the range of flow rates utilised.

Particular attention was paid to the influence the preparation in capillary format had on the resulting morphology of these poly(HIPE)s. It was found that when these materials were prepared in capillaries with i.d.s below 540 µm using low shear emulsification significant alterations in their porous structure was observed. This observation was particularly important as low shear emulsification is commonly employed for the preparation of poly(HIPE)s for LC. In these cases a decrease in void size was observed with decreasing capillary i.d. In addition, all columns prepared using low shear emulsification possessed significant radial heterogeneity. This resulted in significant band broadening when these columns were applied for the separation of a standard protein mixture comprising ribonuclease A, lysozyme and α-chymotrypsinogen A by RPLC.

When high shear emulsification was utilised the resulting poly(HIPE)s exhibited narrower void size distributions and the materials prepared in capillary format reflected those prepared within glass vials, in all cases. The presence of radial heterogeneity was also not observed for these poly(HIPE)s. This resulted in significant improvements in the chromatographic performance for the separation of this protein mixture, in particular when using a 150 µm i.d. capillary. However the presence of a small number of significantly larger voids was observed, which was attributed to the presence of air bubbles from the use of the high energy mixer and/or the capillary filling process. These larger voids have also been observed for other poly(HIPE) systems [1] and would have contributed to band broadening, resulting in a reduction in chromatographic performance.

Given these poly(Sty-*co*-DVB) poly(HIPE)s possessed a rigid backbone and stable attachment to the capillary wall, in contrast to the poly(AAm-*co*-MBAm) monoliths, these monoliths were functionalised by simply including monomers in the internal phase. Initial work focused on the inclusion of the hydrophilic AAm monomer in an effort to increase the surface hydrophilicity. The influence of AAm content and the choice of initiator on the

resulting morphology was investigated. It was found, as previously reported by Gitli and Silverstein [7], that the inclusion of AAm resulted in a reduction the void size as this monomer was acting as a co-stabiliser. In addition, the use of a water-soluble initiator coupled with an increase in the AAm content resulted in the presence of an AAm-based hydrogel that filled the voids of the resulting poly(HIPE). This was related to a higher degree of polymerisation occurring in the internal phase. In contrast when an oil-soluble initiator was utilised, with the same AAm content, a lower degree of polymerisation occurred in the internal phase resulting in a poly(HIPE) with AAm chains grafted to the surface.

The presence of this hydrogel was found to be advantageous for the separation of some components of a peptide mixture in HILIC, which was not possible for the poly(HIPE) prepared using the oil-soluble initiator. However, its presence coupled with a broad void size distribution resulted in inferior performance for the separation of the protein mixture by RPLC, compared to the unmodified column. In contrast the materials prepared using the oil-soluble initiator with AAm present in the internal phase exhibited significantly improved chromatographic performance as a result of their improved column bed homogeneity. In particular the peaks obtained with these materials were narrower and more Gaussian in nature, in comparison to the broad and rear-tailed peaks observed for the unmodified column.

In an attempt to further improve the column homogeneity the weakly hydrophilic monomer PEGDA was included in the internal phase, where it was expected to act as a more efficient co-stabiliser than AAm. When small amounts of PEGDA were included, poly(HIPE)s with narrower void size distributions were obtained and these columns were capable of separating the three proteins from the protein impurity peaks. This allowed these materials to be utilised for a more complex separation involving seven components where a good separation was obtained. However these materials also possessed the presence of these significantly larger voids and the chromatographic performance of these materials overall is still inferior to that of conventional polymer monoliths.

While it is clear that emulsifying under high shear and including co-stabilisers in the emulsion formulation can result in poly(HIPE)s with significantly improved chromatographic performance, their performance is ultimately limited by the presence of these larger voids. Therefore in order to further improve their performance more effort on improving the emulsification process is required. For example, strategies involving microfluidics, which have been used to prepare relatively monodisperse HIPEs [8], may offer an alternative route to the use of high energy mixers. However, the droplet size in these approaches is relatively large. In addition, the void and window structure of these poly(HIPE)s could potentially be acting as mixers [1], resulting in increased dispersion. In accordance the predominately open void structure observed for some of the poly(AAm-*co*-MBAm) monoliths prepared in this work might result in further improvements in chromatographic performance if the same approach can be applied to the poly(Sty-*co*-DVB) system.

Further investigation into the preparation and resulting structure of these materials is required in order to further improve their chromatographic performance to a point where it approaches that of conventional polymer monoliths. However, it is important to point out that direct comparisons between the separations obtained with these materials and that of conventional polymer monoliths are not representative due to the significant differences in porosity. Conventional polymer monoliths are typically prepared with a porosity of 60%, in comparison to the porosities of poly(HIPE)s which exceeds 74%. A higher porosity often results in lower surface areas, which limits both the sample capacity and the interactions occurring between the stationary phase and the analytes.

Additionally, the presence of a larger total pore volume results in differences in flow velocity at the same flow rate. In accordance the analytes in a monolith with a larger pore volume will experience a lower flow velocity and therefore a higher degree of band broadening can occur. For example, Krajnc et al. [1] demonstrated a slight improvement in the chromatographic performance for their poly(GMA-*co*-EDMA) poly(HIPE)s upon reducing the porosity.

While reducing the internal phase volume of the emulsion templates may also allow for further improvements in the chromatographic performance, as discussed, this is often at the expense of interconnectivity and this would detract from the advantage of having a highly porous material with high permeability. For example, the permeabilities for the poly(HIPE)s prepared in this work were found to be an order of magnitude larger than that of conventional polymer monoliths and this allows for the possibility of rapid separations with minimal increase in back pressure, which was also demonstrated in this work. This is particularly important for situations where the pressure of the LC system is limited, for example for miniaturised platforms. These particular features may also allow these materials to be applied in other areas, where the degree of band broadening is not a critical factor. For example the high permeabilities and porosities, typically associated with poly(HIPE)s, have already been demonstrated to be beneficial for the transport of nutrients in tissue engineering [9-10]. They could also potentially be applied as supports for catalysis and combinatorial chemistry or as metal chelating agents, with some additional chemical modifications.

An alternative route for the preparation of poly(styrene)-based monoliths was also explored through the combination of oppositely charged latexes prepared from the soap-free emulsion polymerisation of styrene. The addition of these particles at 20 wt% resulted in cohesive gels, which were then cross-linked by the inclusion of DEGDA in the formulation. This approach potentially offers a greener alternative to the preparation of polymer monoliths in comparison to the use of a porogenic solvent or an emulsion template, with the use of only H_2O and/or MeOH as solvents, the absence of surfactant, and minimal purification the main advantages.

It was also found that these materials could be prepared through the use of a single latex where the addition of the initiator APS promoted both the formation of the gel and the cross-linking process. The use of APS also allowed for these materials to be cured rapidly at room temperature through the addition of TEMED. This approach also offered some unique advantageous over conventional strategies, for example the pore size of these materials was found to be in the order of the particle dimensions, with the use of larger particles resulting in materials with larger pore size. Particles of different size can easily be

prepared using the soap-free emulsion polymerisation approach, thus offering the ability to prepare materials with desired porous properties for particular applications.

Additionally, the mouldability of these gels afforded the possibility to prepare these materials in a variety of formats. They were also able to retain their shape in the absence of an external force allowing for their preparation without the use of a mould, which is not possible when using a porogenic solvent. These materials may find applications in several areas including tissue engineering, catalysis, chromatography, extraction, sample preparation, and as absorbents and this warrants further investigation. This approach is also not limited to the use of poly(styrene)-based particles, as other monomer systems such as methyl methacrylate could potentially be utilised [11-12]. These materials also possessed relatively high porosities and were observed to rapidly uptake solvents of varying polarity by capillary action, suggesting their applicability for TLC and extraction.

7.1 References

[1] Krajnc, P.; Leber, N.; Štefanec, D.; Kontrec, S.; Podgornik, A. *J. Chromatogr. A.* **2005**, *1065*, 69-73.
[2] Nischang, I.; Svec, F.; Fréchet, J. M. *J. Chromatogr. A.* **2009**, *1216*, 2355-2361.
[3] Hua, Y.; Zhang, S.; Zhu, Y.; Chu, Y.; Chen, J. *J. Polym. Sci. A Polym. Chem.* **2013**, *51*, 2181-2187.
[4] Jerenec, S.; Šimić, M.; Savnik, A.; Podgornik, A.; Kolar, M.; Turnšek, M.; Krajnc, P. *React. Funct. Polym.* **2014**, *78*, 32-37.
[5] Luo, Y.; Wang, A.-N.; Gao, X. *Soft Matter.* **2012**, *8*, 7547-7551.
[6] Tunç, Y.; Gölgelioğlu, Ç.; Hasirci, N.; Ulubayram, K.; Tuncel, A. *J. Chromatogr. A.* **2010**, *1217*, 1654-1659.
[7] Gitli, T.; Silverstein, M. S. *Soft Matter.* **2008**, *4*, 2475–2485.
[8] Costantini, M.; Colosi, C.; Guzowski, J.; Barbetta, A.; Jaroszewicz, J.; Święszkowski, W.; Dentini, M.; Garstecki, P. *J. Mater. Chem. B.* **2014**, *2*, 2290–2300.
[9] Barbetta, A.; Dentini, M.; De Vecchis, M. S.; Filippini, P.; Formisano, G.; Caiazza, S. *Adv. Funct. Mater.* **2005**, *15*, 118-124.
[10] Busby, W.; Cameron, N. R.; Jahoda, C. A. B. *Biomacromolecules.* **2001**, *2*, 154-164.
[11] Nagao, D.; Anzai, N.; Kobayashi, Y.; Gu, S.; Konno, M. *J. Colloid Interface Sci.* **2006**, *298*, 232-237.
[12] Kang, K.; Kan, C. Y.; Du, Y.; Liu, D. S. *J. Appl. Polym. Sci.* **2004**, *92*, 433–438.